

**DESIGN, SYNTHESIS AND EVALUATION OF SOME NOVEL
FLUORESCENT CHEMOSENSORS FOR MERCURY (II) ION
DETECTION VIA DIFFERENT MECHANISMS**

Ph.D. THESIS

by

MUZEY BAHTA GEBREMDEHIN



**DEPARTMENT OF CHEMISTRY
INDIAN INSTITUTE OF TECHNOLOGY ROORKEE
ROORKEE – 247 667 (INDIA)
MAY, 2019**

DESIGN, SYNTHESIS AND EVALUATION OF SOME NOVEL FLUORESCENT CHEMOSENSORS FOR MERCURY (II) ION DETECTION VIA DIFFERENT MECHANISMS

A THESIS

*Submitted in partial fulfilment of the
requirements for the award of the degree*

of

DOCTOR OF PHILPSOPHY

in

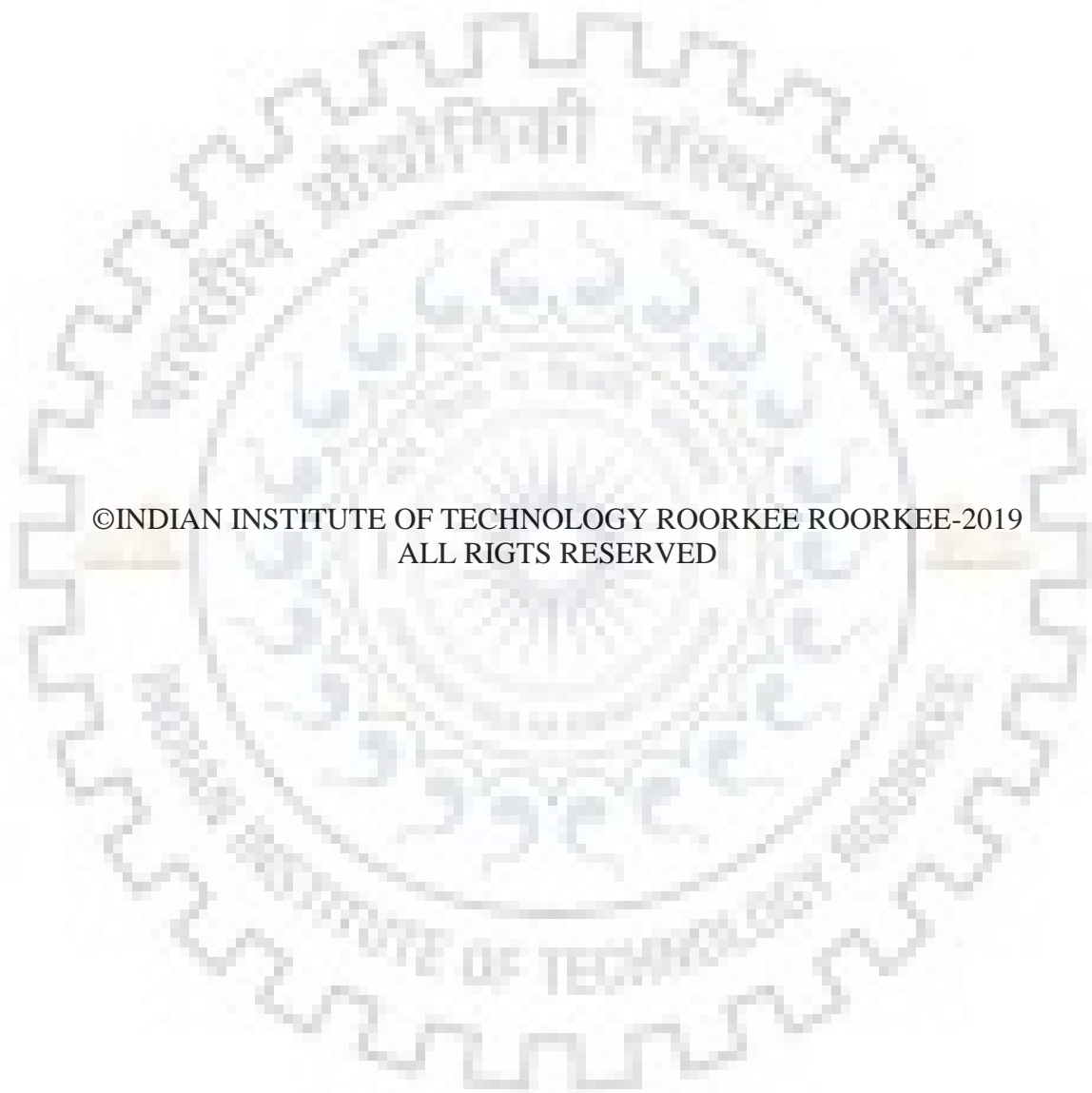
CHEMISTRY

by

MUZEY BAHTA GEBREMDEHIN



**DEPARTMENT OF CHEMISTRY
INDIAN INSTITUTE OF TECHNOLOGY ROORKEE
ROORKEE – 247 667 (INDIA)
MAY, 2019**



©INDIAN INSTITUTE OF TECHNOLOGY ROORKEE ROORKEE-2019
ALL RIGHTS RESERVED



INDIAN INSTITUTE OF TECHNOLOGY ROORKEE ROORKEE

CANDIDATE'S DECLARATION

I hereby certify that the work which is being presented in the thesis entitled “**DESIGN, SYNTHESIS AND EVALUATION OF SOME NOVEL FLUORESCENT CHEMOSENSORS FOR MERCURY (II) ION DETECTION VIA DIFFERENT MECHANISMS**” in partial fulfilment of the requirement of the award of the Degree of Doctor of philosophy and submitted in the Department of chemistry of the Indian Institute of Technology Roorkee, Roorkee, is an authentic record of my own carried out during a period from July, 2015 to May, 2019 under the supervision of Dr. Naseem Ahmed, Professor, Department of Chemistry, Indian Institute of Technology Roorkee, Roorkee.

The matter presented in the thesis has not been submitted by me for the award of any other degree of this or any other Institution.

(Muzey Bahta)

This is to certify that the above statement made by the candidate is correct to the best of my knowledge.

(Naseem Ahmed)
Supervisor

The PhD Viva-Voce Examination of Mrs. Muzey Bahta, Research Scholar, has been held on _____.

Chairman, SRC

Signature of External Examiner

This is to certify that the student has made all the corrections in the thesis.

(Naseem Ahmed)
Supervisor

Head of the Department

Dated: _____.



Dedicated to My Family and Parents



ABSTRACT OF THE THESIS

Increasing demand for fast and accurate environmental pollution monitoring requires new sensing techniques with outstanding performance, high sensitivity, selectivity and reliability and fluorescence chemosensors offer this distinctive reward over other analytical methods and have been considered as an ultimate tool for monitoring trace toxicants. As one of the most toxic heavy metals, Hg^{2+} ion has become an ultimate goal for its prolonged effects and rigorous terrorization to the environment and biological system. Novel organic molecular scaffolds for recognition and sensing of environmentally and biologically toxic Hg^{2+} ions with high selectivity and sensitivity detection in aqueous solution are persistently important for practical research in different fields of science.

The central theme of this present thesis entitled “**DESIGN, SYNTHESIS AND EVALUATION OF SOME NOVEL FLUORESCENT CHEMOSENSORS FOR MERCURY (II) ION DETECTION VIA DIFFERENT MECHANISMS**” discuss about the design, synthesis, characterization and photophysical properties studies of some Hg^{2+} ion receptors. All chemosensors were characterized by different spectroscopic methods and the photophysical behaviors of these chemosensors towards Hg^{2+} ion were observed through UV-visible and fluorescence spectroscopy. In addition to that the binding modes of chemosensors with Hg^{2+} ion were examined by using IR, NMR titration, HRMS and fluorescence lifetime.

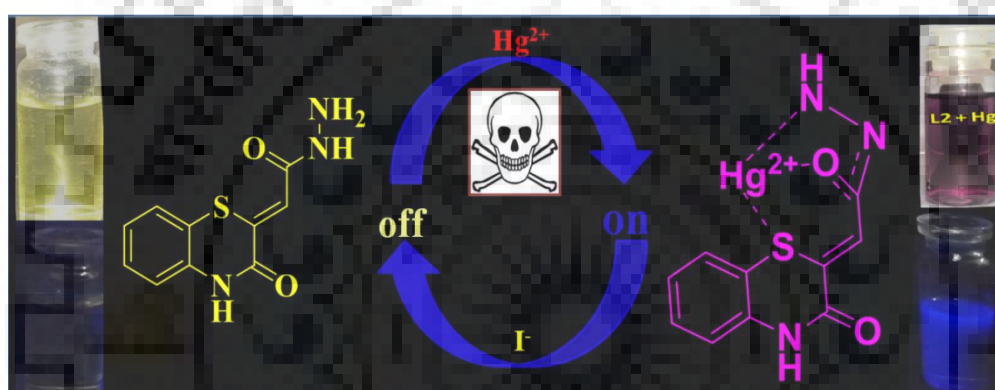
This thesis includes five chapters, the first chapter deals with “General Introduction”, which is providing brief discussions about principle of optical chemosensors, some common photophysical mechanisms of fluorescence chemosensors and review of some recognition mechanisms Hg^{2+} ion.

Chapter 2 presents about design and synthesis of 1,4-benzothiazine hydrazide as selective and sensitive colorimetric and Turn-On fluorometric sensor for Hg^{2+} detection in aqueous medium. A highly colorimetric and fluorimetric chemosensor, 3-oxo-[1,4]-benzothiazin-2-ylidene acetohydrazide (**L2**) is reported for the mercury detection. In HEPES-buffered solution ($\text{CH}_3\text{CN}:\text{H}_2\text{O}$, 1:2, v/v, pH 7.2), **L2** showed a characteristic absorption peak at 340 nm, addition of Hg^{2+} induced colour change from light yellow to purple with significant enhancement in absorbance at 340 nm and a new band centered at 550 nm with red-shift of 110 nm.

Furthermore, the **L2** exhibited high sensitivity and selectivity with overall emission change of more than 100-fold fluorescence intensity enhancement towards Hg^{2+} ion with a 1:1 binding

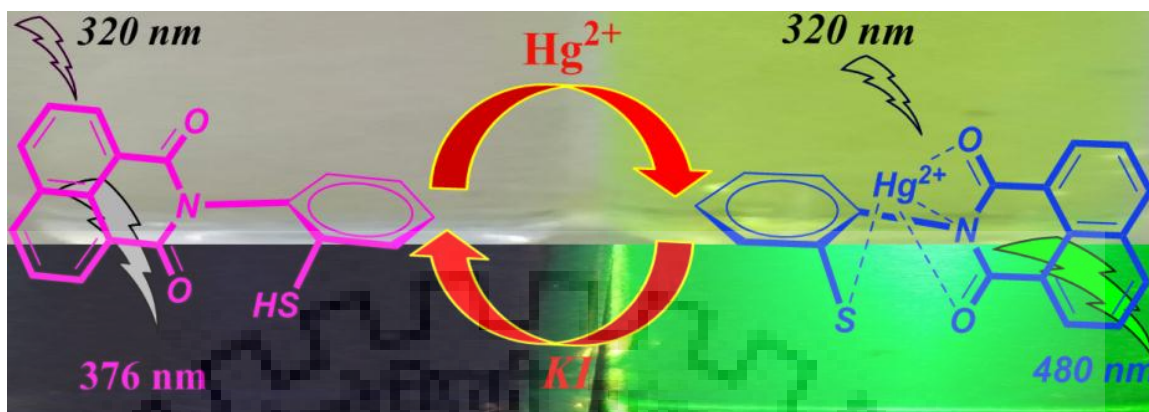
stoichiometry and $1.938 \times 10^3 \text{ M}^{-1}$ binding constant within detection limit as low as $5.4 \times 10^{-8} \text{ M}$.

More importantly, it has good practicability in real water sample. Apart from this, theoretical elucidation of the experimental outcome has also been supported by applying density functional theory (DFT) to the ligand and the complex. Moreover, the solution of *in situ* generated $\text{L2} + \text{Hg}^{2+}$ complex displayed high reversibility by I^- through Hg^{2+} displacement approach. This reversibility in fluorescence suggested that the promising applicability of chemosensor as “off–on–off” naked eye sensor and practical applicability of **L2** as an INHIBIT logic gate based on the emission changes with the inputs of Hg^{2+} and I^- was investigated.

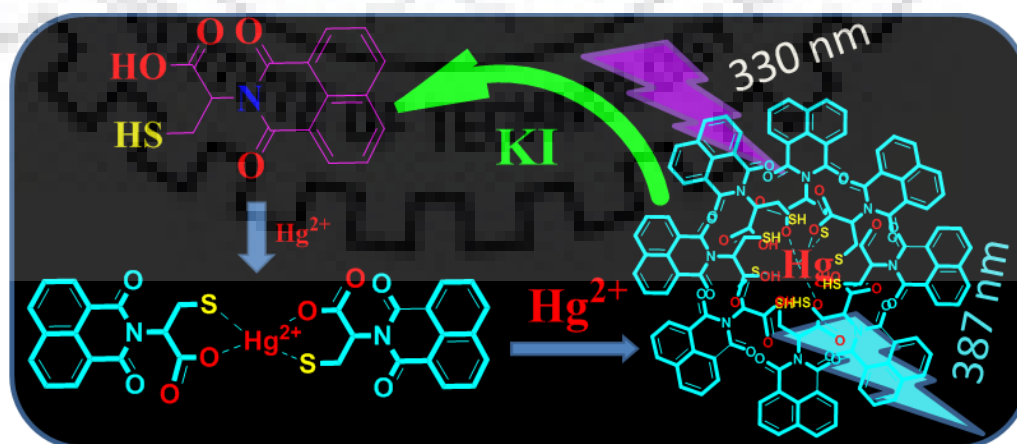


Chapter 3 describes about a novel 1,8-naphthalimide as highly selective naked-eye and ratiometric fluorescent sensor for detection of Hg^{2+} ion. In this chapter a novel chemosensor 2-(2-mercaptophenyl)-1H-benzo[de]isoquinoline-1,3-(2H)-dione (**L3**) is reported for Hg^{2+} ion detection. The selective binding of Hg^{2+} to **L3** afforded new absorbance and fluorescence peaks at 438 nm and 480 nm respectively, in addition to the existing bands of **L3** at 332 nm and 376 nm. It also showed apparent colour change from colourless to yellowish green and weak fluorescent to bright yellowish green strong fluorescent due to selective binding of Hg^{2+} . This sensor forms a 1:1 stoichiometry with high binding constant ($3.89 \times 10^4 \text{ mol}^{-1}\text{L}$) and limit of detection $1.74 \times 10^{-8} \text{ M}$ with high selectivity and sensitivity towards Hg^{2+} in the presence of other interfering metal ions. More importantly, it has good practicability in environmental water sample. The outcome of photo-physical experiment has also been in good accordance with the time-resolved fluorescence lifetime decay and the density functional theory (DFT) estimations. Moreover, the $\text{L3} - \text{Hg}^{2+}$ solution displayed high colorimetric and fluorimetric reversibility *via* the addition of KI . This reversibility in

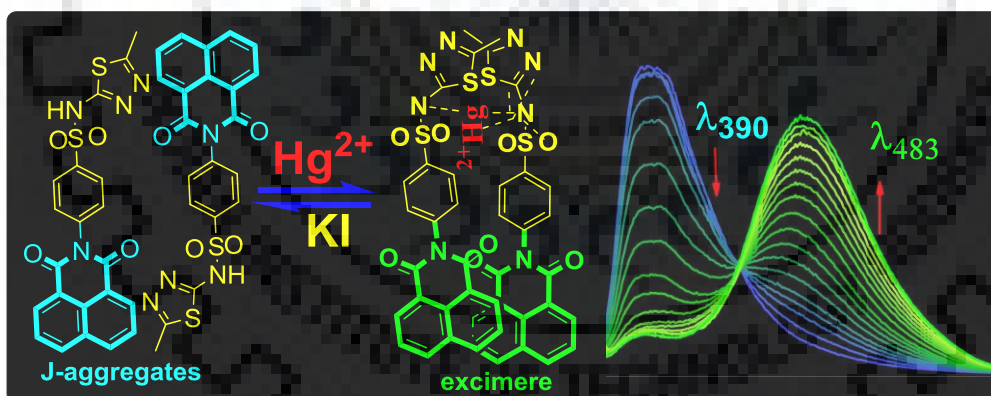
fluorescence showed potential applicability of chemosensor **L3** as “on–off–on” naked eye sensor.



Chapter 4 illustrates naphthalimide-amino acid conjugates chemosensors for Hg^{2+} detection based on chelation mediated emission enhancement in aqueous solution. 1,8-Naphthalimide-Amino acid conjugates (**L4** and **L5**) were designed, synthesized *via* straight forward reaction as Hg^{2+} chemosensors. These chemosensors were found to display aggregation-induced emission (AIE) property along with increment in quantum yield upon changing the medium from methanol to $\text{CH}_3\text{OH}:\text{H}_2\text{O}$ (1:99, v/v). They exhibited a quick response, splendid selectivity and sensitivity toward Hg^{2+} ion over other interfering metal ions through sharp selective Turn-On fluorescence *via* chelation mediated aggregation-induced emission (AIE) in $\text{CH}_3\text{OH}/\text{H}_2\text{O}$ (1:99, v/v) medium. Job’s plot revealed the formation of 2:1 ligand to metal stoichiometric complex. The chemosensors **L4** and **L5** could detect Hg^{2+} ion as low as 22 nM and 5.6 nM respectively. Intriguingly, the fluorescence reversibility study showed good reversibility by adding Hg^{2+} salts and KI sequentially.



Chapter 5 presents synthesis and evaluation of AIEE active sulfamethizole functionalized 1,8-naphthalimide for ratiometric fluorescence sensing of Hg^{2+} ion in aqueous media and anti-microbial activity. A sulfamethizole functionalized 1,8-naphthalimide molecule (**L6**) has been designed and synthesized which exhibited AIEE active, fluorescence sensing of Hg^{2+} ion and Ag^+ complex as anti-microbial activity. The hydrophobic nature of naphthalimide fluorogenic moiety instigated the aggregation induced emission (AIE) in aqueous medium, which led to excimer emission upon intramolecular excimer formation *via* metal ion-induced assembly. The high selectivity of the sensor was due to quenching of the monomeric emission of **L6** at 390 nm with red shift to gradual enhancement in new peak at 483 nm and 478 nm for Hg^{2+} and Ag^+ ions respectively, which resulted in ratiometric detection. The competitive experiment revealed that the chemosensor is selective to Hg^{2+} over Ag^+ ion and selective and sensitive ratiometric response to Hg^{2+} without interference of any other tested metal ions. The limits of detection of Hg^{2+} ion is 14.7 nM in 99% aqueous solution. Meanwhile, visual fluorescence color change of **L6** from blue to green was observed under Uv-lamp upon addition of Hg^{2+} ion to **L6** solution. Anti-microbial activities were tested against Gram negative strain. Under similar concentrations, **L6** and **L6- Ag^+** compounds have shown much better anti-microbial activities than the most of the tested antibiotics available in the market.



ACKNOWLEDGEMENTS

PhD is a long journey harmonized by great efforts, struggle and support of many people. It is a contribution of many faithful companies that proves fruitful after extensive efforts. At this instant, I wish to express my sincere appreciation to those who have contributed to this success and supported me in one way or the other during this amazing journey.

Firstly, I would like to express my Heartfelt thanks to my supervisor Prof. Naseem Ahmed for the continuous support of my PhD study, for his patience, motivation, and immense knowledge. His guidance helped me in all the time of research and writing of this thesis.

Besides my supervisor, my sincere thanks go to the rest of my Student Research Committee members: Prof. Mannar Ram Maurya (Department of Chemistry, IIT Roorkee), Dr. Debasis Banarjee (Department of Chemistry, IIT Roorkee) and Dr. Ranjana Pathania (External member, Department of biotechnology, IIT Roorkee) for their insightful comments and encouragement from various perspectives. And I am highly obliged and express my sincere thanks to, Prof. K. R. Justin Thomas, the present Head Department of Chemistry and Prof. M. R. Mourya, Ex-Head of Department of Chemistry, Department of Chemistry and all other faculty members and Mr. D. C. Meena, Sh. Madan Pal, Mr. Pankaj, Mr. Charan Singh and Mr. Anuj Arjun members of Chemistry Department for providing the basic infrastructural and their needful help for accomplishing my research work.

My sincere thanks to fellow lab mates Dr. Nishant, Dr. Shaily, Dr. Iram Parveen, Dr. Mohammed Wahid, Danish Khan and Zabir for the stimulating discussions, feedback, and cooperation throughout my stay in India, and for all the fun we have had in the last four years. Also I thank my other friends in the institution in particular, I am grateful to Dr. Nirma for her needful help.

A sincere thanks to all Ethiopian friends here in India for really support and all my friends who made my India experience something special, in particular, Special thanks to Abudulkider Shube for all his useful discussions and suggestions when in all ups and downs.

Very special thanks to the Indian institution of technology Roorkee for giving me the opportunity to carry out my doctoral research. A very special gratitude goes out to my host Aksum University, Ethiopian ministry of education and Ethiopian embassy in India for providing the funding for my stay and for their financial support.

Words cannot express the feelings I have for my love Nigus Dimtsu for his constant unconditional support both emotionally and financially, I would not be here if it not for you. A special thanks to the source of my strength my sons Natan Nigus and Yudahie Nigus they have been very patient with me in all my ups and downs.

Finally, I would like to acknowledge the most important person in my life my mother Birizaf Gebremaryiam. She has been a constant source of strength and caring in all my life. There during the past four years for carrying my entire load when everything seemed hopeless and I didn't have any hope. I can honestly say that it was only her determination and constant encouragement that ultimately made it possible for me to see this project through to the end. I owe it all to you.

Last but not the least, I would like to thank my family: my father and to my brothers and sisters for supporting me spiritually throughout this thesis and my life in general.

Many Thanks!

Muzey Bahta

List of Publications

- [1] Bahta, M.; Ahmed, N. Design and synthesis of 1, 4-benzothiazine hydrazide as selective and sensitive colorimetric and Turn-On fluorometric sensor for Hg²⁺ detection in aqueous medium. *J. Photochem. Photobiol. A Chem.* **2018**, *357*, 41–48. DOI: 10.1016/j.jphotochem.2018.02.022.
- [2] Bahta, M.; Ahmed, N. A novel 1, 8-naphthalimide as highly selective naked-eye and ratiometric fluorescent sensor for detection of Hg²⁺ ions. *J. Photochem. Photobiol. A Chem.* **2019**, *373*, 154–161. DOI: 10.1016/j.jphotochem.2019.01.009.
- [3] Bahta, M.; Ahmed, N. Naphthalimide-amino acid conjugates chemosensors for Hg²⁺ detection: Based on chelation mediated emission enhancement in aqueous solution. *J. Photochem. Photobiol. A Chem.* **2019**, *378*, 85–93. DOI: 10.1016/j.jphotochem.2019.04.027.
- [4] Bahta, M.; Ahmed, N. A Synthesis and evaluation of AIEE active sulfamethizole functionalized 1,8-naphthalimide for ratiometric fluorescence sensing of Hg²⁺ ion in aqueous media and anti-microbial activity, **2019**, *Communicated*.

List of Conferences

- [1] Bahta, M.; Ahmed, N. “Poster presentation” in National Conference on Contemporary Facets in Organic Synthesis (CFOS) organized by Department of Chemistry, IIT Roorkee, 22th-24th Dec. **2017**.
- [2] Bahta, M.; Ahmed, N. “Poster presentation” in ACS ON CAMPAS **2018**, organized by ACS, in Department of Chemistry, IIT Roorkee, 7th Feb. **2018**.



LIST OF ABBREVIATIONS

A.U.	Arbitrary Unit
ACN	Acetonitrile
CDCl ₃	Deuterated Chloroform
cm	Centimeter
conc.	Concentration
DMF	N,N'-Dimethylformamide
DMSO	Dimethylsulphoxide
DMSO d ₆	Deuterated Dimethylsulphoxide
equiv.	Equivalents
EtOH	Ethanol
FLS	Fluorescence lifetime
gm	Gram
HCl	Hydrochloric Acid
HEPES	4-(2-Hydroxyethyl)-1-Piperazineethanesulfonic Acid
Hr	Hour
HRMS	High Resolution Mass Spectroscopy
ICP-MS	inductively coupled plasma mass spectrometry
IR	Infrared radiation
K _a	Association constant
KI	Potassium iodide
KOH	Potassium hydroxide
LOD	Limit of Detection
M	Molar
MeOH	Methanol
Mol	Mole
nm	Nano meter
nM	Nano molar
NMR	Nuclear magnetic resonance spectroscopy
°C	Degree Centigrade
ppm	Parts Per Million
TLC	thin-layer chromatography

TMS	Tetramethylsilane
UV-Vis	Ultra-violet and visible wavelength
WHO	World Health Organization
μ	Micro
δ	Chemical Shift
λ	Wave length
Φ	Quantum Yield



List of Figures

Figure 1.1 General host guest interaction of chemosensor and analyte.	3
Figure 1.2 Representation of PET mechanism	4
Figure 1.3 PET based chemosensors for Hg ²⁺ detection.	4
Figure 1.4 Representation of ICT mechanisms.....	6
Figure 1.5 ICT based chemosensors for Hg ²⁺ sensing.....	6
Figure 1.6 Representation of FRET mechanism.....	7
Figure 1.7 FRET based chemosensors for Hg ²⁺ sensing	9
Figure 1.8 Representation of ESIPT mechanism.....	10
Figure 1.9 ESIPT based fluorescence sensors for Hg ²⁺ detection	11
Figure 1.10 CHEF & CHEQ based chemosensors for Hg ²⁺ sensing	12
Figure 1.11 Excimer based chemosensors for Hg ²⁺ sensing.....	13
Figure 1.12 AIE & ACQ based fluorescence sensors for Hg ²⁺ sensing	14
Figure 1.13 Hg ²⁺ selective chemodosimeter based on Hg ²⁺ triggered desulfurization reaction.....	16
Figure 1.14 Hg ²⁺ ion selective chemodosimeters based on Hg ²⁺ ion triggered intermolecular cyclic guanylation of thiourea to imidazoline.	18
Figure 1.15 Hg ²⁺ ion selective chemodosimeter based on Hg ²⁺ triggered desulfurisation and intramolecular cyclization of thiosemicarbazide to 1,3,4-oxadiazole.....	19
Figure 1.16 Hg ²⁺ ion selective chemodosimeter based on Hg ²⁺ triggered desulfurisation / deprotection reaction of dithioacetal/dithioacetal.	21
Figure 1.17 Hg ²⁺ ion selective chemodosimeter based on Hg ²⁺ ion promoted hydration of alkynes to ketones.....	23
Figure 1.18 Hg ²⁺ ion selective chemodosimeter based on Hg ²⁺ ion promoted hydrolysis of vinyl ether and isopropenyl ether.	24
Figure 1.19 Hg ²⁺ ion selective chemodosimeter based on Hg ²⁺ promoted hydrolysis reaction of rhodamine spirolactam ring	25
Figure 1.20 Hg ²⁺ selective chemosensors with pyridine core receptor.....	27
Figure 1.21 Hg ²⁺ selective chemosensors with thioether moieties receptors	27
Figure 1.22 Hg ²⁺ selective chemosensors with sulfonamide receptors	28
Figure 1.23 Hg ²⁺ selective chemosensors with sulfonamide and-amino acids receptors.	29
Figure 1.24 Hg ²⁺ selective chemosensors with dansyl-amino receptors.	29
Figure 1.25 Hg ²⁺ selective chemosensors containing crown thioether or dithia-diazo receptor group.....	30

Figure 1.26 Hg ²⁺ selective chemosensors with S, N, and O atoms coordinating moiety receptor.....	31
Figure 2.1 (a). Absorption spectra of L2 in the presence of 10 equivalents various cations. (b). Absorption titration spectral responses of L2 towards varying Hg ²⁺ ion concentrations (0-3 eq.) Hg ²⁺ (10 μM of L2 in HEPES buffered solution (CH ₃ CN:H ₂ O, 1:2 v/v, pH 7.2).	53
Figure 2.2 (a). Colourimetric. (b). fluorometric naked-eye detection of L2 in the presence of different metal ions in HEPES buffered solution (CH ₃ CN:H ₂ O, 1:2 v/v, pH 7.2).....	53
Figure 2.3 Fluorescence spectra of L2 (10 μM in HEPES buffered solution (CH ₃ CN:H ₂ O, 1:2 v/v, pH 7.2) in the presence of 10.0 equiv. various cations.	54
Figure 2.4 Fluorescence Emission spectral responses of L2 (10 μM) towards varying concentration of Hg ²⁺ (0-4 eq.) in HEPES buffered solution (CH ₃ CN:H ₂ O, 1:2 v/v, pH 7.2). (Inset: (a) visual fluorescence change of L2 with Hg ²⁺ (b). A good liner fit of Benesi-Hildebrand plot confirms the 1:1 stoichiometry.....	54
Figure 2.5 (a). Job's plot, (b). The plot of log ((I-I ₀)/(I _{max} -I)) to log [Hg ²⁺] (μM in HEPES buffered solution (CH ₃ CN:H ₂ O, 1:2 v/v, pH 7.2))	55
Figure 2.6 (a) Linear fit graph of L2 with Hg ²⁺ fluorescence titration. (b) Association constant calculation by Fluorescence titration method of L2 with Hg ²⁺ using linear regression analysis.....	57
Figure 2.7 pH dependent fluorescence of L2 and L2 -Hg ²⁺	57
Figure 2.8 Interference effects of other metal ions in Hg ²⁺ detection by L2 (10 μM) (blue bars represent the fluorescence intensity of L2 +metal ions and red bars show the fluorescence intensity of L2 +Hg ²⁺ + other metal ions in 1:1:10), λ _{ex} = 330 nm, λ _{em} = 429 nm.	58
Figure 2.9 Fluorescence Emission responses of L2 (10 μM, in HEPES buffered solution (CH ₃ CN:H ₂ O, 1:2 v/v, pH 7.2) in the presence of different counter ions.....	59
Figure 2.10 Molecular orbital diagrams and excitation energies of L2 and L2 -Hg ²⁺ complex.	60
Figure 2.11 HOMO–LUMO band gaps of L2 and L2 +Hg ²⁺ optimized structures.	61
Figure 2.12 Theoretical excitation energies UV-vis spectrum of (a) L2 , (b) L2 -Hg ²⁺	61
Figure 2.13 (a). Visual Colorimetric reversibility (b). Fluorescence reversibility of chemosensor L2 upon sequential addition of Hg ²⁺ and KI . (Inset: visual fluorometric reversibility) (c).number of cycles of reversibility of chemosensor	

upon sequential addition of Hg^{2+} and KI (d). Switch circuit diagram and Truth table corresponding to a logic gate based on Hg^{2+} and KI.....	63
Figure 2.14 linear correlation between changes in fluorescence intensity and $[\text{Hg}^{2+}]$ in water samples spiked with different amount of $[\text{Hg}^{2+}]$ standard solutions in the standard addition experiments. (a) Canal water, (b) Drain water. ($[\text{L2}] = 10 \mu\text{M}$, $\lambda_{\text{ex}} = 330 \text{ nm}$, $\lambda_{\text{em}} = 429 \text{ nm}$).....	64
Figure 2.15 $^1\text{H-NMR}$ spectrum of Ethyl (3-oxo-[1,4]Benzothiazin-2-ylidene)acetate in CDCl_3	66
Figure 2.16 $^{13}\text{C-NMR}$ spectrum of Ethyl (3-oxo-[1,4]Benzothiazin-2-ylidene)acetate in CDCl_3	66
Figure 2.17 $^1\text{H-NMR}$ spectrum of L2 in $\text{DMSO-}D_6$	67
Figure 2.18 $^{13}\text{C-NMR}$ spectrum of L2 in $\text{DMSO-}D_6$	67
Figure 2.19 FT-IR spectrum of L2 in KBr pellet.....	68
Figure 2.20 (a) FT-IR spectrum of L2 and L2 + Hg^{2+} in KBr pellet, (b) $^1\text{H-NMR}$ titration of L2 and L2 + Hg^{2+} in $\text{DMSO-}D_6$	68
Figure 3.1 A visual features of detection of Hg^{2+} with L3 in the presence of 10 equivalent of different cations in $\text{CH}_3\text{CN}:\text{H}_2\text{O}$ (1:1 v/v, pH 7.0, HEPES buffer).(a).in sun light and (b). under UV-lamp. (b). under UV lamp.....	78
Figure 3.2 (a). Absorption titrations spectral responses of L3 (10 μM) towards varying Hg^{2+} ion concentration (0-5 equiv.), (b). Fluorescence Emission spectral responses of L3 (10 μM) towards varying Hg^{2+} ion concentration (0-10 equiv.) (in $\text{MeCN}/\text{H}_2\text{O}$ (1:1 v/v, PH 7.0, HEPES buffer)).....	79
Figure 3.3 (a). Absorption spectra (b). Fluorescence Emission spectra of L3 (10 μM) in the presence of 10 equiv. different metal ions (in $\text{MeCN}/\text{H}_2\text{O}$ (1:1 v/v, PH 7.0, HEPES buffer)).....	80
Figure 3.4 Job's plot (the total concentration were 10 μM in $\text{MeCN}/\text{H}_2\text{O}$ (1:1 v/v, PH 7.0, HEPES buffer).....	81
Figure 3.5 (a). The linear fit graph of fluorescence intensity ratio (I_{480}/I_{376}) as a function of Hg^{2+} ion concentration. (b). Benesi-Hildebrand plot of L3 (10 μM) binding with Hg^{2+} . (in $\text{MeCN}/\text{H}_2\text{O}$ (1:1 v/v, PH 7.0, HEPES buffer).....	82
Figure 3.6 Life time decay profile of L3 in the absence and presence of Hg^{2+} .(in $\text{MeCN}/\text{H}_2\text{O}$ (1:1 v/v, PH 7.0, HEPES buffer) $\lambda_{\text{ex}} = 320 \text{ nm}$).....	83
Figure 3.7 Interference effect of various cations with L3-Hg²⁺ in emission spectra (blue bar for fluorescenc intensity ratio(I_{480}/I_{376}) of L3 +cations (1:10 equiv.) and red bars show fluorescence intensity of L3 + Hg^{2+} +other cations (1:1:10 equiv.).....	84

Figure 3.8 Fluorescence Emission responses of L3 (10 μM , in MeCN/H ₂ O (1:1 v/v, PH 7.0, HEPES buffer) in the presence of different counter ions (a) Fluorescence intensity (b) Fluorescence intensity ratio (I_{480}/I_{376}).....	84
Figure 3.9 Fluorescence intensity of (a) L3 , (b) L3-Hg²⁺ at different pH value.	85
Figure 3.10 Fluorescence intensity ratio (I_{480}/I_{376}) for L3 and L3-Hg²⁺ at different pH values.....	86
Figure 3.11 Optimized structures of L3 and L3+Hg²⁺	88
Figure 3.12 HOMO–LUMO band gaps of L3 and L3+Hg²⁺	88
Figure 3.13 TD-DFT of CAM-B3LYP, function combined with 6-31G (d) basis sets for L3 and with Lanl2DZ method for L3-Hg²⁺	89
Figure 3.14 (a). Visual Colorimetric reversibility (b). Fluorometric reversibility. (Inset: visual fluorometric reversibility) (c). “off–on–off” reversibility cycles of chemosensor L3 upon sequential addition of Hg²⁺ and KI . (d). Switch circuit diagram and Truth table corresponding to a logic gate based on Hg²⁺ and KI	91
Figure 3.15 (a). Calibration curve of standard solutions of Hg²⁺ (0.05-0.5 μM), (b). Canal water and drain water, linear correlation of (I_{480}/I_{376}) to [Hg²⁺] in water samples spiked with different concentration of [Hg²⁺] in the standard addition experiments. ([L3]=10 μM , λ_{ex} = 320 nm).....	92
Figure 3.16 IR spectrum of receptor L3 recorded in KBr pellet.	96
Figure 3.17. ¹ H-NMR spectrum of receptor L3 recorded in CDCl ₃	96
Figure 3.18 ¹³ C-NMR spectrum of receptor L3 recorded in CDCl ₃	97
Figure 3.19 HRMS of L3	97
Figure 3.20 HRMS of L3+Hg²⁺	98
Figure 3.21 IR spectrum of receptor L3 , and L3+HgCl₂ recorded in KBr pellet.....	98
Figure 3.22 ¹ H-NMR spectra of L3 with Hg²⁺ as HgCl₂ in CDCl ₃	98
Figure 4.1 Absorption spectra change of (a). L4 , (b). L5 (10 μM) in pure MeOH and MeOH/H ₂ O (1:99, v/v. HEPES buffer, pH 7.0).	110
Figure 4.2 Fluorescence intensity of 10 μM (a) L4 , (b) L5 in CH ₃ OH solution with different fraction of water (0, 10, 20, 40, 60, 80, 99%).....	111
Figure 4.3 Dynamic light scattering results of L4 and L5 in CH ₃ OH and water.....	111
Figure 4.4 Absorption spectra of (a). L4 , (b). L5 (10 μM) MeOH/H ₂ O (1:99, v/v. HEPES buffer, pH 7.0)) in the presence of 10.0 equiv. various cations.	112
Figure 4.5 Absorption titrations spectral responses of (a). L4 , (b). L5 towards varying Hg²⁺ ion concentrations (0-2 equiv.) (In MeOH/H ₂ O (1:99, v/v. HEPES buffer, pH 7.0)).	113

Figure 4.6 Fluorescence spectra of (a). L4 , (b). L5 (10 μM , in MeOH/H ₂ O (1:99, v/v. HEPES buffer, pH 7.0). in the presence of 10.0 equiv. various cations.	113
Figure 4.7 Fluorescence Emission titrations spectral responses of (a). L4 , (b). L5 towards varying Hg ²⁺ ion concentrations ((In MeOH/H ₂ O (1:99, v/v. HEPES buffer, pH 7.0)).	114
Figure 4.8 Dynamic light scattering results of L4 and L5 in the absence and presence of Hg ²⁺ in MeOH/H ₂ O (1:99, v/v. HEPES buffer, pH 7.0).....	115
Figure 4.9 Lifetime decay profile of (a). L4 , (b). L5 in absence and presence of Hg ²⁺ in MeOH/H ₂ O (1:99, v/v. HEPES buffer, pH 7.0). ($\lambda_{\text{ex}}=330$ nm)	116
Figure 4.10 Job's plot (a). L4 +Hg ²⁺ , (b). L5 +Hg ²⁺ (in MeOH/H ₂ O (1:99, v/v. HEPES buffer, pH 7.0).) the total concentration were 10 μM	117
Figure 4.11 The linear fit graph of fluorescence intensity ratio as a function of Hg ²⁺ concentration. (a) L4 , (b) L5	118
Figure 4.12 Benesi-Hilderbrand Plot for K _a determination of (a) L4 , (b) L5 towards Hg ²⁺	118
Figure 4.13 Interference effect of various cations, with (a) L4 emission spectra at 395 nm (Blue bars represent fluorescence intensity of L4 +cations and orange bars show the fluorescence intensity of L4 +Hg ²⁺ +other cations, and (b) L5 emission spectra at 386 nm (green bars represent the fluorescence intensity of L5 +cations and red bars show the fluorescence intensity of L5 +Hg ²⁺ +other cations.....	119
Figure 4.14 Fluorescence intensity of chemosensors (L4 and L5) and complexes (L4 + Hg ²⁺ and L5 + Hg ²⁺) at different pH values.	122
Figure 4.15 Fluorometric reversibility (a) L4 ,(b) L5 upon sequential addition of Hg ²⁺ and KI.	123
Figure 4.16 IR spectrum of receptor L4 recorded in KBr pellet.	124
Figure 4.17 ¹ H-NMR spectrum of receptor L4 recorded in DMSO- <i>d</i> ₆	124
Figure 4.18 ¹³ C-NMR spectrum of receptor L4 recorded in DMSO- <i>d</i> ₆	125
Figure 4.19 HRMS of receptor L4 recorded in CH ₃ CN.	125
Figure 4.20 IR spectrum of receptor L5 recorded in KBr pellet.	126
Figure 4.21 ¹ H-NMR spectrum of receptor L5 recorded in DMSO- <i>d</i> ₆	126
Figure 4.22 ¹³ C-NMR spectrum of receptor L5 recorded in DMSO- <i>d</i> ₆	127
Figure 4.23 HRMS of receptor L5 recorded in CH ₃ CN.	127
Figure 4.24 HRMS of receptor L4 +Hg ²⁺ recorded in CH ₃ CN.	128
Figure 4.25 HRMS of receptor L5 +Hg ²⁺ recorded in CH ₃ CN.	128
Figure 4.26 IR spectrum of receptor L4 +Hg ²⁺ recorded in KBr pellet	129

Figure 4.27 $^1\text{H-NMR}$ spectra of L4 with Hg^{2+} as HgCl_2 in $\text{DMSO-}d_6$	129
Figure 4.28 IR spectrum of receptor L5 + Hg^{2+} recorded in KBr pellet	130
Figure 4.29 $^1\text{H-NMR}$ spectra of L5 with Hg^{2+} as HgCl_2 in $\text{DMSO-}d_6$	130
Figure 5.1 (a) The absorption spectrum of L6 in DMSO and DMSO/water (1:99 v/v), (b) Fluorescence intensity of L6 (10 μM) solution in DMSO with various water fraction (0, 10, 20, 40, 60, 80, 90%).....	144
Figure 5.2 (a). Absorption spectra (b). Fluorescence spectra L6 (10 μM) in the presence of various metal ions (10 equiv.).....	145
Figure 5.3 UV-visible absorption titrations spectra of L6 (10 μM) towards varying concentrations (0-5 equiv.) (a) Hg^{2+} ion, (b) Ag^+ ion (in DMSO/water (1:99, v/v, HEPES buffer, pH 7.2)).	145
Figure 5.4 Fluorescence emission titration responses of L6 (10 μM) towards varying (a) Hg^{2+} ion concentrations, (b) Ag^+ ion concentrations (0 -5 equiv.) ion (in DMSO/water (1:99, v/v, HEPES buffer, pH 7.2)).....	146
Figure 5.5 Interference effect of various cations with L6-Hg²⁺ (fluorescence intensity ratio (I_{483}/I_{390}) of L6 + Hg²⁺ + other cations (1:1:10 equiv.)	147
Figure 5.6 (a) Job's plot (the total concentration were 10 μM), (b) The linear fit graph of intensity ratio (I_{483}/I_{390}) as a function of Hg^{2+} ion concentration. (in DMSO- water (1:99 v/v, HEPES buffer pH 7.2)	148
Figure 5.7 Fluorescence lifetime decay profile of L6 in the absence and presence of Hg^{2+} ion (in DMSO/water (1:99 v/v, HEPES buffer pH 7.2), $\lambda_{\text{ex}} = 340 \text{ nm}$)	148
Figure 5.8 Fluorescence intensity ratio (I_{483}/I_{390}) for L6 and L6-Hg²⁺ at different pH values.....	150
Figure 5.9 (a) Fluorometric reversibility.(b) Truth table corresponding to a logic gate based on Hg²⁺ and KI . (c) Switch circuit diagram.....	152
Figure 5.10 IR spectrum of receptor L6 recorded in KBr pellet.	154
Figure 5.11 $^1\text{H-NMR}$ spectrum of receptor L6 recorded in $\text{DMSO-}d_6$	154
Figure 5.12 $^{13}\text{C-NMR}$ spectrum of receptor L6 recorded in $\text{DMSO-}d_6$	155
Figure 5.13 HRMS of L6	155
Figure 5.14 IR spectrum of receptor L6+Ag⁺ recorded in KBr pellet.	156
Figure 5.15 $^1\text{H-NMR}$ spectrum of receptor L6+Ag⁺ complex recorded in $\text{DMSO-}d_6$	156
Figure 5.16 $^{13}\text{C-NMR}$ spectrum of receptor L6+Ag⁺ recorded in $\text{DMSO-}d_6$	157
Figure 5.17 IR spectrum of L6+HgCl₂ recorded in KBr pellet.....	157
Figure 5.18 $^1\text{H-NMR}$ spectra of L6 with Hg²⁺ (as HgCl_2) in $\text{DMSO-}d_6$	158
Figure 5.19 Fluorescence intensity of (a). L6 , (b). L6-Hg²⁺ at different pH value.	158

List of Tables

Table 2.1 Fluorescence intensity and standard deviation of blank receptor (L2).....	56
Table 2.2 The major electronic transition energies and molecular orbital contributions for L2 and L2-Hg²⁺	60
Table 3.1 Fluorescence intensity and standard deviation of blank receptor (L3).....	82
Table 3.2 Excitation energies and oscillator strengths of L3 opt freq td cam-b3lyp/6- 31g(d) geom=connectivity.....	89
Table 3.3 Determination of Hg ²⁺ ion concentration in real samples by using standard addition method.....	92
Table 3.4 A comparative study of L3 with some previously reported 1,8- Naphthalimide based fluorescence Hg ²⁺ sensors.....	93
Table 4.1 Fluorescence intensity and standard deviation of blank receptors.....	117
Table 5.1 Anti-microbial activities of L6 and L6-Ag⁺ compounds.....	152



Table of Contents

Abstract of the Thesis.....	i
Acknowledgements	v
List of Publications	vii
List of Conferences	vii
List of Abbreviations.....	ix
List of Figures	xi
List of Tables.....	xvii

Chapter 1 GENERAL INTRODUCTION

1.1 Introduction	1
1.2 Fluorescence Sensing	2
1.3 Some Common Photophysical Mechanisms for Fluorescence Sensing	3
1.3.1 Photoinduced Electron Transfer (PET)	3
1.3.2 Intramolecular Charge Transfer (ICT)	5
1.3.3 Fluorescence Resonance Energy Transfer (FRET)	7
1.3.4 Excited State Intramolecular Proton Transfer (ESIPT).....	9
1.3.5 Chelation Enhanced Fluorescence Emission (CHEF) and Chelation Enhanced Quenching (CHEQ)	11
1.3.6 Excimer/Exciplex Formation	12
1.3.7 Aggregation-Induced Emission (AIE)/Aggregation-Caused Quenching (ACQ)	13
1.4 Importance of Mercury ion (Hg^{2+}) Detection	15
1.5 Reaction Based Hg^{2+} Sensors.....	15
1.5.1 Hg^{2+} Detection <i>via</i> Hg^{2+} -Promoted Desulfurisation of Thioamide into Amide	16
1.5.2 Hg^{2+} Detection <i>via</i> Hg^{2+} Promoted Cyclic Guanylationo Thiourea to Imidazoline	17
1.5.3 Hg^{2+} Detection <i>via</i> Hg^{2+} -Promoted Cyclization of Thiosemicarbazide to Oxadiazole	19
1.5.4 Hg^{2+} Detection <i>via</i> Hg^{2+} -Promoted Elimination of Thioether.....	20
1.5.5 Hg^{2+} Detection <i>via</i> Hg^{2+} - Promoted Hydration of Alkynes to Ketones.....	22
1.5.6 Hg^{2+} Detection <i>via</i> Hg^{2+} ion Promoted Hydrolysis of Vinyl Ether and Isopropenyl Acetate	23
1.5.7 Hg^{2+} Promoted Spirolactam Hydrolysis Reaction.....	24

1.6 Coordination Based Hg ²⁺ Sensors	26
1.7 Objective of the Thesis	31
1.8 Reference.....	33

Chapter 2 Design and Synthesis of 1,4-Benzothiazine Hydrazone as Selective and Sensitive Colorimetric and Turn-On Fluorometric Sensor for Hg²⁺ ion Detection in Aqueous Medium

2.1 Introduction	49
2.2 Experimental section	50
2.2.1 Materials and Reagents.....	50
2.2.2 Synthesis of Chemosensor.....	50
2.2.3 Absorbance Measurements.....	51
2.2.4 Fluorescence Measurements.....	51
2.2.5 Theoretical Study.....	52
2.3 Results and Discussion.....	52
2.3.1 Colorimetric and UV-visible Responses of L2 to Hg ²⁺ ion.....	52
2.3.2 Fluorometric Responses of L2 to Hg ²⁺ ion.....	53
2.3.3 Stoichiometry	55
2.3.4 Limit of Detection (LOD) and Association Constant (K _a).....	55
2.3.5 pH Selection	57
2.3.6 Selectivity Experiments.....	58
2.3.7 Theoretical Calculation	59
2.3.8 Binding Nature of L2 and Hg ²⁺ ion	62
2.3.9 Reversibility Studies Applied as Logic Gate Circuit Devices.....	62
2.3.10 Analysis of Real Sample	63
2.4 Conclusion.....	65
2.5 References	69

Chapter 3 A Novel 1,8-Naphthalimide as Highly Selective Naked-Eye and Ratiometric Fluorescent Sensor for Detection of Hg²⁺ ion

3.1 Introduction	75
3.2 Experimental Section	76
3.2.1 Reagents and Instrumentation	76
3.2.2 Synthesis and Characterization of Chemosensors.....	77
3.2.3 Absorbance and Fluorescence Experiments.....	77
3.2.4 Theoretical Study.....	77

3.3 Results and Discussion.....	78
3.3.1 Naked-eye Selectivity	78
3.3.2 Spectroscopic Studies.....	78
3.3.3 Stoichiometry	81
3.3.4 Limit of Detection (LOD) and Association Constant (K_a).....	81
3.3.5 Fluorescence Lifetime	83
3.3.6 Selectivity Studies	83
3.3.7 Solvent System and pH Studies	85
3.3.8 Nature of Binding Interaction of L3 with Hg^{2+}	86
3.3.9 Theoretical Calculation	87
3.3.10 Reversibility Studies Applied as Logic Circuit Devices.....	90
3.3.11 Analysis of Real Sample.....	91
3.4 Comparative Study.....	93
3.5 Conclusion.....	95
3.6 Reference.....	99

**Chapter 4 Naphthalimide-Amino Acid Conjugates Chemosensors for Hg^{2+} ion
Detection: Based on Chelation Mediated Emission Enhancement in
Aqueous Solution**

4.1 Introduction	107
4.2 Experimental Section	108
4.2.1 Reagents and Instrumentation	108
4.2.2 Synthesis and Characterization of Chemosensors.....	108
4.2.3 Absorbance and Fluorescence Measurements.....	109
4.3 Results and Discussion.....	110
4.3.1 Aggregation-Induced Emission (AIE) Properties of L4 and L5	110
4.3.2 Absorption Behaviour towards Various Cations.....	112
4.3.3 Emission Behaviour towards Various Cations.....	113
4.3.4 Fluorescence Lifetime	115
4.3.5 Stoichiometry	116
4.3.6 Limit of Detection (LOD) and Association Constants (K_a).....	117
4.3.7 Selectivity Studies	118
4.3.8 Binding Mode of L4 and L5 with Hg^{2+}	120
4.3.9 pH Selection	121
4.3.10 Reversibility Studies	122

4.4 Conclusion.....	123
4.5 References	131

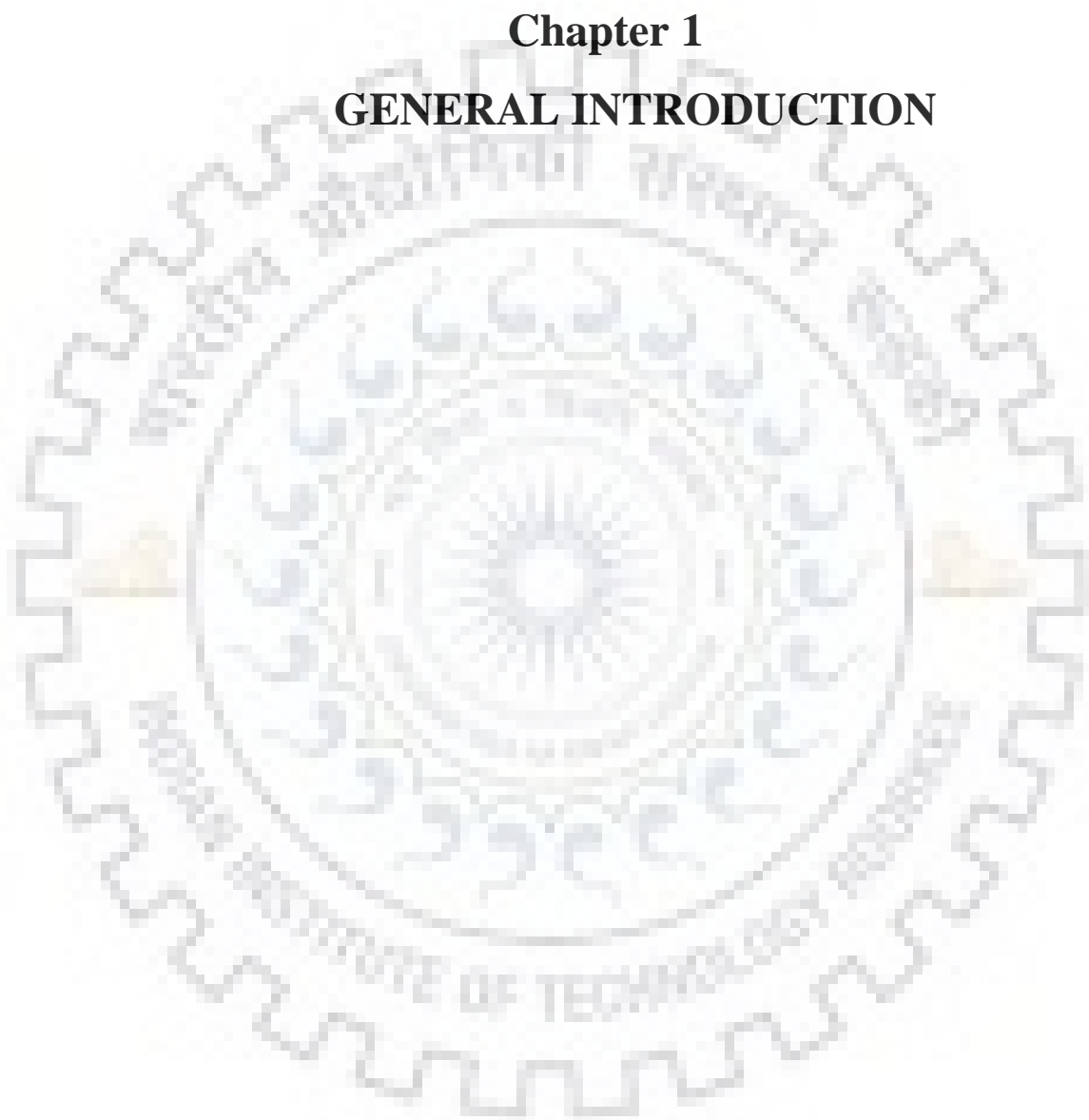
Chapter 5 Synthesis and Evaluation of AIEE Active Sulfamethizole Functionalized 1,8-Naphthalimide for Ratiometric Fluorescence Sensing of Hg²⁺ ion in Aqueous Media and Anti-Microbial Activity

5.1 Introduction	139
5.2 Experimental Section	141
5.2.1 Reagents and Instrumentation	141
5.2.2 General Procedure	141
5.2.3 Synthesis and Characterization of Chemosensor	142
5.2.4 Synthesis and Characterization of Silver Complex	143
5.3 Results and Discussion.....	143
5.3.1 Aggregation Induced Emission (AIE) Character of L6.....	143
5.3.2 Absorption Behaviour towards Various Cations.....	144
5.3.3 Fluorescence Emission Change towards Various Metal ions.....	145
5.3.4 Competitive Experiment.....	146
5.3.5 Stoichiometry and Limit of Detection (LOD)	147
5.3.6 Fluorescence Lifetime	148
5.3.7 Binding Mode of L6 with Hg ²⁺ ion.....	149
5.3.8 pH Selection	150
5.3.9 Reversibility Studies Applied as Logic Circuit Devices	151
5.4 Biological Application of Ligand-Silver Complex	152
5.5 Conclusion.....	153
5.6 Reference.....	159





Chapter 1
GENERAL INTRODUCTION





1.1 Introduction

Metal ions owing to their indispensable importance in different aspects of life [1], there is a great deal of significance for their detection by the scientific community working in different fields of study such as chemical-biology, biochemistry, environmental science and chemistry [2]. Metal ions have been extensively identified and classified into two main categories that attract a special interest of researchers; the first group is biologically essential metal cations, including Ca^{2+} , K^+ , Na^+ , Fe^{2+} , Zn^{2+} , Cu^{2+} , etc. which play important signaling roles in our biological systems. To guarantee their normal biochemical functions, detection of their concentrations level and maintaining within an appropriate range is very crucial. The other group is biologically toxic, such as Hg^{2+} , Cd^{2+} , Cr^{3+} , As^+ , and Pb^{2+} which are toxic pollutants in the environment [3]. Consequently, the development of effective detection system for monitoring their toxic effect is very important as well [4–7].

Among the various available cation detection methods, *viz* flame photometry, atomic absorption spectrometry [8], optical emission spectroscopy (OES) [9], ion sensitive electrodes, cyclic voltammetry, electron microprobe analysis, inductively-coupled plasma-mass spectrometry (ICP-MS) [10], Atomic fluorescence spectrometry, X-ray fluorescence spectrometry [11], etc., are expensive, and often require large samples size and specialized personnel to carry out the operational procedures [12]. On the other hand, the fluorescence based sensors, owing to their attractive reward *viz* robustness, high sensitivity, selectivity, rapidity, long lifetime, ease of measurement, relative low costs, non-destructive methodology and detection of metal ions in living cells, the fluorescence sensors offer unique advantages over other different detection methods [5,13,14] and have been considered as an ultimate tool for monitoring trace amounts of toxic cations and anions. In this regard, design and synthesis of novel fluorescent sensors with improved performance are becoming very active research area in both organic and analytical chemistry and many fluorescent sensors have been synthesized and successfully used. This chapter focuses on over viewing current developments in design, synthesis and application of fluorescent sensors for mercury ion sensing based on different approaches.

1.2 Fluorescence Sensing

Fluorescence is the property of some molecules which can absorb a higher energy radiation at shorter wavelength and excited to high energy level and then re-emit radiation (fluorescence emission) of lower energy at longer wavelength upon relaxation from the excited state on nano seconds time scale. The change in absorbed and emitted radiation wavelength is called stokes shift [15].

Why fluorescence?

Fluorescence based detection is more selective and sensitive than absorption based counterpart. This is because fluorescence measurement is done directly without comparison with reference beam which is relative to dark background, while, absorption is calculated as the difference in light intensity pass through reference and sample [16].

Fluorescent sensors are molecular receptors that transform molecular interaction into analytically useful signals upon specific host-guests binding system. A typical fluorescence sensor contains a recognition site or receptor connected to signal unit or fluorophore which is the functional group responsible for emitting fluorescence which translates the recognition event into fluorescence signal. The basic requirements for fluorescent sensor are; strong affinity and selective binding of the receptor towards the target analyte, sensitive signal recognition unit to the photophysical change in the sensor on analyte binding and stable to environmental interference [17].

Binding of analyte changes the fluorescence nature of the fluorophore; this can accomplished in two ways: by increasing or decreasing the quantum efficiency “Turn On” or “Turn Off ” fluorescence, intensity based fluorophores; or by changing the spectral features, shifting emission wavelengths, dual emission in ratiometric fluorophores.

1.3 Some Common Photophysical Mechanisms for Fluorescence Sensing

The detection of the analyte by fluorescent sensors is based on the change of the photophysical properties of the sensor on the analyte binding to the receptor unit (*via* host-guest interaction) (Figure 1.1) that exhibit a change in emission profile of the fluorophore which can be either “Turn On” or “Turn Off” or both in the case of ratiometric. This phenomenon is guided by a few photophysical interaction mechanisms such as photoinduced electron transfer (PET), intermolecular charge transfer (ICT), fluorescence resonance energy transfer (FRET), excited state intermolecular proton transfer (ESIPT), chelation enhanced fluorescence emission (CHEF) or chelation enhanced quenching (CHEQ), excimer formation, and aggregation-induced emission (AIE) /aggregation-caused quenching (ACQ). This different fluorescence sensing mechanisms with some examples of recently reported Hg²⁺ ion selective chemosensors are briefly discussed in this section.

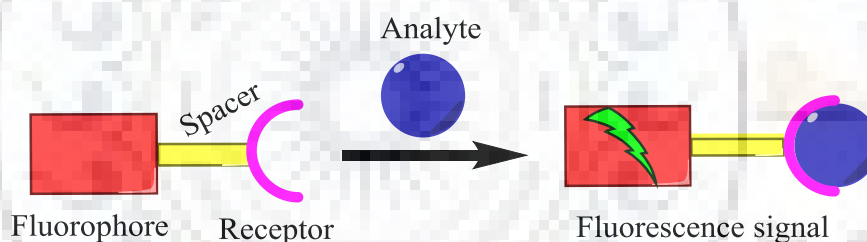


Figure 1.1 General host guest interaction of chemosensor and analyte.

1.3.1 Photoinduced Electron Transfer (PET)

Electron transfer processes in systems containing a donor (D) and acceptor (A) molecular units coupled by a rigid bridge can be easily taking place by applying some kind of fast perturbation energy. The electron transfer in a molecule having the donor and the acceptor linked by rigid aliphatic spacer *via* typical light excitation is called photoinduced electron transfer [18]. PET takes place by electron transfer from the lone pair electrons of N, O, and S of the receptor group to HOMO of the excited fluorophore [19], the photoexcitation localizes the acceptor and the HOMO of the donor atom which is at high energy than the HOMO of the acceptor transfers its electron to the acceptor’s HOMO, this electron transfer process opens PET which quenches the fluorescence of the sensor [20]. Fluorescence sensors that work by PET mechanism are widely accepted mechanism for their fluorescence “Turn-On” character

upon binding with analyte molecule *via* PET inhibition by coordination of the analyte to electron pair of donor atoms of the sensor (Figure 1.2) [21,22].

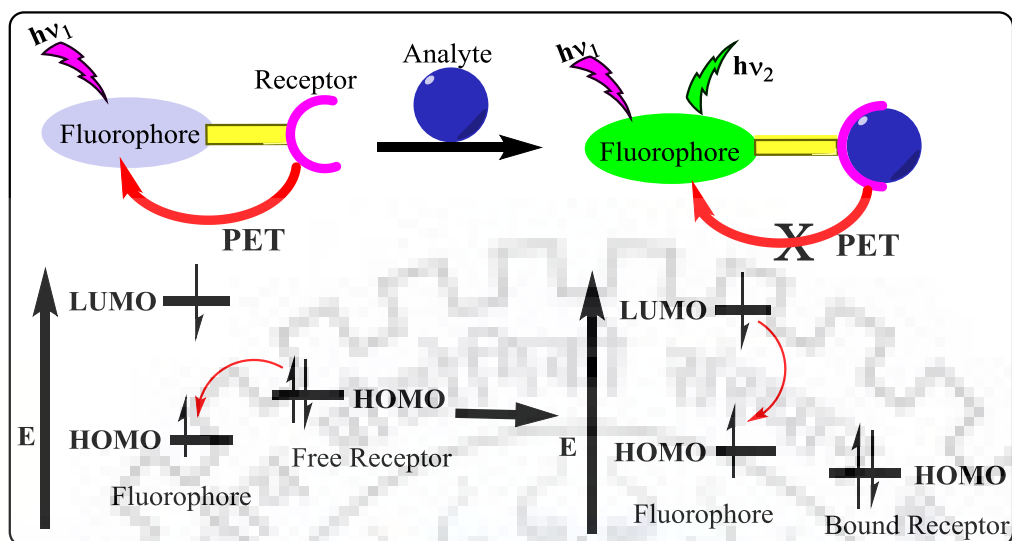


Figure 1.2 Representation of PET mechanism

Lee *et al.* reported PET based fluorescent chemosensor **1** (Figure 1.3) by combining of 2-aminoethyl piperazine receptor and 4-chloro-7-nitrobenz-2-oxa-1,3-diazole fluorophore [19]. Addition of Hg^{2+} ion to chemosensor **1** enhances the fluorescence of the sensor at 542 nm *via* PET inhibition upon Hg^{2+} binding to 2-aminoethyl piperidine. Recently in 2018, Zhoul *et al.* reported a new fluorescent chemosensor **2** (Figure 1.3) based on the BODIPY fluorophore containing carboxyl-thiol as Hg^{2+} receptor [23] for the detection of Hg^{2+} ion in aqueous media. Hg^{2+} binding to chemosensor show “Turn On” fluorescence at 581 nm with about a 630-fold enhancement *via* PET inhibition.

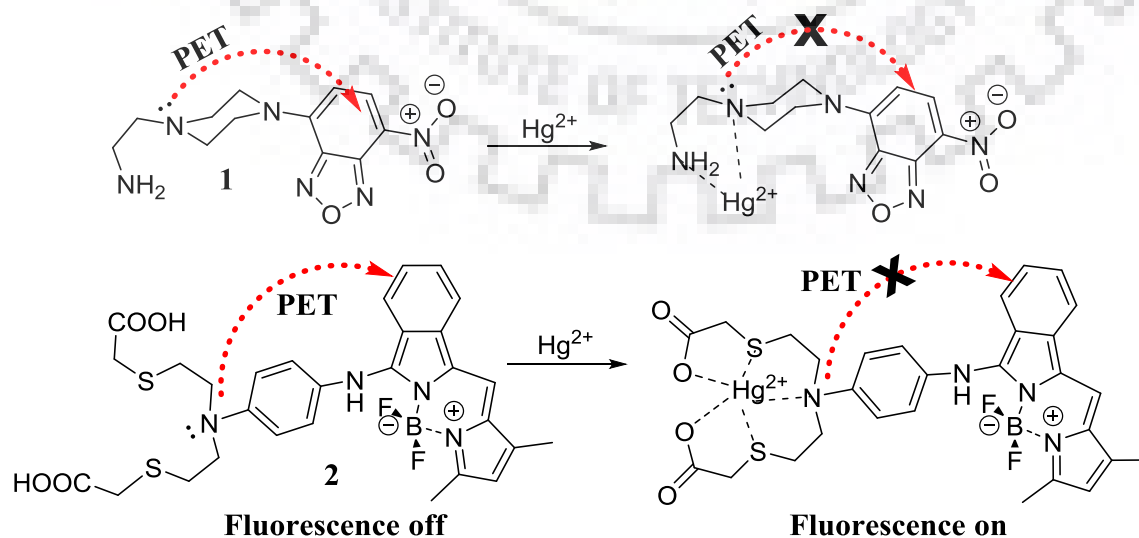


Figure 1.3 PET based chemosensors for Hg^{2+} detection.

1.3.2 Intramolecular Charge Transfer (ICT)

Generally ICT based sensors are molecules containing electron donating linked with electron withdrawing groups by π -spacer, which allows the charge transfer in the excited state from the electron rich donor to the acceptor which accomplished by large stoke shift [24]. The presence of both donor and acceptor in one molecule at the two opposite ends of the spacer results in ICT. Due to their delocalized π -system conjugated organic compounds are considered to be a good bridge for ICT to form donor- π -acceptor (D- π -A) system. The degree of ICT process depends on the donor and acceptor strength, as well as the length of the π system spacer blend the two groups [25]. D- π -A type molecules exhibit large dipole moment ($\Delta\mu$) changes upon photoexcitation which promotes the formation of polaron pairs, the predecessor for charge carriers which causes large stoke shift due to a photoinduced ICT process [26,27]. The binding of analyte with the donor species decreases the electron donating ability of the fluorophore and it causes blue shift, while the analyte binding with the acceptor group increases the electron withdrawing capability of the acceptor moiety and develops a red shift in both absorption and fluorescence spectra of the sensor (Figure 1.4) [28].

Goswami *et al.* [29] reported chromen-2-one derivative containing 7-(diethylamino)-3-(pyrimidin-4-yl)-2H-chromen-2-one chemosensor **3** (Figure 1.5) for Hg^{2+} ion detection in mixed aqueous media. Which shows chelation enhanced quenching of fluorescence (CHEQ) at 509 nm *via* photoinduced electron transfer (PET) from electron lone pairs of nitrogen and simultaneously, 'push-pull' induced ICT between coumarin and pyrimidine moiety upon binding with Hg^{2+} it exhibits red shift around 80 nm in absorption with naked eye color change from green to red, and a new band centered at 575 nm with fluorescence color change from yellowish green to light orange in Hg^{2+} binding. Other ICT based fluorescent chemosensor **4** (Figure 1.5) with strong push-pull system containing aniline nitrogen as electron donor and carbonyl and benzothiazolyl as electron acceptors for Hg^{2+} ion detection was reported by Wang *et al.* in 2006. Addition of Hg^{2+} impose blue shift in both emission and absorption, binding of Hg^{2+} to the receptors responded ratiometrical by blue shift of around 100 nm from 567 to 475 nm [30]. Recently in 2018, Rani *et al.* reported fluorescence Turn Off Hg^{2+} and pyrophosphate ion chemosensor **5** (Figure 1.5) by conjugating of 1H-phenanthro-[9,10d]imidazole as electron donor and anthraquinone as electron acceptor units through the π -system to get push-pull based ICT phenomenon in $\text{H}_2\text{O}/\text{CH}_3\text{CN}$ (1:9; v/v) solution [31].

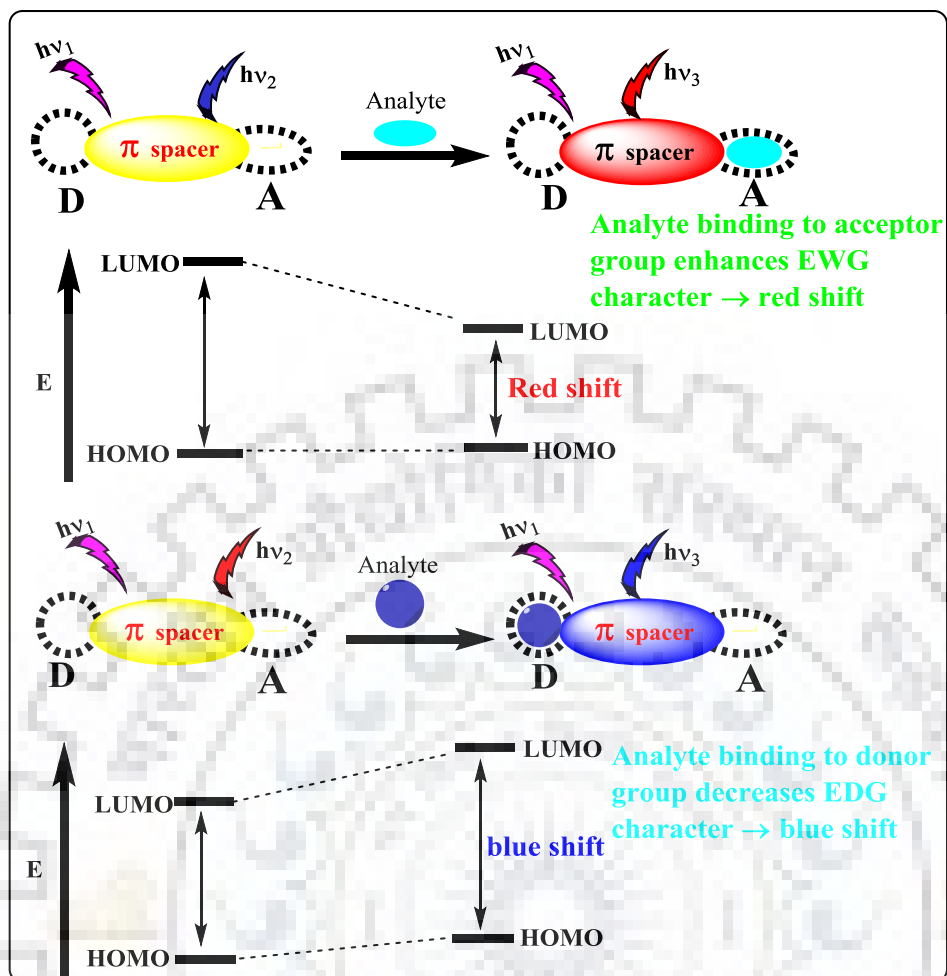


Figure 1.4 Representation of ICT mechanisms

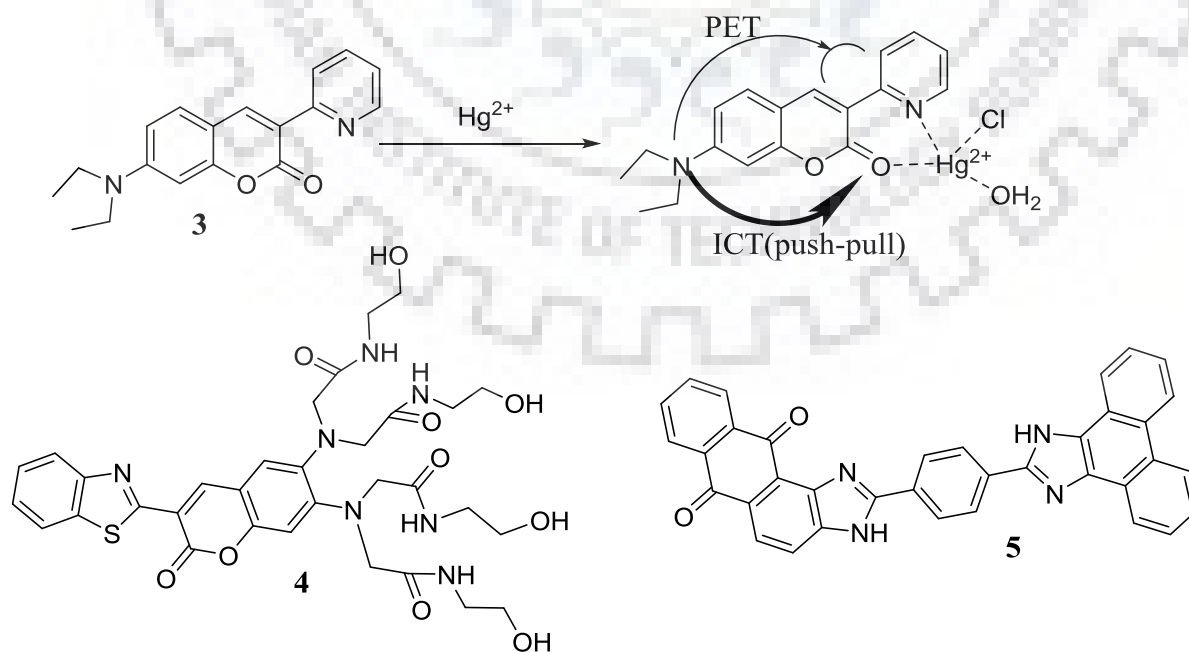


Figure 1.5 ICT based chemosensors for Hg^{2+} sensing

1.3.3 Fluorescence Resonance Energy Transfer (FRET)

FRET are fluorescent sensors based on a distance dependent radiationless energy transfer from high energy excited state donor molecule to low energy ground state acceptor molecule. The term “Resonance Energy Transfer” refers to intermolecular energy transfer of dipolar coupling of emission of donor moiety to the excitation of acceptor moiety [32]. The emission energy of the donor overlaps with the absorption spectrum of the acceptor molecule, the acceptor may be a fluorescent or non-fluorescent molecule (Figure 1.6). If the acceptor is a fluorophore it absorbs the emission of high energy and excited state donor group and gets excited and emits the energy radiatively upon relaxation to its ground state, it is turn on fluorescence. Meanwhile, non-fluorescent acceptor imposes quenching [33]. The rate of energy transfer is strongly dependent on degree of spectral overlap, relative orientation of the transition dipoles, and donor-acceptor proximity [34,35].

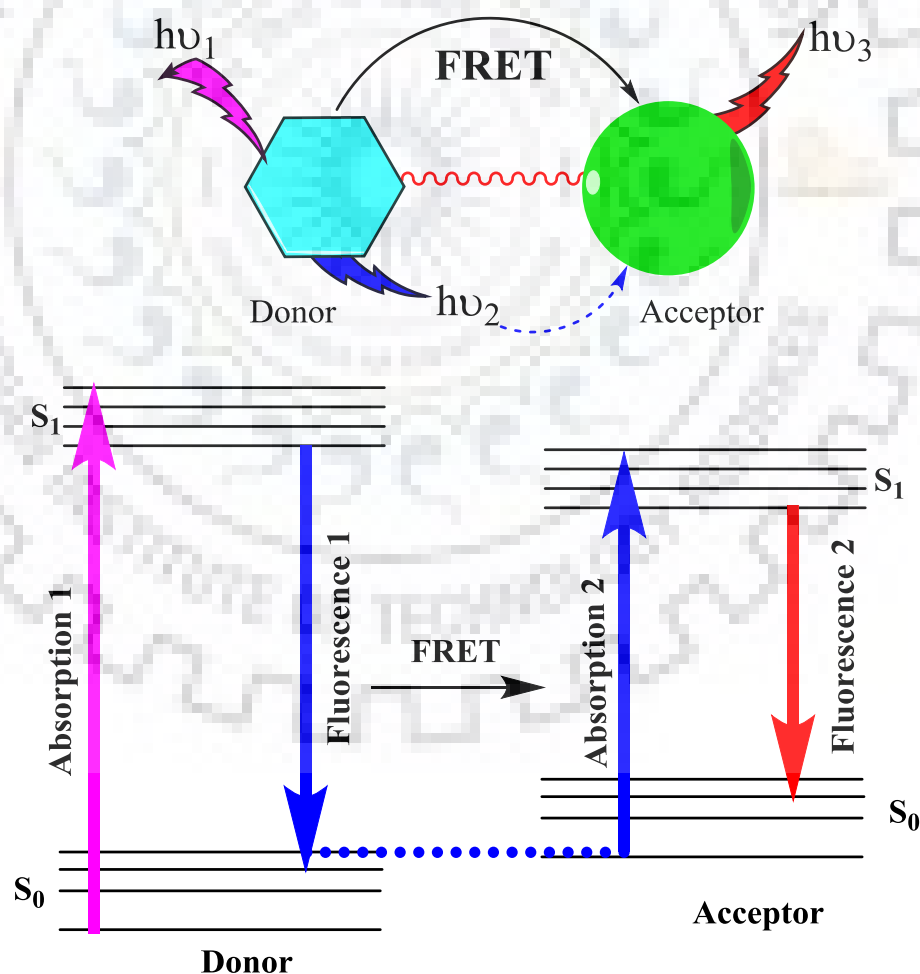


Figure 1.6 Representation of FRET mechanism

Liu *et al.*, reported a ratiometric OFF/ON-type FRET-based fluorescent sensor **6** (Figure 1.7) for Hg^{2+} ion detection using 1,8-naphthalimide as energy donor and rhodamine B as energy acceptor on the basis of spirolactam ring opening followed by mercury promoted desulfurization and intramolecular cyclization to oxadiazole which opens the FRET mechanism. The fluorescent chemosensor with weak band centered at 540 nm 1,8 naphthalimide exhibited strong rhodamine B emission centered at 585 nm upon Hg^{2+} ion addition [36]. Similarly Xu *et al.*, reported another ratiometric sensor **7** (Figure 1.7) containing naphthalimide moiety donor and Rhodamine B acceptor conjugated by ethylenediamine for selective Hg^{2+} detection based on FRET mechanism. Upon treatment of the sensor with Hg^{2+} resulted quenching in the characteristic emission band naphthalimide moiety at 381 nm and new strong emission appeared at 585 nm which increases with Hg^{2+} concentration attributed to FRET mechanism between the naphthalimide donor moiety and the rhodamine acceptor moiety [37].

Two Chemosensor containing pyrido[1,2- a]benzimidazole in sensor **8** [38] and imidazo[1,5- a]pyridine in sensor **9** [39] as energy donors linked with rhodamine energy acceptor, by piperazine for Hg^{2+} detection based on FERT was reported by Ge *et al.* in 2017 (Figure 1.7). Upon addition of Hg^{2+} ions, the imidazo[1,5-a]pyridine emission of **9** centered at 466 nm and the pyrido[1,2-a]benzimidazole of **8** centered at 464 nm gradually quenched and a new emission corresponding to rhodamine ring-opened appears at 584 nm and gradually becomes prominent. The simultaneous “off-on” mechanism of the two fluorescence bands suggested that the structure transformation into open-ring structure *via* Hg^{2+} induced spirolactam ring opening which favours FRET from the donors to ring-opened rhodamine [38,39]. Petdum *et al.* in 2018 developed FRET-based “Turn-On” chemosensor **10** (Figure 1.7) comprising [5]helicene energy donor and rhodamine 6G energy acceptor connected by a hydrazide moiety for selective detection of Hg^{2+} ion. The sensor showed excellent selectivity towards Hg^{2+} through Hg^{2+} ion induced ring opening which allows the FRET process, indicated by a new absorbance centered at 528 nm and Turn On emission at 549 nm, which are characteristic of ring opened rhodamine 6G [40]. Most of the reported FRET-based chemosensors for Hg^{2+} ions sensing used the rhodamine acceptor this is due to the long range absorption fluorescence emission of rhodamine upon Hg- induced spirolactam ring opening.

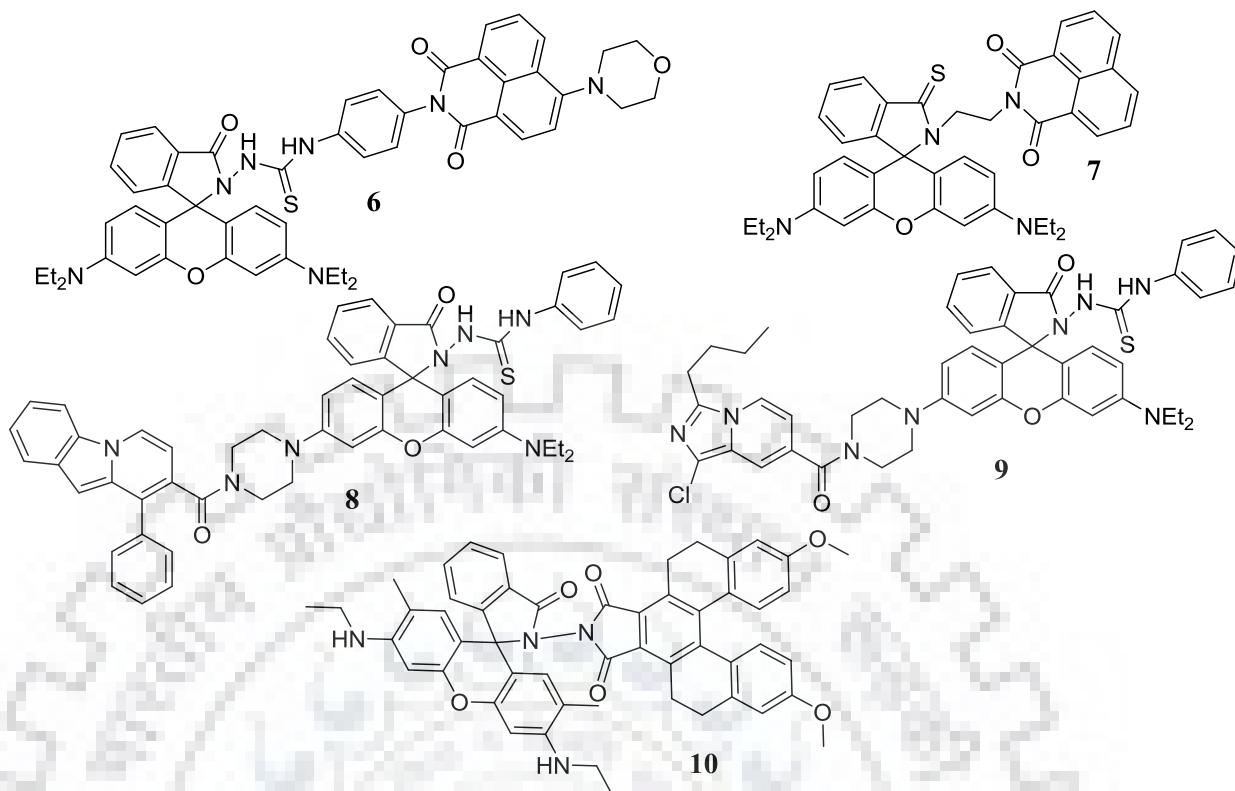


Figure 1.7 FERT based chemosensors for Hg^{2+} sensing

1.3.4 Excited State Intramolecular Proton Transfer (ESIPT)

ESIPET is a photo-induced enol–keto tautomerization of an excited state molecule [41]. Molecules could exhibit ESIPT *via* transfer of proton from hydroxyl or amino hydrogen bond donor to carbonyl oxygen (C=O) or pyridyl nitrogen (=N) hydrogen bond acceptor through a pre-existing intramolecular hydrogen bonding [42,43], this significantly changes the electronic structure and photophysical properties of the molecule in the excited state [44]. The excited enol is swept to its corresponding keto and back to its ground state enol form by emitting radiation [45]. Enol-keto-tautomerization is dependent in the donor-acceptor character and sensitive to acidity/basicity medium and nature of the solvent system. ESIPT fluorophores are ultrafast emitters with a large stokes shift dual emission compared to other fluorophores; this is due to an enormously fast enol to keto photo-tautomerization (Figure 1.8) [46]. Most ESIPT fluorophores are ESIPT Off and ESIPT On ratiometric fluorescent sensors and exhibit dual keto and enol emissions [47–49].

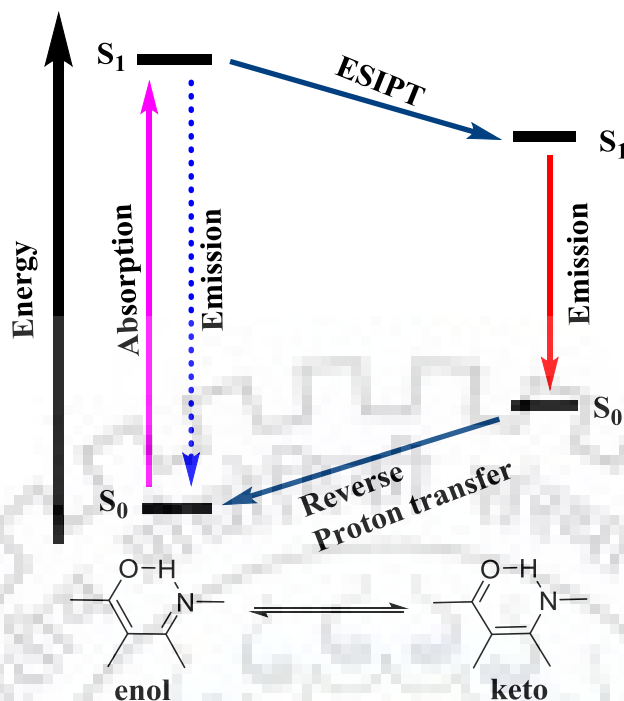


Figure 1.8 Representation of ESIPT mechanism

A ESIPT based ratiometric fluorescence sensor for detection of Hg^{2+} ion based on the Hg^{2+} -promoted hydrolysis of a vinyl ether derivative of 2-(benzothiazol-2-yl)phenol chemodosimeter **11 a-f** (Figure 1.9) in aqueous system was designed and reported by Santra *et al.*, 2011. Addition of Hg^{2+} results quenching of the exciting blue fluorescence and emerges cyan emission at high wavelength responsible for the keto form generated through the ESIPT after hydrolysis of the vinyl ether [50]. Kaur *et al.*, 2019 synthesized an effective chemosensor **12** (Figure 1.9) based on a naphthalene for Hg^{2+} and cysteine recognition in aqueous: CH_3CN (9:1 (v/v), pH 7.0 HEPES buffer). Addition of Hg^{2+} ion and cysteine displays “On-Off-On” emission at 454 nm due to ESIPT procedure, the ESIPT character of sensor terminated by presence of Hg^{2+} ions due to the equilibrium shift from keto to enol form quenches the emission and the high affinity of Hg^{2+} to sulfhydryl group releases the free sensor and the characteristic emission of the free chemosensor emerges back [51].

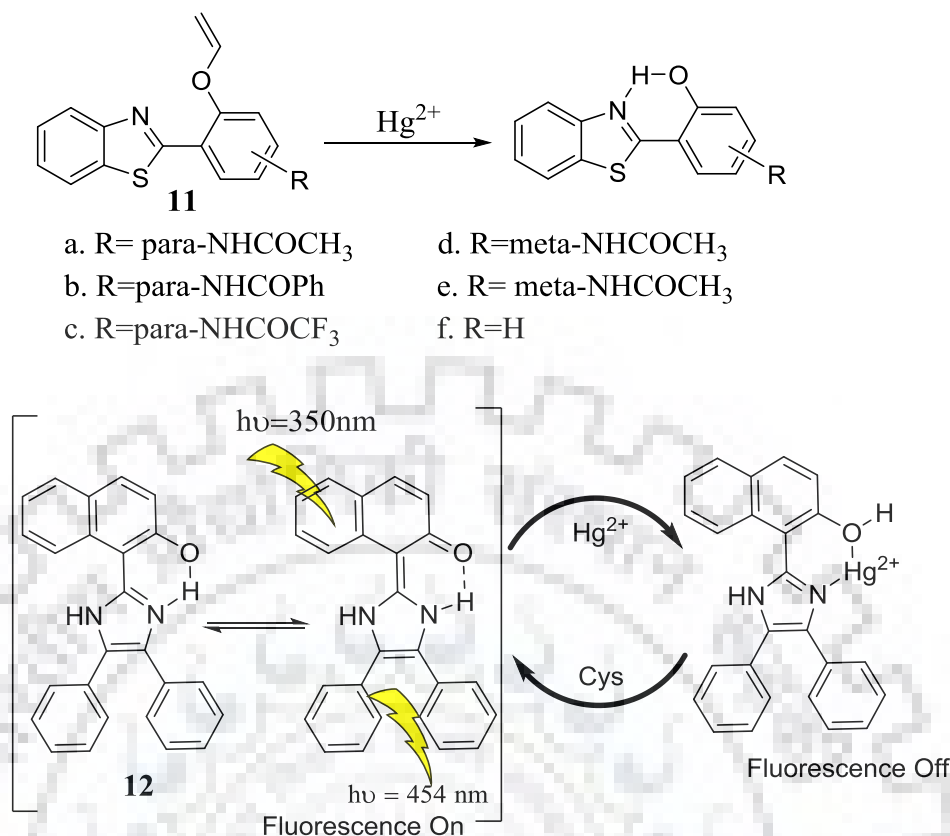


Figure 1.9 ESIP based fluorescence sensors for Hg²⁺ detection

1.3.5 Chelation Enhanced Fluorescence Emission (CHEF) and Chelation Enhanced Quenching (CHEQ)

The fluorescence response of a fluorophore to analyte species is dependent on how the analyte coordinated to the receptor group of the sensor and can be categorized as either “Turn-On” or “Turn-Off”. When the chelation process increases the conjugation of the ligand and thereby it switch-on the fluorescence nature of the sensor, which leads to turn on or fluorescence emission enhancement, this process is called CHEF. When the chelation of the analyte molecules to the receptor turned off the fluorescence nature of the fluorophore, it leads to chelation enhanced fluorescent quenching (CHEQ). Due to better sensitivity of turn on than quenching CHEF approach is most desirable for metal ion sensing. Owing to the chelation tendency of organic donor ligands to form chelated complex with metal ion and fluorescence turn on after the host-guest interaction, number of CHEF based chemosensors for metal ion are reported [52–54].

Ahamed and Ghosh in 2011 reported a selective sensing of Hg²⁺ ion by a chelation induced fluorescent enhancement (CHEF) in acetonitrile. The chemosensor **13** (Figure 1.10)

containing two tris(2-aminoethyl)amine based tripodal amide as chelating agent receptor and 2-quinolyl moiety as both fluorophore and chelating agent, the selective chelation of **13** towards Hg^{2+} induces fluorescence enhancement [55]. Lee *et al.*, 2012 reported CHEQ based fluorescence turn-off chemosensor **14** (Figure 1.10) for Hg^{2+} which strongly quenches the fluorescence of **14** in solution phase by forming covalent bonding to the fluorophore, it could be due to possible π complex formation of Hg^{2+} with the anthracenyl group [54].

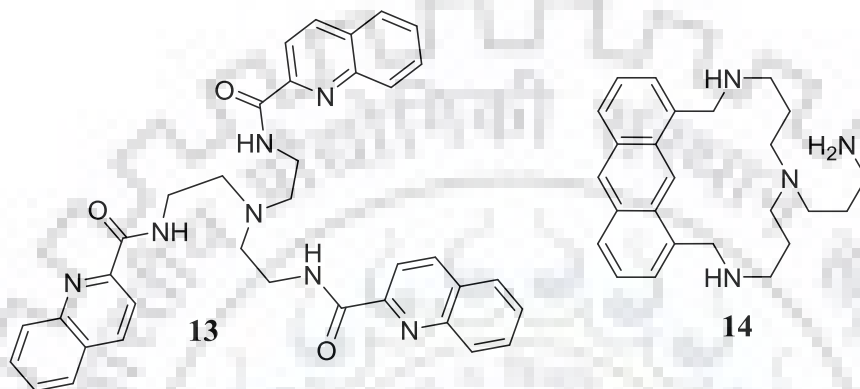


Figure 1.10 CHEF & CHEQ based chemosensors for Hg^{2+} sensing

1.3.6 Excimer/Exciplex Formation

An excimer/excimer is excited state dimer species which are monomers in the ground electronic state; this is due to resonance interactions of excited state molecules with neighbor ground state molecules. The excimer has broad red-shifted fluorescence emission that appears slowly at longer wavelengths than their monomers [56,57] with longer decay time due to the formation of the excimers *via* diffusion of ground state monomer and excited monomer after excitation [58–60]. Excimeric emissions are identified by their two characteristic fluorescence emissions varying with concentration, in concentrated solution, the lower energy long wavelength excimer emission enhanced while the high energy short wavelength monomeric emission is quenched [61]. This is also known to give “ratiometric type of sensors” because the switch between monomer and excimer emission intensity provides a quantitative magnitude of ions present in solution.

Shellaiah *et al.* reported a novel pyrene Schiff base derivative fluorescent chemosensor **15** (Figure 1.11), containing free thiol receptor for Hg^{2+} ion detection, showed fluorescence Turn-On response to Hg^{2+} ions, *via* chelation enhanced fluorescence (CHEF) through excimer formation in $\text{DMSO:H}_2\text{O}$ ($v/v=7/3$) at pH 7.0 Hg^{2+} binds to free thiol receptor and bring pyrene moiety of sensor close together that can encapsulate to form excimer [62]. Razi *et al.*

reported a novel pyrene based derivative **16** (Figure 1.11), having monomer and excimer emissions at 393 nm and 506 nm in the absence and presence of Hg^{2+} ion respectively. Hg^{2+} ion binds to the hydroxyl and diamine receptors and bring pyrene moiety of sensor close together that can encapsulate to form excimer in phosphate buffer [63]. Recently in 2018, Puangsamlee *et al.* developed another pyrene derivative **17** (Figure 1.11) having two pyrenylacetamide moieties covalently bound to 2-[4-(2-aminoethylsulfanyl)butylsulfanyl]ethanamine receptor based sensor, **17** for Hg^{2+} and Cu^{2+} ions sensing *via* intramolecular excimer formation [64].

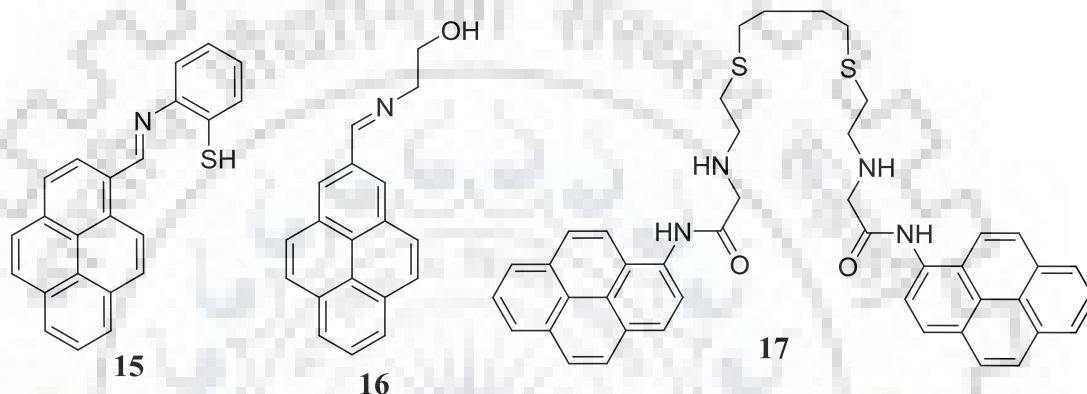


Figure 1.11 Excimer based chemosensors for Hg^{2+} sensing

1.3.7 Aggregation-Induced Emission (AIE)/Aggregation-Caused Quenching (ACQ)

Most organic fluorophores with large delocalized π -conjugated units are strong emitters in diluted solution, but weak or non-fluorescent in high concentration in aggregate state due to aggregation caused quenching (ACQ) effect. This quenching problem has limited the practical application of organic fluorophores to some level. In contrary to the ACQ effect, aggregation induced emission is a novel property of brilliant fluorophores that goes the opposite way, they are weakly or non-fluorescent in diluted solution while exhibiting bright fluorescence upon aggregate formation. This distinctive photophysical property is correlated with a restriction of intramolecular rotation (RIR) mechanism which closes the non-radiative relaxation path and opens radiative pathway [65–68]. Because of their practical applicability in organic electronics, chemical sensing, and fluorescence cell imaging as aggregates or solid films AIE active fluorophores have garnered a significant attention [69,70].

AIE based fluorescent chemosensor **18** (Figure 1.12) for the detection of Hg^{2+} ion in aqueous medium was reported by Neupane *et al.* on the basis of peptide receptor and tetraphenylethylene fluorophore [71]. The peptide receptor selective bound Hg^{2+} ion and give “Off-On” response *via* metal induced aggregation fluorescence enhancement at 470 nm and bring 30 fold enhancements with increasing Hg^{2+} ion concentration. Similarly, Chatterjee *et al.* reported AIE active tetraphenylethylene-boronic acid chemodosimeter **19** (Figure 1.12) chemodosimeter Turn-On sensor *via* Hg-promoted trans-metalation reaction for detection of both inorganic and organic mercury ions species in aqueous solution [72]. Shyamal *et al.* reported AIE active fluorescent sensor 1-(Anthracen-2-yliminomethyl)-naphthalen-2-ol chemosensor **20** (Figure 1.12) for Hg^{2+} *via* disaggregation of sensor in H_2O -THF mixture [73].

Ma *et al.* in 2014 developed a Turn-On fluorescence chemosensor **21** (Figure 1.12) which contains 9,10-distyrylanthracene fluorophore and thymine Hg^{2+} ion receptor groups for Hg^{2+} ion detection *via* thymine- Hg^{2+} -thymine complex based on AIE feature. The AIE active chemosensor **21** shows further fluorescence emission enhancement with red shift from 501 to 521 nm up on chelation with Hg^{2+} ion in 3:2 CH_3CN - H_2O solutions [74]. Similarly in 2019, He *et al.* reported AIE active o-phthalimide based selective turn on fluorescence chemosensor **22** (Figure 1.12) for selective Hg^{2+} detection on the basis of efficient binding of two thymine bases (T) with Hg^{2+} to form a stable T-Hg-T complex aqueous solution.

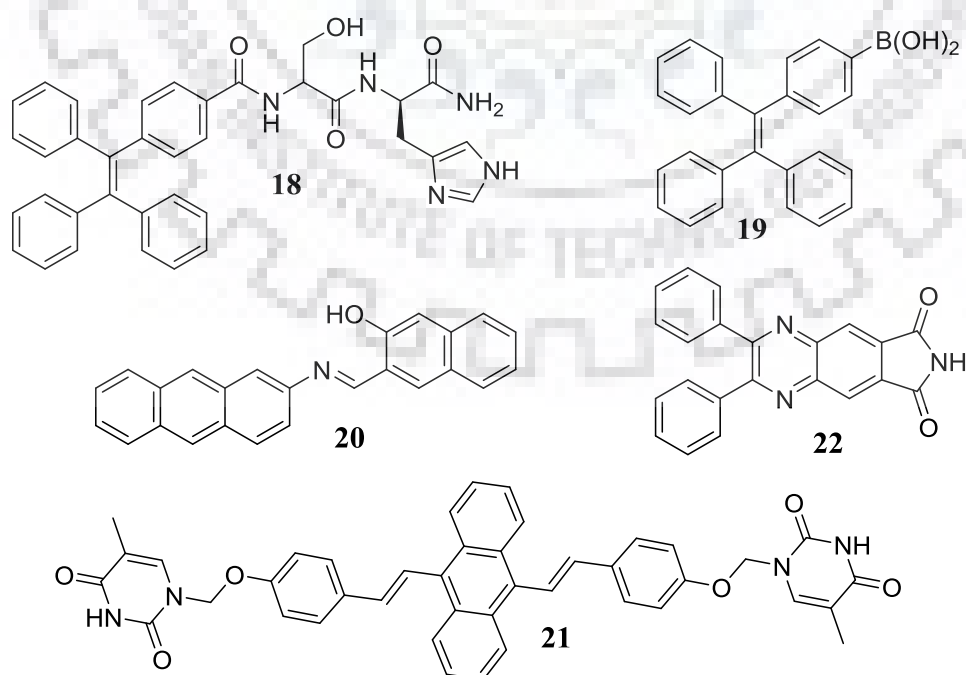


Figure 1.12 AIE & ACQ based fluorescence sensors for Hg^{2+} sensing

1.4 Importance of Mercury ion (Hg^{2+}) Detection

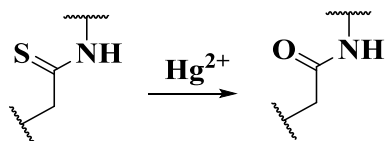
Mercury is a heavy metal that is more painstaking threat to human health and the environment wellbeing. Once inorganic mercury ions enter to the environment, microbes convert them into organic mercury mostly the neurotoxin methyl mercury which can easily pass through the biological membranes [75,76]. Due to its membrane permeability and high affinity to thiol group of proteins and enzymes [77,78], exposure to mercury ion (Hg^{2+}) can destroy human central nervous system, endocrine system and various cognitive and motor disorders and leads to Minamata disease even in very low-dose, especially for children [79–84]. As one of the most toxic heavy metals [85,86], Hg^{2+} has become a focal point for its rigorous terrorization and its prolonged effects to environment and biological systems [78,87–89] and lots of efforts have been engaged to develop and design fluorescent sensors specific for Hg^{2+} determination [88,90].

Fluorescent sensors follow either selective host-guest binding interaction or specific chemical reaction and impose fluorescence properties change in the sensor in re-organization of target analyte. Fluorescent sensors that are governed by reversible none covalent binding between the receptor molecules and analyte species are known as a chemosensor. While, those undertake a specific irreversible chemical reaction between sensor molecule and analyte are called chemodosimeters [46,91]. Based on their recognition mechanisms, Hg^{2+} sensors can be classified into two categories as reaction based and coordination based Hg^{2+} sensors.

1.5 Reaction Based Hg^{2+} Sensors

Reaction based fluorescence sensors which undergo specific irreversible chemical reaction between sensor molecule and analyte species, induce a fluorescence or/and color change in the signal unit are called chemodosimeters [92,93]. The photophysical character of chemodosimeters molecule changes due to the chemical reaction which makes the detection reliable and easier [91]. Owing to their high sensitivity and specificity, chemodosimeter has been getting much attention in fluorescence sensing and bio-imaging research field [94,95]. Reaction based Hg^{2+} sensors are very attractive for selective and sensitive detection of Hg^{2+} ion, the development of Hg^{2+} ion selective chemodosimeters are generally based on Hg^{2+} promoted desulfurization reactions, such as cyclization, hydrolysis, and elimination of thioether [95,96], Hg^{2+} mediated hydration of alkynes to ketones and hydrolysis of the vinyl and alkynes ether [97,98] and Hg^{2+} mediated rhodamine spiro-systems ring opening [99].

1.5.1 Hg²⁺ Detection via Hg²⁺-Promoted Desulfurisation of Thioamide into Amide



In 1992 the first chemodosimeter for Hg²⁺ sensing was reported by Chae and Czarnik this chemodosimeter **23** (Figure 1.13) was used for Hg²⁺ detection via desulfurisation reaction of thioamide group into amide group, which causes turn on fluorescence, due to the desulfurisation of thioamide group which efficiently quenches the fluorescence of the fluorophore via photoinduced electron transfer followed by oxidation to amide group which have no PET effect. The chemodosimeter was selective to Hg²⁺ and Ag⁺ [100]. And in 2006, Song *et al.* reported Hg²⁺ ion selective Off-On dosimeter **24** (Figure 1.13) on the basis of irreversible desulfurization of thioamide into an amide counterpart in similar to Czarink group's work. Rapid recognition with low detection limit of 5.4x10⁻⁷ M and little interferences by Cd²⁺ and Ag⁺ only 10 and 13% respectively among the tested metal ions [101].

Thiocoumarins based Hg²⁺ selective chromogenic and fluorogenic chemodosimeter system **25** (Figure 1.13) based on conversion of thiocoumarin to coumarin by selective Hg²⁺ ion promoted desulfurization reaction was developed by Choi *et al.* in 2009, chemodosimeter **25** was highly selective to Hg²⁺ ion in the presence of potential interfering ions with low detection limit of 8.9x10⁻⁷ M [102]. Zhang *et al.* in 2011 reported the synthesis and application of another chemodosimeter **26** (Figure 1.13) based on oxazine-thione, for selective and sensitive Hg²⁺ ion sensing. The desulfurization reaction of carbonyl sulfide takes advantage of the high affinity of Hg²⁺ for sulphur shows dramatic color change and exhibiting a large blue shift of 100 nm in its absorption spectra and a selective enhancement in fluorescence intensity upon addition of Hg²⁺ ions [103].

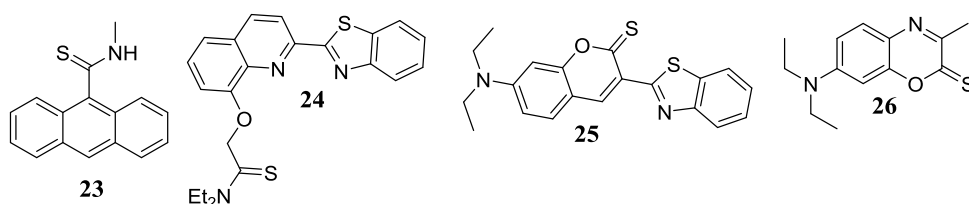
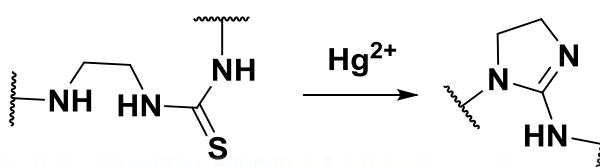


Figure 1.13 Hg²⁺ selective chemodosimeter based on Hg²⁺ triggered desulfurization reaction.

1.5.2 Hg²⁺ Detection via Hg²⁺ Promoted Cyclic Guanylation Thiourea to Imidazoline



Liu and Tian in 2005, reported the first ratiometric fluorescent chemodosimeter **27** (Figure 1.14) for selective and sensitive detection of Hg²⁺ ion based on dehydrothiolazition reaction. Hg²⁺ promoted cyclic guanylation of thiourea to imidazoline moiety was come up with a suitable fluorometric and colorimetric sensing. The absorption spectra of **27** blue shifted from 435 nm to 350 nm with an isosbestic point at 391 nm and the yellow–green fluorescence emission at 530 nm shifted to blue fluorescence at 475 nm an isoemissive point at 510nm [104]. Other Hg²⁺ selective fluorescent chemodosimeters **28** and **29** based on Mercury promoted intramolecular cyclic guanylation of thiourea to imidazoline was also reported in 2007. The Hg²⁺ ion induced ring opening of rhodamine spirolactam leads to cyclic guanylation of thiourea to imidazoline in chemodosimeter **28** (Figure 1.14)and azo-component containing chemodosimeters responsible for the Hg²⁺ ion induced desulfurization and cyclization in chemodosimeter **29** (Figure 1.14) by Lee *et al.* [105] and Wu *et al.* [96] respectively. Subsequently in the year 2009, Lee and his coworkers reported another fluorescent chemodosimeter **30** (Figure 1.14) with absorption wave length of 630 nm and emission at 652 nm for Hg²⁺ ion detection. The reaction of **30** with Hg²⁺ ion causes desulfurization cascade cyclization accompanied by blue shift in both absorption and emission with ratiometric fluorescence enhancement. The chemodosimeter **30** revealed dual absorptions at 592 nm and 630 nm and addition of Hg²⁺ ion induces blue shift to 546 and 583 nm and fluorescence enhancement with blue shift from 652 to 626 nm respectively [106]. A highly selective and sensitive Porphyrin fluorophore with thiourea reactive moiety chemodosimeter **31** (Figure 1.14) for Hg²⁺ ion detection in aqueous solution was synthesized by Lv *et al.* in 2017. Chemodosimeter **31** shows ratiometric response in absorption and fluorescence emission change upon addition of Hg²⁺ ion promoted cyclization to imidazoline in aqueous media induces bathochromic shift both in absorption from 413 nm to 425 nm and emission from 651 nm to 601 nm with isoemission point at 630 nm [107].

Recently in 2018, Singh *et al.* synthesized a multifunctional self-assembled dual-chemodosimeter Schiff base thiourea hybrid with *o*-phenylenediamine based dual

chemodosimeter **32** (Figure 1.14) was used for optical identification of Hg^{2+} , CN^- and $\text{Hg}(\text{CN})_2$ from each other. The chemodosimeter **32** undergoes desulfurization followed by guanylation reaction of the Schiff base thiourea hybrid to form benzimidazole. Addition of Hg^{2+} promotes Hg^{2+} assisted ESIPT phenomena (red shifted in the emission centered at 458nm to 510 nm and hyperchromic effect in absorption between 400 to 480 nm associated with fluorescence quenching at 510 nm. The flake like structure **32** undergoes analyte induced self-assembly to different arrangement, such as a bunch of nano rods with Hg^{2+} , segregated nano-rods with curvy ends with CN^- and spherical with $\text{Hg}(\text{CN})_2$ ion pair [108].

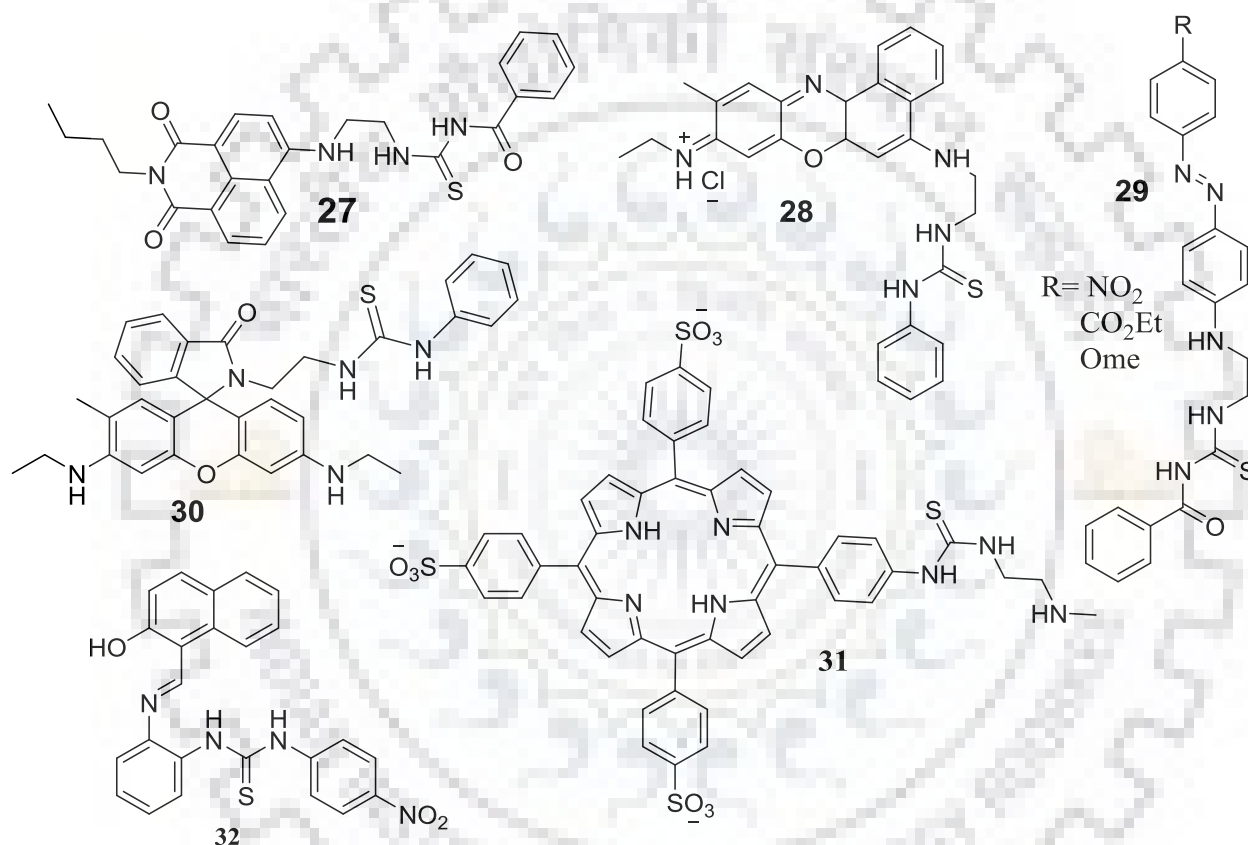
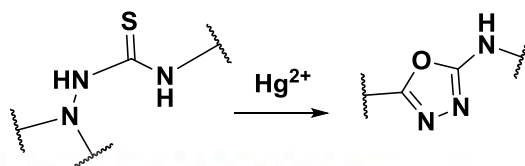


Figure 1.14 Hg^{2+} ion selective chemodosimeters based on Hg^{2+} ion triggered intermolecular cyclic guanylation of thiourea to imidazoline.

1.5.3 Hg^{2+} Detection via Hg^{2+} -Promoted Cyclization of Thiosemicarbazide to Oxadiazole



Mercury promoted desulfurization and intramolecular cyclization reaction of thiosemicarbazide to 1,3,4-oxadiazole of rhodamine derivative fluorescent chemodosimeter with fluorophore conjugated with rhodamine B hydrazide by thiourea as spacer for selective Hg^{2+} ion detection were designed and synthesized by Yang *et al.* in 2005 (chemodosimeter **33**) and Shang *et al.* in 2008 (chemodosimeter **34**). Chemodosimeter **33** (Figure 1.15) showed 26-fold fluorescence enhancement and red shift from 553 to 557 nm in the presence of Hg^{2+} [109]. While, the dual colourimetric and ratiometric fluorescence chemodosimeter **34** (Figure 1.15) with absorption centered at 490 nm and green fluorescence at 520 nm showed a dual ratiometric response both in absorption and emission upon addition of Hg^{2+} ion accompanied by red shifting in absorption peak from 520 to 565 nm and in fluorescence from 520 to 591 nm respectively. This is due to mercury promoted desulfurization and intramolecular cyclization of thiosemicarbazide to 1,3,4-oxadiazole [110]. Another fluorescent chemodosimeter **35** (Figure 1.15) based on spirocyclic ring-opening of rhodamine-based dyes followed by mercury promoted desulfurization and intramolecular cyclization of thiosemicarbazide to 1,3,4-oxadiazole for selective recognition of Hg^{2+} have been reported by Liu *et al.* in 2013. The chemodosimeters **35** showed high sensitivity and selectivity Turn-On fluorescence to Hg^{2+} with color change which can be detected by naked-eye in aqueous media and it was applicable in monitoring the blood Hg^{2+} ions intoxicosis mice [111].

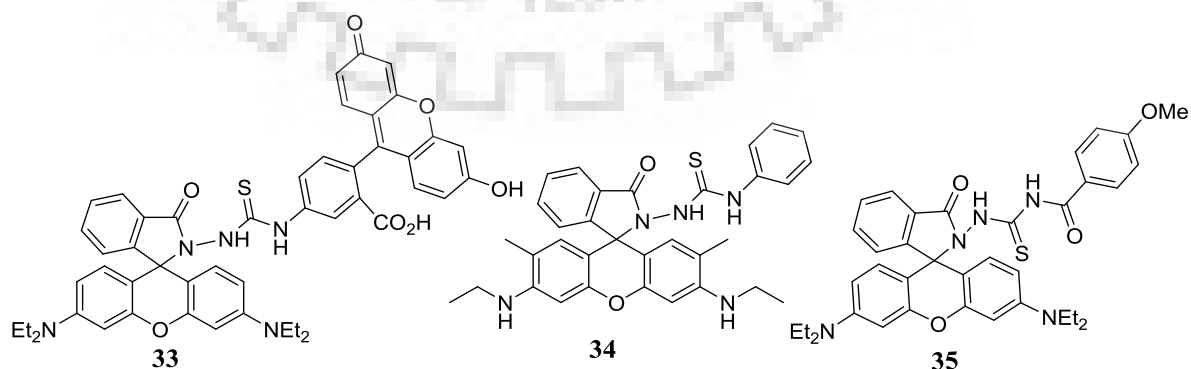
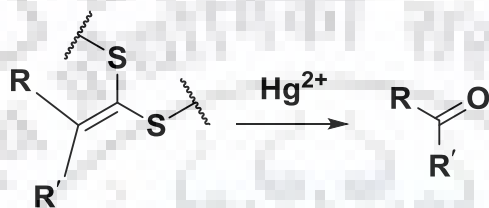


Figure 1.15 Hg^{2+} ion selective chemodosimeter based on Hg^{2+} triggered desulfurisation and intramolecular cyclization of thiosemicarbazide to 1,3,4-oxadiazole.

1.5.4 Hg^{2+} Detection via Hg^{2+} -Promoted Elimination of Thioether

Another important example of desulfurization reaction based fluorescence chemodosimeter are a dithioacetal/dithioketal, a mercapto protected aldehyde or ketone group which could be converted to the previous corresponding carbonyl derivatives by the selective Hg^{2+} promoted desulfurization (deprotection) reaction. Therefore, significant number of Hg^{2+} selective chemodosimeter based on the carbon–sulfur bond cleavage of dithioacetal/dithioketal to corresponding carbonyl derivatives were developed.



By taking the good performance of ratiometric sensors and the selective deprotection reaction of thioacetal into consideration Cheng *et al.* developed two new ratiometric fluorescent chemodosimeter **36a** and **36b** (Figure 1.16) towards Hg^{2+} and Ag^+ ions detection, using ICT photophysical mechanism, in which the fluorophore are conjugated phenyl rings and aldehyde electron acceptor group. Both probes showed selective recognition of Hg^{2+} and Ag^+ among the tested metal ions, this is because of the selective cleavage of thioacetals by Hg^{2+} and Ag^+ [112]. π -extended anthracene-bearing thioacetals **37** (Figure 1.16) was used by Chinna *et al.* in 2018 a Turn-On fluorescence chemodosimetric responses to Hg^{2+} ions via selective Hg^{2+} promoted deprotection/desulfurization reaction of thioacetal leads to formation of ICT based strong fluorescent formyl products [113].

Song *et al.* in 2013 reported as covalent assembly type fluorescent probe **38** (Figure 1.16) for Hg^{2+} detection with a new way of Hg^{2+} promoted cleavage of 1,3 dithiolane results Turn On fluorescence. Coordination one thiolane moieties with Hg^{2+} causes subsequently cleavage of the carbon–sulfur bond which consequently caused alkyl sulfonium ion which is highly electrophile and reacts the nucleophile *N,N*-dithylaniline group to re-aromatization followed by elimination of $\text{Hg}(\text{S}-\text{CH}_2\text{CH}_2-\text{S})$ complex and furnishes fluorescent pyronin B scaffold [114]. And in the year 2018, Pan *et al.* reported a novel thioacetal elimination based reaction coumarin chemodosimeter **39** (Figure 1.4) via the “covalent assembly” principle, which detected Hg^{2+} and CH_3Hg^+ with excellent selectivity and sensitivity. The desulfurization of 1,3-dithiolane to formyl group and the *ortho*-2-aminophenyl group plays key role in condensation to generate cyclic amine with larger conjugation than the probe though the Hg^{2+}

ion promoted desulfurization followed intramolecular condensation which results hetrocyclic product. Probe **39** exhibits absorption and emission maximum at 405 nm and 492 nm respectively. Meanwhile, upon addition of Hg^{2+} or MeHg^+ it shows good ratiometric character both in absorbance and fluorescence and after complete reaction with Hg^{2+} the absorbance and fluorescence shifts to 480 nm and 572 nm respectively. **39** shows detection limit of 27 nM and 5.8 mM for Hg^{2+} ion and CH_3Hg^+ respectively [115].

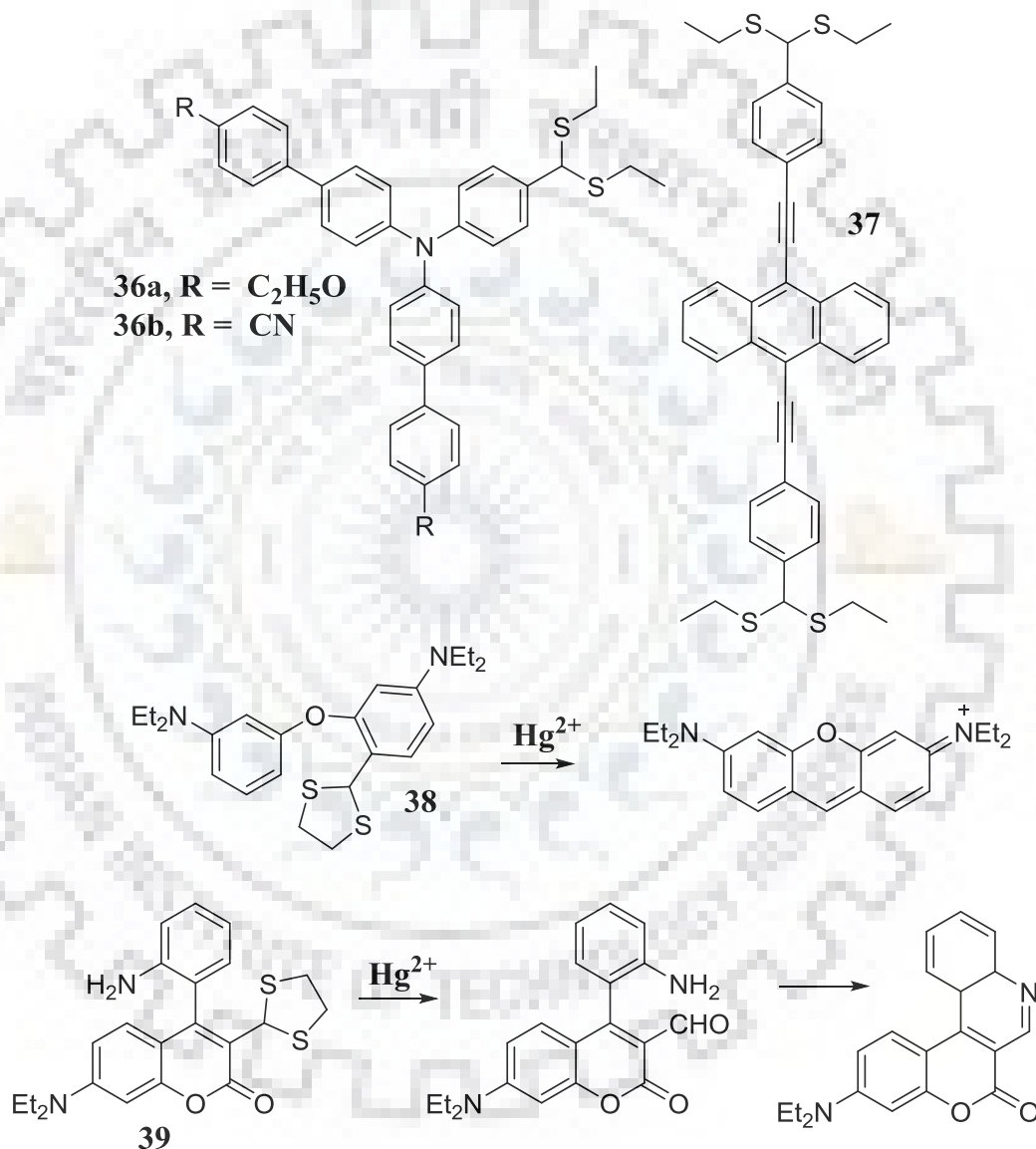


Figure 1.16 Hg^{2+} ion selective chemodosimeter based on Hg^{2+} triggered desulfurisation / deprotection reaction of dithioacetal/dithioacetal.

1.5.5 Hg²⁺ Detection via Hg²⁺- Promoted Hydration of Alkynes to Ketones

Hg²⁺ ion react with electron rich alkynes to undergo hydrolysis reaction to produce carbonyl moieties. The hydration of alkynes to give an enol in water could be promoted by Hg²⁺ ion, in which this enol form is tautomerizes into ketone is known as Kucherov reaction [116]. Formation of acetone by the hydrolysis of isopropenyl acetate promoted by Hg²⁺ ion through an oxymercuration–deoxymercuration mechanisms is one of the known examples [117]. Therefore, significant number of Hg²⁺ ion selective fluorescent sensors based on Hg²⁺ ion promote hydrolysis of vinyl ether and oxymercuration of an alkyne via π -electrophilicity of mercury ion was developed.

Having the alkynophilicity of Hg²⁺ ion into account, coumarin-based alkyne fluorescent chemodosimeter **40** (Figure 1.17) was developed for Hg²⁺ ions detection, via the Hg²⁺ promoted conversion of alkyne to ketone in water by Lee *et al.* in 2009. The Hg²⁺ promoted hydration of alkynes to ketones induces more electron-withdrawing carbonyl group which exhibits bathochromic shift in absorbance from 425 nm to 471 nm with isosbestic point at 450 nm and fluorescence intensity quenching [118]. Subsequently, in 2011 the same group tried to modify the Turn Off chemodosimeter **40** into ‘Turn On’ chemodosimeter **41** (Figure 1.17) by incorporating amide group into the coumarin-based alkyne. Interestingly, the chemodosimeter containing propargyl amide **41** was established a ratiometric result by cyclization of the propargyl amide to corresponding oxazole derivative on the presence of Hg²⁺, along with red shift from 427 nm to 475 nm and isosbestic point at 438 nm and ratiometric fluorescence emission with gradual quenching of at 469 nm, and fluorescence enhancement at 492 nm with an isoemissive point at 472 nm, which detects Hg²⁺ with LOD of 2.7 μ M [119]. Taking the advantage of thiophilicity and alkynophilicity of Hg²⁺ ion. Lin *et.al.* reported chemodosimeter **42** (Figure 1.17) containing both the thiol and alkyne moieties utilized for Hg²⁺ ion recognition. Reaction of Hg²⁺ with the alkyne group triggers a spirocyclic ring opening with a concomitant intramolecular attack by the thioamide sulphur to the alkyne functionality which directs to the thiazole ring formation with mercurated exocyclic double bond which undergoes further Hg²⁺ promoted hydrolysis to corresponding thiozole carbaldehyde with rapid fluorescence enhancement up to 140-fold at 566 nm and color change [120].

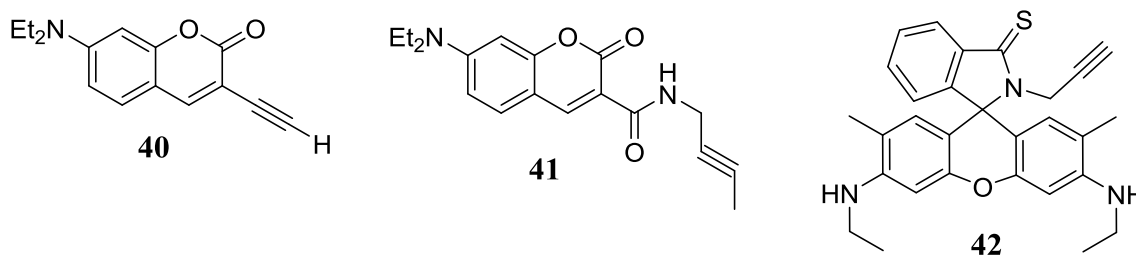


Figure 1.17 Hg²⁺ ion selective chemodosimeter based on Hg²⁺ ion promoted hydration of alkynes to ketones

1.5.6 Hg²⁺ Detection via Hg²⁺ ion Promoted Hydrolysis of Vinyl Ether and Isopropenyl Acetate

It is known that Hg²⁺ catalyzes hydration of alkynes to form the corresponding ketones. A sensitive and specific “Turn On” fluorogenic chemodosimeter **43** (Figure 1.18) for Hg²⁺ ion detection based on the Hg²⁺ promoted cleavage of the fluorescence-masking alkyl group have been developed by Song *et al.* in 2008. Reaction of Hg²⁺ with the alkynes of chemodosimeter **43** first leads to mercuriation reaction followed by hydrolysis/demercuriation, to produces the corresponding ketone which leads to 219 fold emission enhancements at 523 nm in aqueous and it was used for detection of Hg²⁺ ion in fish tissue in ppb level [121]. This mechanism has also been applied in designing chemodosimeter **44** (Figure 1.18) in 2011 by Ando and Koide for selective detection of Hg²⁺ ion. Vinyl-ether has also high affinity to Hg²⁺ ion and ultimately the hydrolysis reaction leads to the corresponding acetaldehyd and phenolate formation. consequently, non-fluorescent chemodosimeter **44** showed ‘Turn On’ fluorescence in the presence of Hg²⁺ at 515 nm, which was applicable for Hg²⁺ ion detection in dental and river water samples with LOD of lower than ppb level [122].

Similarly, naphthalimide derived selective chromogenic and ratiometric fluorometric chemodosimeter **45** (Figure 1.18) for Hg²⁺ ion detection via Hg²⁺ ion promoted hydrolysis of aryl vinyl was reported by Jiang *et al.* in 2014. The hydrolysis of aryl vinyl ether group produced highly fluorescent 4-hydroxynaphthalimide due to the strong donating ability of oxygen anion which opens ICT process, resulting bathochromic shift from 456 nm to 546 nm with isosbestic point at 506 nm accompanied by colorless to light yellow color [123].

Another fluorescent chemodosimeter **46** (Figure 1.18) contains 2-(1(p-tolyl)-phenothro[9,10-d]imidazol-2-yl)phenol as fluorophore scaffold and vinyl group recognition unit have been reported by Gu *et al.* in 2015. The Hg²⁺ ion induced cleavage of the fluorescence masking

vinyl group to results deprotection of OH group in the probe which opens excited state intramolecular proton transfer (ESIPT) that Turn On the fluorescence with shift from short wave length (380 nm) to long wave length (477 nm) with red shift of about 100 nm attributed to ratiometric detection of Hg^{2+} ion with LOD of 7.8 nM and fluorescence naked eye detection under long UV-light with color change from blue to green fluorescence [124].

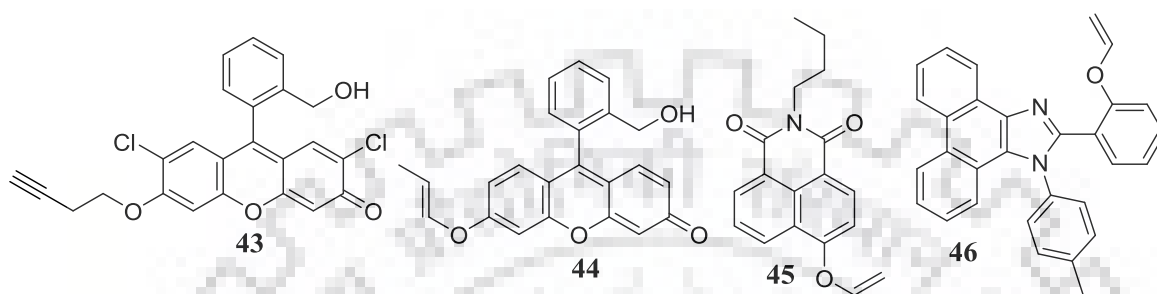


Figure 1.18 Hg^{2+} ion selective chemodosimeter based on Hg^{2+} ion promoted hydrolysis of vinyl ether and isopropenyl ether.

1.5.7 Hg^{2+} Promoted Spirolactam Hydrolysis Reaction

The Rhodamine spirolactam is non-fluorescent and colorless, binding of Hg^{2+} ion induces spirolactam ring-opening *via* Hg-O bond formation followed by Hg^{2+} promoted irreversible hydrolysis in the presence of water, which results an intense colored and high emission. Several Hg^{2+} chemodosimeters have been developed and reported based on this principle.

Du *et al.* in 2010 designed rhodamine B based chemodosimeter **47** (Figure 1.19), for selective Hg^{2+} ion sensing. The Hg^{2+} promoted ring opening of **47** *via* Hg-O bond formation followed by hydrolysis of hydrazide into carboxylic acid to release rhodamine B showed a clear “Turn On” fluorescence. Addition of Hg^{2+} ion to **47** solution enhances the fluorescence intensity at 579 nm significantly by over 370 fold and a new absorption peak emerged at around 554 nm. Chemodosimeter **47** was selective and sensitive to Hg^{2+} with LOD of 0.91 ppb [125]. Ni *et al.* in 2013 [126] and Zhang and Zhu in 2014 [94] designed rhodamine B Schiff bases based chemodosimeter **48** and **49** (Figure 1.19) by conjugation of Rhodamine B hydrazide with glyoxylic acid and glyoxal respectively, as selective and sensitive fluorogenic and chromogenic Hg^{2+} ion detectors. The coordination of Hg^{2+} to chemodosimeter **48** and **49** undergoes rhodamine-B spirolactam ring opening followed by rapid Hg^{2+} promoted hydrolysis of hydrazide to carboxylic acid functionality in aqueous system which transforms the colorless chemodosimeter into a pink colored accompanied by “Turn On” fluorescence. In the presence of Hg^{2+} ion **48** and **49** showed a new absorption maxima at 555 nm and 561 nm

and drastically enhanced “Turn On” emission intensity at 578 nm and 576 nm for **48** and **49** respectively, with distinct color change from colorless to pink which provided “naked eye” detection of Hg^{2+} ion.

Another rhodamine 6G derived chemodosimeter **50** (Figure 1.19), via Hg^{2+} promoted hydrolysis reaction of rhodamine spirolactam has been designed and developed by Bay *et al.* in 2019. The colorless and non-fluorescent chemodosimeter was turned into pink color and yellow fluorescent emitter at 558 nm due to selective Hg^{2+} promoted hydrolysis reaction of rhodamine spirolactam. The chemodosimeter was selective and sensitive to Hg^{2+} with LOD of $0.08 \mu\text{M}$ for colorimetric and $0.008 \mu\text{M}$ for fluorometric methods [127].

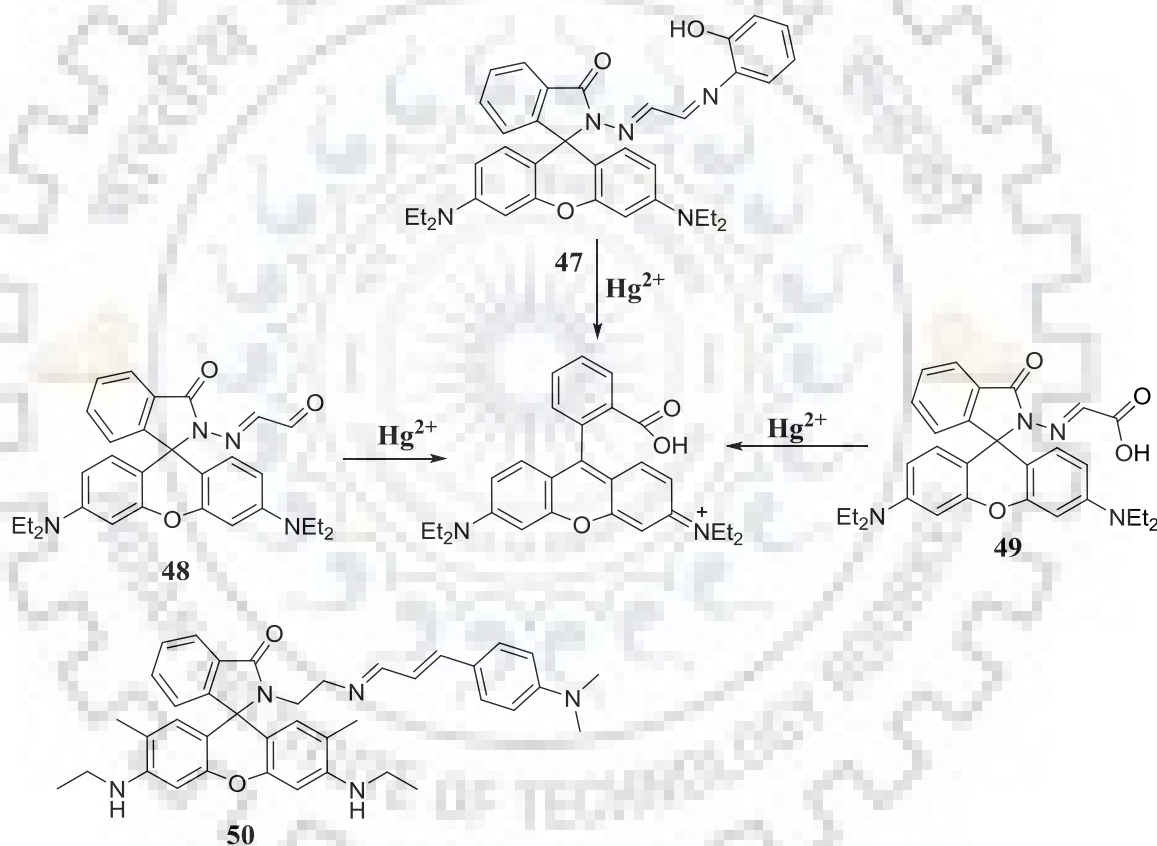


Figure 1.19 Hg^{2+} ion selective chemodosimeter based on Hg^{2+} promoted hydrolysis reaction of rhodamine spirolactam ring.

1.6 Coordination Based Hg²⁺ Sensors

In order to design fluorescent sensor for detection of analyte species, it is imperative to establish a fitting receptor moiety that selectively binds the analyte and change fluorescence properties of the fluorophore. This can be accomplished through careful selection of appropriate binding moiety and signal units. Metal-ligand coordination bonding, by its very nature, fulfils these criteria. Subsequently, integrating fluorescence signal unit with specific receptor moiety for a definite metal ion is common approach to design chemosensor for metal ion detection. Coordination of metal ions to the receptor will alter the photophysical properties of the fluorescence signal unit [128]. Hence, variety of sensors based on direct coordination of metal to ligand has been reported.

Alfonso *et al.* reported two ferrocene-based Heteroditopic receptors for selective detection of Hg²⁺ ion, containing two pyridine ring group as the binding moiety chemosensors **51** [129] and **52** [130] (Figure 1.20). The weak fluorescence at 507 nm of **51** shows 227 fold chelation-enhanced fluorescent (CHEF) towards Hg²⁺ accompanied by red shift of 28 nm with 1:1 stoichiometry detection limit 1.81 μM . While, addition of Hg²⁺ ion to **52** was accomplished by 165 fold fluorescence enhancement based on CHEF process and red-shifted from 512 nm to 544 nm.

Jonaghani and Zali-boeini in 2017 reported quinoline derived naphthothaizole fluorescence probe **53** for selective detection of Hg²⁺ ion in 1:1 of MeCN/water mixture and exhibited absorption maxima centered at 356 nm and emission at 433 nm. Upon Hg²⁺ ion addition a new absorption peak centered at 504 nm emerges with red shift of about 71 nm and observable quenching in the existing fluorescence band with LOD of 34.2 nM, additionally the sensor shows visual blue to green fluorescence color change under UV-light [131]. Other fluorescent chemosensor **54** (Figure 1.20) with anthracene core fluorescence signaling unit bridge by triazole to oxyquinoline to get selective receptor unit with high coordination affinity to Hg²⁺ ion through the nitrogen atom of triazole ring and quinoline ring in water/THF 6:4 mixture and display fluorescence Turn-Off response was reported by Gupta *et al.* in 2017 [132].

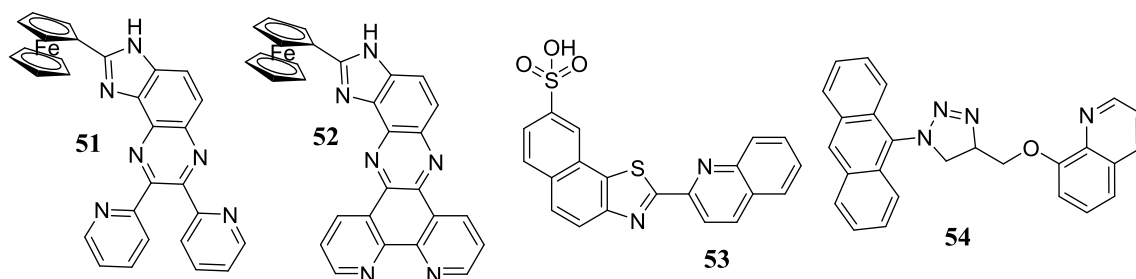


Figure 1.20 Hg^{2+} selective chemosensors with pyridine core receptor

Chen *et al.* in 2011 reported a squaraine containing dithiocarbamate moiety a fluorescent sensor **55** (Figure 1.21) with H-aggregate nature as selective colorimetric and Turn On fluorimetric Hg^{2+} ion detector with 1:2 stoichiometry and LOD of 7.1 nM. The selective coordination of Hg^{2+} with the dithiocarbamate acceptor groups of fluorescent sensor induces a 700 fold emission enhancements and color change from purple to blue which resulted from deaggregation of the H-aggregate [133]. Taki *et al.* reported other reversible selective Hg^{2+} ion sensor containing thioether receptor unit chemosensor **56** (Figure 1.21) bearing hexathioether moieties as metal receptor which preferably binds soft metal Hg^{2+} ion in an aqueous solution. **56** exhibits a swift enhancement in emission intensity of around 20-fold upon Hg^{2+} ion binding with receptor group of **56** with an extremely high femto-molar binding affinity and 1:1 binding stoichiometry. **56** were reversible by addition of Glutathione and applicable in monitoring Hg^{2+} ion level change in the mitochondria of living cells [134].

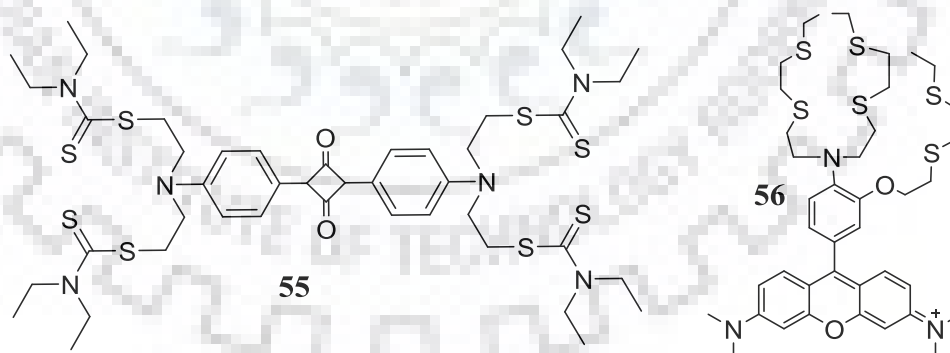


Figure 1.21 Hg^{2+} selective chemosensors with thioether moieties receptors

Tharmaraj and Pitchumani in 2012 reported foluorescent chemosensor **57** (Figure 1.22) by reaction of dansyl chloride with 2-aminothiophenol for detection of Hg^{2+} via twisted ICT in aqueous: CH_3CN (1:1 v/v) solution. The coordination of Hg^{2+} with thio and sulfonamide group results intermolecular charge transfer from the electron rich *N,N*-dimethylamino group to the electron poor sulfonamide moiety exhibits a significant fluorescence quenching accompanied by

red shift from 495 to 514 nm and blue shifts in absorbance from 342 nm to 330 nm with LOD of 1.5 nM [135]. Srivastava *et al.* in 2013 reported other ICT based fluorescent chemosensor **58** (Figure 1.22) containing sulfonamide group for detection of Hg^{2+} in 1:1 MeCN/water solution by introducing benzhydryl and dansyl groups bridged by piperazine to generate a stable configuration by acquiring an efficient electron rich ICT probe to work on the push-pull mechanism. The coordination of Hg^{2+} with nitrogen atoms of piperazine unit and sulfonamide group activates the charge transfer from *N,N*-dimethylamine to sulfonamide moiety induces quenching and detects Hg^{2+} as sensitive as 20 nM [136].

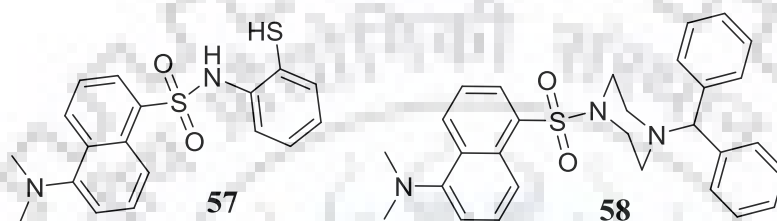


Figure 1.22 Hg^{2+} selective chemosensors with sulfonamide receptors

Dimerized cysteine amino acid residues with dansyl fluorophore based fluorescent chemosensor **59** (Figure 1.23) containing sulfonamide and cysteine dimer as receptors in the designing of selective Hg^{2+} sensor were reported by Joshi *et al.* in 2010. **59** exhibited an outstanding selective Turn-On response to Hg^{2+} with blue shift from 541 to 507 nm upon excitation with 330 nm in 100% aqueous solution. The sensor showed LOD of 7.8 nM with good reversibility *via* addition of EDTA solution [137]. Other Amino acid based fluorescence chemosensors containing pyrene fluorophore and sulfonamide and methionine receptors **60** [138] and tryptophan as a receptor **61** (Figure 1.23) [139], were designed and reported by Lee and his coworkers in 2011 and 2013 respectively. The addition of Hg^{2+} to **60** induced decreasing in intensity of absorption spectra at 352 nm and a ratiometric response by a significant decreasing the intensity of the monomer emission centered at 385 nm and enhancement in excimer emission of the pyrene moiety at 480 nm with increasing Hg^{2+} concentration as indication of dimerization of two pyrene fluorophores in binding with Hg^{2+} with binding stoichiometry of 2:1 in pH 7.4 HEPES buffer (10 nM) containing 2% DMF. The PET mechanism of **61** from indole to pyrene with absorption at 352 nm and fluorescence at 390 nm was inhabited by the coordination of Hg^{2+} to the indole and amino acid groups and exhibited significant decrease in the absorbance and progressively increasing excimeric emission at 480 nm due to the stacked dimerization of two pyrene fluorophores in binding with Hg^{2+} with binding stoichiometry of 2:1 in 5:95 MeCN/water 10 mM HEPES buffer pH of 7.4.

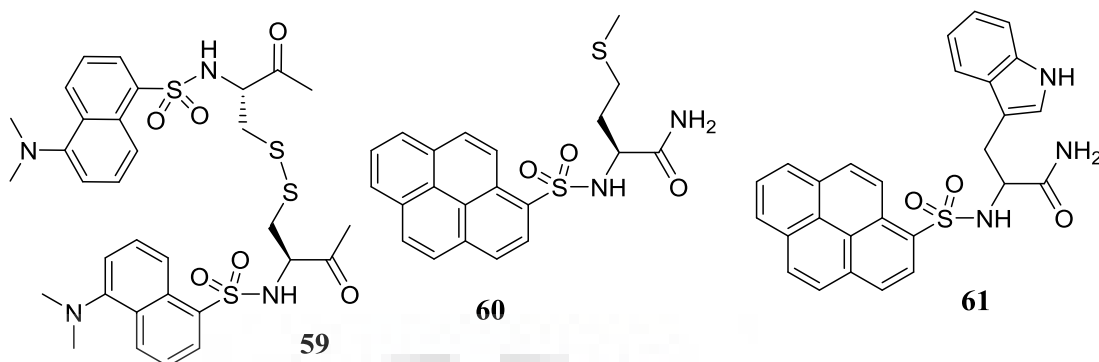


Figure 1.23 Hg^{2+} selective chemosensors with sulfonamide and-amino acids receptors.

Recently, Aliberti *et al.* reported a set of dansyl-amino acids based fluorescent chemosensors **62a-e** (Figure 1.24) for Hg^{2+} ions recognition using methionine and cysteine derivatives as receptors *via* different fluorescence emission modes in aqueous buffers [140]. **62a** shows quenching at low concentration of Hg^{2+} ion (0.02-0.4 equiva.) and enhancement upon increasing the concentration above 0.6 equivalents with blue shift from 550 nm to 500 nm. Suggesting that formation of two different stoichiometric ratio of metal-ligand complexes 1:1 and 2:1 complexation for lower and higher amounts of Hg^{2+} ions respectively. In case of **62b** which also contains thioether group, shows modest fluorescence enhancement in comparing to **62a**. While the strong emitter **62c** exhibited strong quenching on binding to Hg^{2+} with slight blue shift from 520 to 510nm. Similarly Hg^{2+} induces strong fluorescence quenching into **62d** and **62e**.

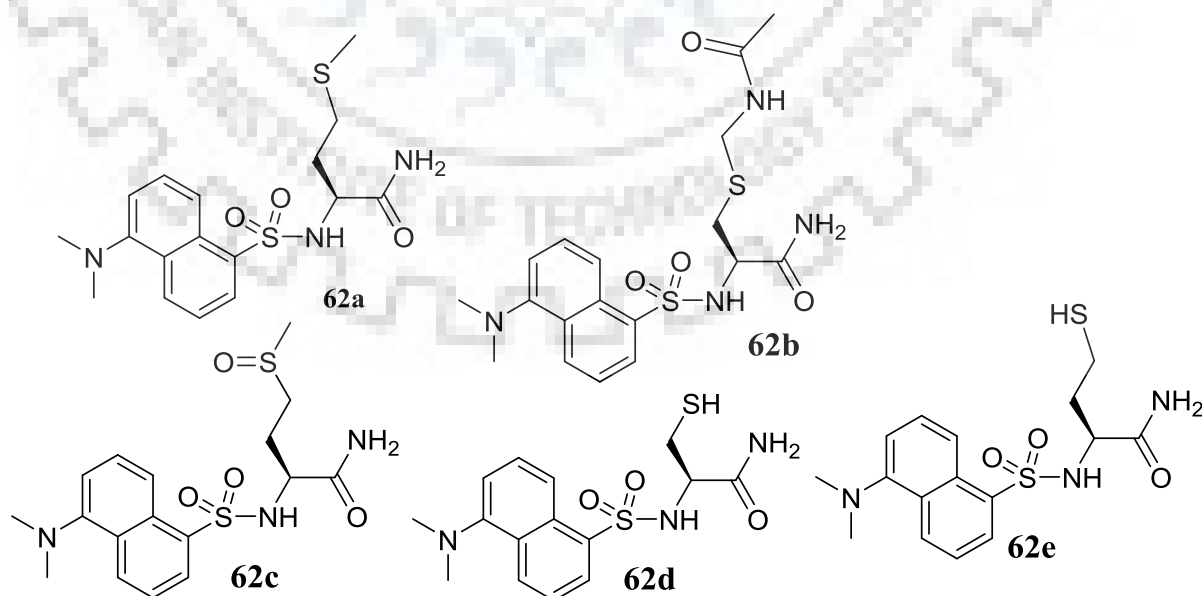


Figure 1.24 Hg^{2+} selective chemosensors with dansyl-amino receptors.

A fluorescent chemosensor **63** (Figure 1.25) containing a crown thioether group as the binding moiety and naphthalimide as fluorophore exhibited Turn On for Hg^{2+} and Turn Off for Ag^+ dual signaling properties in aqueous solution was reported by Chen *et al.* in 2010 [141]. Likewise, Atilgan *et al.* synthesized near-IR emitting based ratiometric chemosensor **64** (Figure 1.25), using dithia-dioxa-aza macrocycle as Hg^{2+} ion recognition unit linking with BODIPY fluorophore. The binding of Hg^{2+} ion to **64** induced a blue shift from 720 nm to 630 nm, which induced by blocking of the electron donating ability of the amino groups due to the coordination of heavy metal mercury, this decreases the conjugation and blocks ICT and causes blue shift followed by color change from blue to green [142].

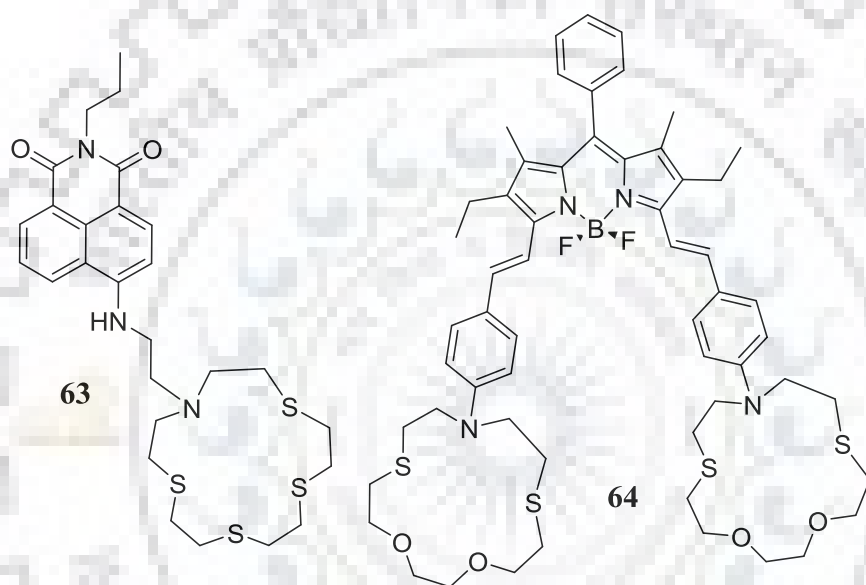


Figure 1.25 Hg^{2+} selective chemosensors containing crown thioether or dithia-diazo receptor group.

Highly selective and reversible Hg^{2+} ion receptor with free thiol recognition unit containing rhodamine based fluorescent sensor **65** (Figure 1.26) with a light “Off–On” system was reported by Liu *et al.* in 2012. Addition of Hg^{2+} to **65** induces distinct fluorescence and color change in 80:20 ethanol/water solution which resulted from the spirolactam ring opening. Strong affinity of the thiol for Hg^{2+} starts up the opening of spirolactam ring through Hg-S and Hg-O bond formation. This induces emission enhancement at 576 nm with swift color change from colorless to pink and emission at 558 nm with LOD of 2.5 μM . And good reversibility was acquired by addition of tetra-butyl ammonium iodide (TBAI) [143]. Chemosensor **66** (Figure 1.26) with S, N, O possible coordinating atoms to Hg^{2+} ion binding was reported by S. Gwon and his co-workers in 2015.

The chemosensor **66** was dual mode chemosensor for Hg^{2+} and CN^- ions based on styrylbenzothiazolium having hydroxyl, thioether and aniline nitrogen as a receptor group for selective binding of Hg^{2+} . the ligation of electron rich aniline nitrogen with Hg^{2+} ion favors ICT process leads to a evident color change from pink to colorless with blue shift from 516 nm to 383 nm in absorption and fluorescence quenching [144].

Recently, other S, N, O atoms coordinating moiety Hg^{2+} ion receptors chemosensor **67** (Figure 1.26) with the coumarin Schiff base fluorophore for selective colorimetric and fluorometric Hg^{2+} ions detection in nano-molar level in mixed aqueous-organic solution was developed and reported by Shaily *et al.* in 2017. Addition of Hg^{2+} ions to the chemosensor tune the yellowish green solution into orange which can be detected by naked eye accompanied by fluorescence intensity quenching, more importantly, it was used for elective detection of CN^- ion by displacement of Hg^{2+} ions [145].

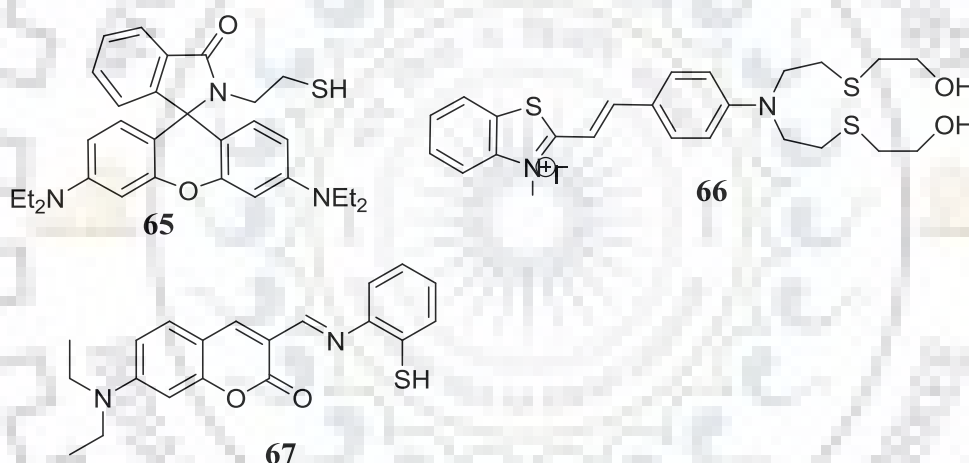


Figure 1.26 Hg^{2+} selective chemosensors with S, N, and O atoms coordinating moiety receptor.

1.7 Objective of the Thesis

From above discussion, it is evident that the detection and estimation of toxic metals is very important and relevant in the context of human health and environmental protection. The literature survey discloses that, even though there are numerous reported Hg^{2+} sensors, the search for fluorescence sensors with precise high sensitivity, selectivity and good response time is still needs more exploration. And owing to its hazardous and biotoxicity to the environment and ecosystem, recognition of Hg^{2+} is creditable.

The central theme of this thesis is designing and synthesis of some novel fluorescent chemosensors with high selectivity and sensitivity, and their photochemical studies for

selective recognition of Hg^{2+} ion in aqueous system. In this thesis, synthesis, characterizations, binding and sensing mechanisms of the synthesized ligands have been analyzed *via* different instrumental techniques *viz* FTIR, ^1H and ^{13}C NMR, HRMS, UV-Vis, fluorescence spectroscopy and lifetime analysis have been used for the entire studies. Furthermore, density functional theory (DFT), molecular logic gate and anti-microbial behavior have been applied in some schemes.

This thesis work is summarized into five chapters, the first chapter is about general introduction which defines fluorescence sensing, and importance of metal sensing particularly focuses on the selective recognition of Hg^{2+} ion, and brief discussion on principle of some common photophysical mechanisms of fluorescence sensors and reviews some common type of Hg^{2+} ion receptors in different mechanistic approaches.

Second chapter presents the design and synthesis of 1,4-benzothiazine hydrazide (**L2**) for selective and sensitive colorimetric and Turn On fluorometric detection of Hg^{2+} ion in 1:2 MeCN/water HEPES buffer at pH of 7.2, which is applicable in real sample analysis. The experimental findings were supported by applying density functional theory (DFT) and further the reversible behavior of receptors applied as INHIBIT logic gate.

The third chapter discusses a novel colorimetric and ratiometric fluorescence chemosensor 2-(2-mercaptophenyl)-1H-benzo[de]isoquinoline-1,3-(2H)dione (**L3**) for detection of Hg^{2+} ions applied in environmental water sample. The outcome of photo-physical experiment has also been in good accordance with the DFT estimations. The 'On-Off-On' emission reversibility works in the principle of IMPLICATION logic gate.

The fourth chapter describes two AIE active naphthalimide-amino acid conjugates chemosensors (**L4** and **L5**) for Hg^{2+} detection based on selective chelation mediated emission enhancement in MeCN/water (1:99, v/v) medium.

The fifth chapter discloses the AIEE active and monomer-excimer switching emission *via* metal ion-induced assembly based ratiometric fluorescent chemosensor sulfamethizole functionalized 1,8-naphthalimide (**L6**) for Hg^{2+} ion detection in aqueous medium and anti-microbial activity of the ligand and its silver complex. All the synthesized chemosensors in this thesis are working in aqueous medium either by Turn On or by ratiometric methods which makes them more attractive and desirable.

1.8 Reference

- [1] X. Qian, Z. Xu, Fluorescence imaging of metal ions implicated in diseases, *Chem. Soc. Rev.* 44 (2015) 4487–4493. doi:10.1039/c4cs00292j.
- [2] B. Valeur, I. Leray, Design principles of fluorescent molecular sensors for cation recognition, *Coord. Chem. Rev.* 205 (2000) 3–40. doi:10.1016/S0010-8545(00)00246-0.
- [3] M. Jaishankar, T. Tseten, N. Anbalagan, B.B. Mathew, K.N. Beeregowda, Toxicity, mechanism and health effects of some heavy metals, *Interdiscip. Toxicol.* 7 (2014) 60–72. doi:10.2478/intox-2014-0009.
- [4] E.S. Cho, J. Kim, B. Tejerina, T.M. Hermans, H. Jiang, H. Nakanishi, M. Yu, A.Z. Patashinski, S.C. Glotzer, F. Stellacci, B.A. Grzybowski, Ultrasensitive detection of toxic cations through changes in the tunnelling current across films of striped nanoparticles, *Nat. Mater.* 11 (2012) 978–985. doi:10.1038/nmat3406.
- [5] Y. Ding, Y. Tang, W. Zhu, Y. Xie, Fluorescent and colorimetric ion probes based on conjugated oligopyrroles, *Chem. Soc. Rev.* 44 (2015) 1101–1112. doi:10.1039/c4cs00436a.
- [6] N. Ullah, M. Mansha, I. Khan, A. Qurashi, Nanomaterial-based optical chemical sensors for the detection of heavy metals in water: Recent advances and challenges, *Trends Anal. Chem.* 100 (2018) 155–166. doi:10.1016/j.trac.2018.01.002.
- [7] L. Basabe-desmots, D.N. Reinhoudt, M. Crego-calama, Design of fluorescent materials for chemical sensing, *Chem. Soc. Rev.* 36 (2007) 993–1017. doi:10.1039/b609548h.
- [8] S.K. Pandey, K. Kim, R.J.C. Brown, Measurement techniques for mercury species in ambient air, *Trends Anal. Chem.* 30 (2011) 899–917. doi:10.1016/j.trac.2011.01.017.
- [9] P. Gardinalli, R.K. Singhal, B. Ferreira, S. Pe, A.A. Mozeto, Analytical chemistry of metallic nanoparticles in natural environments, *Trends Anal. Chem.* 30 (2011). doi:10.1016/j.trac.2011.01.008.
- [10] J. Wang, E.H. Hansen, on-line sample pre-treatment schemes for trace-level determinations of metals by coupling flow injection or sequential injection with ICP-MS, *Trends Anal. Chem.* 22 (2003) 836–846. doi:10.1016/S0165-9936(03)01207-X.
- [11] E. Marguá, B. Zawisza, R. Sitko, Trace and ultratrace analysis of liquid samples by X-ray fluorescence spectrometry, *Trends Anal. Chem.* 53 (2014) 73–83. doi:10.1016/j.trac.2013.09.009.

- [12] K. Duarte, C.I.L. Justino, A.C. Freitas, A.M.P. Gomes, A.C. Duarte, T.A.P. Rochasantos, Disposable sensors for environmental monitoring of lead, cadmium and mercury, *Trends Anal. Chem.* 64 (2015) 183–190. doi:10.1016/j.trac.2014.07.006.
- [13] D. Kukkar, K. Vellingiri, V. Kumar, A. Deep, K. Kim, A critical review on the metal sensing capabilities of optically active nanomaterials: Limiting factors, mechanism, and performance evaluation, *Trends Anal. Chem.* 109 (2018) 227–246. doi:10.1016/j.trac.2018.09.009.
- [14] M. Dutta, D. Das, Recent developments in fluorescent sensors for trace-level determination of toxic-metal ions, *Trends Anal. Chem.* 32 (2012) 113–132. doi:10.1016/j.trac.2011.08.010.
- [15] J.R. Lakowicz, *Principles of fluorescence spectroscopy*, 3rd Edition, Joseph R. Lakowicz, editor, 2006. doi:10.1007/978-0-387-46312-4.
- [16] T. Ueno, T. Nagano, Fluorescent probes for sensing and imaging, *Nat. Methods.* 8 (2011) 642–645. doi:10.1038/nmeth.1663.
- [17] Z. Xu, J. Yoon, D.R. Spring, Fluorescent chemosensors for Zn²⁺, *Chem. Soc. Rev.* 39 (2010) 1996–2006. doi:10.1039/b916287a.
- [18] M. Natali, S. Campagna, F. Scandola, Photoinduced electron transfer across molecular bridges: electron and hole-transfer superexchange pathways, *Chem. Soc. Rev.* 43 (2014) 4005–4018. doi:10.1039/c3cs60463b.
- [19] J.J. Lee, Y.S. Kim, E. Nam, S.Y. Lee, M.H. Lim, C. Kim, A PET-based fluorometric chemosensor for the determination of mercury(II) and pH, and hydrolysis reaction-based colorimetric detection of hydrogen sulfide, *Dalton Trans.* 45 (2016) 5700–5712. doi:10.1039/c6dt00147e.
- [20] N. Boens, V. Leen, W. Dehaen, Fluorescent indicators based on BODIPY, *Chem. Soc. Rev.* 41 (2012) 1130–1172. doi:10.1039/c1cs15132k.
- [21] T. Kowalczyk, Z. Lin, T. Van Voorhis, Fluorescence quenching by photoinduced electron transfer in the Zn²⁺ sensor Zinpyr-1: a computational investigation, *J. Phys. Chem. A.* 114 (2016) 10427–10434. doi:10.1021/jp103153a.
- [22] L.J. Fan, W.E.J. Jr, Studies of Photoinduced Electron Transfer and Energy Migration in a Conjugated Polymer System for Fluorescence “Turn-On” Chemosensor Applications, *J. Phys. Chem. B.* 110 (2006) 7777–7782. doi:10.1021/jp056381q.Studies.
- [23] B. Zhou, S. Qin, B. Chen, Y. Han, A new BODIPY-based fluorescent “Turn-On” probe for highly selective and rapid detection of mercury ions, *Tetrahedron Lett.* 59 (2018) 4359–4363. doi:10.1016/j.tetlet.2018.10.068.

- [24] Y. Dong, R. Fan, W. Chen, P. Wang, Y. Yang, A simple quinolone Schiff-base containing CHEF based fluorescence ‘Turn-On’ chemosensor for distinguishing Zn^{2+} and Hg^{2+} with high sensitivity, selectivity and reversibility, *Dalton Trans.* 46 (2017) 6769–6775. doi:10.1039/c7dt00956a.
- [25] S.K. Panja, N. Dwivedi, S. Saha, Tuning the intramolecular charge transfer (ICT) process in push–pull systems: effect of nitro groups, *RSC Adv.* 6 (2016) 105786–105794. doi:10.1039/c6ra17521j.
- [26] P. Roy, A. Jha, V.B. Yasarapudi, T. Ram, B. Puttaraju, S. Patil, J. Dasgupta, Ultrafast bridge planarization in donor- π -acceptor copolymers drives intramolecular charge transfer, *Nat. Commun.* 8 (2017) 1716. doi:10.1038/s41467-017-01928-z.
- [27] S. Sumalekshmy, K.R. Gopidas, Photoinduced Intramolecular Charge Transfer in Donor - Acceptor Substituted Tetrahydropyrenes, *J. Phys. Chem. B.* 108 (2004) 3705–3712. doi:10.1021/jp022549l.
- [28] M. Liu, X. Yu, M. Li, N. Liao, A. Bi, Y. Jiang, S. Liu, Z. Gong, W. Zeng, Fluorescent probes for the detection of magnesium ions (Mg^{2+}): from design to application, *RSC Adv.* 8 (2018) 12573–12587. doi:10.1039/c8ra00946e.
- [29] S. Goswami, A.K. Das, S. Maity, ‘PET’ vs ‘push–pull’ induced ICT: a remarkable coumarinyl-appended pyrimidine based naked eye colorimetric and fluorimetric sensor for the detection of Hg^{2+} ions in aqueous media with test trips, *Dalton Trans.* 42 (2013) 16259. doi:10.1039/c3dt52252k.
- [30] J. Wang, X. Qian, J. Cui, Detecting Hg^{2+} ions with an ICT Fluorescent Sensor Molecule: Remarkable Emission Spectra Shift and Unique Selectivity, *J. Org. Chem.* 71 (2006) 4308–4311. doi:10.1021/jo052642g.
- [31] R. Rani, G. Kumar, K. Paul, V. Luxami, Donor- π -acceptor (D- π -A) dyad for ratiometric detection of Hg^{2+} and PPI, *New J. Chem.* 42 (2018) 12729–12736. doi:10.1039/c8nj00741a.
- [32] P. Rajdev, S. Ghosh, Fluorescence Resonance Energy Transfer (FRET): A Powerful Tool for Probing Amphiphilic Polymer Aggregates and Supramolecular Polymers, *J. Phys. Chem. B.* 123 (2018) 327–342. doi:10.1021/acs.jpcc.8b09441.
- [33] L. Ma, F. Yang, J. Zheng, Application of fluorescence resonance energy transfer in protein studies, *J. Mol. Struct.* 1077 (2014) 87–100. doi:10.1016/j.molstruc.2013.12.071.
- [34] G. Chen, F. Song, X. Xiong, X. Peng, Fluorescent Nanosensors Based on Fluorescence Resonance Energy Transfer (FRET), *Ind. Eng. Chem. Res.* 52 (2013) 11228–11245.

doi:10.1021/ie303485n.

- [35] N. Kumar, V. Bhalla, M. Kumar, Resonance energy transfer-based fluorescent probes for Hg^{2+} , Cu^{2+} and $\text{Fe}^{2+}/\text{Fe}^{3+}$ ions, *Anal. Methods*. 139 (2014) 543–558. doi:10.1039/c3an01896b.
- [36] Y. Liu, X. Lv, Y. Zhao, M. Chen, J. Liu, P. Wang, W. Guo, A naphthalimide rhodamine ratiometric fluorescent probe for Hg^{2+} based on fluorescence resonance energy transfer, *Dye. Pigment*. 92 (2012) 909–915. doi:10.1016/j.dyepig.2011.07.020.
- [37] N. Xu, M. Liu, M. Ye, Y. Yao, Y. Zhou, G. Wu, A Rhodamine-naphthalimide conjugated chemosensor for ratiometric detection Hg^{2+} in actual aqueous samples, *J. Lumin*. 188 (2017) 135–140. doi:10.1016/j.jlumin.2017.03.067.
- [38] Y. Ge, A. Liu, R. Ji, S. Shen, X. Cao, Detection of Hg^{2+} by a FRET ratiometric fluorescent probe based on a novel pyrido [1, 2-a] benzimidazole-rhodamine system, *Sensors Actuators B. Chem*. 251 (2017) 410–415. doi:10.1016/j.snb.2017.05.097.
- [39] Y. Ge, X. Xing, A. Liu, R. Ji, S. Shen, X. Cao, Dyes and Pigments A novel imidazo [1,5-a] pyridine-rhodamine FRET system as an efficient ratiometric fluorescent probe for Hg^{2+} in living cells, *Dye. Pigment*. 146 (2017) 136–142. doi:10.1016/j.dyepig.2017.06.067.
- [40] A. Petdum, W. Panchan, J. Sirirak, V. Promarak, T. Sooksimuang, N. Wanichacheva, Colorimetric and fluorescent sensing of a new FRET system via [5]helicene and rhodamine 6G for Hg^{2+} detection, *New J. Chem*. 42 (2018) 1396–1402. doi:10.1039/c7nj04129b.
- [41] R. Daengngern, N. Kungwan, Electronic and photophysical properties of 2-(2'-hydroxyphenyl) benzoxazole and its derivatives enhancing in the excited-state intramolecular proton transfer processes: A TD-DFT study on substitution effect, *J. Lumin*. 167 (2015) 132–139. doi:10.1016/j.jlumin.2015.06.001.
- [42] F.S. Santos, E. Ramasamy, V. Ramamurthy, F.S. Rodembusch, Excited state behavior of benzoxazole derivatives in a confined environment afforded by a water soluble octaacid capsule, *J. Photochem. Photobiol. A Chem*. 317 (2016) 175–185. doi:10.1016/j.jphotochem.2015.08.019.
- [43] W. Chansen, R. Salaeh, C. Prommin, K. Kerdpol, R. Daengngern, N. Kungwan, Theoretical study on influence of geometry controlling over the excited-state intramolecular proton transfer of 10-hydroxybenzo [h] quinoline and its derivatives, *Comput. Theor. Chem*. 1113 (2017) 42–51. doi:10.1016/j.comptc.2017.05.008.
- [44] H. Lin, X. Chang, D. Yan, W.-H. Fanga, G. Cui, Tuning excited-state-intramolecular-

- proton-transfer (ESIPT) process and emission by cocystal formation: a combined experimental and theoretical study, *Chem. Sci.* 8 (2017) 2086–2090. doi:10.1039/c6sc04354b.
- [45] A.C. Sedgwick, L. Wu, H. Han, S.D. Bull, X. He, T.D. James, J.L. Sessler, B.Z. Tang, H. Tian, J. Yoon, Excited-state intramolecular proton-transfer (ESIPT) based fluorescence sensors and imaging agents, *Chem. Soc. Rev.* 47 (2018) 8842–8880. doi:10.1039/c8cs00185e.
- [46] K. Keshav, M.K. Kumawat, R. Srivastava, M. Ravikanth, Benzothiazoles-substituted tetraphenylethylenes: synthesis, structure, aggregation-induced emission and biological studies, *Mater. Chem. Front.* 1 (2017) 1207–1216. doi:10.1039/c6qm00374e.
- [47] S. Pascal, S. Denis-Quanquin, F. Appaix, A. Duperray, A. Grichine, B. Le Guennic, D. Jacquemin, J. Cuny, S.-H. Chi, J.W. Perry, B. van der Sanden, C. Monnereau, C. Andraud, O. Maury, Keto-polymethines: a versatile class of dyes with outstanding spectroscopic properties for in cellulo and in vivo two-photon microscopy imaging, *Chem. Sci.* 8 (2017) 381–394. doi:10.1039/c6sc02488b.
- [48] V.S. Padalkar, S. Seki, Excited-state intramolecular proton-transfer (ESIPT)-inspired solid state emitters, *Chem. Soc. Rev.* 45 (2016) 169–202. doi:10.1039/c5cs00543d.
- [49] S. Budzak, D. Jacquemin, Excited state intramolecular proton transfer in julolidine derivatives: an ab initio study, *Phys.Chem.Chem.Phys.* 20 (2018) 25031–25038. doi:10.1039/c8cp04356f.
- [50] M. Santra, B. Roy, K.H. Ahn, A “Reactive” Ratiometric Fluorescent Probe for Mercury Species, *Org Lett.* 13 (2011) 3422–3425. doi:10.1021/ol2011693.
- [51] N. Kaur, G. Jindal, Sukhvinder, S. Kumar, Cascade recognition of Hg²⁺ and cysteine using a naphthalene based ESIPT sensor and its application in a set/reset memorized device, *New J. Chem.* 43 (2019) 436–443. doi:10.1039/c8nj03909g.
- [52] S. Goswami, K. Aich, S. Das, C. Das Mukhopadhyay, D. Sarkar, T.K. Mondal, A new visible-light-excitable ICT-CHEF-mediated fluorescence ‘Turn-On’ probe for the selective detection of Cd²⁺ in a mixed aqueous system with live-cell imaging, *Dalton Trans.* 44 (2015) 5763–5770. doi:10.1039/c4dt02463j.
- [53] A.T. Afaneh, G. Schreckenbach, Fluorescence Enhancement/Quenching Based on Metal Orbital Control: Computational Studies of a 6-Thienyllumazine-Based Mercury Sensor, *J. Phys. Chem. A.* 119 (2015) 8106–8116. doi:10.1021/acs.jpca.5b04691.
- [54] H. Lee, H. Lee, J.H. Reibenspies, R.D. Hancock, Mechanism of “Turn-On” Fluorescent Sensors for Mercury(II) in Solution and Its Implications for Ligand

- Design, *Inorg. Chem.* 51 (2012) 10904–10916. doi:10.1021/ic301380w.
- [55] B.N. Ahamed, P. Ghosh, A chelation enhanced selective fluorescence sensing of Hg^{2+} by a simple quinoline substituted tripodal amide receptor, *Dalton Trans.* 40 (2011) 12540–12547. doi:10.1039/c1dt10923e.
- [56] A.J. Musser, S.K. Rajendran, K. Georgiou, L. Gai, R.T. Grant, Z. Shen, M. Cavazzini, A. Ruseckas, G.A. Turnbull, I.D.W. Samuel, J. Clarka, D.G. Lidzey, Intermolecular states in organic dye dispersions: excimers vs. aggregates, *J. Mater. Chem. C* 5 (2017) 8380–8389. doi:10.1039/c7tc02655b.
- [57] P. Debnath, S. Chakraborty, S. Deb, J. Nath, D. Bhattacharjee, S.A. Hussain, Reversible Transition between Excimer and J-Aggregate of Indocarbocyanine Dye in Langmuir–Blodgett (LB) Films, *J. Phys. Chem. C* 119 (2015) 9429–9441. doi:10.1021/acs.jpcc.5b02111.
- [58] W.T. Yip, D.H. Levy, Excimer/Exciplex Formation in van der Waals Dimers of Aromatic Molecules, *J. Phys. Chem.* 3654 (1996) 11539–11545. doi:10.1021/jp9537668.
- [59] H. Saigusa, Excimer and Exciplex Formation in van der Waals Dimers of Toluene and Benzene, *J. Phys. Chem. A* 105 (2001) 7334–7340. doi:10.1021/jp010910i.
- [60] O.P. Dimitriev, Y.P. Piryatinski, Y.L. Slominskii, Excimer Emission in J-Aggregates, *J. Phys. Chem. Lett.* 9 (2018) 2138–2143. doi:10.1021/acs.jpcclett.8b00481.
- [61] A.I. Sulatskaya, A. V Lavysh, A.A. Maskevich, I.M. Kuznetsova, K.K. Turoverov, Thioflavin T fluoresces as excimer in highly concentrated aqueous solutions and as monomer being incorporated in amyloid fibrils, *Sci. Rep.* 7 (2017) 1–11. doi:10.1038/s41598-017-02237-7.
- [62] M. Shellaiah, Y.C. Rajan, P. Balu, A. Murugan, A pyrene based Schiff base probe for selective fluorescence Turn-On detection of Hg^{2+} ions with live cell application, *New J. Chem.* 39 (2015) 2523–2531. doi:10.1039/c4nj02367f.
- [63] S.S. Razi, R. Ali, P. Srivastava, A. Misra, Smart excimer fluorescence probe for visual detection, cell imaging and extraction of Hg^{2+} , *RSC Adv.* 5 (2015) 79538–79547. doi:10.1039/c5ra13021b.
- [64] T. Puangsamlee, Y. Tachapermpon, P. Kammalun, K. Sukrat, C. Wainiphithaponga, J. Siriraka, N. Wanichacheva, Solvent control bifunctional fluorescence probe for selective detection of Cu^{2+} and Hg^{2+} via the excimer of pyrenylacetamide subunits, *J. Lumin.* 196 (2018) 227–235. doi:10.1016/j.jlumin.2017.11.048.
- [65] N. Meher, S. Panda, S. Kumarb, P.K. Iyer, Aldehyde group driven aggregation-induced

- enhanced emission in naphthalimides and its application for ultradetection of hydrazine on multiple platforms, *Chem. Sci.* 9 (2018) 3978–3985. doi:10.1039/C8SC00643A.
- [66] Y.-R. Jheng, M.G. Mohamed, and S.-W. Kuo, Supramolecular Interactions Induce Unexpectedly Strong Emissions from Triphenylamine-Functionalized Polytyrosine Blended with Poly(4-vinylpyridine), *Polymers (Basel)*. 9 (2017) 503. doi:10.3390/polym9100503.
- [67] W.Z. Yuan, Y. Gong, S. Chen, X.Y. Shen, J.W.Y. Lam, P. Lu, Y. Lu, Z. Wang, R. Hu, N. Xie, H.S. Kwok, Y. Zhang, J.Z. Sun, B.Z. Tang, Efficient Solid Emitters with Aggregation-Induced Emission and Intramolecular Charge Transfer Characteristics: Molecular Design, Synthesis, Photophysical Behaviors, and OLED Application, *Chem. Mater.* 24 (2012) 1518–1528. doi:org/10.1021/cm300416y.
- [68] X.Q. Ma, Y. Wang, T.B. Wei, L.H. Qi, X.M. Jianga, J.D. Ding, W. Zhu, H. Yao, Y. Zhang, Q. Lin, A novel AIE chemosensor based on quinoline functionalized Pillar [5]arene for highly selective and sensitive sequential detection of toxic Hg^{2+} and CN^- , *Dye. Pigment.* 164 (2019) 279–286. doi:10.1016/j.dyepig.2019.01.049.
- [69] H. Nie, K. Hu, Y. Cai, Q. Peng, Z. Zhao, R. Hu, J. Chen, S. Su, A. Qin, B.Z. Tang, Tetraphenylfuran: aggregation-induced emission or aggregation-caused quenching?, *Mater. Chem Front.* 1 (2017) 1125–1129. doi:10.1039/c6qm00343e.
- [70] R.R. Maar, J.B. Gilroy, Aggregation-Induced Emission Enhancement in Boron Difluoride Complexes of 3-Cyanoformazanates, *J. Mater. Chem. C.* 4 (2016) 6478–6482. doi: 10.1039/C6TC01782G.
- [71] L.N. Neupane, E. Oh, H.J. Park, K. Lee, Selective and Sensitive Detection of Heavy Metal Ions in 100% Aqueous Solution and Cells with a Fluorescence Chemosensor Based on Peptide Using Aggregation-Induced Emission, *Anal. Chem.* 88 (2016) 3333–3340. doi:10.1021/acs.analchem.5b04892.
- [72] A. Chatterjee, M. Banerjee, D.G. Khandare, R.U. Gawas, S.C. Mascarenhas, A. Ganguly, R. Gupta, H. Joshi, Aggregation-Induced Emission-Based Chemodosimeter Approach for Selective Sensing and Imaging of Hg(II) and Methylmercury Species, *Anal. Chem.* 89 (2017) 12698–12704. doi:10.1021/acs.analchem.7b02663.
- [73] M. Shyamal, S. Maity, A. Maity, R. Maity, S. Roy, A. Misra, Aggregation induced emission based “turn-off” fluorescent chemosensor for selective and swift sensing of mercury (II) ions in water, *Sensors Actuators B. Chem.* 263 (2018) 347–359. doi:10.1016/j.snb.2018.02.130.
- [74] K. Ma, X. Li, B. Xu, W. Tian, A sensitive and selective “Turn-On” fluorescent probe

- for Hg^{2+} based on thymine- Hg^{2+} -thymine complex with an aggregation-induced emission feature, *Anal. Methods*. 6 (2014) 2338–2342. doi:10.1039/c3ay42255k.
- [75] Q. Duan, M. Zhang, C. Sheng, C. Liu, L. Wu, Z. Ma, Q. Zhao, Z. Wang, B. Zhu, Rhodol-derived Colorimetric and Fluorescent Probe with the Receptor of Carbonothioate for the Specific Detection of Mercury Ions, *Anal. Sci.* 33 (2017) 1169–1173. doi:10.2116/analsci.33.1169.
- [76] J. Park, W. Zheng, Human Exposure and Health Effects of Inorganic and Elemental Mercury, *J. Prev. Med. Public Heal.* 45 (2012) 344–352. doi:10.3961/jpmph.2012.45.6.344.
- [77] N. Mori, M. Yamamoto, E. Tsukada, T. Yokooji, N. Matsumura, M. Sasaki, T. Murakami, Comparison of InVivo with InVitro Pharmacokinetics of Mercury Between Methylmercury Chloride and Methylmercury Cysteine Using Rats and Caco2 Cells, *Arch. Environ. Contam. Toxicol.* 63 (2012) 628–636. doi:10.1007/s00244-012-9800-5.
- [78] B.D. de Greñu, J. García-Calvo, J. Cuevas, G. García-Herbosa, B. García, N. Busto, S. Ibeas, T. Torroba, B. Torroba, A. Herrera, S. Pons, Chemical Science solution and HEK cells nuclei by means of DNA interacting fluorogenic probes, *Chem. Sci.* 6 (2015) 3757–3764. doi:10.1039/c5sc00718f.
- [79] M.S. Alam, G. Kaur, Z. Jabbar, K. Javed, M. Athar, Eruca sativa seeds possess antioxidant activity and exert a protective effect on mercuric chloride induced renal toxicity, *Food and Chemical Toxicology*. 45 (2007) 910–920. doi:10.1016/j.fct.2006.11.013.
- [80] P.A. Olsvik, H. Amlund, B.E. Torstensen, Dietary lipids modulate methylmercury toxicity in Atlantic salmon, *Food and Chemical Toxicology*. 49 (2011) 3258–3271. doi:10.1016/j.fct.2011.09.025.
- [81] I. Onyido, A.R. Norris, E. Buncl, Biomolecule–Mercury Interactions: Modalities of DNA Base–Mercury Binding Mechanisms. Remediation Strategies, *Chem. Rev.* (2004) 5911–5929. doi:10.1021/cr030443w.
- [82] L. Li, Y. Wen, L. Xu, Q. Xu, S. Song, X. Zuo, J. Yan, W. Zhang, G. Liu, Development of mercury (II) ion biosensors based on mercury-specific oligonucleotide probes, *Biosens. Bioelectron.* 75 (2016) 433–445. doi:10.1016/j.bios.2015.09.003.
- [83] F.M.M. Morel, A.M.L. Kraepiel, M. Amyot, The Chemical Cycle and Bioaccumulation of Mercury, *Annu. Rev. Ecol. Syst.* (1998).
- [84] B. Kaur, N. Kaur, S. Kumar, Colorimetric metal ion sensors, A comprehensive review of the years 2011–2016, *Coord. Chem. Rev.* 358 (2018) 13–69.

doi:10.1016/j.ccr.2017.12.002.

- [85] H.S. So, B.A. Rao, J. Hwang, K. Yesudas, Y.A. Son, Synthesis of novel squaraine-bis(rhodamine-6G): A fluorescent chemosensor for the selective detection of Hg^{2+} , *Sensors Actuators, B Chem.* 202 (2014) 779–787. doi:10.1016/j.snb.2014.06.013.
- [86] E.A. Sondreal, S.A. Benson, J.H. Pavlish, Status of research on air quality: mercury, trace elements, and particulate matter, *Fuel Process. Technol.* 65–66 (2000) 5–19.
- [87] Y. Ding, S. Wang, J. Li, L. Chen, Nanomaterial-based optical sensors for mercury ions, *Trends Anal. Chem.* 82 (2016) 175–190. doi:10.1016/j.trac.2016.05.015.
- [88] S.A. El-Safty, M.A. Shenashen, S.A. El-Safty, Mercury-ion optical sensors, *Trends Anal. Chem.* 38 (2012) 98–115. doi:10.1016/j.trac.2012.05.002.
- [89] G. Chen, Z. Guo, L. Tang, Fluorescent and colorimetric sensors for environmental mercury detection, *Analyst.* 140 (2015) 5400–5443. doi:10.1039/c5an00389j.
- [90] P.D. Selid, H. Xu, E.M. Collins, M.S. Face-collins, J.X. Zhao, Sensing Mercury for Biomedical and Environmental Monitoring, *Sensors.* 9 (2009) 5446–5459. doi:10.3390/s90705446.
- [91] H. Tang, Y. Gao, B. Li, C. Li, Y. Guo, Reaction-based colorimetric and ratiometric fluorescent probe for highly selective detection of silver ions, *Sensors Actuators B. Chem.* 270 (2018) 562–569. doi:10.1016/j.snb.2018.05.064.
- [92] R. An, D. Zhang, Y. Chen, Y. Cui, A “Turn-On” fluorescent and colorimetric sensor for selective detection of Cu^{2+} in aqueous media and living cells, *Sensors Actuators B. Chem.* 222 (2016) 48–54. doi:10.1016/j.snb.2015.08.035.
- [93] M.J. Culzoni, A.M. de la Peña, A. Machuca, H.C. Goicoechea, R. Babiano, Rhodamine and BODIPY chemodosimeters and chemosensors for the detection of Hg^{2+} , based on fluorescence enhancement effect, *Anal. Methods.* 5 (2013) 30–49. doi:10.1039/c2ay25769f.
- [94] X. Zhang, Y.Y. Zhu, A new fluorescent chemodosimeter for Hg^{2+} selective detection in aqueous solution based on Hg^{2+} -promoted hydrolysis of rhodamine-glyoxylic acid conjugate, *Sensors Actuators, B Chem.* 202 (2014) 609–614. doi:10.1016/j.snb.2014.05.121.
- [95] J. Du, M. Hu, J. Fan, X. Peng, Fluorescent chemodosimeters using “mild” chemical events for the detection of small anions and cations in biological and environmental media, *Chem. Soc. Rev.* 41 (2012) 4511–4535. doi:10.1039/c2cs00004k.
- [96] S. Madhu, S. Josimuddin, M. Ravikanth, 3,5-Bis(dithioacetal) meso-aryl BODIPYs: selective chemodosimeters for $\text{Hg}(\text{II})$ ions, *New J. Chem.* 12 (2014) 3770–3776.

doi:10.1039/c4nj00593g.

- [97] M. Kaur, M.J. Cho, D.H. Choi, A phenothiazine-based “naked-eye” fluorescent probe for the dual detection of Hg^{2+} and Cu^{2+} : Application as a solid state sensor, *Dye. Pigment.* 125 (2016) 1–7. doi:10.1016/j.dyepig.2015.09.030.
- [98] P. Mahato, S. Saha, P. Das, H. Agarwallad, A. Das, An overview of the recent developments on Hg^{2+} recognition, *RSC Adv.* 4 (2014) 36140–36174. doi:10.1039/c4ra03594a.
- [99] J. Qin, H. Yao, S. He, X. Zeng, Design and synthesis of a rhodol isomer and its derivatives with high selectivity and sensitivity for sensing Hg^{2+} and F^- in aqueous media, *RSC Adv.* 6 (2016) 75570–75577. doi:10.1039/c6ra14287g.
- [100] M. Chae, A.W. Czarnik, Fluorometric chemodosimetry. Mercury(II) and silver(I) indication in water via enhanced fluorescence signaling, *J. Am. Chem. Soc.* 114 (1992) 9704–9705. doi:10.1021/ja00050a085.
- [101] K.C. Song, J.S. Kim, S.M. Park, K. Chung, S. Ahn, S. Chang, Fluorogenic Hg^{2+} -Selective Chemodosimeter Derived from 8-Hydroxyquinoline, *Org. Lett.* 8 (2006) 3413–3416. doi:10.1021/ol060788b.
- [102] M.G. Choi, Y.H. Kim, J.E. Namgoong, S. Chang, Hg^{2+} selective chromogenic and fluorogenic chemodosimeter based on thiocoumarins, *Chem. Commun.* (2009) 3560–3562. doi:10.1039/b905612b.
- [103] Q. Zhang, J. Ge, Q. Xu, X. Yang, X. Cao, N. Li, J. Lu, A selective, sensitive probe for mercury (II) ions based on oxazine-thione, *Tetrahedron Lett.* 52 (2011) 595–597. doi:10.1016/j.tetlet.2010.11.130.
- [104] B. Liu, H. Tian, A selective fluorescent ratiometric chemodosimeter for mercury ion, *Chem. Commun.* (2005) 3156–3158. doi:10.1039/b501913c.
- [105] M.H. Lee, B. Cho, J. Yoon, J.S. Kim, Selectively Chemodosimetric Detection of $\text{Hg}(\text{II})$ in Aqueous Media, *Org. Lett.* 9 (2007) 4515–4518. doi:10.1021/ol7020115.
- [106] M.H. Lee, S.W. Lee, S.H. Kim, C. Kang, J.S. Kim, Nanomolar $\text{Hg}(\text{II})$ Detection Using Nile Blue Chemodosimeter in Biological Media, *Org. Lett.* 11 (2009) 2101–2104. doi:10.1021/ol900542y.
- [107] Y. Lv, W. Gu, J. Wang, W. Huang, W. Shen, Xiao-Yi Sun, A ratiometric fluorescence chemodosimeter for detecting Hg^{2+} in aqueous solutions and living cells, *Sensors Actuators B. Chem.* 246 (2017) 1017–1024. doi:10.1016/j.snb.2017.02.171.
- [108] H. Singh, G. Bhargava, S. Kumar, P. Singh, Microstructural (self-assembly) and optical based discrimination of Hg^{2+} , CN^- and $\text{Hg}(\text{CN})_2$ ion-pair; Hg^{2+} promoted-

- ESIPT assisted guanylation of thiourea, *Sensors Actuators B. Chem.* 272 (2018) 43–52. doi:10.1016/j.snb.2018.05.104.
- [109] Y. Yang, K. Yook, J. Tae, A Rhodamine-Based Fluorescent and Colorimetric Chemodosimeter for the Rapid Detection of Hg^{2+} ions in Aqueous Media, *J. Am. Chem. Soc.* 1 (2005) 16760–16761. doi:10.1021/ja054855t.
- [110] G.Q. Shang, X. Gao, M.X. Chen, H. Zheng, J.G. Xu, A Novel Hg^{2+} Selective Ratiometric Fluorescent Chemodosimeter Based on an Intramolecular FRET Mechanism, *J Fluoresc.* 18 (2008) 1187–1192. doi:10.1007/s10895-008-0365-7.
- [111] W. Liu, S. Shen, H. Li, J. Miao, B. Zhao, Fluorescence Turn-On chemodosimeter for rapid detection of mercury (II) ions in aqueous solution and blood from mice with toxicosis, *Anal. Chim. Acta.* 791 (2013) 65–71. doi:10.1016/j.aca.2013.07.022.
- [112] X. Cheng, Q. Li, J. Qin, Z. Li, A New Approach to Design Ratiometric Fluorescent Probe for Mercury (II) Based on the Hg^{2+} Promoted Deprotection of Thioacetals, *ACS Appl. Mater. Interfaces.* 2 (2010) 1066–1072. doi:10.1021/am900840q.
- [113] C. Swamy P, J. Shanmugapriya, S. Singaravadeivel, G. Sivaraman, D. Chellappa, Anthracene-Based Highly Selective and Sensitive Fluorescent “Turn-On” Chemodosimeter for Hg^{2+} , *ACS Omega.* 3 (2018) 12341–12348. doi:10.1021/acsomega.8b01142.
- [114] L. Song, Z. Lei, B. Zhang, Z. Xu, Z. Li, Y. Yang, A zero-background fluorescent probe for Hg^{2+} designed via the “covalent-assembly” principle, *Anal. Methods.* 6 (2014) 7597–7600. doi:10.1039/c4ay01729c.
- [115] S. Pan, K. Li, L. Li, M. Li, L. Shi, Y. Liu, X. Yu, A reaction-based ratiometric fluorescent sensor for the detection of Hg (II) ions in both cells and bacteria, *Chem. Commun.* 54 (2018) 4955–4958. doi:10.1039/c8cc01031e.
- [116] A. Hintermann, L. Lukas, Catalytic Hydration of Alkynes and its Application in Synthesis, *Synthesis (Stuttg).* (2007) 1121–1150. doi:10.1055/s-2007-966002.
- [117] J.E. Byrd, J. Halpern, Mercury(II)-catalysed Hydrolysis of Isopropenyl Acetate, *J. Chem. Soc. D.* (1970) 1332–1333. doi:10.1039/C29700001332.
- [118] D. Lee, G. Kim, H. Kim, A Fluorescent coumarinylalkyne probe for the selective detection of mercury(II) ion in water, *Tetrahedron Lett.* 50 (2009) 4766–4768. doi:10.1016/j.tetlet.2009.06.017.
- [119] H. Lee, H. Kim, Ratiometric fluorescence chemodosimeter for mercuric ions through the Hg (II) -mediated propargyl amide to oxazole transformation, *Tetrahedron Lett.* 52 (2011) 4775–4778. doi:10.1016/j.tetlet.2011.07.019.

- [120] W. Lin, X. Cao, Y. Ding, L. Yuan, L. Long, A highly selective and sensitive fluorescent probe for Hg^{2+} imaging in live cells based on a rhodamine–thioamide–alkyne scaffold, *Chem. Commun.* 46 (2010) 3529–3531. doi:10.1039/b927373e.
- [121] F. Song, S. Watanabe, P.E. Floreancig, K. Koide, Oxidation-Resistant Fluorogenic Probe for Mercury Based on Alkyne Oxymercuration, *J. Am. Chem. Soc.* 130 (2008) 16460–16461. doi:10.1021/ja805678r.
- [122] S. Ando, K. Koide, Development and Applications of Fluorogenic Probes for Mercury (II) Based on Vinyl Ether Oxymercuration, *J. Am. Chem. Soc.* 133 (2011) 2556–2566. doi:10.1021/ja108028m.
- [123] H. Jiang, J. Jiang, J. Cheng, W. Dou, X. Tang, L. Yang, A sensitive colorimetric and ratiometric fluorescent chemodosimeter for Hg^{2+} and its application for bioimaging, *New J. Chem.* 38 (2014) 109–114. doi:10.1039/c3nj00766a.
- [124] B. Gu, L. Huang, N. Mi, P. Yin, Y. Zhang, X. Tu, X. Luo, S. Luo, S. Yao, An ESIPT-based fluorescent probe for highly selective and ratiometric detection of mercury (II) in solution and in cells, *Analyst.* 140 (2015) 2778–2784. doi:10.1039/c5an00273g.
- [125] J. Du, J. Fan, X. Peng, P. Sun, J. Wang, H. Li, S. Sun, A New Fluorescent Chemodosimeter for Hg^{2+} : Selectivity, Sensitivity, and Resistance to Cys and GSH, *Org Lett.* 12 (2010) 476–479. doi:10.1021/ol902590g.
- [126] J. Ni, Q. Li, B. Li, L. Zhang, A novel fluorescent probe based on rhodamine B derivative for highly selective and sensitive detection of mercury (II) ion in aqueous solution, *Sensors Actuators B. Chem.* 186 (2013) 278–285. doi:10.1016/j.snb.2013.06.011.
- [127] M. Van Bay, N.K. Hien, S. Son, N.D. Trinh, N.T. Trung, P.C. Nam, J.S. Kim, D.T. Quang, Hg^{2+} -Promoted Spirolactam Hydrolysis Reaction: A Design Strategy for the Highly Selective Sensing of Hg^{2+} over other Metal ions in Aqueous Media, *Sensors.* 19 (2019) 1–14. doi:10.3390/s19010128.
- [128] Z. Liu, W. He, Z. Guo, Metal coordination in photoluminescent sensing, *Chem. Soc. Rev.* 42 (2013) 1568–1600. doi:10.1039/c2cs35363f.
- [129] M. Alfonso, A. Tárraga, P. Molina, Ferrocene-based multichannel molecular chemosensors with high selectivity and sensitivity for Pb (II) and Hg (II) metal cations, *Dalton Trans.* 39 (2010) 8637–8645. doi:10.1039/c0dt00450b.
- [130] M. Alfonso, A. Tárraga, P. Molina, Ferrocene-Based Heteroditopic Receptors Displaying High Selectivity toward Lead and Mercury Metal Cations through Different Channels, *J. Org. Chem.* 76 (2011) 939–947. doi:10.1021/jo102243e.

- [131] M.Z. Jonaghani, H. Zali-boeini, Highly selective fluorescent and colorimetric chemosensor for detection of Hg^{2+} ion in aqueous media, *Spectrochim. Acta Part A Mol. Biomol. Spectrosc.* 178 (2017) 66–70. doi:10.1016/j.saa.2017.01.065.
- [132] R.C. Gupta, S.S. Razi, R. Ali, S.K. Dwivedi, P. Srivastava, P. Singh, B. Koch, H. Mishra, A. Misra, An efficient Hg^{2+} ensemble based on a triazole bridged anthracene and quinoline system for selective detection of cyanide through fluorescence Turn Off–on response in solution and live cell, *Sensors Actuators B. Chem.* 251 (2017) 729–738. doi:10.1016/j.snb.2017.04.096.
- [133] C. Chen, R. Wang, L. Guo, N. Fu, H. Dong, Y. Yuan, A Squaraine-Based Colorimetric and “Turn On” Fluorescent Sensor for Selective Detection of Hg^{2+} in an Aqueous Medium, *Org Lett.* 13 (2011) 1162–1165. doi:10.1021/ol200024g.
- [134] M. Taki, K. Akaoka, S. Iyoshi, Y. Yamamoto, Rosamine-Based Fluorescent Sensor with Femtomolar Affinity for the Reversible Detection of a Mercury Ion, *Inorg. Chem.* 51 (2012) 13075–13077. doi:doi.org/10.1021/ic301822r.
- [135] V. Tharmaraj, K. Pitchumani, An acyclic, dansyl based colorimetric and fluorescent chemosensor for $\text{Hg}(\text{II})$ via twisted intramolecular charge transfer (TICT), *Anal. Chim. Acta.* 751 (2012) 171–175. doi:10.1016/j.aca.2012.09.016.
- [136] P. Srivastava, R. Ali, S.S. Razi, M. Shahid, S. Patnaik, A. Misra, A simple blue fluorescent probe to detect Hg^{2+} in semiaqueous environment by intramolecular charge transfer mechanism, *Tetrahedron Lett.* 54 (2013) 3688–3693. doi:10.1016/j.tetlet.2013.05.014.
- [137] B.P. Joshi, C.R. Lohani, K. Lee, A highly sensitive and selective detection of $\text{Hg}(\text{II})$ in 100% aqueous solution with fluorescent labeled dimerized Cys residues, *Org. Biomol. Chem.* 8 (2010) 3220–3226. doi:10.1039/b925744f.
- [138] M. Yang, P. Thirupathi, K. Lee, Selective and Sensitive Ratiometric Detection of $\text{Hg}(\text{II})$ Ions Using a Simple Amino Acid Based Sensor, *Org Lett.* 13 (2011) 5028–5031. doi:10.1021/ol201683t.
- [139] L.N. Neupane, J. Park, J.H. Park, K. Lee, Turn-On Fluorescent Chemosensor Based on an Amino Acid for Pb (II) and Hg (II) ions in Aqueous Solutions and Role of Tryptophan for Sensing, *Org Lett.* 15 (2013) 254–257. doi:10.1021/ol3029516.
- [140] A. Aliberti, P. Vaiano, A. Caporale, M. Consales, M. Ruvo, A. Cusano, Fluorescent chemosensors for Hg^{2+} detection in aqueous environment, *Sensors Actuators B. Chem.* 247 (2017) 727–735. doi:10.1016/j.snb.2017.03.026.
- [141] T. Chen, W. Zhu, Y. Xu, S. Zhang, X. Zhang, X. Qian, A thioether-rich crown-based

- highly selective fluorescent sensor for Hg^{2+} and Ag^+ in aqueous solution, *Dalton Trans.* 39 (2010) 1316–1320. doi:10.1039/b908969a.
- [142] S. Atilgan, I. Kutuk, T. Ozdemir, A near IR di-styryl BODIPY-based ratiometric fluorescent chemosensor for Hg(II) , *Tetrahedron Lett.* 51 (2010) 892–894. doi:10.1016/j.tetlet.2009.12.025.
- [143] W. Liu, J. Chen, L. Xu, J. Wu, H. Xu, H. Zhang, P. Wang, Reversible “off-on” fluorescent chemosensor for Hg^{2+} based on rhodamine derivative, *Spectrochim. Acta Part A Mol. Biomol. Spectrosc.* 85 (2012) 38–42. doi:10.1016/j.saa.2011.08.071.
- [144] S. Gwon, B. Ananda, H. Kim, Y. Son, S. Kim, Novel styrylbenzothiazolium dye-based sensor for mercury, cyanide and hydroxide ions Benzenoid form Quinoid form, *Spectrochim. ACTA PART A Mol. Biomol. Spectrosc.* 144 (2015) 226–234. doi:10.1016/j.saa.2015.02.094.
- [145] Shaily, A. Kumar, N. Ahmed, Indirect Approach for CN^- Detection: Development of “Naked-Eye ” Hg^{2+} -Induced Turn-Off Fluorescence and Turn-On Cyanide Sensing by the Hg^{2+} Displacement Approach, *Ind. Eng. Chem. Res.* 56 (2017) 6358–6368. doi:10.1021/acs.iecr.7b00188.





Chapter 2

Design and Synthesis of 1,4-Benzothiazine Hydrazone as Selective and Sensitive Colorimetric and Turn-On Fluorometric Sensor for Hg²⁺ ion Detection in Aqueous Medium

Bahta, M.; Ahmed, N. *J. Photochem. Photobiol. A Chem.* **2018**, 357, 41–48.

DOI: 10.1016/j.jphotochem.2018.02.022.





2.1 Introduction

Development of selective and efficient detection methods for range of toxic heavy metal ions and anions is at the center of attention for researchers over the past few decades due to their wide range applications in biological, industrial and environmental processes [1–3]. In the viwe, researchers across the universe have been putting lot of efforts in designing and synthesis of novel chromogenic and fluorogenic organic molecules for as chemosensors which are efficiently competent to detect toxic cations and anions [4,5]. Among all heavy metal ions mercury ion gets substantial attention due to its notorious history [6,7]. The toxicity of mercury and its prolonged effect to human health and the ecosystem is well known [8,9]. Contamination of mercury ion is extensive and come up from a array of natural processes as well as anthropogenic activities, such as thermometers, barometers, mercury lamps, caustic soda, gold mining, fertilizer industries and waste incineration [10,11]. Both inorganic mercury ion and elemental mercury can be transformed into methylmercury (CH_3HgX) by microbial in the environment [12]. Owing to its non-biodegradability methylmercury accumulated through the food chain in animal and human leads to cell dysfunctions [13,14]. As a result, it induces serious health problems, such as damage to brain, nervous system and kidneys due to permeability of Hg^{2+} ion through biological membranes [15]. The United State environmental protection agency (USEPA) has set the highest tolerable level of mercury in drinking water to be 2 ppb; this is due to the extreme toxicity of mercury ion [16].

Given these environmental and toxicological concerns, effort to create new sensitive and selective mercury detection strategies in different sources has been increased [17]. So, several classical analytical techniques for Hg^{2+} screening have been established, mainly includes anodic stripping voltammetry [18], inductively coupled mass spectroscopy, atom is emission and absorption spectroscopy, x-ray absorption and fluorescence, surface enhance roman spectroscopy etc. [19–23]. Though these techniques are selective and sensitive, the expensive instrumentation and necessitates for skilled manpower, controlled experimental conditions and time taking sample pre-treatment procedure make them disadvantageous. Apart from these classical analytical techniques, a variety of sensors have been proven to be powerful tools for detection of mercury ion to list some electrochemical sensors [24], DNA functionalized sensors [25], fluorescence sensors [26,27] and colorometric sensors [28–30] etc. among these sensors colorometric and fluorscence sensores are more attractive and widely investigated, this is due to their advantages like fast detection, nondestructive analysis high

sensitivity and selectivity, naked eye visual detection and operational simplicity [31–33]. Therefore, designing a new fluorometric/colorimetric mercury sensor with high selectivity and sensitivity in aqueous medium is highly recommended. Bearing this idea in mind, we designed and efficiently synthesized 3-oxo-[1,4]-benzothiazin-2-ylidene acetohydrazide, which is highly sensitive and selective colorimetric and fluorimetric mercury sensor.

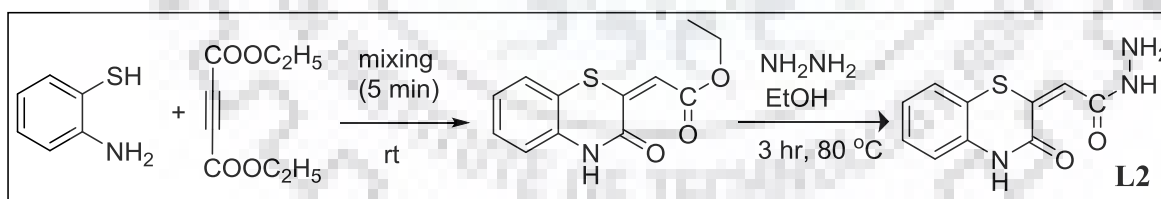
2.2 Experimental section

2.2.1 Materials and Reagents

2-aminothiophenol, diethyl-acetylenedicarboxylate and hydrazine hydrate were purchased and used without further purification all stock solutions of cations were prepared using their perchlorate. The NMR spectra were recorded in JEOL 400 MHz spectrophotometer and TMS as internal standard. Perkin-Elmer FT-IR 1000 spectrophotometer were used for IR spectra with the help of KBr solid film. Absorption and emission spectra were recorded using Specord S600 PC double beam spectrophotometer with cell of 1 cm path length and Horiba RF-5301 PC with 1 cm path length standard quartz cell. Inductively coupled plasma mass spectrometry (ICP-MS) was used for water sample analysis.

2.2.2 Synthesis of Chemosensor

Chemosensor was prepared in two steps [34–36].



Scheme 2.1. Synthesis of L2 (3-oxo-[1,4]-benzothiazin-2-ylidene acetohydrazide).

Synthesis of Ethyl (3-oxo-[1,4]Benzothiazin-2-ylidene)acetate: To 2-aminothiophenol (2 mmol), 2 mmol of diethyl-acetylenedicarboxylate was added slowly and mixed for 5 min with spatula, the homogeneous paste was allowed to stand at room temperature for 5 min to get to a yellow solid product; the product was collected and washed with ethanol to obtain analytically pure product in quantitative yield. The reaction progress was monitored by thin layer chromatograph (TLC).

Ethyl (3-oxo-[1,4]Benzothiazin-2-ylidene)acetate: ^1H NMR (400 MHz, CDCl_3) δ (ppm): 10.27 (s, 1H), 7.28 (d, $J = 8.3$ Hz, 1H), 7.20 (t, $J = 7.6$ Hz, 2H), 7.19 (s, 1H), 7.08 (t, $J = 8.0$ Hz, 1H), 7.02 (d, $J = 8.3$ Hz, 1H), 4.28 (q, $J = 7.6$, 2H), 1.34 (t, $J = 7.6$ Hz, 3H). ^{13}C NMR (100 MHz, CDCl_3) δ (ppm): 169.9, 156.0, 140.0, 138.0, 125.6, 124.1, 122.7, 117.0, 114.8, 91.1, 60.3, 14.2. (Figure 2.15-2.16).

Synthesis of 3-oxo-[1,4]-benzothiazin-2-ylidene acetohydrazide (L2): 2 mmol ethyl (3-oxo-[1,4]-benzothiazin-2-ylidene)acetate with hydrazine hydrate (2 mmol) in 4ml of ethanol was refluxed at 80 °C for 3 hr to get light yellow precipitate of 3-oxo-[1,4]-benzothiazin-2-ylidene acetohydrazide after completion of the reaction indicated by TLC the reaction mixture was cooled to room temperature and product was collected by filtration and washed with ethanol to obtain analytically pure product, Yield: 91%.

3-oxo-[1,4]-benzothiazin-2-ylidene acetohydrazide (L2): ^1H NMR (400 MHz, $\text{DMSO-}d_6$) δ (ppm): 11.60 (s, 1H), 9.14 (s, 1H), 7.28 (d, $J = 7.2$ Hz, 1H), 7.09 (m, 1H), 6.97 (t, $J = 7.2$ Hz, 1H), 6.88 (t, $J = 7.2$ Hz, 1H), 5.57 (s, 1H), 4.29 (s, 2H). ^{13}C NMR (100 MHz, $\text{DMSO-}d_6$) δ (ppm): 165.3, 149.8, 137.4, 135.5, 131.2, 122.9, 119.0, 116.5, 116.1, and 114.8. IR (KBr): λ_{max} 3377, 3298, 3063, 1612, 1586, 1471, 1443, 1303, 1244, 1154, 1021, 859, 751, 697, 545, 465 (Figure 2.17-2.19).

2.2.3 Absorbance Measurements

The photophysical properties of the chemosensor **L2** was studied through colorimetric and UV-visible absorption at room temperature in HEPES buffered solution ($\text{CH}_3\text{CN}:\text{H}_2\text{O}$, 1:2 v/v, pH 7.2). A stock solution of 1 mM of **L2** was prepared in CH_3CN and diluted to get 10 μM sample solution in HEPES buffered solution ($\text{CH}_3\text{CN}:\text{H}_2\text{O}$, 1:2 v/v, pH 7.2) and sample was analyzed by taking 3 ml of 10 μM **L2** followed by addition of 10 μL of aqueous stock (1mM) solution of the metal salts. Perchlorate salts of various metal ions such as Ag^+ , Mn^{2+} , Mg^{2+} , Na^+ , K^+ , Ca^{2+} , Ba^{2+} , Hg^{2+} , Cd^{2+} , Fe^{2+} , Cu^{2+} , Zn^{2+} , Co^{2+} , Al^{3+} , Sn^{2+} , and Ni^{2+} were used to investigate the photo chemical properties of **L2**.

2.2.4 Fluorescence Measurements

The photophysical properties of the chemosensor **L2** was studied through colorimetric and UV-visible absorption at room temperature in HEPES buffered solution ($\text{CH}_3\text{CN}:\text{H}_2\text{O}$, 1:2 v/v, pH 7.2). A stock solution of 1 mM of **L2** was prepared in CH_3CN and diluted to get 10 μM sample solution in HEPES buffered solution ($\text{CH}_3\text{CN}:\text{H}_2\text{O}$, 1:2 v/v, pH 7.2).

The fluorescence emission changes were monitored upon addition of 10 equivalents of different cations including Ag^+ , Mn^{2+} , Mg^{2+} , Hg^{2+} , Na^+ , K^+ , Ca^{2+} , Ba^{2+} , Cd^{2+} , Fe^{2+} , Cu^{2+} , Zn^{2+} , Cr^{3+} , Co^{2+} , Sn^{2+} , and Ni^{2+} in water to 3 mL of 10 μM solution of ligand in HEPES buffered solution ($\text{CH}_3\text{CN}:\text{H}_2\text{O}$, 1:2 v/v, pH 7.2). All fluorescence spectra were recorded using excitation wavelength of with the slit width of 2 nm.

2.2.5 Theoretical Study

The structural optimizations of the ligand and ligand- Hg^{2+} complexes were performed with Gaussian 09 program using the Density Functional Theory (DFT) method. All the calculations were performed in the gas phase with the hybrid functional B3LYP using the basis sets 6-31G(d,p) for C, H, N, O, and S of **L2** and LANL2DZ for **L2-Hg²⁺**.

2.3 Results and Discussion

2.3.1 Colorimetric and UV-visible Responses of **L2** to Hg^{2+} ion

L2 exhibited a characteristic peak at 340 nm in UV-visible absorbance spectrum. Upon addition of Hg^{2+} ion to the **L2** (10 μM) in HEPES buffered solution, absorbance at 340 nm was significantly enhanced and a new band centered at 550 nm with significant red shift of 110nm was appeared (Figure 2.1(a)), resulting drastic color change from light yellow into purple which can be easily detect by 'naked eye' which was entirely different from the other cations (Figure 2.2(a)). The binding titration of chemosensor **L2** with Hg^{2+} ion was also studied by absorbance titration, by adding different concentration of Hg^{2+} (0-3 equiva.) to **L2** (10 μM) solution and absorption band centered at 550 nm increased gradually (Figure 2.1(b)). The appearance of a new peak and radical color change indicated that the formation of new species, possibly charge transfer complex of **L2-Hg²⁺** the formation of charge transfer complex between **L2** and Hg^{2+} . In contrast, other cations did not exhibit any colorimetric or spectral change within **L2**.

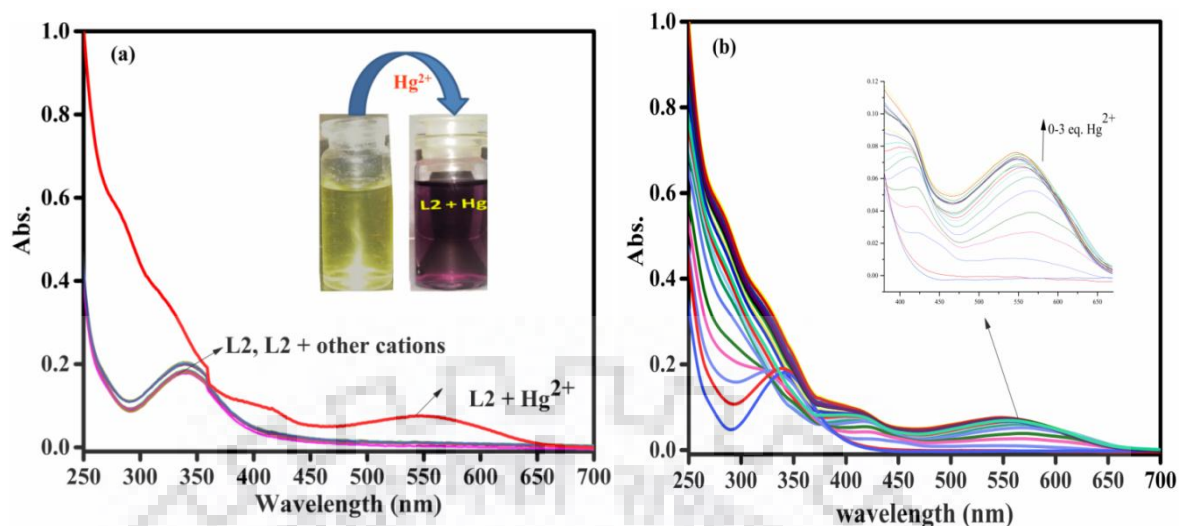


Figure 2.1 (a). Absorption spectra of **L2** in the presence of 10 equivalents various cations. (b). Absorption titration spectral responses of **L2** towards varying Hg^{2+} ion concentrations (0-3 eq.) Hg^{2+} ($10 \mu\text{M}$ of **L2** in HEPES buffered solution ($\text{CH}_3\text{CN}:\text{H}_2\text{O}$, 1:2 v/v, pH 7.2)).

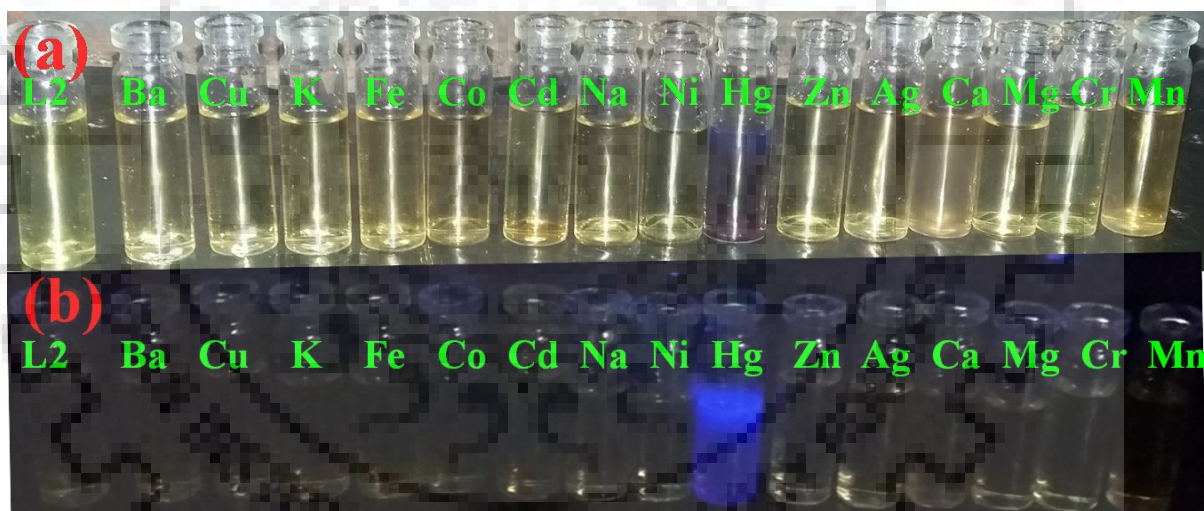


Figure 2.2 (a). Colourimetric. (b). fluorometric naked-eye detection of **L2** in the presence of different metal ions in HEPES buffered solution ($\text{CH}_3\text{CN}:\text{H}_2\text{O}$, 1:2 v/v, pH 7.2).

2.3.2 Fluorometric Responses of **L2** to Hg^{2+} ion

A weak fluorescent solution of **L2** was turned to strong fluorescent in the presence of Hg^{2+} ion, no significant change was observed upon addition of other tested metal ions except Hg^{2+} (Figure 2.3). the fluorescence change could be easily observed from the emission spectra by introducing Hg^{2+} into the solution of **L2** (1.0×10^{-5} M) in HEPES buffered solution ($\text{CH}_3\text{CN}:\text{H}_2\text{O}$, 1:2 v/v, pH 7.2). The emission peak of **L2** was appeared at 416 nm after gradual addition of Hg^{2+} (upto 4.0 equivalents), the emission peak at 416 nm leisurely shifted

to 429 nm along with extremely high enhancement in intensity (Figure 2.4) with a red shift of 13 nm. In addition, the enhancement of the fluorescence was observed by naked eye upon irradiation with long UV=light (Figure 2.2 (b)).

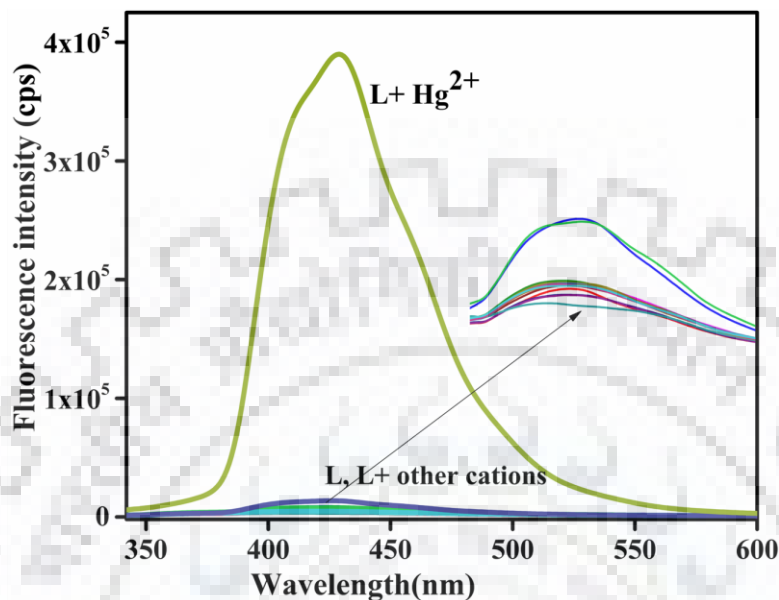


Figure 2.3 Fluorescence spectra of **L2** (10 μM in HEPES buffered solution ($\text{CH}_3\text{CN}:\text{H}_2\text{O}$, 1:2 v/v, pH 7.2) in the presence of 10.0 equiv. various cations.

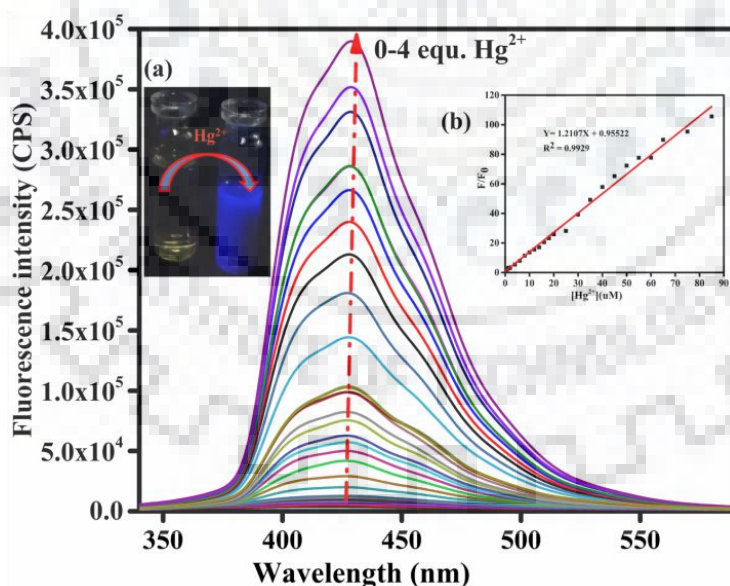


Figure 2.4 Fluorescence Emission spectral responses of **L2** (10 μM) towards varying concentration of Hg^{2+} (0-4 eq.) in HEPES buffered solution ($\text{CH}_3\text{CN}:\text{H}_2\text{O}$, 1:2 v/v, pH 7.2). (Inset: (a) visual fluorescence change of **L2** with Hg^{2+} (b). A good liner fit of Benesi-Hildebrand plot confirms the 1:1 stoichiometry.

2.3.3 Stoichiometry

Job's plot have been applied to inspect the stoichiometry of the **L2**+**Hg**²⁺ complex, the fluorescence intensities revealed a maximum at 0.5 mole fraction, which indicated a 1:1 binding stoichiometry (Figure 2.5(a)) with a good linear fit plot of Benesi-Hildebrand plot of $[\text{Hg}^{2+}]$ to change in fluorescence intensity of the sensor concomitant plot of $\log((I-I_0)/(I_{\text{max}}-I))$ to $\log[\text{Hg}^{2+}]$, is a straight line with slope of 0.96202 (Figure 2.5 (b)) this indicated the stoichiometry of **L2** to **Hg**²⁺ is 1:1 binding.

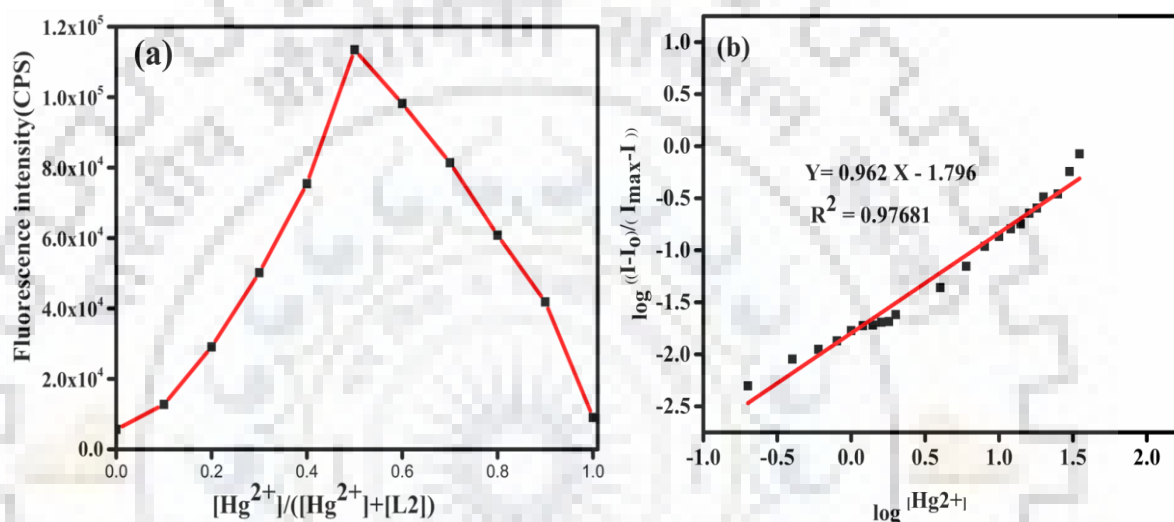


Figure 2.5 (a). Job's plot, (b). The plot of $\log((I-I_0)/(I_{\text{max}}-I))$ to $\log[\text{Hg}^{2+}]$ (μM in HEPES buffered solution ($\text{CH}_3\text{CN}:\text{H}_2\text{O}$, 1:2 v/v, pH 7.2))

2.3.4 Limit of Detection (LOD) and Association Constant (K_a)

Limit of detection (LOD)

The fluorescence titration data was used to calculate the limit of detection (LOD) [37–41]. The fluorescence intensity standard deviation of for the blank receptor was determined from 10 times measurement of fluorescence of blank receptor and the standard deviation of the blank receptor (**L2**) solution was found to be 80.57 (Table 2.1). From the linear fit graph of fluorescence intensity to concentration of **Hg**²⁺ we get slope 4.47×10^9 (Figure 2.6a).

Then the LOD of the receptors for sensing **Hg**²⁺ was determined from the following equation:

$$LOD = \sigma \times S.d/k$$

Where σ is 2 or 3 (in this case 3 was taken); SD is the standard deviation of the blank receptor (**L2**) K is slope of the linear fit in the titration experiment.

Thus using the above formula we get very low detection limit value of 5.4×10^{-8} M, which is sufficiently low to detect micro-molar concentration of Hg^{2+} by fluorescence technique.

Table 2.1 Fluorescence intensity and standard deviation of blank receptor (**L2**)

S.no.	Fluorescence intensity
1	4777.841
2	4815.693
3	4850.369
4	4855.337
5	4895.811
6	4912.887
7	4929.382
8	4981.604
9	5001.231
10	5018.887
Standard deviation	80.57029

The association constant (K_a)

The association constant (K_a) calculated by Benesi-Hildebrand linear regression analysis [42,43]. The association constant K_a was calculated from a plot of reciprocal of intensity difference ($1/\Delta I$), where $\Delta I = (I - I_0)$, against the reciprocal of concentration of mercury ion ($1/[\text{Hg}^{2+}]$) was plotted and the association constant was calculated from the following equation where association constant

$$K_a = \text{intercept/slope}$$

$$1/(I - I_0) = 1/(I_\infty - I_0)K_a[\text{Hg}^{2+}] + 1/(I_\infty - I_0)$$

The association constant (K_a) calculated by Benesi-Hildebrand linear regression analysis was found to be $1.938 \times 10^3 \text{ M}^{-1}$ (Figure 2.6(b)), advocating high binding affinity of **L2** towards Hg^{2+} .

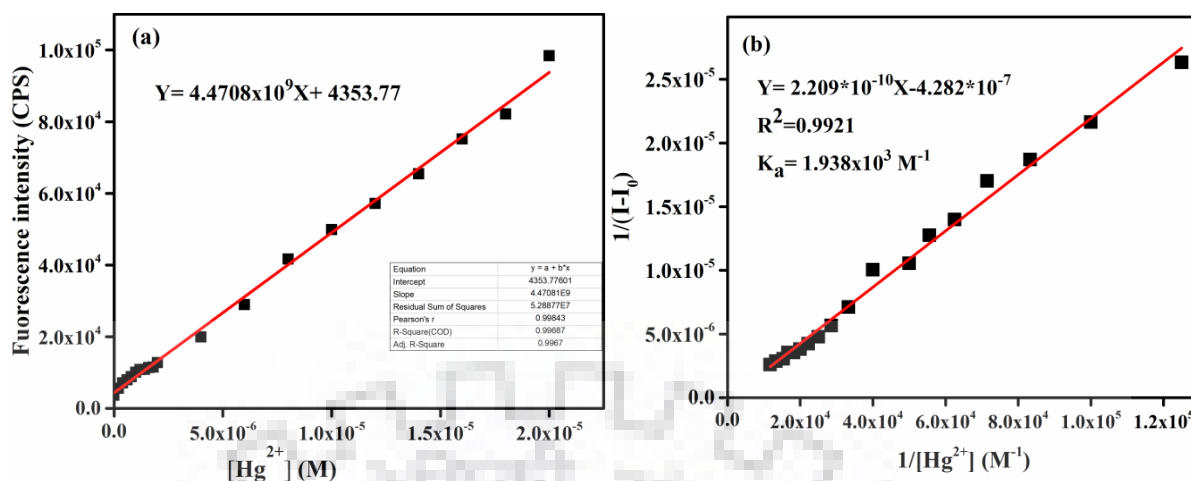


Figure 2.6 (a) Linear fit graph of **L2** with Hg^{2+} fluorescence titration. (b) Association constant calculation by Fluorescence titration method of **L2** with Hg^{2+} using linear regression analysis.

2.3.5 pH Selection

The pH value has enormous significance for the detection procedure. To determine the appropriate pH of the Hg^{2+} detection, the effect of pH on the fluorescence emission of **L2** in absence and presence of Hg^{2+} were investigated in a pH range of 1.0-12.0 (Figure 2.7). **L2** and **L2+Hg²⁺** showed stability in wide pH range of 3-10 which improved its practical applicability in the biological pH range.

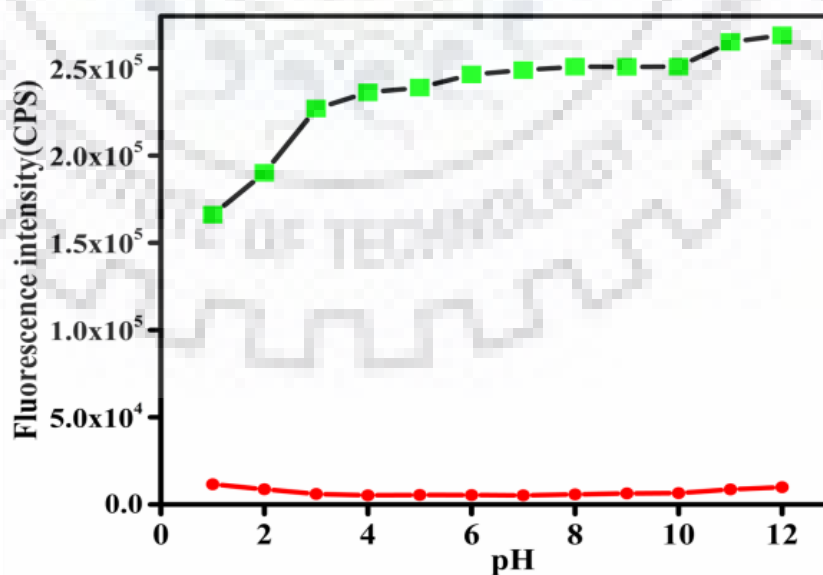


Figure 2.7 pH dependent fluorescence of **L2** and **L2-Hg²⁺**.

2.3.6 Selectivity Experiments

In order to check the practical applicability of the receptor **L2** for selective detection of Hg^{2+} ion, the selectivity of the fluorescence chemosensor was assessed by competitive experiment to determine the possible interferences of other cations. The competitive experiment of fluorescence changes of $10\ \mu\text{M}$ **L2** in HEPES buffered solution ($\text{CH}_3\text{CN}:\text{H}_2\text{O}$, 1:2 v/v, pH 7.2) solution in the presence of 1 equivalent of Hg^{2+} ion mixed with 10 equivalent of various metal ions was carried out including (Ag^+ , Mn^{2+} , Mg^{2+} , Na^+ , K^+ , Ca^{2+} , Ba^{2+} , Fe^{2+} , Cd^{2+} , Cr^{3+} , Cu^{2+} , Zn^{2+} , Co^{2+} , Al^{3+} , Sn^{2+} , and Ni^{2+}). The fluorescence enhancement of **L2** by addition of Hg^{2+} remained the same in the presence and absence of other interfering metals (Figure 2.8). All the results confirmed the selectivity and sensitivity of **L2** towards Hg^{2+} . In addition, to investigate the counter ions effect, we have checked **L2** with different Hg^{2+} salts other than $\text{Hg}(\text{ClO}_4)_2$ such as $\text{Hg}(\text{NO}_3)_2$, HgCl_2 , and $\text{Hg}(\text{SO}_4)_2$. Chemosensor **L2** emission intensity in all cases induced similar change (Figure 2.9). It demonstrated that the counter anions exerted no significant effect on Hg^{2+} sensing.

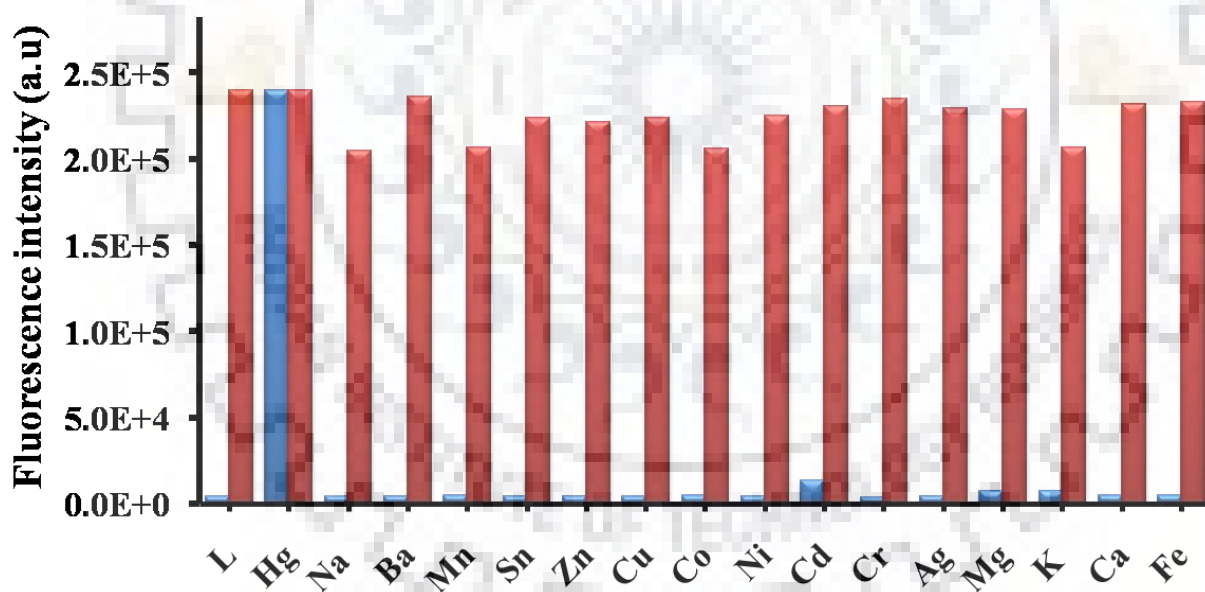


Figure 2.8 Interference effects of other metal ions in Hg^{2+} detection by **L2** ($10\ \mu\text{M}$) (blue bars represent the fluorescence intensity of **L2**+metal ions and red bars show the fluorescence intensity of **L2**+ Hg^{2+} + other metal ions in 1:1:10), ($\lambda_{\text{ex}} = 330\ \text{nm}$, $\lambda_{\text{em}} = 429\ \text{nm}$).

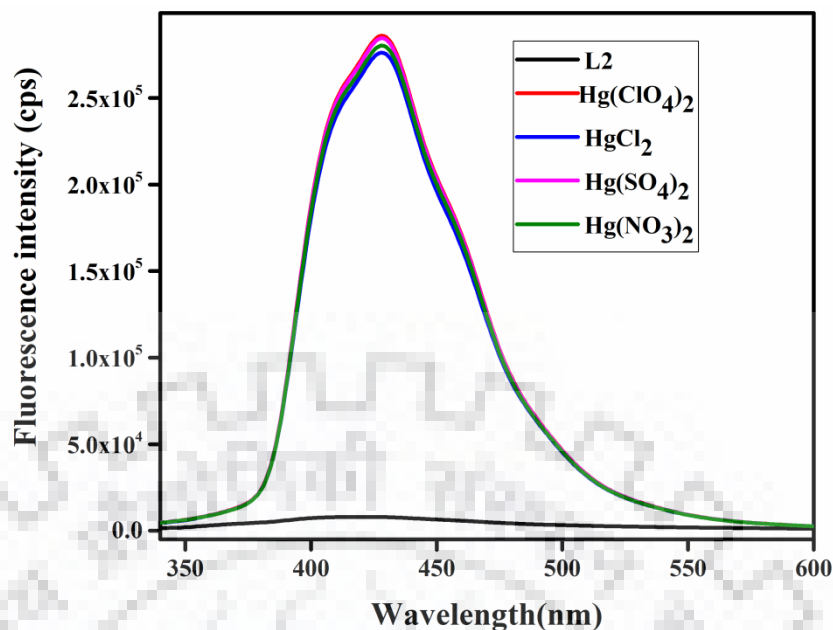


Figure 2.9 Fluorescence Emission responses of L2 (10 uM, in HEPES buffered solution (CH₃CN:H₂O, 1:2 v/v, pH 7.2) in the presence of different counter ions.

2.3.7 Theoretical Calculation

To understand the binding mechanism of **L2** to Hg²⁺, density functional theory (DFT) and time dependent DFT (TD-DFT) calculations were implemented using Gaussian 09 program. The geometries of **L2** and **L2-Hg²⁺** have been optimized by density functional theory (DFT) based on the hybrid B3LYP function combined with 6-31G (d) basis sets for **L2** and LanL2DZ method for **L2-Hg²⁺** [44]. TD-SCF calculations were conducted to provide more information about the electronic characters of **L2** and **L2-Hg²⁺**. In **L2**, the HOMO is spread all over the molecule; whereas the LUMO mostly localized on the hetero-atoms; and the main molecular orbital contribution to absorbance was of the 1st excited state from HOMO to LUMO transition with excitation energy of 355.45 nm and oscillator strength 0.2574 (Table 2.2). With the binding of Hg²⁺ the HOMO of complex is mainly laid in Hg²⁺ central metal ion and NH₂ and C=O moieties, but the LUMO is spread over entire molecule. The 2nd excited state was determined for the main molecular orbital contribution to absorbance was transition from HOMO to LUMO+1 (Figure 2.10) with excitation energy and oscillator strength of 550.82 nm and 0.0002 respectively (Table 2.2).

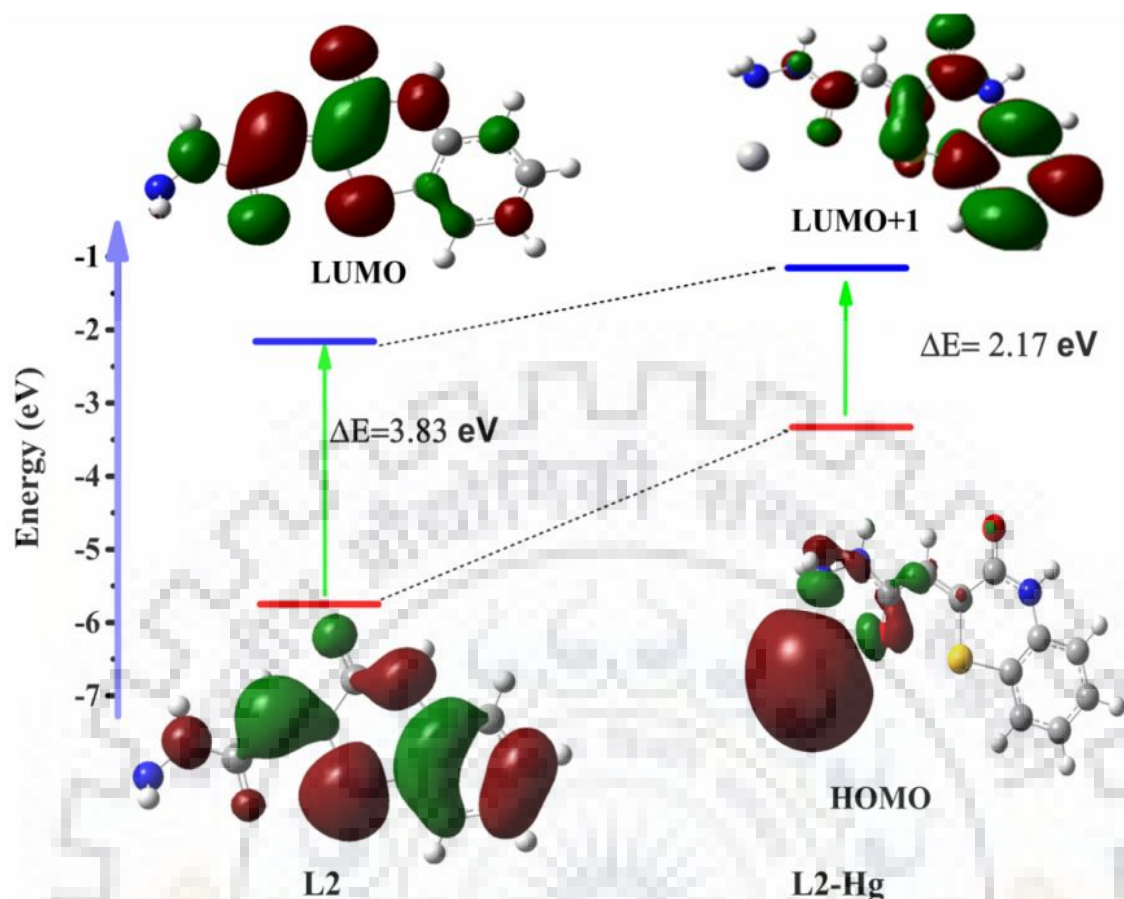


Figure 2.10 Molecular orbital diagrams and excitation energies of **L2** and **L2-Hg²⁺** complex.

Complex formation of **L2** with **Hg²⁺** destabilizes the HOMO and stabilizes the LUMO, this drop off HOMO-LUMO energy difference from 3.83 eV in **L2** to 0.75 eV in **L2-Hg²⁺** (Figure 2.11). This has been supported by red shifting of absorption band to longer wavelength on coordination with **Hg²⁺** (340 nm in **L2** shift to 550 nm in **L2-Hg²⁺**). The calculated absorption band was reliable with the experimental absorption data (Figure 2.12). Upon complexation with **Hg²⁺**, the intramolecular rotation of the sensor is restricted, which blocks the pathway for non-radiative decay and converts into strong emitters.

Table 2.2 The major electronic transition energies and molecular orbital contributions for **L2** and **L2-Hg²⁺**.

	Excited state		Theoretical Wavelength (nm)	Oscillator strength	Experimental (nm)
L2	1 st	HOMO to LUMO	355.45	0.2574	340
L2 + Hg²⁺	2 nd	HOMO to LUMO+1	550.82	0.0002	550

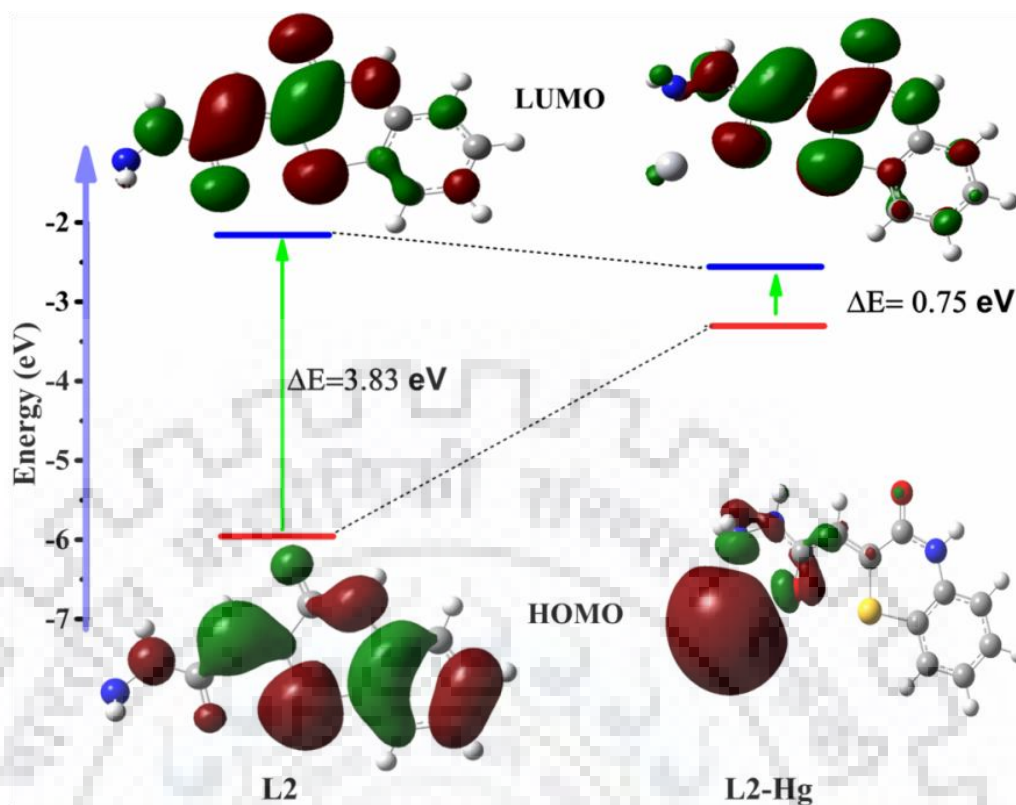


Figure 2.11 HOMO-LUMO band gaps of L2 and L2+Hg²⁺ optimized structures.

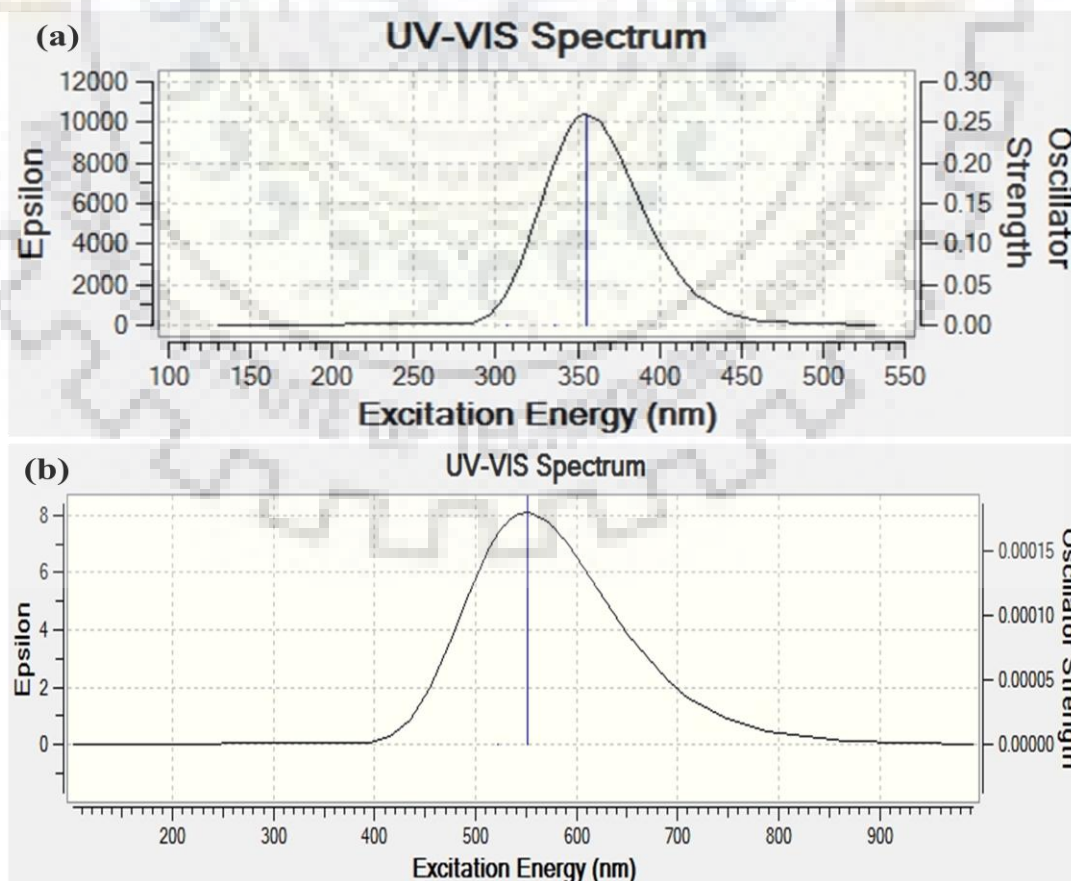
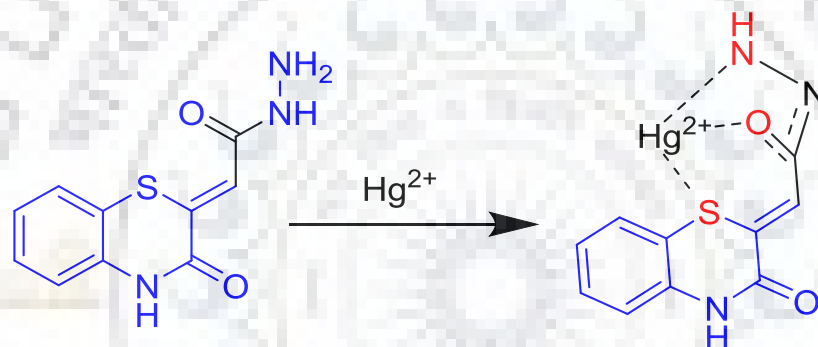


Figure 2.12 The theoretical excitation energies UV-vis spectrum of (a) L2, (b) L2+Hg²⁺.

2.3.8 Binding Nature of L2 and Hg²⁺ ion

Furthermore, the complex formation was established by using IR and ¹H-NMR. In the IR spectra, the hydrazide carbonyl peak at 1743 cm⁻¹ and N-H peaks at 3377 and 3298 cm⁻¹ of **L2** disappeared due to the interaction of Hg²⁺ which indicated that the interaction of nitrogen atoms and the hydrazide oxygen of ligand with Hg²⁺ (Figure 2.20(a)). In the ¹H NMR titration spectra of **L2** with Hg²⁺, the NH peak at 9.14 ppm disappear and NH₂ proton signal shift from 4.29 to 4.18 ppm upon the addition of Hg²⁺, this indicated that Hg²⁺ binds to NH, and NH₂. In addition to that, NH peak at 11.60 ppm shift to 10.64 ppm and all protons of the sensor showed shift because of the electropositive Hg²⁺ ion binding (Figure 2.20 (b)). The proposed structure of **L2** + Hg²⁺ complex is as shown in Scheme 2.2.



Scheme 2.2: proposed binding mechanism of **L2** with Hg²⁺

2.3.9 Reversibility Studies Applied as Logic Gate Circuit Devices

In order to understand the reusability of ligand, we study the chemical reversibility of the binding of **L2** to Hg²⁺. Addition of KI to **L2**-Hg²⁺ solution established good reversibility which was revealed by restoration of the original spectrum for **L2** up on KI addition in HEPES buffered solution (CH₃CN:H₂O, 1:2 v/v, pH 7.2). I⁻ ions have a strong affinity for Hg²⁺, and it causes de-metallation of **L2**-Hg²⁺ to HgI₂ or [HgI₄]²⁻ and regeneration of free sensor [11].

The solution of **L2**+Hg²⁺ complex displayed high reversibility in colorimetric and fluorimetric by I⁻ through Hg²⁺ displacement approach. This has been designated by purple to light yellow color change (Figure 2.13(a)) and fluorescence quenching with visual fluorometric change (Figure 2.13(b)) upon addition of KI to in situ generated **L2**-Hg²⁺ solution. This indicated that the free **L2** was regenerated from the complex (**L2**-Hg²⁺) which can be used for further sensing. This reversibility character advocated the promising usage of chemosensor **L2** as “off–on–off” naked eye and fluorescence sensor. Furthermore, the “off–

on-off” cycle was repeated several times by subsequent addition of Hg^{2+} and KI (Figure 2.13 (c)). Subsequently, the reversibility of the chemical sensor **L2** by KI has been used to build an INHIBIT logic gate on the basis of these two input signals, which can be symbolized as a combination of NOT and AND gates [45,46], using Hg^{2+} (input 1) and KI (input 2) and the fluorescence enhancement at 429 nm as an output (Figure 2.13 (d)).

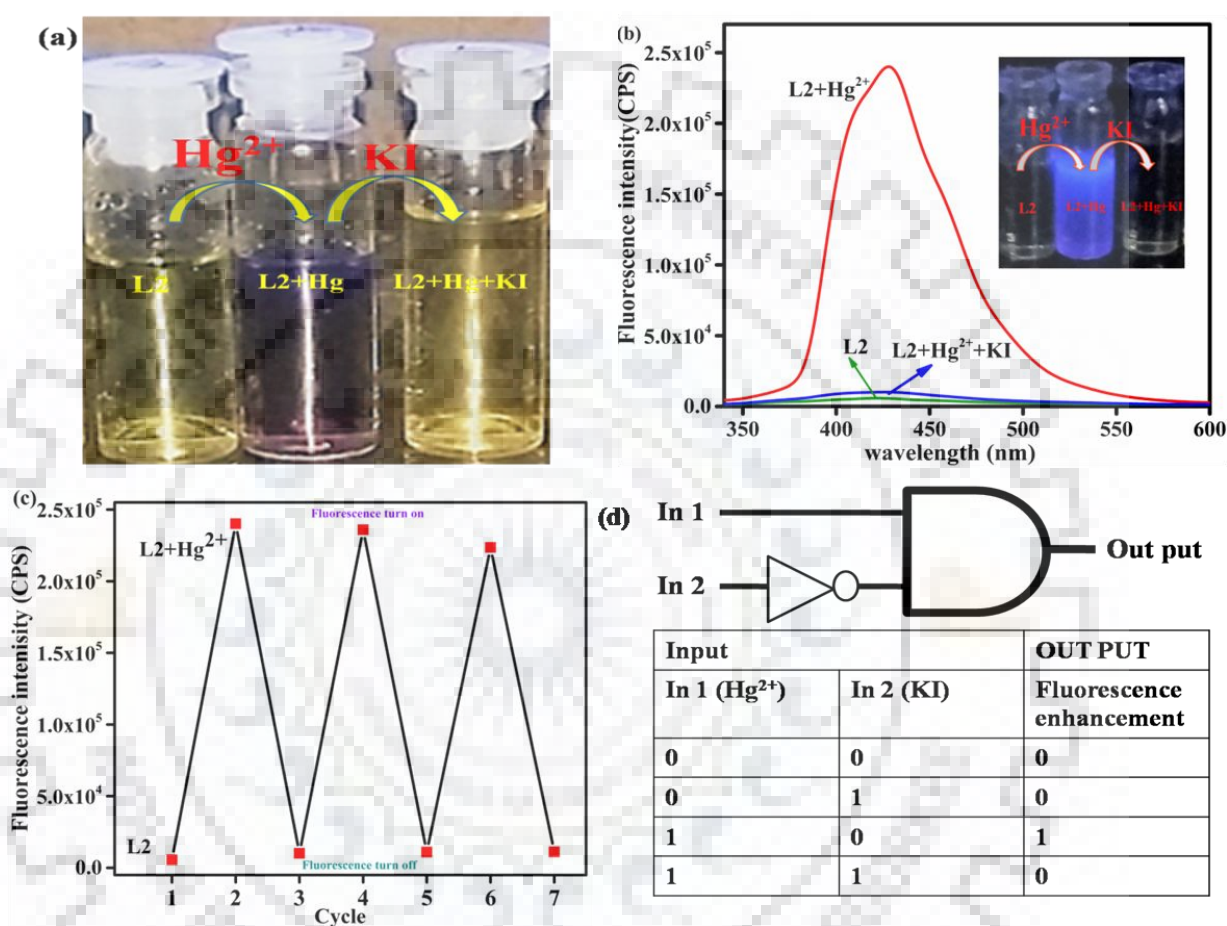


Figure 2.13 (a). Visual Colorimetric reversibility (b). Fluorescence reversibility of chemosensor **L2** upon sequential addition of Hg^{2+} and **KI**. (Inset: visual fluorometric reversibility) (c). number of cycles of reversibility of chemosensor upon sequential addition of Hg^{2+} and KI (d). Switch circuit diagram and Truth table corresponding to a logic gate based on Hg^{2+} and **KI**.

2.3.10 Analysis of Real Sample

To investigate the reliability and analytical applicability of chemosensor **L2**, **L2** was used for detection of Hg^{2+} ion in canal water and drain water samples, a standard addition method was used to eliminate matrix effect. A water sample from a Ganga canal and Khanjarpur drain water around Roorkee was filtered through a 0.2 μm nylon filter and used for analysis without

any further pre-treatment. 1 mL of the water samples were mingled with standard solutions of Hg^{2+} to prepare 3.0 mL solution at the range of 0.1-1.0 μM concentration in HEPES buffered solution ($\text{CH}_3\text{CN}:\text{H}_2\text{O}$, 1:2 v/v, pH 7.2). The mixtures were analyzed by fluorescence titration against **L2** solution (Figure 2.14). The Hg^{2+} concentrations were found to be 6.46×10^{-7} M and 5.58×10^{-7} M for canal water and drain water respectively. For further verification of accuracy of the method, the water samples were also analyzed by ICPMS; and the obtained results (Hg^{2+} concentration in canal water and drain water were 6.41×10^{-7} M and 5.55×10^{-7} M respectively) were in good agreement with calculated concentration from fluorescence analysis and it reveals the effectiveness of the chemosensor for Hg^{2+} ion detection In actual samples.

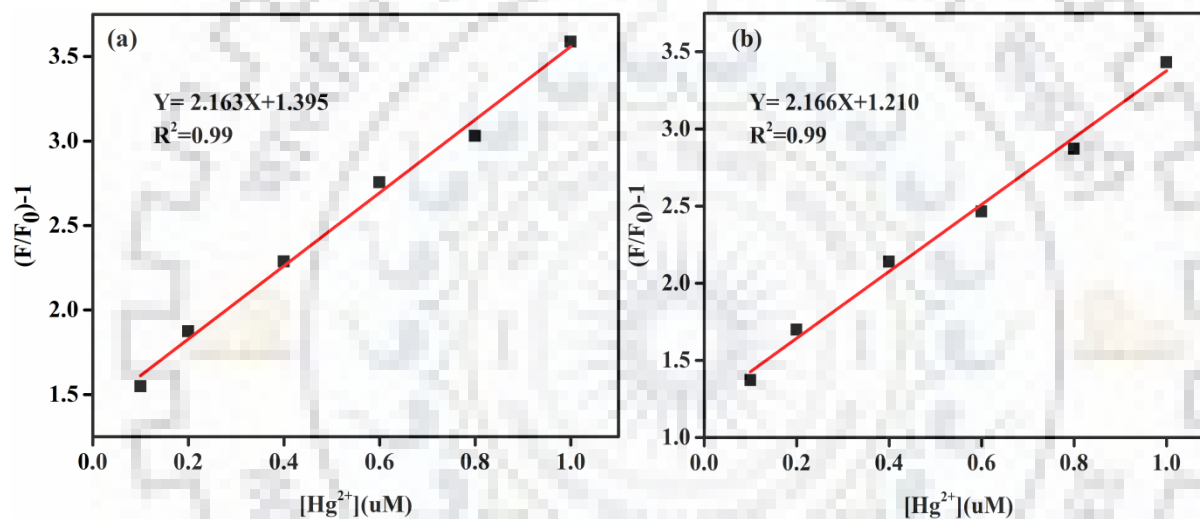


Figure 2.14 linear correlation between changes in fluorescence intensity and $[\text{Hg}^{2+}]$ in water samples spiked with different amount of $[\text{Hg}^{2+}]$ standard solutions in the standard addition experiments. (a) Canal water, (b) Drain water. ($[\text{L2}] = 10 \mu\text{M}$, $\lambda_{\text{ex}} = 330 \text{ nm}$, $\lambda_{\text{em}} = 429 \text{ nm}$).

2.4 Conclusion

We have prepared a highly reversible, selective and sensitive naked eye and Turn On fluorescence chemosensor for Hg^{2+} ion detection in aqueous medium. Addition of Hg^{2+} ion induced a new absorption band centered at 550 nm and clear color change from light yellow to purple accompanied by giant fluorescence emission enhancement. The prepared chemical sensor **L2** is highly selective for Hg^{2+} with detection limit of 5.4×10^{-8} M which is low enough for sensing sub-micromolar concentration of Hg^{2+} . The binding mode of chemosensor **L2** with Hg^{2+} was nicely demonstrated *via* DFT computer-based theoretical calculation, the theoretical studies supported this sensing process. **L2** was used for fast determination of Hg^{2+} ion in water samples and the result obtained from direct determination of Hg^{2+} in environmental sample without any further purification was adequately comparable with the corresponding ICP-MS result. Furthermore, the chemical sensor **L2** was reversible by KI, the original color and fluorescence intensity of **L2** was restored upon addition of KI solution to the **L2**- Hg^{2+} solution and the “off–on–off” reversible has been used to build the logic gate method.

Spectral characterization of intermediate, L2, and L2+Hg²⁺ by NMR and

IR

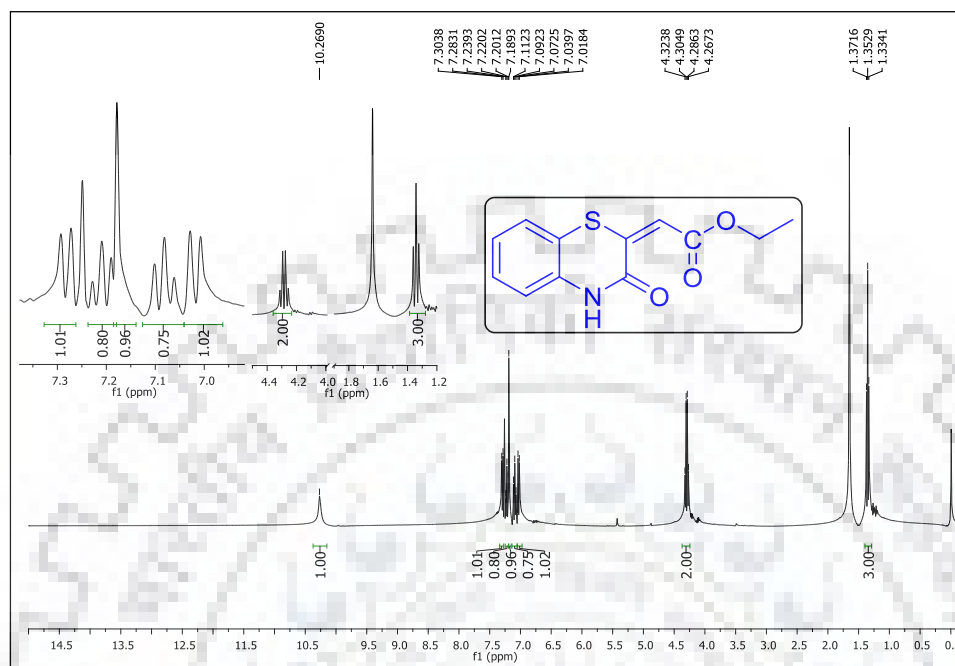


Figure 2.15 ¹H-NMR spectrum of Ethyl (3-oxo-[1,4]Benzothiazin-2-ylidene)acetate in CDCl₃.

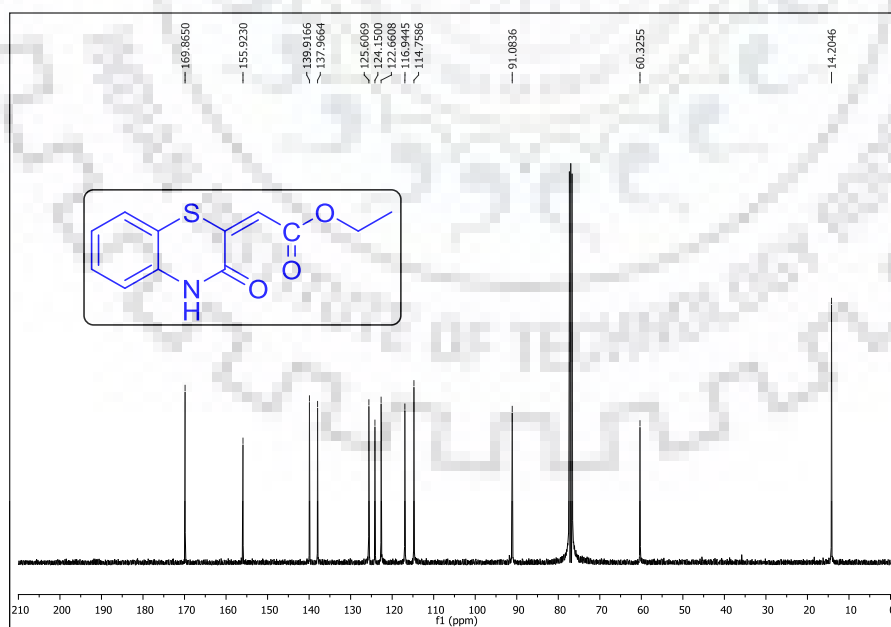


Figure 2.16 ¹³C-NMR spectrum of Ethyl (3-oxo-[1,4]Benzothiazin-2-ylidene)acetate in CDCl₃.

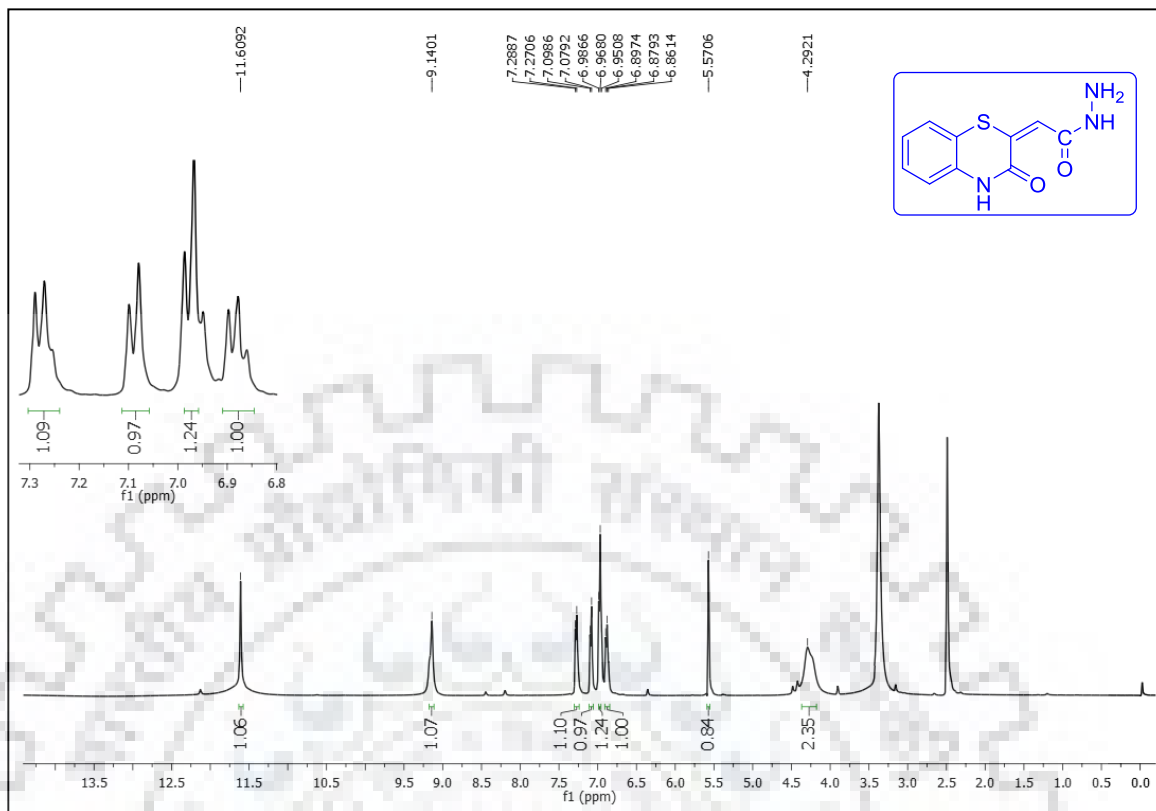


Figure 2.17 $^1\text{H-NMR}$ spectrum of L2 in $\text{DMSO-}D_6$

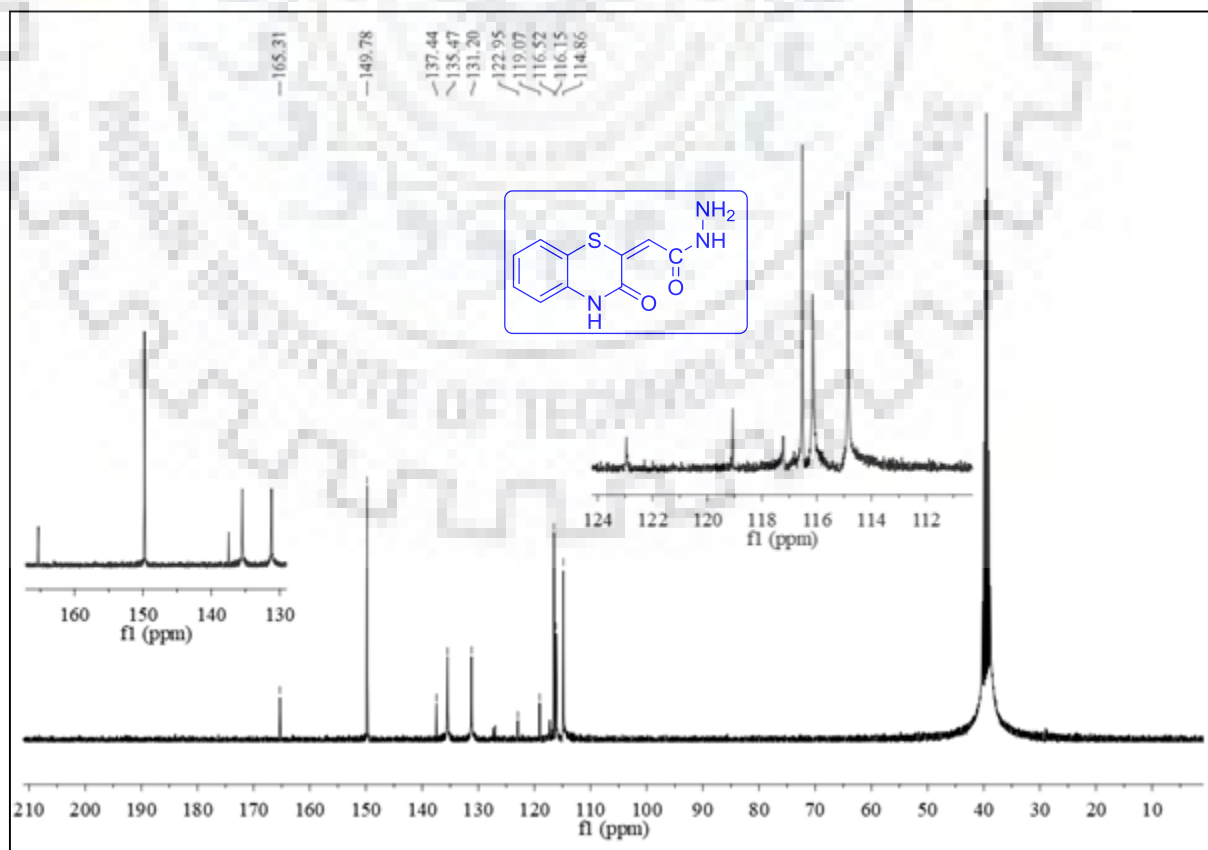


Figure 2.18 $^{13}\text{C-NMR}$ spectrum of L2 in $\text{DMSO-}D_6$

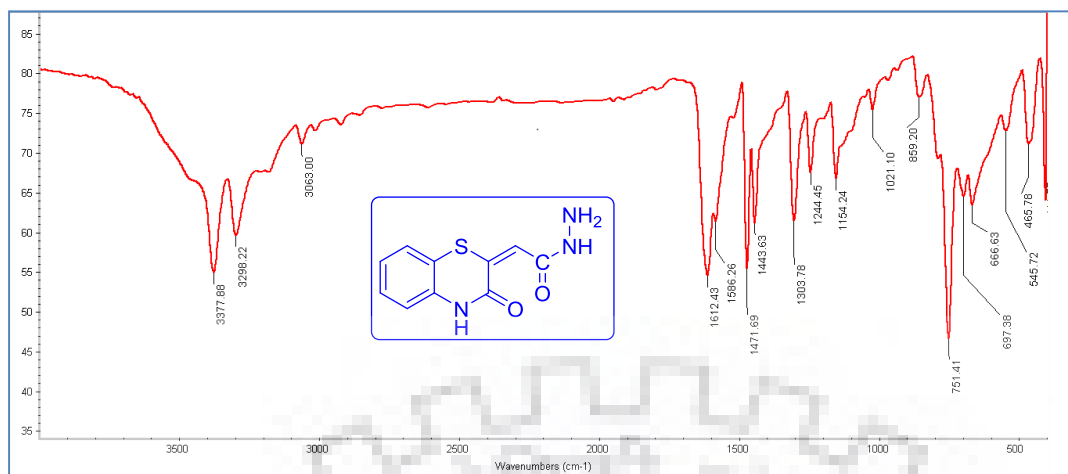


Figure 2.19 FT-IR spectrum of L2 in KBr pellet.

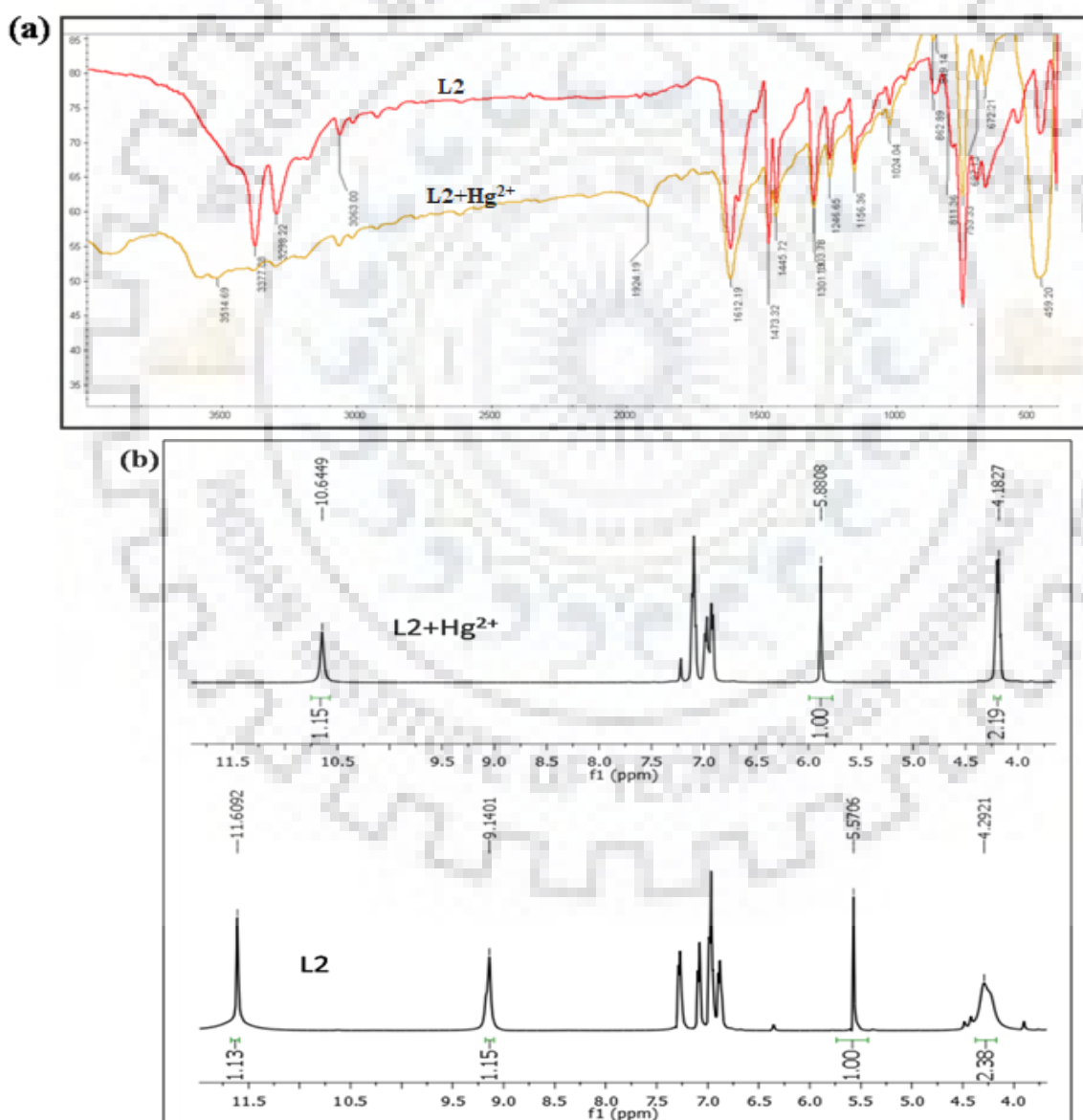


Figure 2.20 (a) FT-IR spectrum of L2 and L2 +Hg²⁺ in KBr pellet, (b) ¹H-NMR titration of L2 and L2 +Hg²⁺ in DMSO-*D*₆.

2.5 References

- [1] H.N. Kim, W.X. Ren, J.S. Kim, J. Yoon, Fluorescent and colorimetric sensors for detection of lead, cadmium, and mercury ions, *Chem. Soc. Rev.* 41 (2012) 3210–3244. doi:10.1039/C1CS15245A.
- [2] L.E. Santos-Figueroa, M.E. Moragues, E. Climent, A. Agostini, R. Martínez-Máñez, F. Sancenón, Chromogenic and fluorogenic chemosensors and reagents for anions. A comprehensive review of the years 2010–2011, *Chem. Soc. Rev.* 42 (2013) 3489. doi:10.1039/c3cs35429f.
- [3] M.E. Moragues, R. Martínez-Máñez, F. Sancenón, Chromogenic and fluorogenic chemosensors and reagents for anions, *Chem. Soc. Rev.* 40 (2011) 2593–2643. doi:10.1039/c0cs00015a.
- [4] S. Goswami, A.K. Das, S. Maity, ‘PET’ vs. ‘push–pull’ induced ICT: a remarkable coumarinyl-appended pyrimidine based naked eye colorimetric and fluorimetric sensor for the detection of Hg^{2+} ions in aqueous media with test strips, *Dalton Trans.* 42 (2013) 16259. doi:10.1039/c3dt52252k.
- [5] R. Martínez-Máñez, F. Sancenón, Fluorogenic and chromogenic chemosensors and reagents for anions, *Chem. Rev.* 103 (2003) 4419–4476. doi:10.1021/cr010421e.
- [6] X. Gan, W. Li, C. Li, Z. Wu, D. Liu, B. Huang, H. Zhou, Y. Tian, Two analogously structural triphenylamine-based fluorescent “off-on” probes for Al^{3+} *via* two distinct mechanisms and cell imaging application, *Sensors Actuators, B Chem.* 239 (2017) 642–651. doi:10.1016/j.snb.2016.08.042.
- [7] Renzoni, F. Zino, E. Franchi, Mercury levels along the food chain and risk for exposed populations, *Environ. Res.* 77 (1998) 68–72. doi:10.1006/enrs.1998.3832.
- [8] M. Suresh, S. Mishra, S.K. Mishra, E. Suresh, A.K. Mandal, A. Shrivastav, A. Das, Resonance energy transfer approach and a new ratiometric probe for Hg^{2+} in aqueous media and living organism, *Org. Lett.* 11 (2009) 2740–3. doi:10.1021/ol900810q.
- [9] P. Mahato, A. Ghosh, S. Saha, S. Mishra, S.K. Mishra, A. Das, Recognition of Hg^{2+} using diametrically disubstituted cyclam unit, *Inorg. Chem.* 49 (2010) 11485–11492. doi:10.1021/ic1014797.
- [10] E.M. Nolan, S.J. Lippard, Tools and tactics for the optical detection of mercuric ion, *Chem. Rev.* 108 (2008) 3443–3480. doi:10.1021/cr068000q.
- [11] P. Xie, F. Guo, L. Wang, S. Yang, D. Yao, G. Yang, A dansyl-rhodamine ratiometric fluorescent probe for Hg^{2+} based on FRET mechanism, *J. Fluoresc.* 25 (2015) 319–325.

doi:10.1007/s10895-015-1511-7.

- [12] F. Di Natale, A. Lancia, A. Molino, M. Di Natale, D. Karatza, D. Musmarra, Capture of mercury ions by natural and industrial materials, *J. Hazard. Mater.* 132 (2006) 220–225. doi:10.1016/j.jhazmat.2005.09.046.
- [13] C.M.L. Carvalho, E.H. Chew, S.I. Hashemy, J. Lu, A. Holmgren, Inhibition of the human thioredoxin system: A molecular mechanism of mercury toxicity, *J. Biol. Chem.* 283 (2008) 11913–11923. doi:10.1074/jbc.M710133200.
- [14] T. Zhang, B. Kim, C. Levard, B.C. Reinsch, G. V. Lowry, M.A. Deshusses, H. Hsu-Kim, Methylation of mercury by bacteria exposed to dissolved, nanoparticulate, and microparticulate mercuric sulfides, *Environ. Sci. Technol.* 46 (2012) 6950–6958. doi:10.1021/es203181m.
- [15] T.W. Clarkson, L. Magos, G.J. Myers, The Toxicology of Mercury Current Exposures and Clinical Manifestations, *N. Engl. J. Med.* 349 (2003) 1731–1737. doi:10.1056/NEJMra022471.
- [16] U. States, E.P.F. shit Agency, Fact Sheet Mercury Update : Impact on Fish Advisories, 2001. doi:http://www.epa.gov/ost/fish/listing.html U.S.
- [17] A. Ben Othman, W.L. Jeong, J.S. Wu, S.K. Jong, R. Abidi, P. Thuéry, J.M. Strub, A. Van Dorsselaer, J. Vicens, Calix[4]arene-based, Hg²⁺-induced intramolecular fluorescence resonance energy transfer chemosensor, *J. Org. Chem.* 72 (2007) 7634–7640. doi:10.1021/jo071226o.
- [18] J. Li, H. Wang, Z. Guo, Y. Wang, H. Ma, X. Ren, B. Du, A “turn-off” fluorescent biosensor for the detection of mercury (II) based on graphite carbon nitride, *Talanta*. 162 (2017) 46–51. doi:10.1016/j.talanta.2016.09.066.
- [19] H.T. Wang, B.S. Kang, T.F. Chancellor, T.P. Lele, Y. Tseng, F. Ren, S.J. Pearton, W.J. Johnson, P. Rajagopal, J.C. Roberts, E.L. Piner, K.J. Linthicum, Fast electrical detection of Hg(II) ions with AlGaN/GaN high electron mobility transistors, *Appl. Phys. Lett.* 91 (2007) 42114–421143. doi:10.1063/1.2764554.
- [20] K. Leopold, M. Foulkes, P. Worsfold, Methods for the determination and speciation of mercury in natural waters A review, *Anal. Chim. Acta.* 663 (2010) 127–138. doi:10.1016/j.aca.2010.01.048.
- [21] A. Bernaus, X. Gaona, J.M. Esbrí, P. Higuera, G. Falkenberg, M. Valiente, Microprobe techniques for speciation analysis and geochemical characterization of mine environments: The mercury district of Almadén in Spain, *Environ. Sci. Technol.* 40 (2006) 4090–4095. doi:10.1021/es052392l.

- [22] T. Senapati, D. Senapati, A.K. Singh, Z. Fan, R. Kanchanapally, P.C. Ray, Highly selective SERS probe for Hg(II) detection using tryptophan-protected popcorn shaped gold nanoparticles, *Chem. Commun. (Camb)*. 47 (2011) 10326–10328. doi:10.1039/c1cc13157e.
- [23] Y. Chen, L. Wu, Y. Chen, N. Bi, X. Zheng, H. Qi, M. Qin, X. Liao, H. Zhang, Y. Tian, Determination of Mercury(II) by surface-enhanced Raman scattering spectroscopy based on thiol-functionalized silver nanoparticles, *Microchim. Acta*. 177 (2012) 341–348. doi:10.1007/s00604-012-0777-6.
- [24] T.Z.J. Gong, D. Song, L. Zhang, X. Hu, Stripping Voltammetric Detection of Mercury(II) Based on a Bimetallic Au–Pt Inorganic–Organic Hybrid Nanocomposite Modified Glassy Carbon Electrode, *Anal. Chem.* 82 (2010) 567–573. doi:10.1021/ac901846a.
- [25] Z. Guo, J. Duan, F. Yang, M. Li, T. Hao, S. Wang, D. Wei, A test strip platform based on DNA-functionalized gold nanoparticles for on-site detection of mercury (II) ions, *Talanta*. 93 (2012) 49–54. doi:10.1016/j.talanta.2012.01.012.
- [26] Shaliy, A. Kumar, N. Ahmed, Indirect Approach for CN⁻ Detection: Development of “Naked-Eye” Hg²⁺-Induced Turn-Off Fluorescence and Turn-On Cyanide Sensing by the Hg²⁺ Displacement Approach, *Ind. Eng. Chem. Res.* 56 (2017) 6358–6368. doi:10.1021/acs.iecr.7b00188.
- [27] X. Lu, Z. Guo, M. Feng, W. Zhu, Sensing Performance Enhancement via Acetate-Mediated N-Acylation of Thiourea Derivatives: A Novel Fluorescent Turn-On Hg²⁺ Chemodosimeter., *ACS Appl. Mater. Interfaces*. (2012). doi:10.1021/am300751p.
- [28] Y.R. Kim, R.K. Mahajan, J.S. Kim, H. Kim, Highly sensitive gold nanoparticle-based colorimetric sensing of Mercury(II) through simple ligand exchange reaction in aqueous Media, *ACS Appl. Mater. Interfaces*. 2 (2010) 292–295. doi:10.1021/am9006963.
- [29] L. Chen, L. Chan, X. Fu, W. Lu, Highly sensitive and selective colorimetric sensing of Hg²⁺ based on the morphology transition of silver nanoprisms, *ACS Appl. Mater. Interfaces*. 5 (2013) 284–290. doi:10.1021/am3020857.
- [30] A. Kumar, Sahaliy, N. Ahmed, ‘Naked-eye’ colorimetric/fluorimetric detection of F⁻ ions by biologically active 3-((1H-indol-3-yl)methyl)-4-hydroxy-2H-chromen-2-one derivatives, *RSC Adv.* 6 (2016) 108105–108112. doi:10.1039/c6ra24597h.
- [31] P. Srivastava, S.S. Razi, R. Ali, R.C. Gupta, S.S. Yadav, G. Narayan, A. Misra, Selective naked-eye detection of Hg²⁺ through an efficient Turn-On photoinduced

- electron transfer fluorescent probe and its real applications, *Anal. Chem.* 86 (2014) 8693–8699. doi:10.1021/ac501780z.
- [32] K. Kanagaraj, K. Bavanidevi, T.J. Chow, K. Pitchumani, Selective “turn-off” fluorescent sensing of mercury ions using aminocyclodextrin:3-hydroxy-N-phenyl-2-naphthamide complex in aqueous solution, *RSC Adv.* 4 (2014) 11714. doi:10.1039/c3ra45837g.
- [33] D. Singhal, N. Gupta, A.K. Singh, Chromogenic ‘naked eye’ and fluorogenic ‘Turn On’ sensor for mercury metal ion using thiophene-based Schiff base, *RSC Adv.* 5 (2015) 65731–65738. doi:10.1039/C5RA11043B.
- [34] G. Choudhary, R.K. Peddinti, Introduction of a clean and promising protocol for the synthesis of β -amino-acrylates and 1,4-benzoheterocycles: an emerging innovation, *Green Chem.* 13 (2011) 3290. doi:10.1039/c1gc15701a.
- [35] Y.A. Ammar, M.M.F. Ismail, M.K. Ibrahim, H.S.A. El-Zahaby, 3-thoxycarbonylmethylenequinoxalin-2-one in heterocyclic synthesis. Part 1: Synthesis of new substituted and condensed quinoxalines, *Afinidad.* 62 (2005).
- [36] K. Tokimatsu, Y. Yoshimi, K. Ariizumi, NII-Electronic Library Service, *Soils Found.* 30 (1990) 153–158. doi:10.1248/cpb.37.3229.
- [37] Y. Yang, T. Cheng, W. Zhu, Y. Xu, X. Qian, Highly selective and sensitive near-infrared fluorescent sensors for cadmium in aqueous solution, *Org Lett.* 13 (2011) 264–267. doi:10.1021/ol102692p.
- [38] Z. Su, K. Chen, Y. Guo, H. Qi, X.F. Yang, M. Zhao, A coumarin-based fluorescent chemosensor for Zn^{2+} in aqueous ethanol media, *J. Fluoresc.* 20 (2010) 851–856. doi:10.1007/s10895-010-0628-y.
- [39] W. Lin, L. Yuan, Z. Cao, Y. Feng, L. Long, A Sensitive and Selective Fluorescent Thiol Probe in Water Based on the conjugate 1,4- addition of thiols to α , β Unsaturated ketones, *Chem. Eur. J.* 15 (2009) 5096–5103. doi:10.1002/chem.200802751.
- [40] G.L. Long, J.D. Winefordner, Limit of Detection: A Closer Look at the IUPAC Definition, *Anal. Chem.* 55 (1983) 712A–724A. doi:10.1021/ac00258a001.
- [41] A. Caballero, R. Martinez, V. Lloveras, I. Ratera, J. Vidal-Gancedo, K. Wurst, A. Tarraga, P. Molina, J. Veciana, Highly selective chromogenic and redox or fluorescent sensors of Hg^{2+} in aqueous environment based on 1,4-disubstituted azines, *J. Am. Chem. Soc.* 127 (2005) 15666–15667. doi:10.1021/ja0545766.
- [42] H.A. Benesi, J.H. Hildebrand, A Spectrophotometric Investigation of the Interaction of Iodine with Aromatic Hydrocarbons, *J. Am. Chem. Soc.* 71 (1949) 2703–2707.

doi:10.1021/ja01176a030.

- [43] P. T. Chou, G. R. Wu, C. Y. Wei, C. C. Cheng, C. P. Chang, F. T. Hung, Excited-State Amine–Imine Double Proton Transfer in 7-Azaindoline, *J. Phys. Chem. B.* 104 (2000) 7818–7829. doi:10.1021/jp001001g.
- [44] T. Chatterjee, S. Areti, M. Ravikanth, Synthesis, Structure, and Hg²⁺ ion Sensing Properties of Stable Calixazasmaragdyrins, *Inorg. Chem.* 54 (2015) 2885–2892. doi:10.1021/ic503028k.
- [45] W. Zhai, C. Du, X. Li, A series of logic gates based on electrochemical reduction of Pb(2+) in self-assembled G-quadruplex on the gold electrode., *Chem. Commun. (Camb).* 1 (2014) 2–4. doi:10.1039/c3cc47763k.
- [46] V.K. Gupta, A.K. Jain, S.K. Shoor, New “on–off” optical probe based on Schiff base responding to Al³⁺ ions: Logic gate application, *Sensors Actuators B Chem.* 219 (2015) 218–231. doi:10.1016/j.snb.2015.05.026.







Chapter 3

A Novel 1,8-Naphthalimide as Highly Selective Naked-Eye and Ratiometric Fluorescent Sensor for Detection of Hg^{2+} ion

Bahta, M.; Ahmed, N. *J. Photochem. Photobiol. A Chem.* **2019**, *373*, 154–161.

DOI: 10.1016/j.jphotochem.2019.01.009.



3.1 Introduction

Industrialization has been tremendously accelerating in recent years throughout the world. Consequently, it gave rise to serious air pollution and discharges toxic heavy metal ions, which ultimately accumulate in human bodies through food chain [1]. Mercury pollution is a serious hazard to our environment. It finds its way into water through point-source discharges with its environmentally mobile and prevalent form [2,3]. Inorganic mercury ion and metallic mercury can be easily converted into methyl-mercury (CH_3Hg^+) by micro-organisms [4] which is the main source of organic mercury and more noxious form of mercury ion [5,6] thereby it builds up in aquatic organisms and consequently accumulates in higher organisms through the food chain [7]. The extreme toxicity of Hg^{2+} instigates from its strong affinity to thio moieties of proteins and enzymes [8,9] causing dys-function of cells and consequently leads to many health problems. Exposure to trace amount of mercury ions can cause serious damages [10] to prenatal brains, nervous system [11,12] the endocrine system [13] immune system [14] and other biological systems. Therefore, concerns about the serious toxic damages of mercury ion have provoked these arching of reliable and fast with high selectivity and sensitivity method of detection for mercury ion and many mercury-ion sensors have been recently reported, yet environmentally benign, operationally simple mercury sensor with high selectivity and sensitivity in real samples is still urgent.

Due to low cost instrumentation, rapid detection, high selectivity, sensitivity and relatively simple handling, a fluorescent probes are widely used as powerful tools to detect cations, anions, and neutral molecules [15,16]. Owing to their photo-physical properties, such as high fluorescence quantum yields and inherent photo-stability, 1,8-naphthalimides are extensively used as colorimetric and fluorometric probes [17–19]. The optical and photo-physical properties of N-aryl-1,8-naphthalimides are very sensitive to substitutes in the 1,8-naphthalimides ring or that of the N-aryl moiety [20–22]. This feature has been extensively applied in designing and preparation of colorimetric and fluorometric chemosensors based on 1,8-naphthalimide [18,23–27]. Chemosensors with free thiol or sulphur moieties in their metal receptor unit are highly selectivity for Hg^{2+} due to high binding affinity of Hg^{2+} for soft sulphur donors. Hence, various explorations of thiol based fluorescent Hg^{2+} sensors have been developed [28–30]. Based on the above ideas, the conjugation of 1,8-naphthalimide fluorophores with thiol as Hg^{2+} receptor part is promising development for designing of a new fluorescent Hg^{2+} sensor. The measurement of emission intensities at two different

wavelengths is an important aspect of ratiometric fluorescent probes which make them more attractive over intensity-based probes [31]. Ratiometric fluorescent probes are not influenced by microenvironment, concentration of probe, excitation light intensity, *etc.* This eliminates major limitation of intensity based probes, *via* the ratio of two emissions at different wavelengths [25,26,32–35]. Though, wide-ranging of 1,8-naphthalimide based chemosensors with a different substituent in the 1,8-naphthalimides rings have been reported, a simple dual colorimetric and ratiometric mercury sensor is still imperative.

In this study, we present a new sensitive colorimetric and dual ratiometric chemosensor **L3** for selective recognition of Hg^{2+} , by integration of 1,8-naphthalimide with a 2-mercapto-phenyl moiety in which the amide and thiol groups are responsible for the specific recognition of Hg^{2+} . The synthesis of **L3** is a straight forward involving single step amidation of 1,8-naphthalic anhydride to achieve the desired chemosensor. And this chemosensor was found to detect Hg^{2+} with reasonable selectivity and sensitivity against several competing metal ions. Moreover the chemosensor gives adequately comparable results with corresponding data from inductively coupled plasma mass spectrometry (ICP-MS) for applications in direct determination of Hg^{2+} in water samples.

3.2 Experimental Section

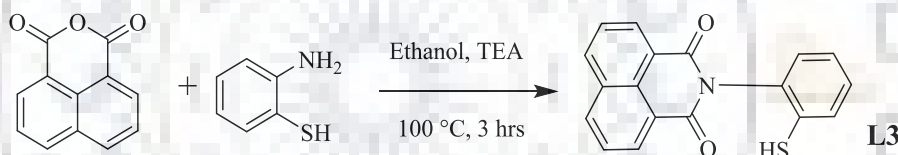
3.2.1 Reagents and Instrumentation

Stock solutions of all cations were prepared using their corresponding perchlorates purchased from Himedia and Loba Chemie, India. Spectroscopic grade MeCN and deionized water was used for photophysical experiments. IR spectra were recorded with the KBr pellet on the Alpha-FTIR spectrometer BRUKER in the range 4000-400 cm^{-1} . $^1\text{H-NMR}$ and $^{13}\text{C-NMR}$ spectra of compounds were recorded in CDCl_3 on a Bruker spectrosin DPX 500 MHz spectrometry with TMS internal standard were used, and the chemical shift were reported as parts per million (ppm) scale downfield from TMS. The multiplicities were reported as abbreviations *viz* s= singlet, d= doublet, t= triplet and m = multiplet. Absorption and emission spectra were recorded using Specord S600 PC double beam spectrophotometer with cell of 1 cm path length and Horiba RF-5301 PC with 1 cm path standard quartz cell. Melting points was measured by Optimelt melt system. The fluorescence quantum yield was calculated using FLS 980 fluorescence spectrometry (Edinburgh Instruments). Fluorescence life cycle was recorded by HORIBA jobin Yvon, fluorocube lifetime system and ICP-MS was used for water sample analysis.

3.2.2 Synthesis and Characterization of Chemosensors

To a stirring suspension of 1,8-naphthalicanhydride (1 mmol) in ethanol (5ml), 2-aminobenzenethiol (1.2 mmol) and 10 drops of triethylamine were added and the resulting suspension was stirred at 100 °C for 3hrs (Scheme 3.1). As such, when the reaction is completed as indicated by thin-layer chromatography (TLC), it was cooled down to room temperature with stirring. The solid precipitate product was filtered and washed with ethanol [36]. A white solid was obtained in 80% yield; the structure of **L3** was characterized by IR, ¹H-NMR, ¹³C-NMR, and HRMS spectroscopy (Figure 3.16-3.19).

2-(2-mercaptophenyl)-1H-benzo[de]isoquinoline-1, 3-(2H)-dione (L3): white solid, 80% yield; M.P: 210.6 °C; IR (KBr, $\bar{\nu}/\text{cm}^{-1}$): 2518 (-SH), 1702, 1662 (N-C=O), 1587, 1376, 1354 (C=C aromatic frame); ¹H NMR (500 MHz, CDCl₃, δ/ppm): 8.70 (d, $J = 7.2$ Hz, 2H), 8.32 (d, $J = 8.1$ Hz, 2H), 7.84 (t, $J = 7.7$ Hz, 2H), 7.63 (d, $J = 7.7$ Hz, 1H), 7.45-7.39 (m, 2H), 7.32 (d, $J = 7.7$ Hz, 1H), 3.33 (s, 1H). ¹³C NMR (125 MHz, CDCl₃, δ/ppm): 163.7, 135.3, 134.5, 132.8, 131.8, 130.1, 129.8, 129.6, 128.7, 127.8, 127.1, 122.6 HRMS (ESI+) m/z calcd. C₁₈H₁₁NO₂S [M]⁺: 305.0510 found 305.1574.



Scheme 3.1. Synthesis of chemosensor **L3**.

3.2.3 Absorbance and Fluorescence Experiments

Stock solution of **L3** (1.0 mM) was prepared in CH₃CN and then sample solution of **L3** (10 μM) was prepared in MeCN/H₂O (1:1 v/v, PH 7.0, HEPES buffer) in quartz cuvette followed by 10 μl aqueous solution (1mM) perchlorates salt metal ions (Na⁺, K⁺, Mg²⁺, Ba²⁺, Mn²⁺, Zn²⁺, Cu²⁺, Co²⁺, Ni²⁺, Ag⁺, Al³⁺, Fe²⁺, Fe³⁺, Pb²⁺, Cd²⁺, Cr³⁺, and Hg²⁺), all emission experiments were carried out with slit width of 2 nm and excitation wave length of 320 nm.

3.2.4 Theoretical Study

The optimization of the structure of the ligand and ligand-Hg²⁺ complexes and their absorption energy and oscillation strength (f) calculation were carried out with Gaussian 09 program by density functional theory (DFT) and time-dependent density functional theory (TD-DFT) methods. All calculations were carried out in gas phase with B3LYP hybrid function and 6-31G (d) basis set for **L3** and LANL2DZ for **L3-Hg²⁺** complex. And the long range corrected functionality CAM-B3LYP, using 631+G(d,p) basis set for **L3** and LANL2DZ method for **L3-Hg²⁺** complex.

3.3 Results and Discussion

3.3.1 Naked-eye Selectivity

The naked-eye recognition properties of **L3** were studied toward different metal ions by colorimetric and fluorescence methods. The colorless solution of **L3** turned into yellowish green colour and non-fluorescence to bright yellowish green fluorescent with Hg^{2+} , no significant colour change was observed in the presence of other examined metal ions (Figure 3.1). These results clearly show that **L3** can be used for selective naked-eye detection of Hg^{2+} ion in normal light and under UV-lamp.

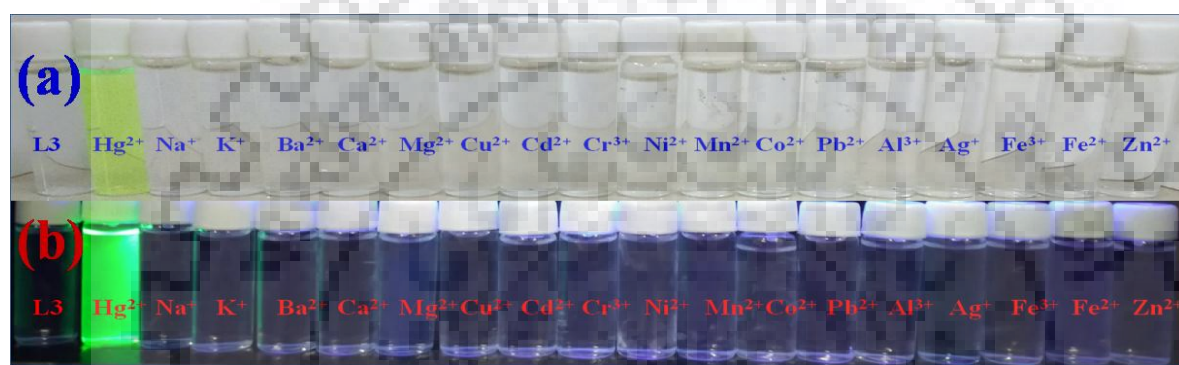


Figure 3.1 A visual features of detection of Hg^{2+} with **L3** in the presence of 10 equivalent of different cations in $\text{CH}_3\text{CN}:\text{H}_2\text{O}$ (1:1 v/v, pH 7.0, HEPES buffer). (a). in sun light and (b). under UV-lamp. (b). under UV lamp.

3.3.2 Spectroscopic Studies

The chemosensor **L3** exhibits a strong absorbance centered at 332 nm and relatively weaker fluorescence emission at 376 nm ($\lambda_{\text{ex}}=320$ nm). In order to investigate the optical sensing competence of the chemosensor the photo-physical studies were performed in the presence of 10 equivalent of different metal ions (Na^+ , K^+ , Mg^{2+} , Ba^{2+} , Mn^{2+} , Zn^{2+} , Cu^{2+} , Co^{2+} , Ni^{2+} , Ag^+ , Al^{3+} , Fe^{2+} , Fe^{3+} , Pb^{2+} , Cd^{2+} , Cr^{3+} , and Hg^{2+}). These experiments disclose that only Hg^{2+} ion imposes significant change in the photophysical character of **L3**, while there were no reactions from other metal ions. Upon adding different concentration of Hg^{2+} (0-10 equiv.) **L3** solution, the absorption intensity centered at 332 nm decrease coupled with swift increasing and a new absorption band centered at 438 nm with isosbestic point at 356 nm emerges (Figure 3.2a). Similarly in fluorescence spectra a progressive enhanced emission at 480 nm and a corresponding modest decrease in 376 nm with an isoemission point at 427 nm (Figure 3.4b), which indicated clear ratiometric absorbance and fluorescence changes. It is known that when Hg^{2+} chelating with O, S moiety, a bathochromic shift in both emission and absorption

is predictable [37], as expected when Hg^{2+} is binding to the amide oxygen, and thiol group of the chemosensor. It shows 106 nm and 104 nm red shift in absorption and emission spectra respectively, due to coordination of metal to the receptor. This indicates the opening of intramolecular charge transfer (ICT) mechanism in the chemical sensor after coordination with Hg^{2+} [23,24,38–40]. Besides this, no significant change was revealed in the absorbance or fluorescence of **L3** on the addition of other metal ions (Figure. 3.3).

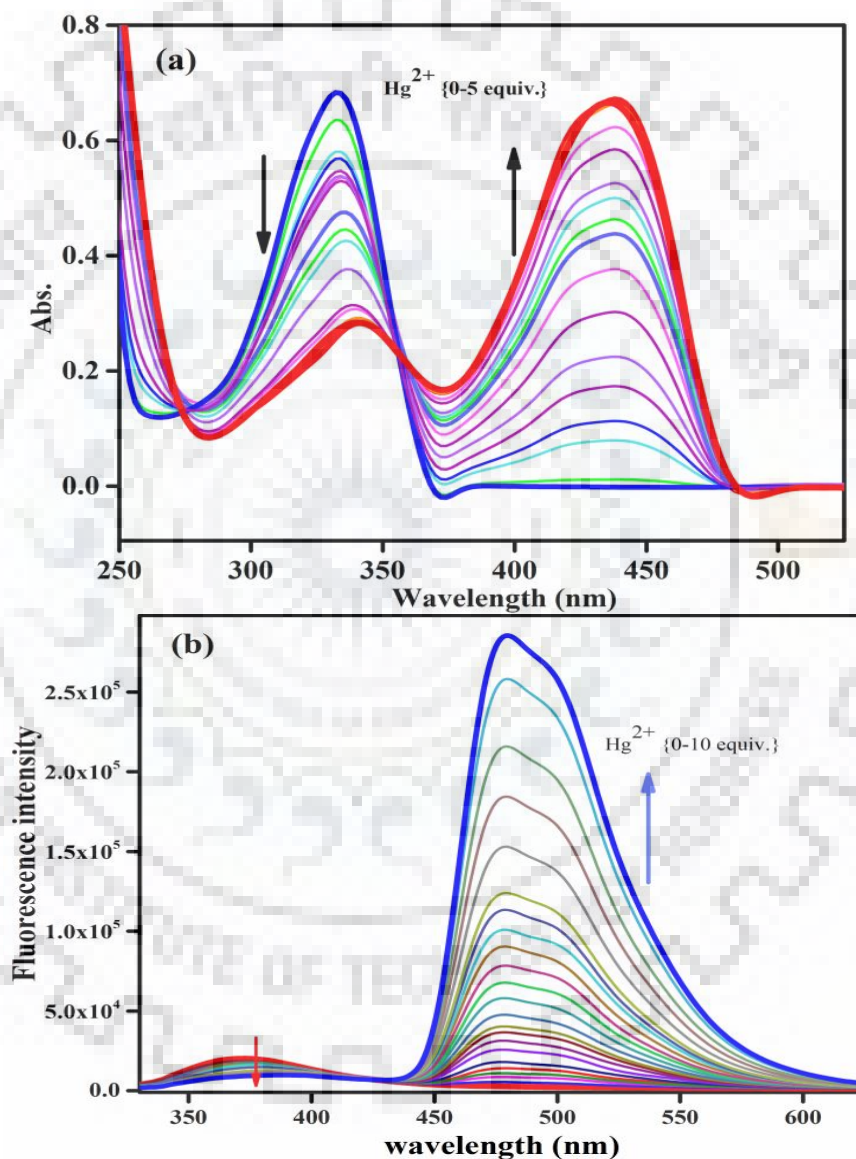


Figure 3.2 (a). Absorption titrations spectral responses of **L3** (10 μM) towards varying Hg^{2+} ion concentration (0-5 equiv.), (b). Fluorescence Emission spectral responses of **L3** (10 μM) towards varying Hg^{2+} ion concentration (0-10 equiv.)(in MeCN/ H_2O (1:1 v/v, PH 7.0, HEPES buffer)).

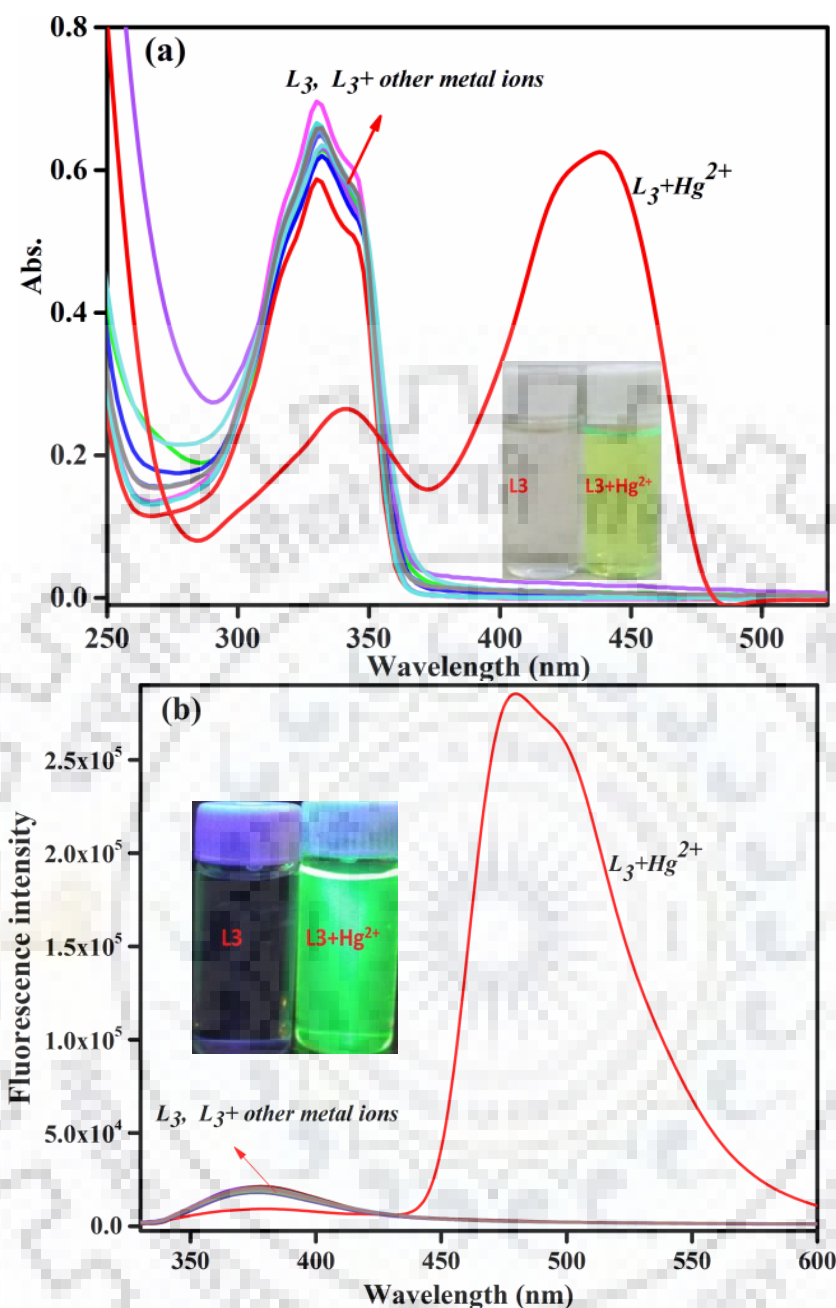


Figure 3.3 (a). Absorption spectra (b). Fluorescence Emission spectra of **L3** (10 μM) in the presence of 10 equiv. different metal ions (in MeCN/H₂O (1:1 v/v, PH 7.0, HEPES buffer)).

Based on the spectral results, the Turn-On fluoresce mechanism of **L3**-Hg²⁺ is probably as follows: before the addition of Hg²⁺, the intramolecular rotation of **L3** was free that weakened the intramolecular charge transfer (ICT) shows a weak fluorescence emission ($\Phi_F = 0.01$). After binding of Hg²⁺ to the amide oxygen, and the thiol group of the sensor, the intramolecular rotation of the chemosensor restricted which opens the intramolecular charge transfer (ICT) state and displays a very strong fluorescence ($\Phi_F = 0.81$).

3.3.3 Stoichiometry

The Job's plot of absorption ratio (A_{438}/A_{332}) and fluorescence intensity ratio (I_{480}/I_{376}) (Figure 3.4) that is dependent on the complex formation was plotted as a function of the mole fractions of Hg^{2+} to determine the stoichiometry between **L3** and Hg^{2+} and the maximum of the plot was obtained at 0.5 mole fraction both plots, which indicates that the formation of 1:1 stoichiometry between **L3** and Hg^{2+} [41]. The stoichiometry was studied by HRMS, the mass of **L3**+ Hg^{2+} complex has appeared at 546.2862 (Figure 3.20) and Cal. [**L3**+ Hg^{2+} + $\text{CH}_3\text{CN}-2\text{H}$] $^+$ is 546.0315. This advocates the stoichiometry of **L3** to Hg^{2+} is 1:1 binding.

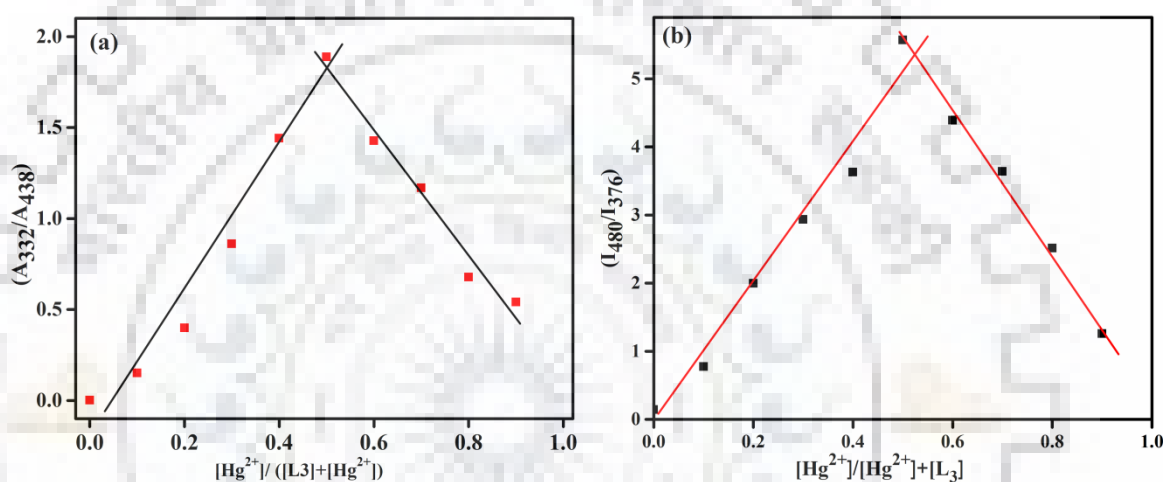


Figure 3.4 Job's plot (a) absorption, (b) fluorescence (the total concentration were 10 mM in MeCN/ H_2O (1:1 v/v, PH 7.0, HEPES buffer)

3.3.4 Limit of Detection (LOD) and Association Constant (K_a)

Limit of detection (LOD)

The detection limit was calculated based on a fluorescence titration and standard deviation of the ligand fluorescence intensity ratio (I_{480}/I_{376}). The fluorescence emission of ligand was measured 5 times, and the standard deviation of the fluorescence intensity ratio was calculated, and the emission intensity ratio from the titration experiment in the presence of increasing Hg^{2+} concentrations was plotted as a function of the Hg^{2+} concentration to determine the slope. The fluorescence intensity ratio (I_{480}/I_{376}) fit into straight line as give in (Figure 3.5a) and the slope of linear fit graph was used to calculate the detection limit using the following equation according to the IUPAC definition [42,43] and found to be 1.74×10^{-8} M.

$$LOD = 3 \cdot \sigma / K$$

Where σ is the standard deviation of blank receptor L3 standard solution, and K is the slope of the liner graph.

$$LOD = 3 \cdot 0.0023 / 4.025 = 0.017 \cdot 10^{-6} \text{ molar}$$

Table 3.1 Fluorescence intensity and standard deviation of blank receptor (L3)

S.no.	I ₃₇₆	I ₄₈₀	I ₄₈₀ /I ₃₇₆
1	2685.724	18073.73	0.148598
2	2564.019	18020.42	0.142284
3	2624.872	18047.07	0.145446
4	2594.446	18033.74	0.143866
5	2609.659	18040.41	0.144656
	STDEV		0.002341

Association constant (K_a): the Benesi-Hildebrand plot between The linearity of Benesi-Hildebrand plot between $1/(I - I_0)$ to $1/[\text{Hg}^{2+}]$ supports the 1:1 stoichiometry. The values of association constant (K_a) was calculated from the slope of the liner graph at 376 nm were $3.89 \times 10^4 \text{ mol}^{-1}\text{L}$ (Figure 3.5b), high K_a value indicates strong binding of ligand to metal [27,44], the calculated K_a was good enough to form strong complex between L3 and Hg²⁺ ion.

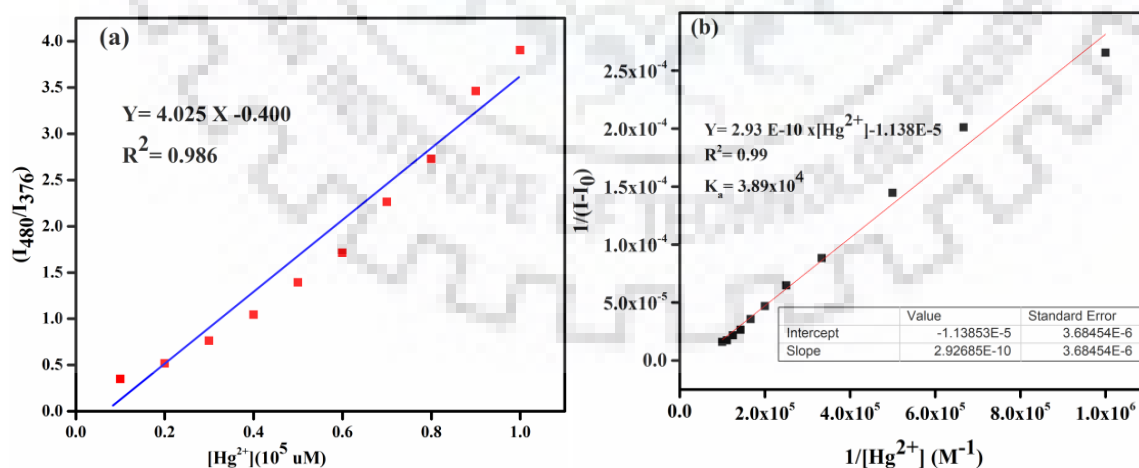


Figure 3.5 (a). The linear fit graph of fluorescence intensity ratio (I_{480}/I_{376}) as a function of Hg²⁺ ion concentration. (b). Benesi-Hildebrand plot of L3 (10 μM) binding with Hg²⁺. (in MeCN/H₂O (1:1 v/v, PH 7.0, HEPES buffer).

3.3.5 Fluorescence Lifetime

For further support of the new absorption and emission enhancement is obtained from the absorbance and fluorescence experiment and to get more insight into the coordination of **L3** with Hg^{2+} , time-resolved decays of **L3** were carried out in the absence and presence of Hg^{2+} ($\lambda_{\text{ex}}=320$ nm) the decay was monitored at 376 and 480 nm. As shown in figure 3.6, after the addition of Hg^{2+} , the fluorescence lifetime of **L3** at 376 nm was decreased from 1.63 ns to 1.55 ns, and increased to 5.74 ns at 480 nm. These results validate the red shift in the absorbance and fluorescence experiments, and fluorescence quenching at 376 and enhancement at 480 nm. From this outcome, the fluorescence enhancement at 480 nm could be due to blocking of intramolecular rotation of **L3** by formation of rigid complex on binding to Hg^{2+} which slams the non radiative relaxation path way and opens the radiative relaxation.

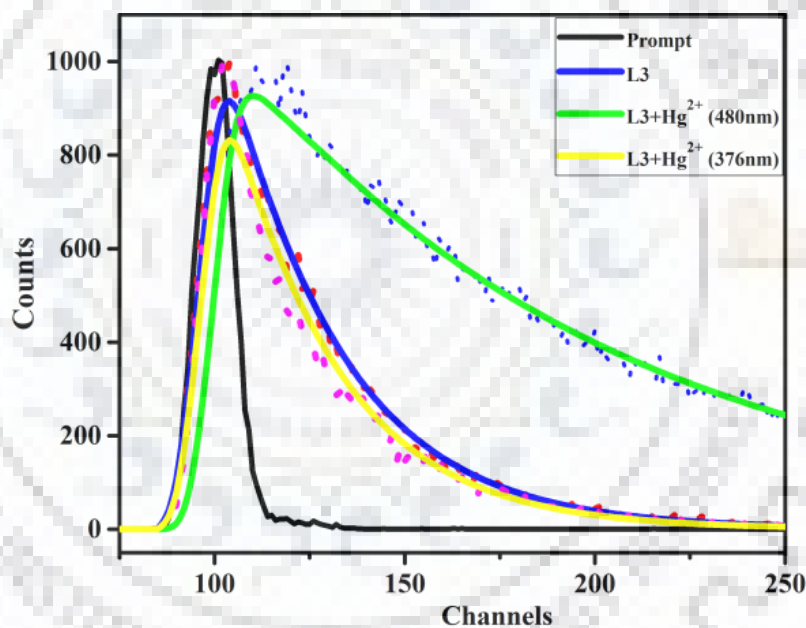


Figure 3.6 Life time decay profile of **L3** in the absence and presence of Hg^{2+} . (in MeCN/ H_2O (1:1 v/v, PH 7.0, HEPES buffer) $\lambda_{\text{ex}} = 320$ nm)

3.3.6 Selectivity Studies

In order to evaluate the selectivity of **L3** for Hg^{2+} ion, we investigated the fluorescence change of **L3** towards Hg^{2+} ion, via treating **L3** with 1 equivalent of Hg^{2+} blend with 10 equivalents various metal ions. As shown in Figure 3.7, the presence of other competitive metal ions did not induce a significant change in the ratiometric fluorescence emission (I_{480}/I_{376}) of **L3**- Hg^{2+} . From this, we can conclude that **L3** exhibited an excellent selectivity towards Hg^{2+} in the presence of potential interfering metal ions. Additionally, to investigate

the counter ions effect, we have checked **L3** with different Hg^{2+} salts other than $\text{Hg}(\text{ClO}_4)_2$ such as $\text{Hg}(\text{ClO}_4)_2$ such as $\text{Hg}(\text{NO}_3)_2$, HgCl_2 and $\text{Hg}(\text{SO}_4)_2$. Chemosensor **L3** emission ratio (I_{480}/I_{376}) in all cases induced similar change (Figure 3.8). It confirmed that the Hg^{2+} sensing is not affected by counter anions.

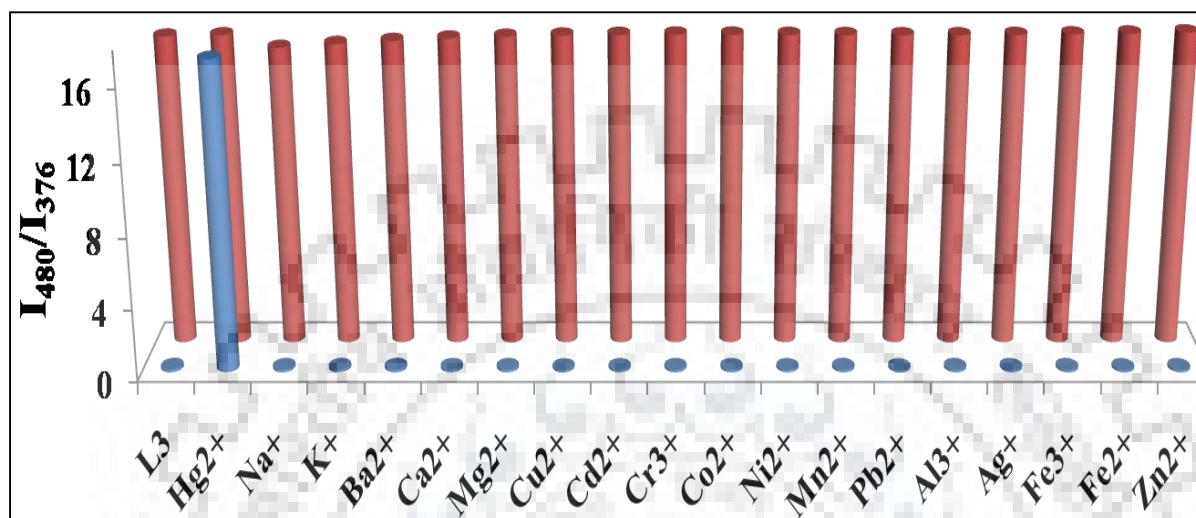


Figure 3.7 Interference effect of various cations with **L3**- Hg^{2+} in emission spectra (blue bar for fluorescence intensity ratio (I_{480}/I_{376}) of **L3**+cations (1:10 equiv.) and red bars show fluorescence intensity of **L3**+ Hg^{2+} +other cations (1:1:10 equiv.)

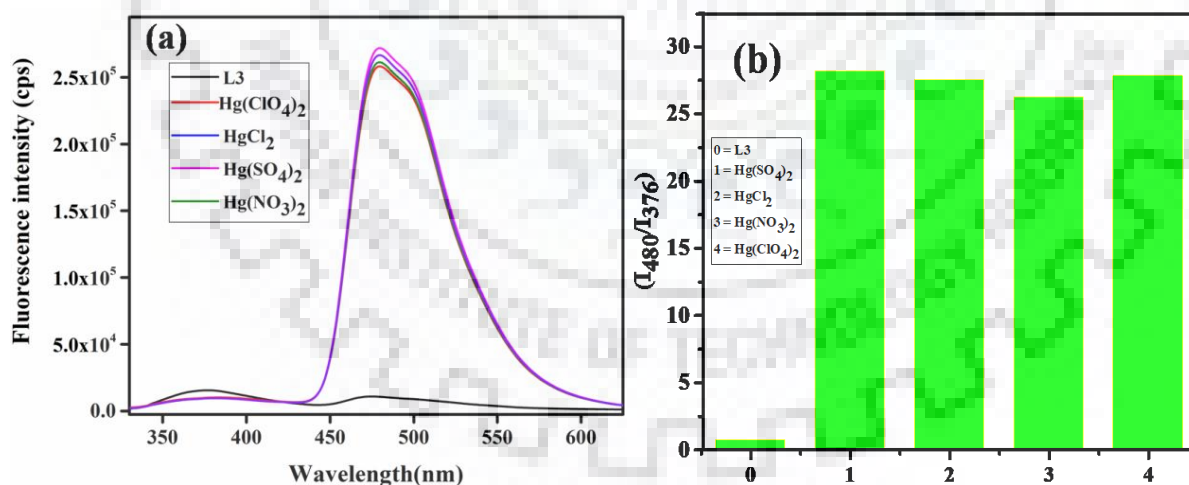


Figure 3.8 Fluorescence Emission responses of **L3** (10 μM , in $\text{MeCN}/\text{H}_2\text{O}$ (1:1 v/v, PH 7.0, HEPES buffer) in the presence of different counter ions (a) Fluorescence intensity (b) Fluorescence intensity ratio (I_{480}/I_{376}).

3.3.7 Solvent System and pH Studies

To find out the most suitable solvent system for fluorescence studies, the proportion of $\text{CH}_3\text{CN}:\text{H}_2\text{O}$ was varied to identify the ratio of CH_3CN to H_2O at which **L3** is effectively detecting Hg^{2+} . **L3** was readily soluble in pure CH_3CN and insoluble in water. The solvent selection was done by gradual addition of water into CH_3CN solution of **L3**, keeping its concentration fixed at $10\ \mu\text{M}$, and monitoring the fluorescence intensity of **L3** in the absence and presence of Hg^{2+} upon excitation at $320\ \text{nm}$, the fluorescence intensity of **L3** was almost constant but the intensity of **L3**+ Hg^{2+} starts to decrease as the water volume fractions increases over 1:1 (V/V) of CH_3CN to H_2O which allowed setting the ideal working solvent system as 1:1(V/V) of $\text{CH}_3\text{CN}:\text{H}_2\text{O}$ mixtures.

To investigate the suitable pH range for sensing application, the pH dependence of **L3** on the ratiometric detection performance of **L3** towards Hg^{2+} were studied at pH range of (2-12) in the absence and presence of Hg^{2+} . It was observed that the **L3** was stable in pH range of 3-9 (Figure 3.9a), and pH of 5-9 was the stable range for **L3**- Hg^{2+} (Figure 3.9b). However a decrease in the intensity was observed in both **L3** and **L3**- Hg^{2+} at lower and higher pH ranges. The overall pH effect for the fluorescence intensity ratio (I_{480}/I_{376}) for the **L3** and **L3**- Hg^{2+} was constant in the pH range of 5-9 (Figure 3.10). This wide range pH stability is an important for using the chemosensor for Hg^{2+} ion sensing in both biological and environmental samples. Hence, all the experiments were carried out in neutral pH [in $\text{MeCN}/\text{H}_2\text{O}$ (1:1 v/v, PH 7.0, HEPES buffer)] as optimized experimental condition.

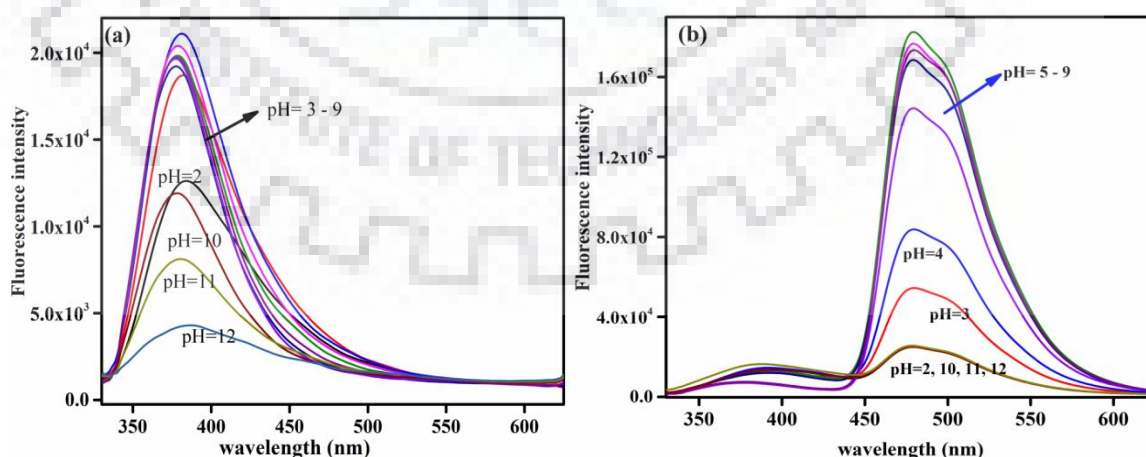


Figure 3.9 Fluorescence intensity of (a) **L3**, (b) **L3**- Hg^{2+} at different pH value.

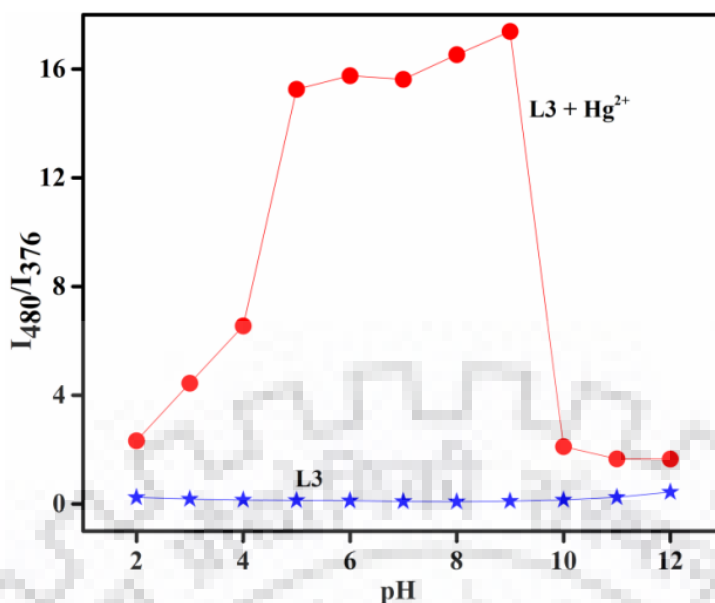
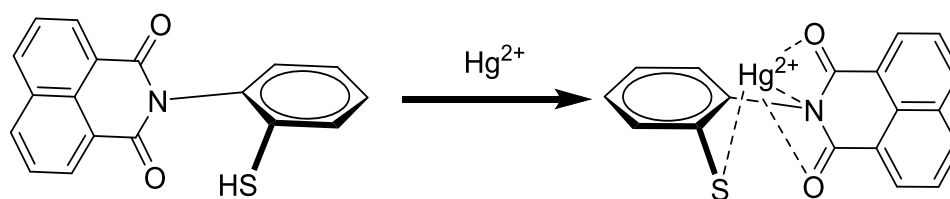


Figure 3.10 Fluorescence intensity ratio (I_{480}/I_{376}) for **L3** and **L3-Hg²⁺** at different pH values.

3.3.8 Nature of Binding Interaction of L3 with Hg²⁺

The complex formation was established by IR, and ¹H-NMR to understand the binding mode of **L3** with Hg²⁺. The FT-IR spectra were recorded with and without Hg²⁺. **L3** exhibited a characteristic series of stretching vibrations among which the (-SH), (-C=O) and (C-N) bands at 2518 cm⁻¹, 1702 and 1662 cm⁻¹, and 1239 cm⁻¹, respectively. Upon addition of Hg²⁺, the peak corresponding to (-SH) was disappeared and the (-C=O) peaks were decreased in intensity and the (-C-N) peak shifting to 1253 cm⁻¹, (Figure 3.21), which implies the coupling with (-SH), (-C=O) and (C-N) groups of the 1,8-Naphthalimide moiety. Furthermore, ¹H NMR titration shows -SH proton peak appeared as a singlet at 3.33 ppm in free **L3** gradually vanished upon addition of Hg²⁺, this signifies that the deprotonation of -SH proton by Hg²⁺ (Figure 3.22).

Accordingly, the observed spectroscopic data from IR and NMR clearly demonstrate that chemosensor **L3** coordinate with Hg²⁺ through amide oxygen and sulphur of thiol group. We have also found that the melting temperature of **L3** is increased in the presence of Hg²⁺. When **L3** coordinate to Hg²⁺, the binding of cation stabilizes the structure and the temperature at which the **L3** dissociates increased from 210.6 to 265°C. Thus, the probable mechanism is depicted in scheme 3.2.



Scheme 3.2. Proposed sensing mechanism of **L3** with Hg^{2+} .

3.3.9 Theoretical Calculation

For further understanding of the interaction mechanism of **L3** with Hg^{2+} in terms of molecular and electronic level, the structure of **L3** and **L3-Hg²⁺** have been optimized by density functional theory (DFT) and the vertical excitation (absorption) energy and oscillation strength (*f*) using time-dependent density functional theory (TD-DFT) calculation methods were carried out with Gaussian 09 program. All calculations have been done in gas phase with B3LYP hybrid function and 6-31G (d) basis set for **L3** and LANL2DZ for **L3-Hg²⁺** complex. And the long range corrected functionality CAM-B3LYP, using 631+G(d,p) basis set for **L3** and LANL2DZ method for **L3-Hg²⁺** complex [45–48]. As shown in Figure 3.11, the optimized structure of **L3** appeared to be in twisted through the amide linkage in such a way that the 2-mercapto-phenyl moiety and 1,8-naphthalimide are almost in perpendicular planes and in the **L3-Hg²⁺** they are in the same plane. This could be due to the relaxation in the structure of **L3** is blocked in **L3-Hg²⁺** complex.

The electron density in HOMO-LUMO levels in **L3**, the HOMO is localized on 2-mercapto-phenyl moiety, whereas the LUMO mostly restricted on the 1,8-naphthalimide ring. With the introduction of Hg^{2+} , HOMO of the complex spread over the Hg^{2+} central metal ion and 2-mercapto-phenyl moiety, on the other hand the LUMO is mainly laid on 1,8-naphthalimide. Complex formation of **L3** with Hg^{2+} stabilizes the molecule and decreases the HOMO-LUMO energy gap from 3.563 eV in **L3** to 2.223 eV in **L3-Hg²⁺** (Figure 3.12); this was supported by red shift of absorbance and fluorescence bands to longer wavelength (332 nm to 438 nm, and 376 nm to 480 nm respectively) via coordination with Hg^{2+} . This result was also in good accordance with fluorescence lifetime experiment result, which show upon complexation with Hg^{2+} , the intramolecular rotation of the **L3** is restricted, which blocks the pathway for non-radiative processes and converts into strong emitters. In addition to that the TD-DFT CAM-B3LYP provided the best agreement with experimental results (Table 3.2). According to our TD-DFT of CAM-B3LYP/6-31+G(d,p) calculations, the vertical transition energies of **L3** are 329 and 319 nm for S2 and S3 excited states respectively. The absorption wavelengths of

these two states lie closely and agree with the experiment result. So, S3 the transition from HOMO-1 to LUMO that have large oscillator strengths (0.3182) transitions is considered to the experimental absorption peak at 332 nm. The 3rd extention (S3) the transition from HOMO-2 to LUMO that have transition energies of **L3**+Hg²⁺ of 2.7786 eV and wavelength 446 nm large oscillator strengths (0.2156) transitions is considered to the experimental absorption peak at 438 nm (Figure 3.13).

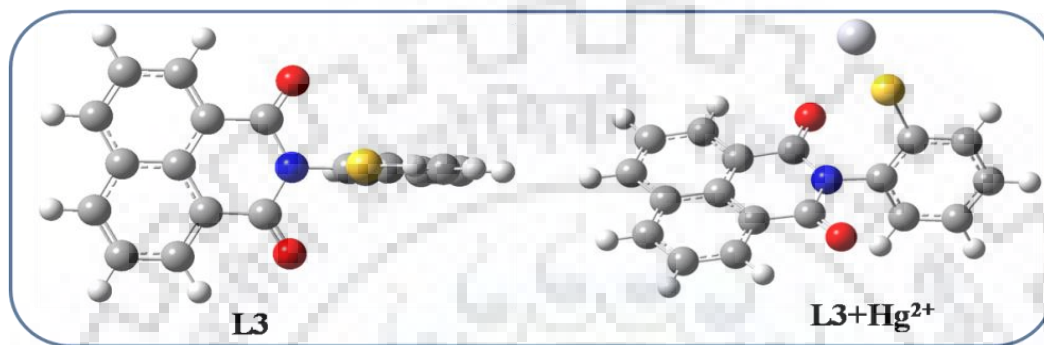


Figure 3.11 Optimized structures of **L3** and **L3+Hg²⁺**

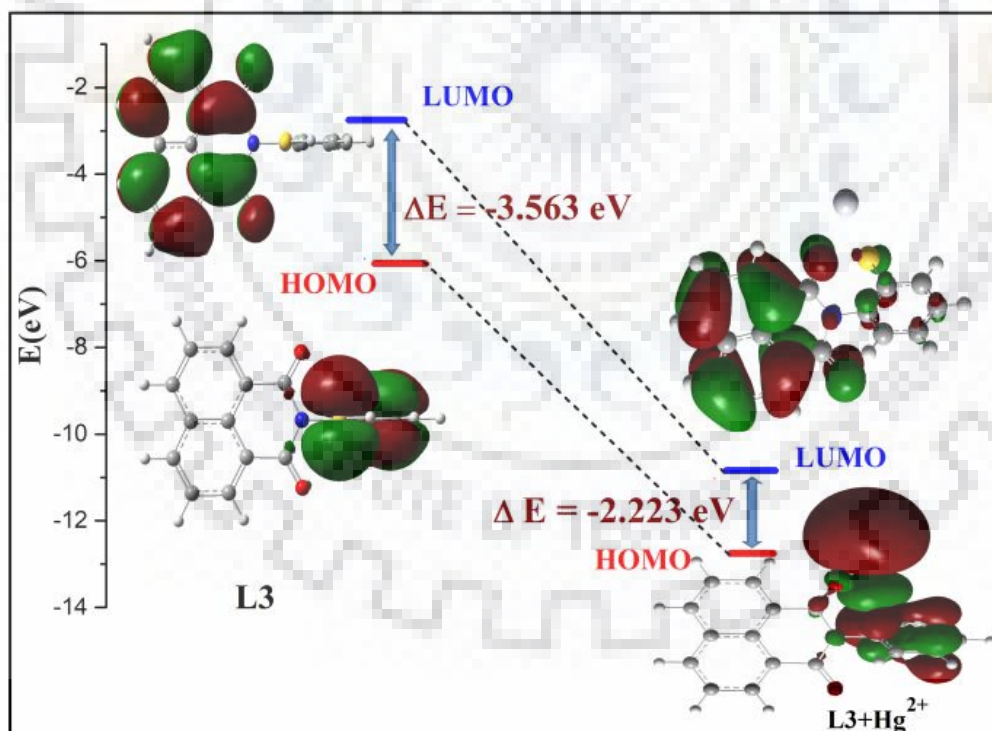


Figure 3.12 HOMO–LUMO band gaps of **L3** and **L3+Hg²⁺**

Table 3.2 Excitation energies and oscillator strengths of **L3** opt freq td cam-b3lyp/6-31g(d) geom=connectivity

	Excited State	Excitation energies (eV)	Wavelength (nm)	oscillator strengths(f)
L3	1	3.6236	342.16	0.0007
	2	3.7663	329.19	0.0001
	3	3.8755	319.91	0.3182
L3-Hg²⁺	1	2.0415	607	0.0033
	2	2.1844	567	0.0165
	3	2.7786	446	0.2156

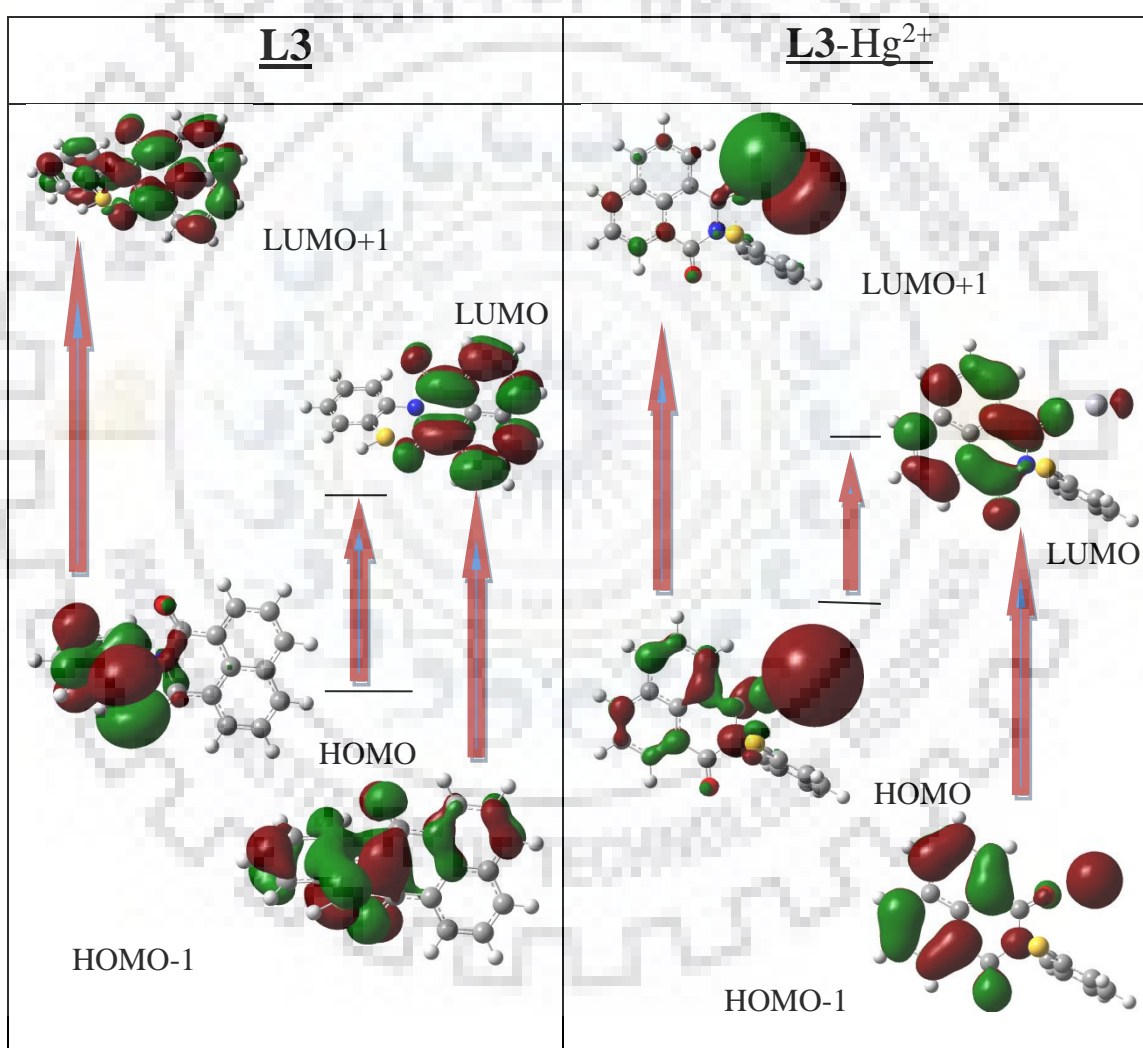


Figure 3.13 TD-DFT of CAM-B3LYP, function combined with 6-31G (d) basis sets for **L3** and with Lan12DZ method for **L3-Hg²⁺**.

3.3.10 Reversibility Studies Applied as Logic Circuit Devices

It is very practical if a sensor can be reversed and reused. As it is well known, iodide ions (I^-) have strong binding ability to Hg^{2+} ; therefore, we use KI for competitive bind Hg^{2+} from the **L3**- Hg^{2+} complex. To identify the reusability of **L3** for Hg^{2+} sensing, the reversibility of **L3** coordination toward Hg^{2+} via addition of KI to **L3**- Hg^{2+} solution in (in MeCN/ H_2O (1:1 v/v, PH 7.0, HEPES buffer) was studied. Importantly, high reversibility in colorimetric and ratiometric fluorimetric was obtained (Figure. 3.14a, b). On titration of **L3**- Hg^{2+} with KI, the fluorescence intensity at 480 nm is apparently decreasing and that of 376 nm is increasing gradually, after the addition of 10 equiv. of KI the fluorescence intensity returns almost to the free sensor **L3** which can be used for further sensing. This phenomenon is because of stable mercury-iodide complex formation due to the strong affinity I^- for Hg^{2+} [49–52]. This reversibility character advocates the applicability of **L3** as “Off–On–Off” naked eye and ratiometric sensor.

Furthermore, the “off-on-off” cycle could be repeated numerous times with negligible reduction in emission ratio (I_{480}/I_{376}) by alternate addition of Hg^{2+} and KI (Figure 3.14c). Subsequently, INHIBIT logic gate has been constructed on the basis of the repeated On-Off behaviour of **L3** by Hg^{2+} and KI as two input signals, which can be symbolized as a combination of AND and NOT gates, [53,54] using input 1 (Hg^{2+}) and input 2 (KI) and emission intensity ratio (I_{480}/I_{376}) as an output as revealed in the truth table (Figure 3.14d).

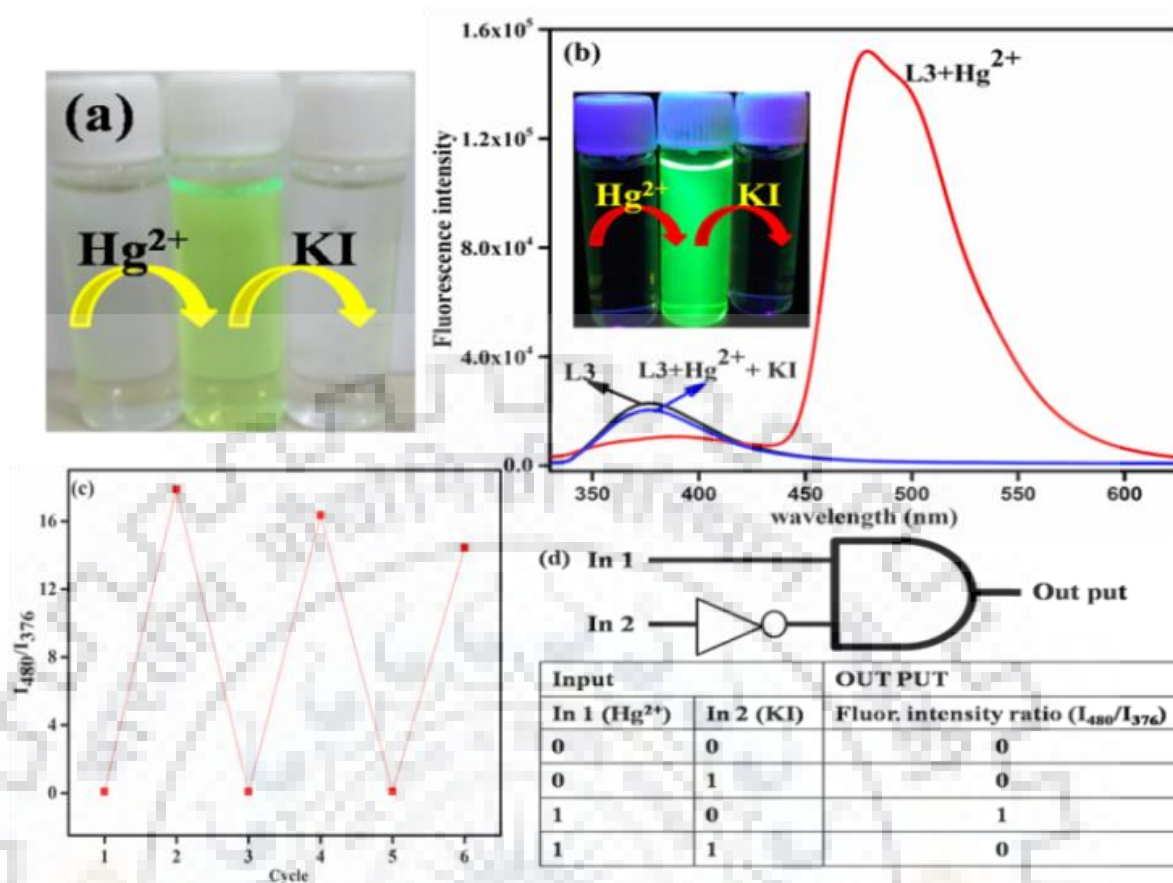


Figure 3.14 (a). Visual Colorimetric reversibility (b). Fluorometric reversibility. (Inset: visual fluorometric reversibility) (c). "off-on-off" reversibility cycles of chemosensor **L3** upon sequential addition of Hg^{2+} and **KI**. (d). Switch circuit diagram and Truth table corresponding to a logic gate based on Hg^{2+} and **KI**.

3.3.11 Analysis of Real Sample

To investigate the reliability and practical applicability of our method, the analysis of Hg^{2+} concentration in water samples was applied; to eliminate matrix effect a standard addition method was used [55–57]. A 0.2 μm nylon filtered water sample from a Ganga canal and drain water around IIT Roorkee were used for analysis without advance pre-treatment. 1 mL of the water samples were blended with standard solutions of Hg^{2+} at (0.1, 0.2, and 0.4 μM) concentration (HEPES-buffered solution ($\text{CH}_3\text{CN}:\text{H}_2\text{O}$, 1:1, v/v, pH 7.0) to prepare 3.0 mL solution [58,59]. The mixtures were analyzed by fluorescence titration against **L3** solution (Figure 3.15). The concentration of standards is subtracted from the calculated Hg^{2+} concentration to obtain Hg^{2+} concentration in the water sample. The concentration Hg^{2+} is calculated from the fluorescence intensity ratio (I_{480}/I_{376}) of mingled solution by the Linear correlation equation of ($Y = 3.724[\text{Hg}^{2+}] - 0.1446$).

The Hg^{2+} concentrations were found to be $0.022 \mu\text{M}$ and $0.043 \mu\text{M}$ for canal water and drain water respectively. As shown in table 3.3 the samples were also analyzed by ICP-MS for the verification of accuracy of the method; and concentration of Hg^{2+} in canal water and drain water were obtained as $0.021 \mu\text{M}$ and $0.041 \mu\text{M}$ respectively, which are in good accordance with calculated concentration from fluorescence analysis. This reveals the efficiency of the chemosensor for detection of Hg^{2+} in actual samples.

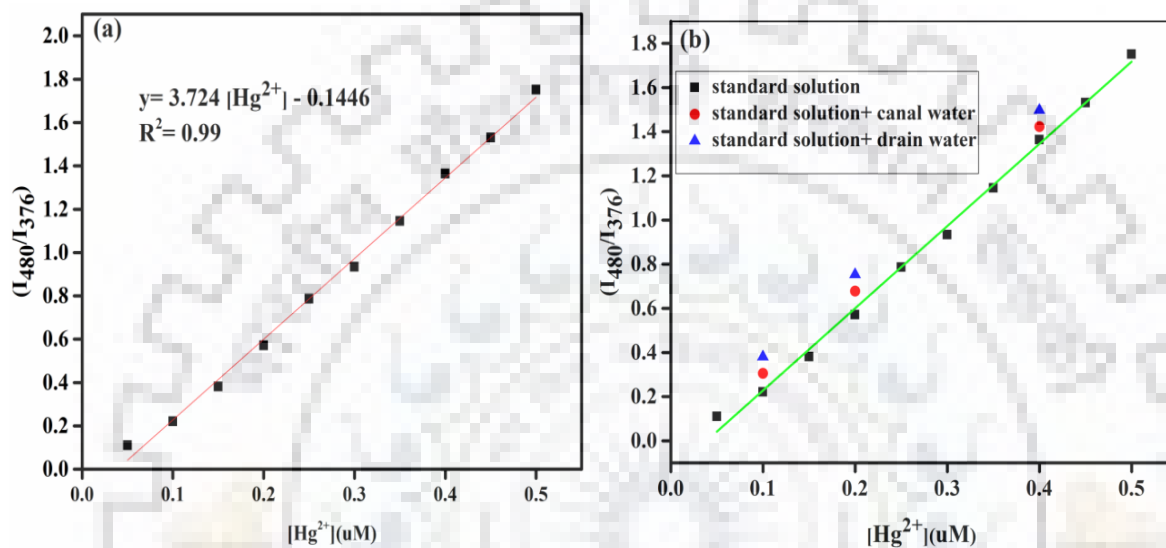


Figure 3.15 (a). Calibration curve of standard solutions of Hg^{2+} ($0.05\text{-}0.5\mu\text{M}$), (b). Canal water and drain water, linear correlation of (I_{480}/I_{376}) to $[\text{Hg}^{2+}]$ in water samples spiked with different concentration of $[\text{Hg}^{2+}]$ in the standard addition experiments. ($[\text{L3}] = 10 \mu\text{M}$, $\lambda_{\text{ex}} = 320 \text{ nm}$).

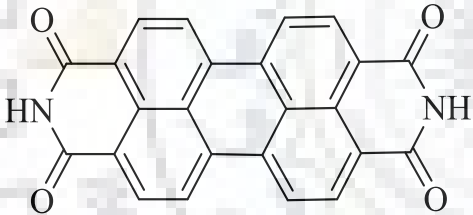
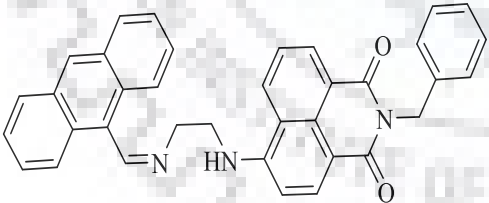
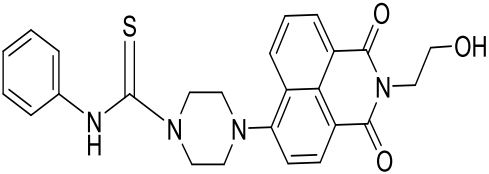
Table 3.3 Determination of Hg^{2+} ion concentration in real samples by using standard addition method

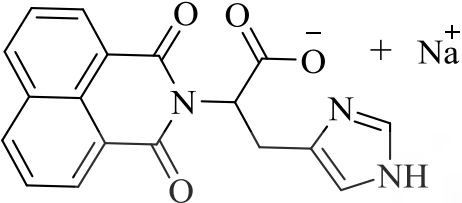
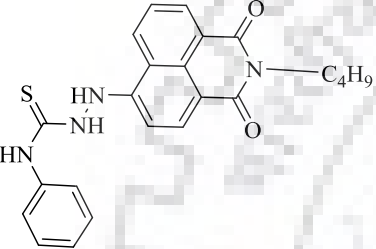
Sample	Added $[\text{Hg}^{2+}]$ (μM)	(I_{480}/I_{376})	Total recovered $[\text{Hg}^{2+}]$ (μM)	Percentage recovery (%)	$[\text{Hg}^{2+}]$ (μM)	
					by L3	by IPC-MS
Canal	0.1	0.307	0.121267454	121.2675	$0.022073 \pm$	$0.02135 \pm$
	0.2	0.6874	0.223415682	111.7078	0.000956	0.000197
	0.4	1.4252	0.421535983	105.384		
Drain	0.1	0.38548	0.142342	142.3416	$0.042803 \pm$	$0.04117 \pm$
	0.2	0.75888	0.24261	121.305	0.000476	0.010824
	0.4	1.50684	0.443459	110.8647		

3.4 Comparative Study

The performance of **L3** which is recognized for selective detection of Hg^{2+} ion and it was also compared with some recently reported 1,8-Naphthalimide based fluorescent chemosensors for Hg^{2+} detection (Table 3.4). The chemosensor is synthesized easily in single straight forward reaction from commercially available starting materials, and it exhibits comparable performance with most of recently reported fluorescence chemosensors in detection of Hg^{2+} in aqueous solution. In addition, its colorimetric and ratiometric behaviour could make it more attractive over intensity-based probes and it could be used as competent method for monitoring of Hg^{2+} ion level in different samples in good extent.

Table 3.4 A comparative study of **L3** with some previously reported 1,8-Naphthalimide based fluorescence Hg^{2+} sensors.

Fluorescence sensor	LOD	linear ranges	Mode of analyse	Ref.
Perylene bisimide 	5 nM	$0.1-1 \times 10^{-7}$ M	Quenching	[60]
Naphthalimide based fluorescent dyad 	-		Quenching	[61]
1,8-naphthalimide fragment with a phenyl- thiourea unit 	1×10^{-7} M	$0-1.3 \times 10^{-6}$ M	Enhancement	[62]

<p>Histidine-functionalized 1,8-naphthalimide based fluorescent chemosensor</p> 	$1.785 \times 10^{-7} \text{ M}$	$0.1 - 2 \times 10^{-6} \text{ M}$	Quenching	[63]
<p>A single thiourea-appended 1,8-naphthalimide chemosensor</p> 	82.1 nM	$0 - 90 \times 10^{-6} \text{ M}$	Enhancement	[64]
<p>1,8-Naphthalimide based Naked-Eye and Ratiometric Fluorescent Sensor</p>	$1.74 \times 10^{-8} \text{ M}$	$0 - 1.2 \times 10^{-6} \text{ M}$	Ratiometric	This work

3.5 Conclusion

The designed and synthesized 2-(2-mercaptophenyl)-1H-benzo[de]isoquinoline-1,3(2H)-dione (**L3**) a highly sensitive, selective and reusable naked eye and ratiometric chemosensor for detection of Hg^{2+} . **L3** exhibits maximum absorption at 332 nm and fluorescence emission at 376 nm after Hg^{2+} ion addition to **L3** solution a new absorption at 438 nm accompanied with color change from colorless to yellowish green and the new yellowish green fluorescence emission was enhanced rapidly with increasing Hg^{2+} ion concentration. The prepared chemosensor **L3** selectively detect Hg^{2+} with detection limit of 1.74×10^{-8} M which is low enough for sensing submicromolar concentration of Hg^{2+} ion. The binding mechanism of **L3** with Hg^{2+} also adequately demonstrated by IR, $^1\text{H-NMR}$ and DFT computer-based theoretical calculations. Furthermore, the photo-physical properties of **L3** has been restored and reused through metal displacement approach via addition of KI as strong coordinator of Hg^{2+} . The “*off-on-off*” reversibility has been used to build the logic gate method. Assessing the performance by fluorescence, we found that the fluorescent probe **L3** can efficiently detect Hg^{2+} and more suitable for real-time analysis.

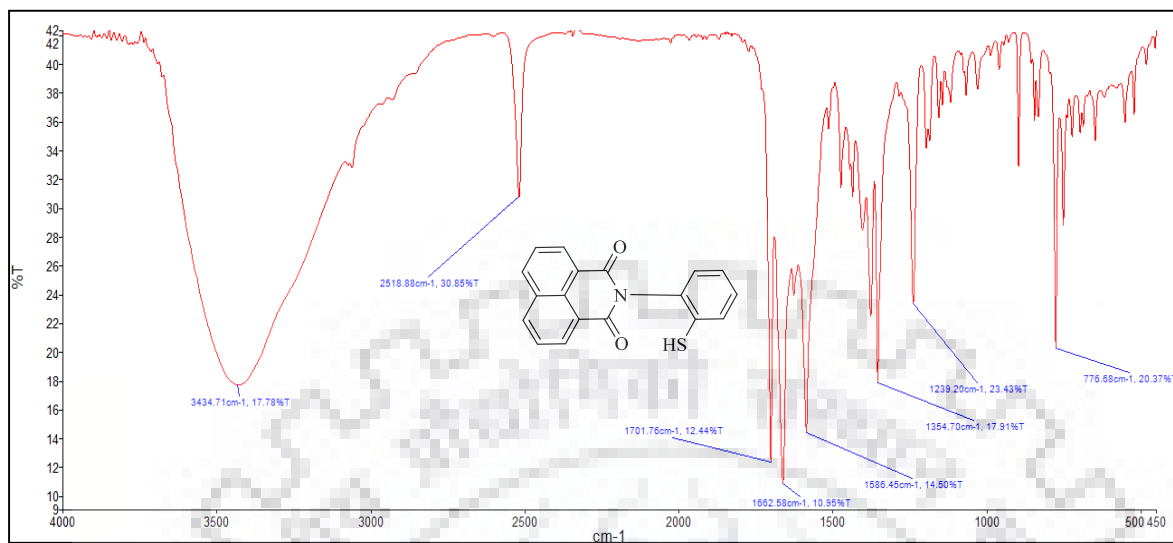
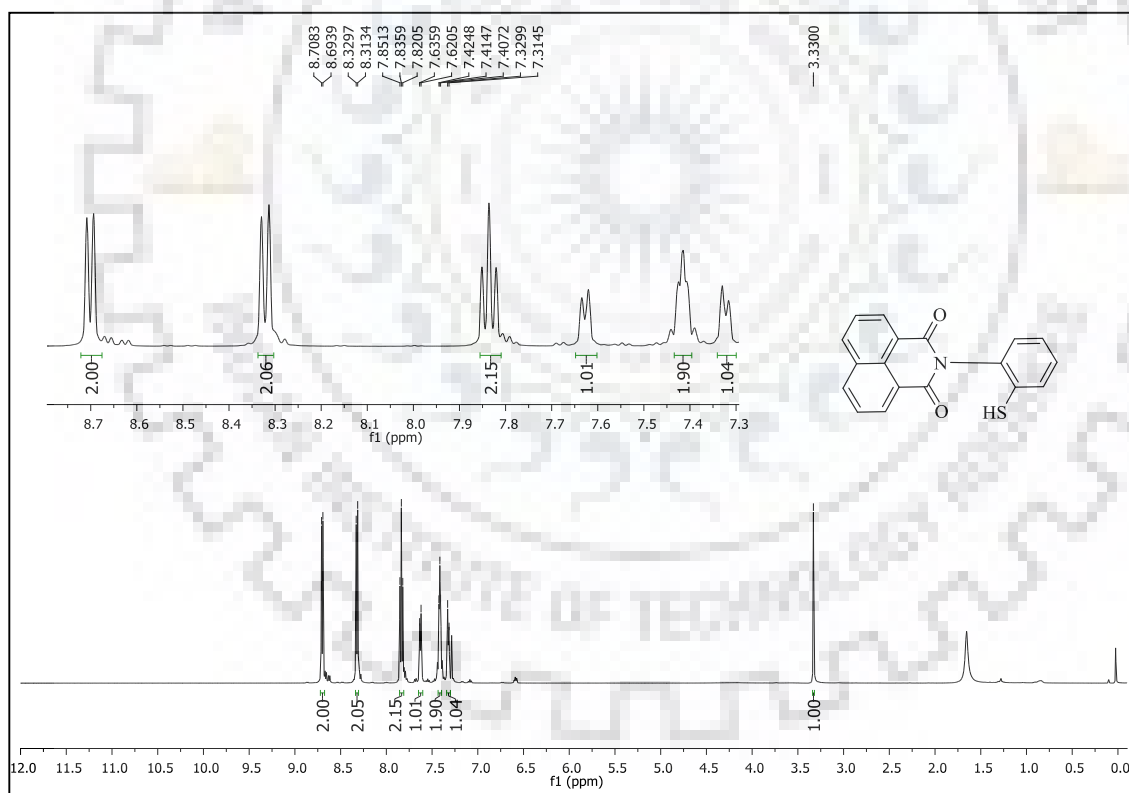
Spectral characterization of L3, and L3+Hg²⁺ by IR, NMR and HRMS

Figure 3.16 IR spectrum of receptor L3 recorded in KBr pellet.

Figure 3.17. ¹H-NMR spectrum of receptor L3 recorded in CDCl₃.

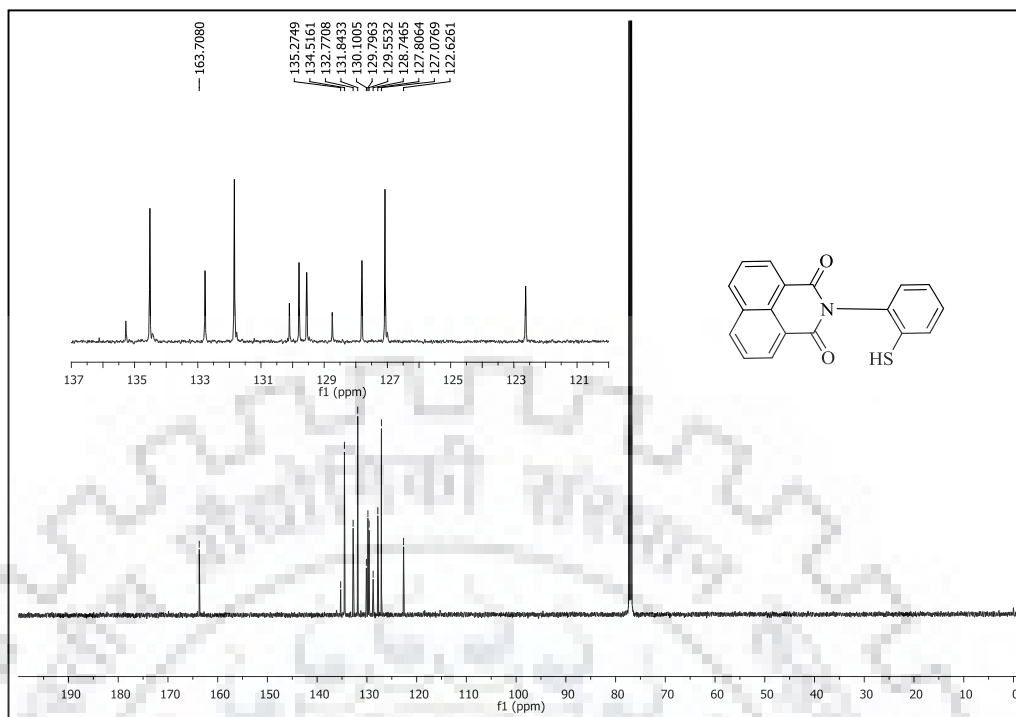
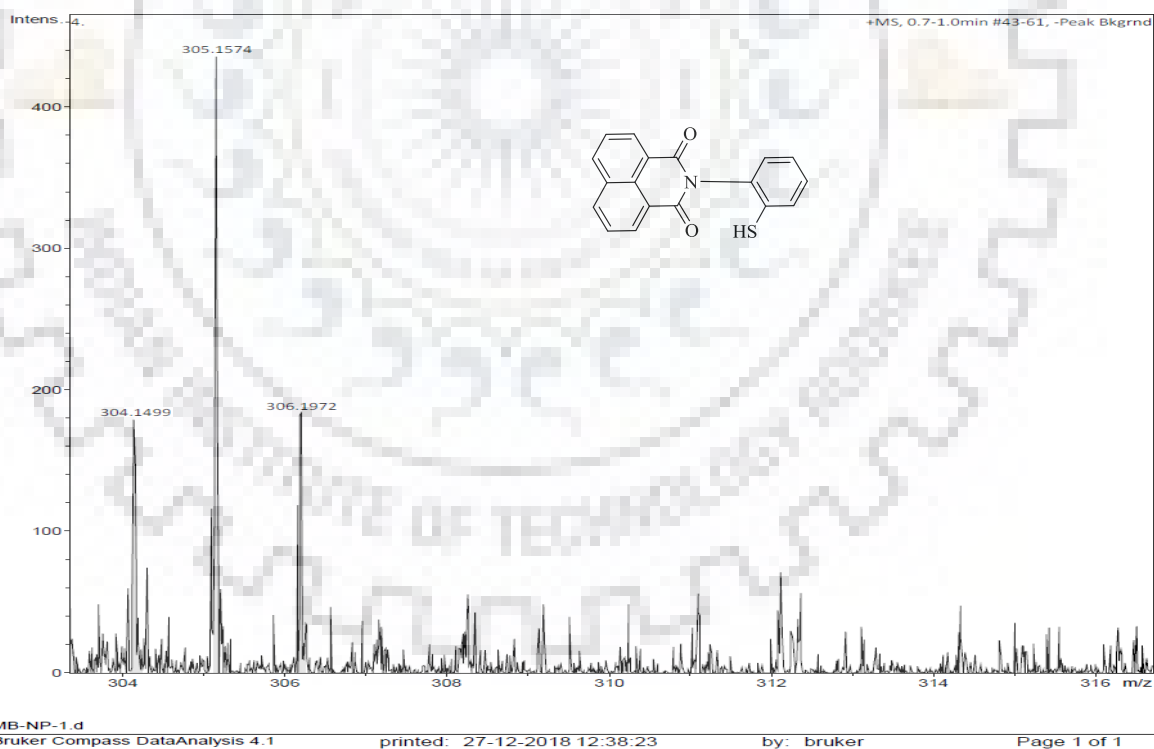


Figure 3.18 ^{13}C -NMR spectrum of receptor L3 recorded in CDCl_3



WB-NP-1.d

Bruker Compass DataAnalysis 4.1

printed: 27-12-2018 12:38:23

by: bruker

Page 1 of 1

Figure 3.19 HRMS of L3

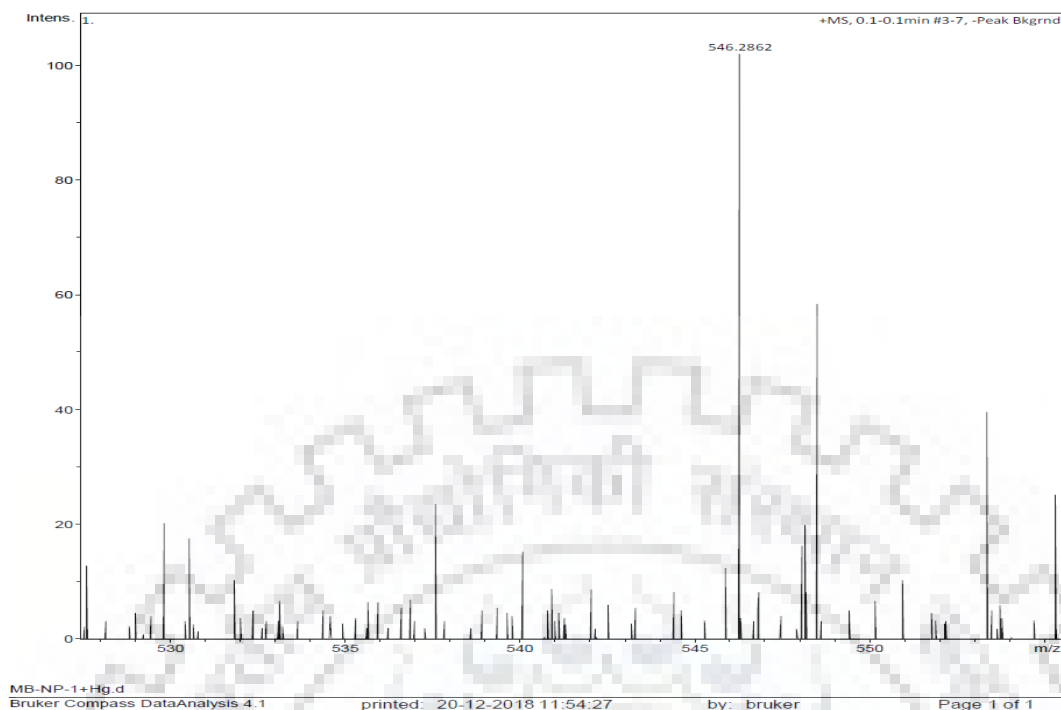


Figure 3.20 HRMS of L3+Hg²⁺

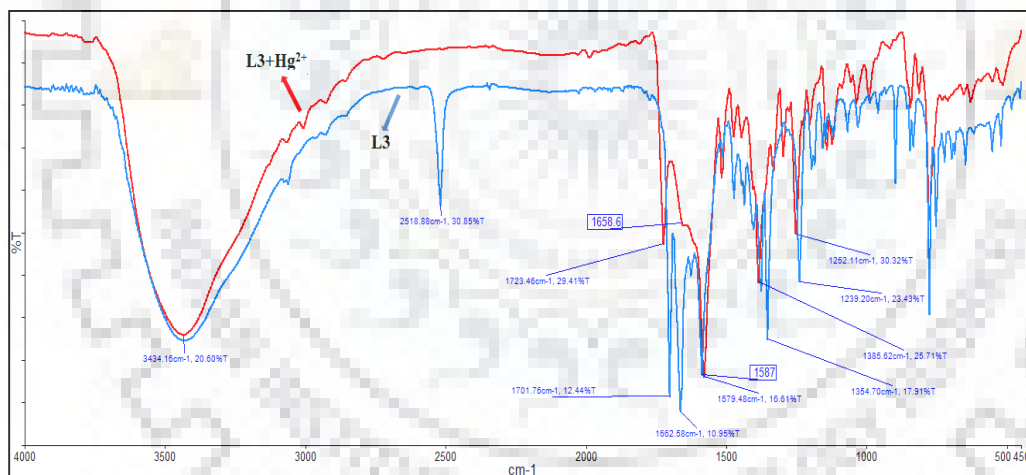


Figure 3.21 IR spectrum of receptor L3, and L3+HgCl₂ recorded in KBr pellet.

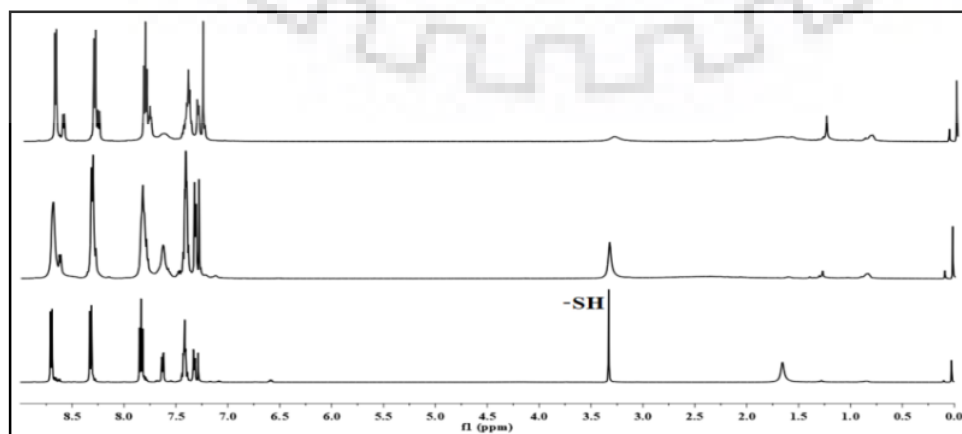


Figure 3.22 ¹H-NMR spectra of L3 with Hg²⁺ as HgCl₂ in CDCl₃.

3.6 Reference

- [1] G.H. Chen, W.Y. Chen, Y.C. Yen, C.W. Wang, H.T. Chang, C.F. Chen, Detection of mercury(II) ions using colorimetric gold nanoparticles on paper-based analytical devices, *Anal. Chem.* 86 (2014) 6843–6849. doi:10.1021/ac5008688.
- [2] A.B. Kobal, J. Snoj Tratnik, D. Mazej, V. Fajon, D. Gibičar, A. Miklavčič, D. Kocman, J. Kotnik, A. Sešek Briški, J. Osredkar, M. Krsnik, M. Prezelj, Knap, B. Križaj, L. Liang, M. Horvat, Exposure to mercury in susceptible population groups living in the former mercury mining town of Idrija, Slovenia, *Environ. Res.* 152 (2017) 434–445. doi:10.1016/j.envres.2016.06.037.
- [3] F. Zahir, S.J. Rizwi, S.K. Haq, R.H. Khan, Low dose mercury toxicity and human health, *Environ. Toxicol. Pharmacol.* 20 (2005) 351–360. doi:10.1016/j.etap.2005.03.007.
- [4] L. Deng, Y. Li, X. Yan, J. Xiao, C. Ma, J. Zheng, S. Liu, R. Yang, Ultrasensitive and highly selective detection of bioaccumulation of methyl-mercury in fish samples *via* Ag⁰/Hg⁰ amalgamation, *Anal. Chem.* 87 (2015) 2452–2458. doi:10.1021/ac504538v.
- [5] A.F. Castoldi, C. Johansson, N. Onishchenko, T. Coccini, E. Roda, M. Vahter, S. Ceccatelli, L. Manzo, Human developmental neurotoxicity of methylmercury: Impact of variables and risk modifiers, *Regul. Toxicol. Pharmacol.* 51 (2008) 201–214. doi:10.1016/j.yrtph.2008.01.016.
- [6] B. Subramaniam, Colonial legacies, postcolonial biologies: Gender and the promises of biotechnology, *Asian Biotechnol. Dev. Rev.* 17 (2015) 15–36. doi:10.1080/10643389.2012.728825.
- [7] S. Liu, H. Nie, J. Jiang, G. Shen, R. Yu, Electrochemical Sensor for Mercury (II) Based on Conformational Switch Mediated by Interstrand, *Anal. Chem.* 81 (2009) 5724–5730. doi:10.1021/ac900527f.
- [8] Z. Yan, M.-F. Yuen, L. Hu, P. Sun, C.-S. Lee, Advances for the colorimetric detection of Hg²⁺ in aqueous solution, *RSC Adv.* 4 (2014) 48373–48388. doi:10.1039/C4RA07930B.
- [9] Z. Sun, D. Guo, L. Zhang, H. Li, B. Yang, S. Yan, Multifunctional fibrous silica composite with high optical sensing performance and effective removal ability toward Hg²⁺ ions, *J. Mater. Chem. B.* 3 (2015) 3201–3210. doi:10.1039/C5TB00038F.
- [10] E. Ha, N. Basu, S. Bose-O'Reilly, J.G. Dórea, E. McSorley, M. Sakamoto, H.M. Chan, Current progress on understanding the impact of mercury on human health, *Environ. Res.* 152 (2017) 419–433. doi:10.1016/j.envres.2016.06.042.

- [11] B.M. Kim, A.L. Choi, E.H. Ha, L. Pedersen, F. Nielsen, P. Weihe, Y.C. Hong, E. Budtz-Jørgensen, P. Grandjean, Effect of hemoglobin adjustment on the precision of mercury concentrations in maternal and cord blood, *Environ. Res.* 132 (2014) 407–412. doi:10.1016/j.envres.2014.04.030.
- [12] B. Fernandes Azevedo, L. Barros Furieri, F.M. Peçanha, G.A. Wiggers, P. Frizzera Vassallo, M. Ronacher Simões, J. Fiorim, P. Rossi de Batista, M. Fioresi, L. Rossoni, I. Stefanon, M.J. Alonso, M. Salaces, D. Valentim Vassallo, Toxic Effects of Mercury on the Cardiovascular and Central Nervous Systems, *J. Biomed. Biotechnol.* 2012 (2012) 1–11. doi:10.1155/2012/949048.
- [13] K.M. Rice, E.M. Walker, M. Wu, C. Gillette, E.R. Blough, Environmental mercury and its toxic effects, *J. Prev. Med. Public Heal.* 47 (2014) 74–83. doi:10.3961/jpmph.2014.47.2.74.
- [14] L.L. Hui, M.H.M. Chan, H.S. Lam, P.H.Y. Chan, K.M. Kwok, I.H.S. Chan, A.M. Li, T.F. Fok, Impact of fetal and childhood mercury exposure on immune status in children, *Environ. Res.* 144 (2016) 66–72. doi:10.1016/j.envres.2015.11.005.
- [15] M. Bahta, N. Ahmed, Design and synthesis of 1, 4-benzothiazine hydrazide as selective and sensitive colorimetric and Turn-On fluorometric sensor for Hg^{2+} detection in aqueous medium, *Journal Photochem. Photobiol. A Chem.* 357 (2018) 41–48. doi:10.1016/j.jphotochem.2018.02.022.
- [16] Shaily, A. Kumar, N. Ahmed, Imidazo[1,2-a]pyridine-substituted coumarin as a selective ratiometric sensor for Cu^{2+} ion, *Supramol. Chem.* 29 (2017) 1–7. doi:10.1080/10610278.2016.1190453.
- [17] K.N. Hearn, T.D. Nalder, R.P. Cox, H.D. Maynard, T.D.M. Bell, F.M. Pfeffer, T.D. Ashton, Modular synthesis of 4-aminocarbonyl substituted 1,8-naphthalimides and application in single molecule fluorescence detection, *Chem. Commun.* 53 (2017) 12298–12301. doi:10.1039/c7cc07922b.
- [18] H. Ulla, B. Garudachari, M.N. Satyanarayan, G. Umesh, A.M. Isloor, Blue organic light emitting materials: Synthesis and characterization of novel 1,8-naphthalimide derivatives, *Opt. Mater.* 36 (2014) 704–711. doi:10.1016/j.optmat.2013.11.017.
- [19] J.S. Chen, R.Z. Liu, Y. Yang, T.S. Chu, Intramolecular charge transfer and sensing mechanism for a colorimetric fluoride sensor based on 1,8-naphthalimide derivatives, *Theor Chem Acc.* 133 (2014) 1411. doi:10.1007/s00214-013-1411-3.
- [20] S. Banerjee, E.B. Veale, C.M. Phelan, S.A. Murphy, G.M. Tocci, L.J. Gillespie, D.O. Frimannsson, J.M. Kelly, T. Gunnlaugsson, Recent advances in the development of 1,8-naphthalimide based DNA targeting binders, anticancer and fluorescent cellular imaging agents, *Chem. Soc. Rev.* 42 (2013) 1601–1618. doi:10.1039/c2cs35467e.

- [21] S. Sergio, A.Y.Y. Wooo, B. Thomas, Electron-accepting p-conjugated species with 1,8-naphthalic anhydride or diketophosphanyl units, *Mater. Chem. Front.* 1 (2017) 2324–2334. doi:10.1039/C7QM00336F.
- [22] G. Saito, D. Velluto, M. Resmini, Synthesis of probes with fluorescent switch triggered by flufenamic acid, *R. Socitey Open Secince.* 5 (2018) 172137.
- [23] H. Yang, A. Han, X. Yang, L. Zang, A Ratiometric Fluorescent Sensor for Cd^{2+} Based on Internal Charge Transfer, *Sensors.* 17 (2017) 1–10. doi:10.3390/s17112517.
- [24] L. Wang, W. Li, W. Qu, Y. Fan, H. Yao, Q. Lin, Y. Zhang, A Water Soluble Naphthalimide-Based Chemosensor for Fluorescent Detection CN^- in Pure Water and Its Application in Practical Samples, *J. Braz. Chem. Soc.* 29 (2018) 1563–1569. doi:org/10.21577/0103-5053.20180030.
- [25] Z. Xu, X. Qian, J. Cui, R. Zhang, Exploiting the deprotonation mechanism for the design of ratiometric and colorimetric Zn^{2+} fluorescent chemosensor with a large red-shift in emission, *Tetrahedron.* 62 (2006) 10117–10122. doi:10.1016/j.tet.2006.08.050.
- [26] L. Long, L. Zhou, L. Wang, S. Meng, A. Gong, C. Zhang, ratiometric fluorescent probe for iron (III) and its application for detection of iron (III) in human blood serum, *Anal. Chim. Acta.* 812 (2014) 145–151. doi:10.1016/j.aca.2013.12.024.
- [27] A. Thakur, S. Sardar, S. Ghosh, A Highly Selective Redox , Chromogenic, and Fluorescent Chemosensor for Hg^{2+} in Aqueous Solution Based on Ferrocene À Glycine Bioconjugates, *Inorg. Chem.* 50 (2011) 7066–7073. doi:10.1021/ic200573m.
- [28] M. Shellaiah, T. Simon, P. Venkatesan, K. Wen, F. Ko, Applied Surface Science Cysteamine-modified diamond nanoparticles applied in cellular imaging and Hg^{2+} ions detection, *Appl. Surf. Sci.* 465 (2019) 340–350. doi:10.1016/j.apsusc.2018.09.175.
- [29] E.M. Nolan, M.E. Racine, S.J. Lippard, Selective $\text{Hg}(\text{II})$ Detection in Aqueous Solution with Thiol Derivatized Fluoresceins, *Inorg. Chem.* 45 (2006) 2394–2397. doi:10.1021/ic052083w.
- [30] M. Shellaiah, Y.C. Rajan, P. Balu, A. Murugan, A pyrene based Schiff base probe for selective fluorescence Turn-On detection of Hg^{2+} ions with live cell application, *New J. Chem.* 39 (2015) 2523–2531. doi:10.1039/c4nj02367f.
- [31] X. Guan, W. Lin, W. Huang, Development of a new rhodamine-based FRET platform and its application as a Cu^{2+} probe., *Org. Biomol. Chem.* 12 (2014) 3944–9. doi:10.1039/c4ob00131a.
- [32] Y. Zhou, X. He, H. Chen, Y. Wang, S. Xiao, N. Zhang, D. Li, K. Zheng, Chemical An ES IPT/ICT modulation based ratiometric fluorescent probe for sensitive and selective sensing Hg^{2+} , *Sensors Actuators B. Chem.* 247 (2017) 626–631. doi:10.1016/j.snb.2017.03.085.

- [33] L. Chen, X. Tian, Y. Zhao, Y. Li, C. Yang, Z. Zhou, X. Liu, A ratiometric fluorescence nanosensor for highly selective and sensitive detection of selenite, *Analyst*. 141 (2016) 4685–4693. doi:10.1039/c6an00740f.
- [34] R. Ohgaki, Y. Teramura, D. Hayashi, L. Quan, S. Okuda, Ratiometric fluorescence imaging of cell surface pH by poly (ethylene glycol)-phospholipid conjugated with fluorescein isothiocyanate, *Sci. Rep.* (2017) 1–9. doi:10.1038/s41598-017-17459-y.
- [35] L. Wu, Y. Wang, T.D. James, A hemicyanine based ratiometric fluorescence probe for mapping lysosomal pH during heat stroke in living cells, *Chem. Commun.* 54 (2018). doi:10.1039/c8cc02330a.
- [36] K.A. Macgregor, M.J. Robertson, K.A. Young, L. Von Kleist, W. Stahlschmidt, A. Whiting, N. Chau, P.J. Robinson, V. Haucke, A. McCluskey, Development of 1,8-Naphthalimides as Clathrin Inhibitors, *J. Med. Chem.* 57 (2014) 131–143. doi:10.1021/jm4015263.
- [37] J. Wang, X. Qian, J. Cui, Detecting Hg^{2+} ions with an ICT Fluorescent Sensor Molecule: Remarkable Emission Spectra Shift and Unique Selectivity, *J. Org. Chem.* 71 (2006) 4308–4311. doi:10.1021/jo052642g.
- [38] S. Sun, B. Qiao, N. Jiang, J. Wang, S. Zhang, X. Peng, Naphthylamine–RhodamineBased Ratiometric Fluorescent Probe for the Determination of Pd^{2+} ions, *Org. Lett.* 16 (2014) 1132–1135. doi:10.1021/ol500284p.
- [39] C. Satriano, T. Sfrazzetto, E. Amato, F.P. Ballistreri, A. Copani, L. Giuffrida, G. Grasso, A. Pappalardo, E. Rizzarelli, A. Tomaselli, A ratiometric naphthalimide sensor for live cell imaging of copper(I), *Chem. Commun.* 49 (2013) 5565–5567. doi:10.1039/c3cc42069h.
- [40] C. Lu, Z. Xu, J. Cui, Ratiometric and Highly Selective Fluorescent Sensor for Cadmium under Physiological pH Range: A New Strategy to Discriminate Cadmium from Zinc, *J. Org. Chem.* 72 (2007) 3554–3557. doi:10.1021/jo070033y.
- [41] S. Qu, C. Zheng, G. Liao, C. Fan, G. Liu, S. Pu, A fluorescent chemosensor for Sn^{2+} and Cu^{2+} based on a carbazole-containing diarylethene, *RSC Adv.* 7 (2017) 9833–9839. doi:10.1039/C6RA27339D.
- [42] M. Li, W. Feng, H. Zhang, G. Feng, An aza-coumarin-hemicyanine based near-infrared fluorescent probe for rapid, colorimetric and ratiometric detection of bisulfite in food and living cells, *Sensors Actuators, B Chem.* 243 (2017) 51–58. doi:10.1016/j.snb.2016.11.132.
- [43] Z. Li, Y. Zhou, K. Yin, Z. Yu, Y. Li, J. Ren, A new fluorescence “Turn-On” type chemosensor for Fe^{3+} based on naphthalimide and coumarin, *Dye. Pigment.* 105 (2014) 7–11. doi:10.1016/j.dyepig.2013.12.032.
- [44] W. Gong, S. Wang, Y. Wei, L. Ding, Y. Fang, A pyrene-based fluorescent sensor for ratiometric detection of heparin and its complex with heparin for reversed ratiometric

- detection of protamine in aqueous solution, *Spectrochim. Acta Part A.* 170 (2017) 198–205. doi:10.1016/j.saa.2016.07.026.
- [45] Y. Zhang, J. Leng, Theoretical Studies on Two-Photon Fluorescent Hg²⁺ Probes Based on the Coumarin-Rhodamine System, *Sensors.* 17 (2017) 1672. doi:10.3390/s17071672.
- [46] Y. Huo, S. Wang, T. Lu, C. Pan, Y. Lu, X. Yang, D. Hu, S. Hu, Highly selective and sensitive colorimetric diaminomaleonitrile derivatives, *RSC Adv.* 6 (2016) 5503–5511. doi:10.1039/c5ra21474b.
- [47] S. Joshi, S. Kumari, A. Sarmah, D.D. Pant, R. Sakhuja, Detection of Hg²⁺ ions in aqueous medium using an indole-based fluorescent probe: Experimental and theoretical investigations, *J. Mol. Liq.* 248 (2017) 668–677. doi:10.1016/j.molliq.2017.10.081.
- [48] J. Min, C. Kim, R.G. Harrison, A dual sensor selective for Hg²⁺ and cysteine detection, *Sensors Actuators B. Chem.* 255 (2018) 2756–2763. doi:10.1016/j.snb.2017.09.090.
- [49] E.M. Nolan, M.E. Racine, S.J. Lippard, Selective Hg(II) Detection in Aqueous Solution with Thiol Derivatized Fluoresceins, *Inorg. Chem.* 45 (2008) 2742–2749. doi:10.1021/ic052083w.
- [50] E. Coronado, R. Gala, C. Martí, E. Palomares, J.R. Durrant, M. Gratzel, Reversible Colorimetric Probes for Mercury Sensing, *J. Am. Chem. Soc.* 127 (2005) 12351–12356. doi:10.1021/ja0517724.
- [51] Z. Wang, J. Yang, Y. Li, Q. Zhuang, J. Gu, Zr-Based MOFs integrated with a chromophoric ruthenium complex for specific and reversible Hg²⁺ sensing, *Dalton Trans.* 47 (2018) 5570–5574. doi:10.1039/c8dt00569a.
- [52] G. Gangatharan, V. Kumar, M. Palsamy, A. Tamilselvi, A reversible fluorescent chemosensor for the rapid detection of Hg²⁺ in an aqueous solution: Its logic gates behavior, *Sensors Actuators B. Chem.* 273 (2018) 305–315. doi:10.1016/j.snb.2018.06.067.
- [53] W. Zhai, C. Du, X. Li, A series of logic gates based on electrochemical reduction of Pb(2+) in self-assembled G-quadruplex on the gold electrode., *Chem. Commun. (Camb).* 1 (2014) 2–4. doi:10.1039/c3cc47763k.
- [54] V.K. Gupta, A.K. Jain, S.K. Shoor, New “on–off” optical probe based on Schiff base responding to Al³⁺ ions: Logic gate application, *Sensors Actuators B Chem.* 219 (2015) 218–231. doi:10.1016/j.snb.2015.05.026.
- [55] T. Khantaw, C. Boonmee, T. Tuntulani, W. Ngeontae, Selective Turn-On fluorescence sensor for Ag⁺ using cysteamine capped CdS quantum dots: Determination of free Ag⁺ in silver nanoparticles solution, *Talanta.* 115 (2013) 849–856. doi:10.1016/j.talanta.2013.06.053.

- [56] E. Bertozzini, L. Galluzzi, A. Penna, M. Magnani, Application of the standard addition method for the absolute quantification of neutral lipids in microalgae using Nile red, *J. Microbiol. Methods*. 87 (2011) 17–23. doi:10.1016/j.mimet.2011.06.018.
- [57] E. Vanlı, M.N. Mısırlı, H. Alp, T. Ak, N. Özbek, Ü. Ocak, M. Ocak, Ion Sensor Properties of Fluorescent Schiff Bases Carrying Dipicolylamine Groups. A Simple Spectrofluorimetric Method to Determine Cu(II) in Water Samples, *J. Fluoresc.* 27 (2017) 1759–1766. doi:10.1007/s10895-017-2114-2.
- [58] A. Yari, F. Papi, Ultra trace mercury(II) detection by a highly selective new optical sensor, *Sensors Actuators, B Chem.* 160 (2011) 698–704. doi:10.1016/j.snb.2011.08.051.
- [59] K.D. Bhatt, D.J. Vyas, B.A. Makwana, S.M. Darjee, V.K. Jain, H. Shah, Turn-On fluorescence probe for selective detection of Hg(II) by calixpyrrole hydrazide reduced silver nanoparticle: Application to real water sample, *Chinese Chem. Lett.* 27 (2016) 731–737. doi:10.1016/j.ccllet.2016.01.012.
- [60] Y. Ruan, A. Li, J. Zhao, J. Shen, Y. Jiang, Specific Hg²⁺-mediated perylene bisimide aggregation for highly sensitive detection of cysteine, *Chem. Commun.* 46 (2010) 4938–4940. doi:10.1039/c0cc00630k.
- [61] M. Shahid, P. Srivastava, A. Misra, An efficient naphthalimide based fluorescent dyad (ANPI) for F⁻ and Hg²⁺ mimicking OR, XNOR and INHIBIT logic functions, *New J. Chem.* 35 (2011) 1690–1700. doi:10.1039/c1nj20058e.
- [62] Y. Yan, Y. Zhang, H. Xu, A Selective “Turn-On” Fluorescent Probe for Recognition of Mercury(II) Ions in Aqueous Solution Based on a Desulfurization Reaction, *ChemPulsChem.* 78 (2013) 628–631. doi:10.1002/cplu.201300150.
- [63] Y.M. Zhang, K.P. Zhong, J.X. Su, X.P. Chen, H. Yao, T.B. Wei, Q. Lin, A novel histidine-functionalized 1,8-naphthalimide-based fluorescent chemosensor for the selective and sensitive detection of Hg²⁺ in water, *New J. Chem.* 41 (2017) 3303–3307. doi:10.1039/c6nj03930h.
- [64] Z. Zhang, S. Lu, C. Sha, D. Xu, A single thiourea-appended 1,8-naphthalimide chemosensor for three heavy metal ions: Fe³⁺, Pb²⁺, and Hg²⁺, *Sensors Actuators, B Chem.* 208 (2015) 258–266. doi:10.1016/j.snb.2014.10.136.

Chapter 4

Naphthalimide-Amino Acid Conjugates Chemosensors for Hg²⁺ ion Detection: Based on Chelation Mediated Emission Enhancement in Aqueous Solution

Bahta, M.; Ahmed, N. *J. Photochem. Photobiol. A Chem.* **2019**, *378*, 85–93.

DOI: 10.1016/j.jphotochem.2019.04.027.



4.1 Introduction

Accumulation of heavy metals in the body of humans and animals could lead to many adverse health effects and serious illnesses over time [1,2]. Owing to its high affinity towards thiol group of proteins and enzymes, Hg^{2+} ion is one of the most hazardous and widespread global pollutants [3–5]. Due to its widespread exposure and its deleterious effects on human health, myriad of qualitative and quantitative detection methods of mercury have been devised, and the search for new Hg^{2+} ion detection with high selectivity, sensitivity and environmentally and biologically compatible chemosensor is still on progress [6,7]. Owing to their Turn-On character and high selectivity and sensitivity AIE based fluorescent chemosensors have been rapidly developing and thereby attracted tremendous research interest. AIE active molecules are fluorogenic molecules with high emission intensity in an aggregated or solid state, but weak or non-fluorescent when diluted [8,9]. The aggregate formation happens in poor solvents, especially, when hydrophobic organic fluorophores dissolve in aqueous media. AIE is very important aspect in fluorescence chemosensing to overcome the aggregation induced quenching in hydrophobic organic fluorophores.

Amino acids are highly water-soluble and environmentally and biologically compatible [10], and they can act as one of the best receptor units owing to their effective coordination with metal ions through their chelating moieties [11,12]. Hence, a variety of amino acids based chemosensors for different metal ions detection in aqueous system have been reported [13–19]. Amino acids containing thio group are known to form a very stable complex with Hg^{2+} ion [20–22], and are very effective Hg^{2+} receptors as per HSAB principles [23–25]. Due to this, it is an important aspect to incorporate thio-amino acids as a core scaffold in designing and preparation of new Hg^{2+} ion chemosensors. The conjugation of fluorophores signal unit with amino acid as a receptor part is a promising development for designing of a new water-soluble fluorescent chemosensor [26–28]. Among the various fluorophores, 1,8-naphthalimides have been extensively used in a wide variety of fluorescent chemosensors due to their high fluorescence quantum yield and natural photo-stability [29–35].

In continuation to our line of designing suitable Hg^{2+} chemosensors in the previous work [36,37], herein, we report relatively simple and straightforward preparation and photophysical characterization of amino acid functionalized 1,8-naphthalimides for impressively selective and sensitive detection of Hg^{2+} ions in aqueous solution. Developing Turn-On chemosensors in aqueous solution is more vital strategy in constructing fluorescence sensors, the presence of

carboxylic and thiol groups in the chemosensor helps to increase water solubility and its selectivity for Hg^{2+} ion detection. The amino acid functionalized 1,8-naphthalimides **L4** and **L5** are designed and synthesized by treating 1,8-naphthalic anhydride with thiol containing amino acids, L-methionine and L-cysteine respectively. The collective effect of hydrophobic 1,8-naphthalic core fluorophore with the specific amino acid functionalities leads the chemosensors to AIE active species and structurally optimized receptor which plays an important role in achieving a specific substrate for Hg^{2+} detection in aqueous media through chelation induced AIE.

4.2 Experimental Section

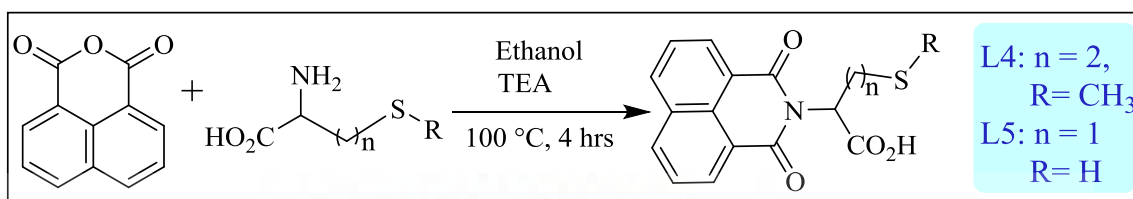
4.2.1 Reagents and Instrumentation

Stock solutions of all cations were prepared using their perchlorates which were purchased from Himedia and Loba Chemie, India. CH_3OH and deionized water were used for electronic spectral and fluorescence studies. IR spectra were recorded with KBr pellet on the Bruker Alpha FT-IR spectrometry in the range of $4000\text{--}400\text{ cm}^{-1}$. $^1\text{H-NMR}$ and $^{13}\text{C-NMR}$ spectra of compounds were recorded in $\text{DMSO-}d_6$ on a Bruker spectropin DPX 500 MHz spectrometry with TMS internal standard were used, and the chemical shift were reported as parts per million (ppm) scale downfield from TMS. The multiplicities were reported as abbreviations viz s = singlet, d = doublet, t = triplet and m = multiplet. Absorption and emission spectra were recorded using Specord S600 PC double beam spectrophotometer (path length 1cm) and Horiba RF-5301PC (path length 1cm) with standard quartz cell. Melting points were measured in the optimelt system and particle size by using Beckman Coulter Delsa Nano particle size analyzer. The fluorescence quantum yield and lifetime were measured and analyzed using fluorescence spectrometer FLS 980 (Edinburgh Instruments) and HORIBA Jobin Yvon, fluorocube fluorescence lifetime system respectively.

4.2.2 Synthesis and Characterization of Chemosensors

To a stirring suspension of 1,8-naphthalic anhydride (1 mmol) in ethanol (5 ml), 1.5 mmol amino acid (L-methionine or L-cysteine) and 10 drops of triethylamine were added and the resulting suspension was stirred at $100\text{ }^\circ\text{C}$ for 4 hrs (Scheme 4.1). After the completion of the reaction as indicated by TLC, it cooled down to room temperature, and triturated with diluted HCl, the solid product formed was collected by filtration, washed with water and air dried

[38]. A white solid product was obtained in 75% yield. The structures of **L4** and **L5** were characterized by IR, $^1\text{H-NMR}$, $^{13}\text{C-NMR}$, and HRMS spectroscopy (Figure 4.16-4.19).



Scheme 4.1. Synthesis of chemosensors **L4** and **L5**.

2-(1,3-dioxo-1H-benzo[de]isoquinolin-2(3H)-yl)-4-(methylthio)butanoic acid (L4): MP: 201.7 °C; IR (KBr, $\bar{\nu}/\text{cm}^{-1}$): 3258 (acid -OH), 1759 (acid -C=O), 1695, 1656 (amide -C=O), 1588, 1437, 1382, 1354 (aromatic frame), 722, 667 (C-S-C); $^1\text{H NMR}$ (500 MHz, $\text{DMSO-}d_6$, δ/ppm): 12.75 (s, 1H), 8.53 (d, $J = 7.2$ Hz, 2H), 8.50 (d, $J = 8.1$ Hz, 2H), 7.90 (t, $J = 7.7$ Hz, 2H), 5.71 (dd, $J = 8.1, 3.8$ Hz, 1H), 2.55 (s, 4H), 2.00 (s, 3H). $^{13}\text{C NMR}$ (126 MHz, $\text{DMSO-}d_6$, δ/ppm): 171.3, 163.8, 135.2, 131.8, 131.7, 128.0, 127.82, 122.2, 52.5, 31.0, 28.6, 15.0. HRMS (ESI+) m/z calcd. $\text{C}_{17}\text{H}_{15}\text{NO}_4\text{S}$ $[\text{M}+\text{Na}]^+$: 352.0619 found 352.0625 (Figure 4.16-4.19).

2-(1,3-dioxo-1H-benzo[de]isoquinolin-2(3H)-yl)-3-mercaptopropanoic acid (L5): MP: 273.2 °C, IR (KBr, $\bar{\nu}/\text{cm}^{-1}$): 3476, 2927 (acid -OH), 2604 (-SH), 1771, 1743 (acid -C=O), 1701, 1650 (amide -C=O), 1587, 1437, 1378, 1354 (aromatic frame), 655 (C-SH); $^1\text{H NMR}$ (500 MHz, $\text{DMSO-}d_6$, δ/ppm): 13.03 (s, 1H), 8.47 (d, $J = 8.1$ Hz, 2H), 8.40 (d, $J = 7.1$ Hz, 2H), 7.83 (t, $J = 7.7$ Hz, 2H), 5.86 (dd, $J = 8.9, 5.0$ Hz, 1H), 3.63 (dd, $J = 14.5, 4.9$ Hz, 1H), 3.44 (dd, $J = 14.4, 9.2$ Hz, 1H), 2.55 (s, 1H). $^{13}\text{C NMR}$ (126 MHz, $\text{DMSO-}d_6$, δ/ppm): 170.4, 163.6, 135.4, 131.8, 131.7, 127.8, 121.8, 115.0, 52.9, 37.4, HRMS (ESI+) m/z calcd. $\text{C}_{15}\text{H}_{11}\text{NO}_4\text{S}$ $[\text{M}+\text{H}]^+$: 302.3240 found 302.3058 (Figure 4.20-4.23).

4.2.3 Absorbance and Fluorescence Measurements

Both the absorption and fluorescence emission measurement experiments were conducted in $\text{MeOH}/\text{H}_2\text{O}$ (1:99, v/v. HEPES buffer, pH 7.0) using 1 cm path length quartz cuvette. A stock solution of **L4** and **L5** (1.0 mM) were prepared in CH_3OH and diluted to 10 μM within $\text{MeOH}/\text{H}_2\text{O}$ (1:99, v/v. HEPES buffer, pH 7.0), then the absorption and fluorescence measurements were carried out by placing 2 ml of 10 μM solution of **L4** or **L5** followed by 10 μl aqueous solution (1 mM) perchlorates salt metal ions (Na^+ , K^+ , Mg^{2+} , Ba^{2+} , Mn^{2+} , Zn^{2+} , Cu^{2+} , Co^{2+} , Ni^{2+} , Ag^+ , Al^{3+} , Fe^{2+} , Fe^{3+} , Pb^{2+} , Cd^{2+} , Cr^{3+} , and Hg^{2+}) in 1.0 cm path length

quartz cuvette. All fluorescence spectra of **L4** and **L5** have been carried out in 1 nm slit width. Freshly prepared 10 μM solution of each species were used for quantum yield and fluorescence lifetime measurements using 330 nm as excitation wavelength. The quantum yield was measured using fluorescence spectrometer FLS 980 and calculated *via* an integrating sphere method. While, fluorescence lifetime measurement was done by fluorescence lifetime spectroscopy (**FLS**) with manual lifetime scan process and calculated by exponential fit to determine their fluorescence decay time.

4.3 Results and Discussion

4.3.1 Aggregation-Induced Emission (AIE) Properties of **L4** and **L5**

Due to the combined effect of the hydrophobic 1,8-naphthalimide with the hydrophilic amino acidic functionalities, the chemosensors are soluble in methanol but slightly soluble in pure water, which leads to slight aggregation behaviours and weak fluorescence in aqueous media. The absorption peaks of **L4** and **L5** in methanol are located at 331 nm and 332 nm respectively. Meanwhile, the absorption spectra showed tailing caused by the Mie-scattering effect in water, and red-shift to 343 and 341 nm for **L4** and **L5** respectively (Figure 4.1), which implies the formation of nano-aggregates [39–41]. The bathochromic shift with spectral broadening is the attribute of strong possibility of J-aggregates formation [42].

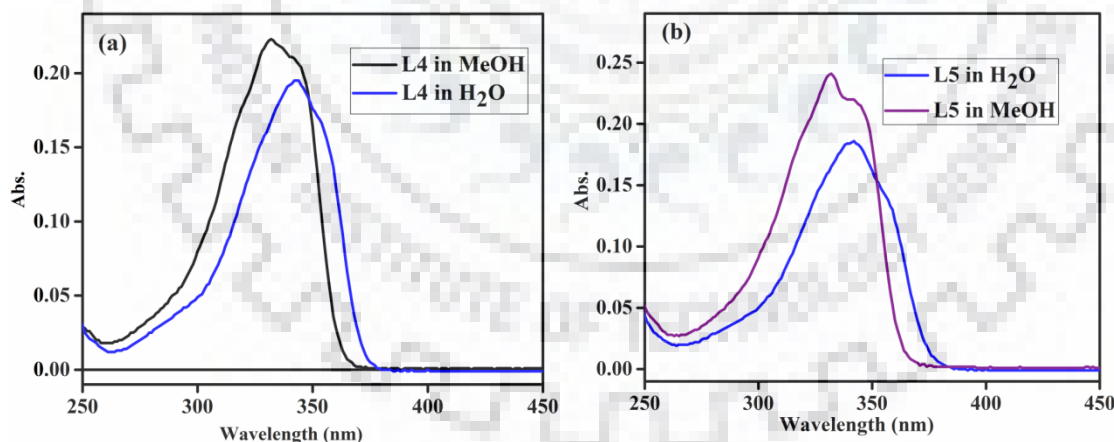


Figure 4.1 Absorption spectra change of (a). **L4**, (b). **L5** (10 μM) in pure MeOH and MeOH/H₂O (1:99, v/v. HEPES buffer, pH 7.0).

In general AIE active compounds are non-fluorescent in dilute solution turned into strong emitter upon aggregation [43,44] in the presence of poor solvents and in solid state due to effective restriction of the intermolecular rotations and vibrations suppress the non-radiative relaxation pathways [45–48]. Interestingly, the AIE characteristics of chemosensors (**L4** and

L5) were further confirmed by emission intensity enhancement with red shift 377 to 395 nm and 381 to 386 nm for **L4** and **L5** respectively. Upon increasing in fraction of water (Figure 4.2) and remarkable increase in quantum yield from ($\Phi_{\text{in MeOH}} = 0.033$ for **L4**, 0.053 for **L5**) to ($\Phi_{\text{water}} = 0.089$ for **L4**, 0.095 for **L5**). The formation of small nano aggregates of chemosensors in water was also supported by dynamic light scattering (DLS) technique. As shown in Figure 4.3 the particle size of **L4** and **L5** in water is greater than in MeOH, showing the chemosensors are slightly aggregated in water. All the above findings apparently signify that the chemosensors agree with the AIE features.

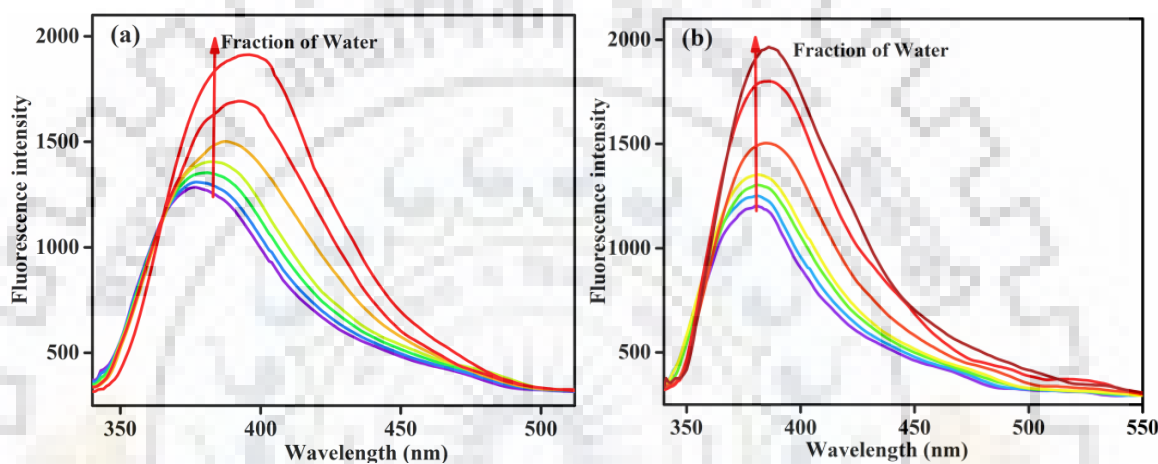


Figure 4.2 Fluorescence intensity of 10 μM (a) **L4**, (b) **L5** in CH_3OH solution with different fraction of water (0, 10, 20, 40, 60, 80, 99%).

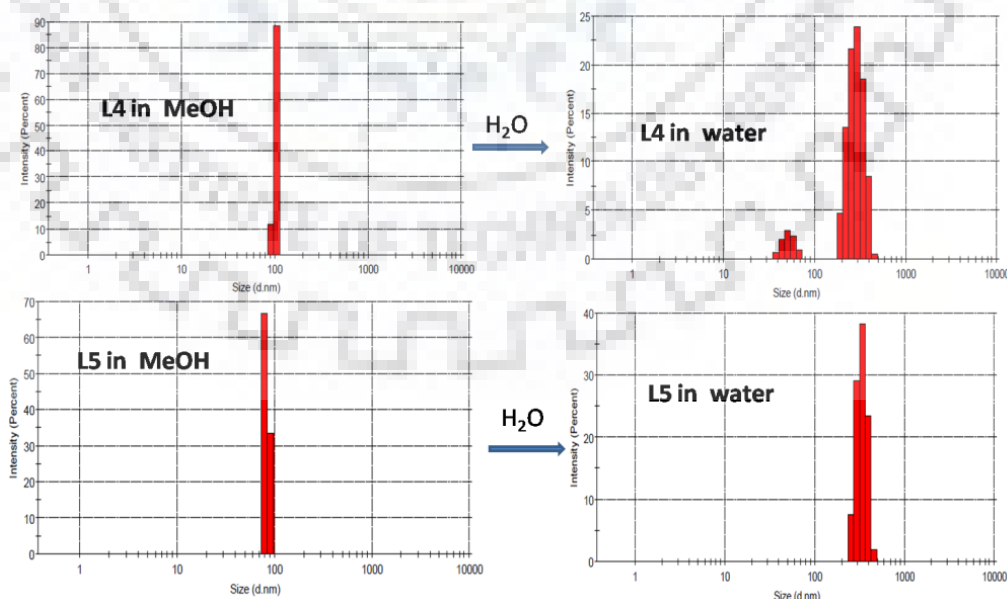


Figure 4.3 Dynamic light scattering results of **L4** and **L5** in CH_3OH and water.

4.3.2 Absorption Behaviour towards Various Cations

The interaction of the chemosensors with different metal ions in UV-vis absorption spectra were tested in the presence of a variety of metal ions (Na^+ , K^+ , Mg^{2+} , Ba^{2+} , Mn^{2+} , Zn^{2+} , Cu^{2+} , Co^{2+} , Ni^{2+} , Ag^+ , Al^{3+} , Fe^{2+} , Fe^{3+} , Pb^{2+} , Cd^{2+} , Cr^{3+} , and Hg^{2+}) in MeOH/H₂O mixtures (1:99 v/v). The chemosensors **L4** and **L5** in MeOH/H₂O (1:99, v/v.) solution revealed absorption maxima at 343 nm and 341 nm for **L4** and **L5** respectively, associated with the π - π^* transition of 1,8-naphthalimide. The absorption intensity remained unchanged for various metal ions, except, for Hg^{2+} (Figure 4.4). Furthermore, the binding properties of the chemosensors with Hg^{2+} ion were studied by UV-visible absorption titration, upon gradual addition of Hg^{2+} , the absorbance at 343 and 341 nm were decreased gradually with two isosbestic points at 311 and 364 nm for **L4**, and at 306 and 362 nm for **L5** (Figure 4.5). The presence of two isosbestic points during UV-Visible absorption titrations indicates the formation of two inter-converting species [49], most probably, ligand and ligand- Hg^{2+} complex.

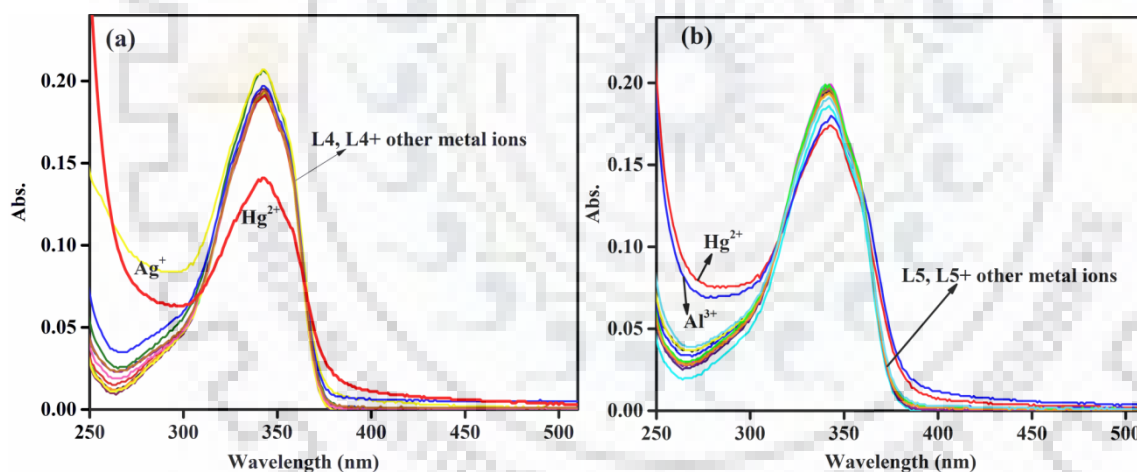


Figure 4.4 Absorption spectra of (a). **L4**, (b). **L5** (10 μM) in MeOH/H₂O (1:99, v/v. HEPES buffer, pH 7.0)) in the presence of 10.0 equiv. various cations.

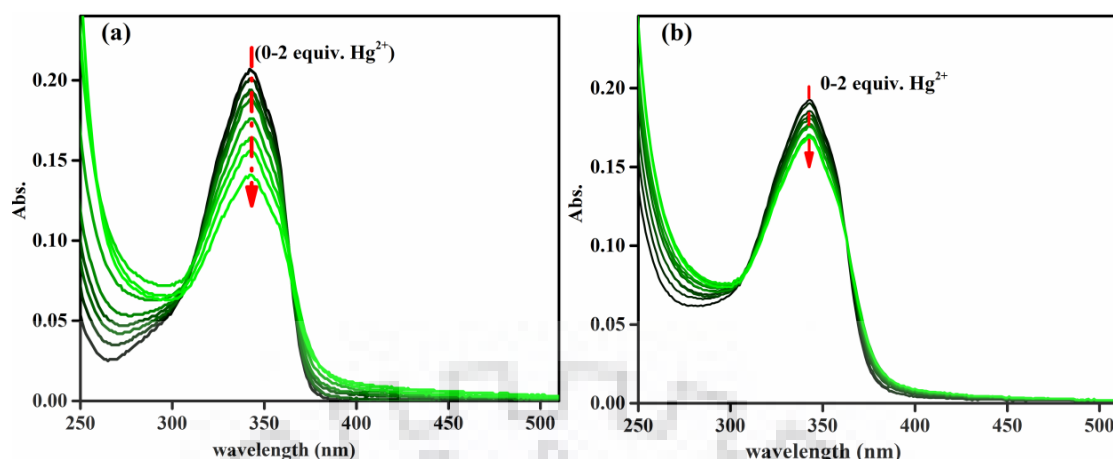


Figure 4.5 Absorption titrations spectral responses of (a). **L4**, (b). **L5** towards varying Hg^{2+} ion concentrations (0-2 equiv.) (In MeOH/ H_2O (1:99, v/v. HEPES buffer, pH 7.0).

4.3.3 Emission Behaviour towards Various Cations

In order to investigate the potential of the chemosensors to be applied for metal ion-sensing and to understand the effect of various metal ions on the photoemission property of chemosensors, the fluorescence spectra of chemosensors were tested in the presence of a variety of metal ions (Na^+ , K^+ , Mg^{2+} , Ba^{2+} , Mn^{2+} , Zn^{2+} , Cu^{2+} , Co^{2+} , Ni^{2+} , Ag^+ , Al^{3+} , Fe^{2+} , Fe^{3+} , Pb^{2+} , Cd^{2+} , Cr^{3+} , and Hg^{2+}) in MeOH/ H_2O (1:99, v/v. HEPES buffer, pH 7.0). As shown in Figure 4.6, Hg^{2+} ion drastically enhanced the fluorescence intensity of the chemosensors and there were trivial response by other metal ions.

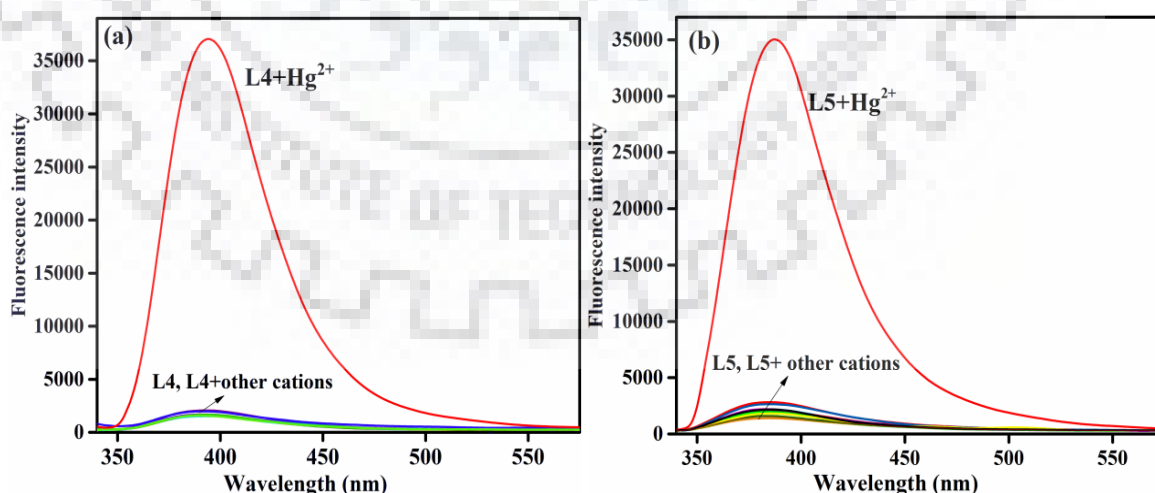


Figure 4.6 fluorescence spectra of (a). **L4**, (b). **L5** (10 μM , in MeOH/ H_2O (1:99, v/v. HEPES buffer, pH 7.0). in the presence of 10.0 equiv. various cations.

For further understanding of sensing mechanism and sensitivity, the fluorescence spectra were monitored with consecutive addition of Hg^{2+} under the optimized condition (Figure 4.7). The fluorescence intensity increased with gradual increase of Hg^{2+} concentrations, after the addition 5 equivalent of Hg^{2+} , the fluorescence intensity of **L4** at 395 nm was significantly enhanced by 20-folds and quantum yield increased from ($\Phi = 0.089$) to ($\Phi = 0.77$) while the fluorescence intensity of **L5** at 386 nm was enhanced by around 21-folds and quantum yield increased from ($\Phi = 0.095$) to ($\Phi = 0.75$) only by addition of 3 equivalents of Hg^{2+} , and the fluorescence intensity was not further enhanced by addition of excess Hg^{2+} . The fluorescent enhancement of the chemosensors is possible due to the selective chelation induced fluorescence enhancement (CHEF) effect. The coordination of receptors with Hg^{2+} increases the rigidity of the molecular assembly by restricting the free rotations of the chemosensors resulting in significant enhancement of the fluorescence intensity *via* CHEF effect. Moreover, increasing in Hg^{2+} ion concentration induces further aggregation of the chemosensor- Hg^{2+} complex thereby facilitates the aggregation induced emission enhancement (AIEE) behaviour of the chemosensors and drastically enhancing fluorescence intensity. Likewise, the fluorescence sensing ability of the sensor can be observed by the naked eye under UV irradiation shows a visible emission color change in the chemosensor with Hg^{2+} (inset Figure 4.7).

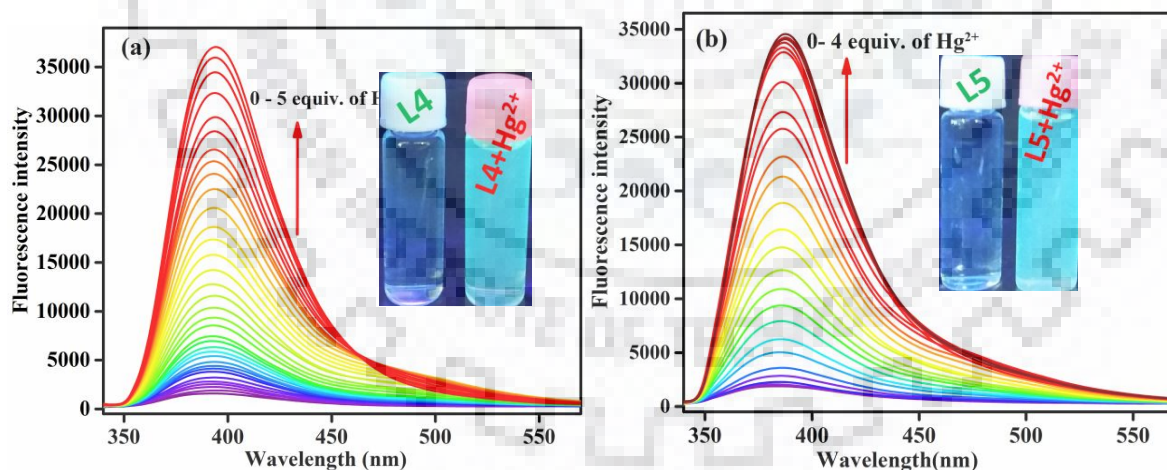


Figure 4.7 Fluorescence Emission titrations spectral responses of (a). **L4**, (b). **L5** towards varying Hg^{2+} ion concentrations ((In MeOH/ H_2O (1:99, v/v. HEPES buffer, pH 7.0)).

In verifying the grounds for enhancement of fluorescence intensity, the dynamic light scattering (DLS) and fluorescence life time techniques were performed to visualize the aggregation of the chemosensor- Hg^{2+} ion complex. Though the chemosensors grouped into slight aggregates in aqueous, still due to the slight solubility in water most of chemosensors

are in free state and the aggregates are small in size. Hence, the slightly aggregated chemosensors were further aggregated into 10 times larger size particles due to addition of Hg^{2+} as observed by DLS (Figure 4.8). This supports the formation of nano aggregates which could prompt the AIEE property *via* CHEF.

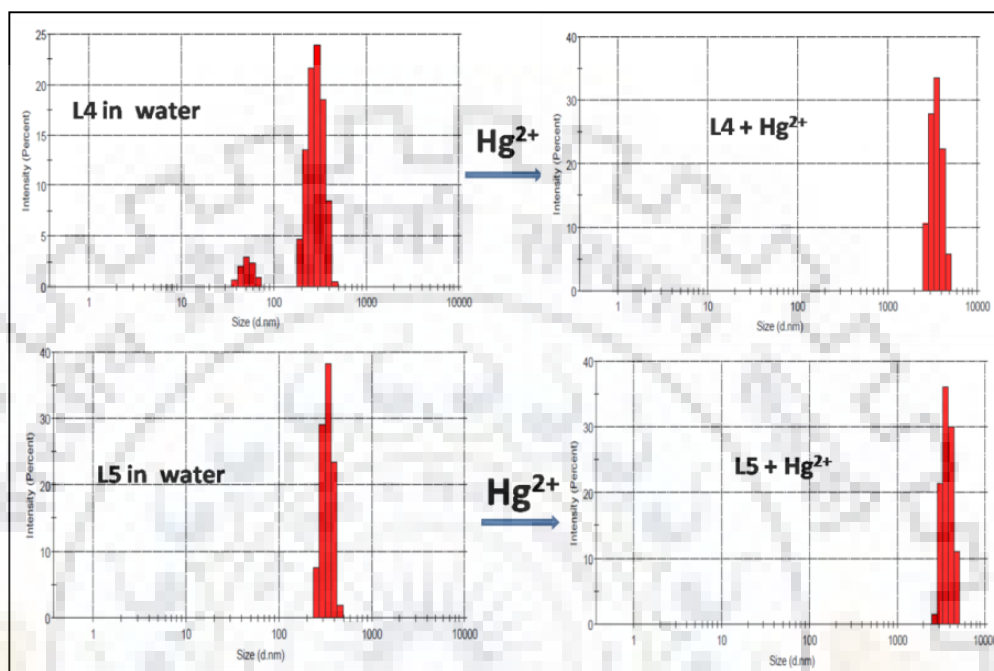


Figure 4.8 Dynamic light scattering results of **L4** and **L5** in the absence and presence of Hg^{2+} in MeOH/ H_2O (1:99, v/v. HEPES buffer, pH 7.0).

4.3.4 Fluorescence Lifetime

The fluorescence lifetime is one of the most important characteristics of light-emitting materials. The lifetime determines the time available for the fluorophore to interact with its environment, and the information can be available from its emission [50]. The time-resolved decays of **L4** and **L5** in methanol, water and upon addition of Hg^{2+} were measured using excitation wavelength of 330 nm and the decays were monitored at 395 and 386 nm for **L4** and **L5** respectively. The fluorescence lifetime of **L4** in methanol increased from 0.46 ns to 2.5 ns and 7.7 ns in water and upon addition of Hg^{2+} ion respectively (Figure 4.9a), as well as the fluorescence lifetime of **L5** was increased from 0.40 ns to 2.3 ns, and 8.5 ns in water and in the presence of Hg^{2+} ion respectively (Figure 4.9b). Prolonged fluorescence lifetime is an indication of aggregation and molecular interaction [51–53]. This increase in lifetime of ligand metal complex advocates stabilization of excited complex which increases the fluorescence intensity by over-crowding the intramolecular rotation of the chemosensors by

formation of rigid aggregates which can transfer them into strong emitters by beating the non-radiative relaxation pathway.

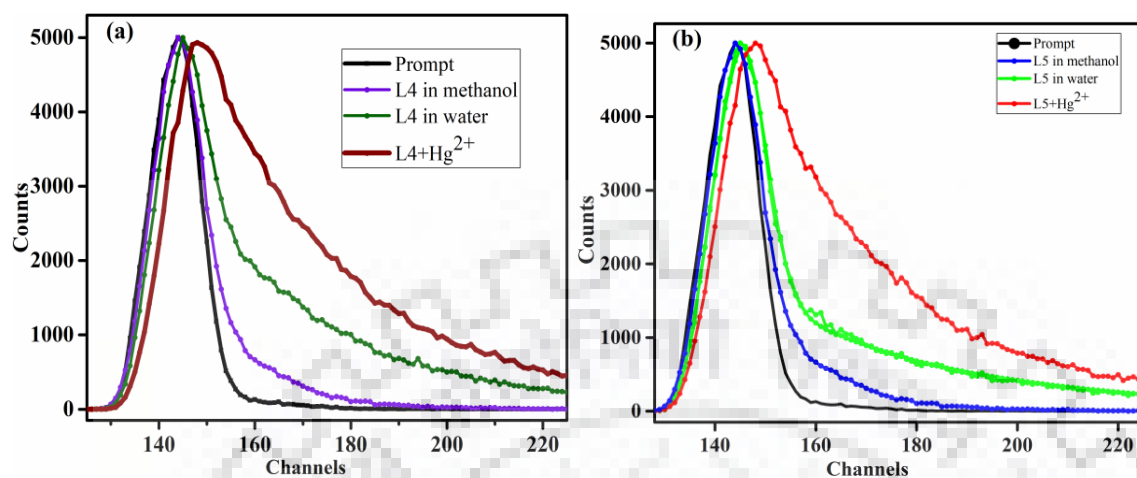


Figure 4.9 Lifetime decay profile of (a). **L4**, (b). **L5** in absence and presence of Hg^{2+} in MeOH/ H_2O (1:99, v/v. HEPES buffer, pH 7.0). ($\lambda_{\text{ex}}=330$ nm)

4.3.5 Stoichiometry

The stoichiometry of coordinating species was examined by the method of continuous variation (Job's plot) and found to be 2:1 with respect to chemosensor to Hg^{2+} (Figure 4.10) for both **L4** and **L5**. The mass spectra provides additional evidence of 2:1 stoichiometry, the HRMS (ESI+) m/z measurement of the mixture of **L4** and 2 equivalent of Hg^{2+} shows a peak at m/z 881.65 which corresponds to $\text{Hg}^{2+}(\text{L4})_2$ complex (Figure 4.24) as the calculated $[\text{2L4}+\text{Hg}^{2+}+\text{Na}]^+$ mass is 881.08 and the peak for the mixture of **L5** and 2 equivalent of Hg^{2+} appeared at m/z 803.54 which corresponds to $\text{Hg}^{2+}(\text{L5})_2$ complex (Figure 4.25) as calculated mass of $[\text{L5}+\text{Hg}^{2+}+\text{H}]^+$ is 803.04.

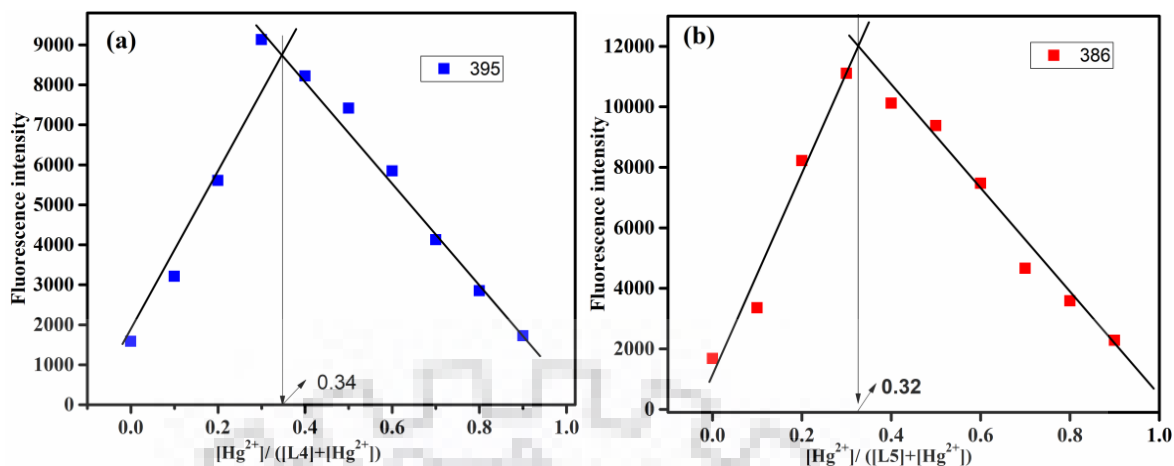


Figure 4.10 Job's plot (a). **L4**+Hg²⁺, (b). **L5**+Hg²⁺ (in MeOH/H₂O (1:99, v/v. HEPES buffer, pH 7.0).) the total concentration were 10 μ M.

4.3.6 Limit of Detection (LOD) and Association Constants (K_a)

The detection limit was calculated through standard deviations and linear fitting according to the IUPAC definition [54–56] and found to be 22 nM for **L4** and 5.6 nM for **L5** from the fluorescence titration result fit into the straight line as given in Figure 4.11.

$$LOD = 3.3 * \sigma / K$$

Where σ is the standard deviation of standard solution of regression lines and K is the slope of the graph

Table 4.1 Fluorescence intensity and standard deviation of blank receptors

	L4	L5	
S.NO	F. intensity	F. intensity	L4
1	1572.774	1869.305	$3.3 * 7.3227 / 1054.5 = 0.0229 * 10^{-6} \text{ molar} = 22 \text{ nM}$
2	1575.594	1877.407	
3	1588.008	1889.368	
4	1576.639	1887.398	
5	1579.392	1892.82	L5
6	1592.309	1878.517	$3.3 * 8.231 / 4827.8 = 0.00565 * 10^{-6} \text{ molar} = 5.6 \text{ nM}$
7	1586.395	1886.937	
STDEV	7.327887	8.273156	
K	1054.526	4827.87	

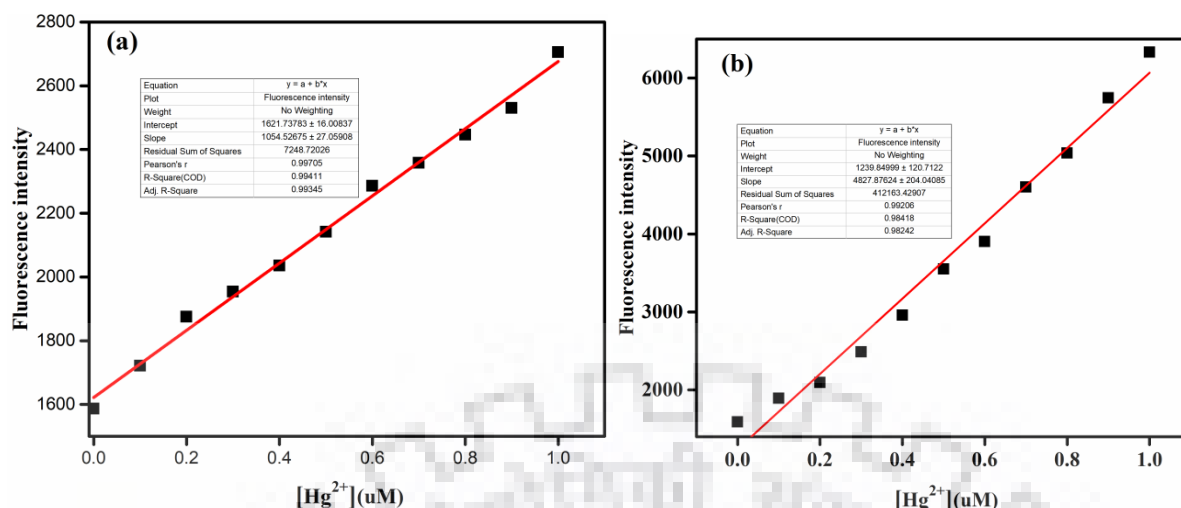


Figure 4.11 The linear fit graph of fluorescence intensity ratio as a function of Hg^{2+} concentration. (a) **L4**, (b) **L5**.

Considering the 2:1 complex formation, the binding constant (K_a) was calculated on the basis of modified Benesi-Hildebrand linear regression analysis [10,19,57] from the titration curve (Figure 4.12), and found to be 3.4×10^9 and $4.6 \times 10^9 \text{ M}^{-2}$ for **L4** and **L5** respectively, this advocates high binding affinity of **L4** and **L5** towards Hg^{2+} .

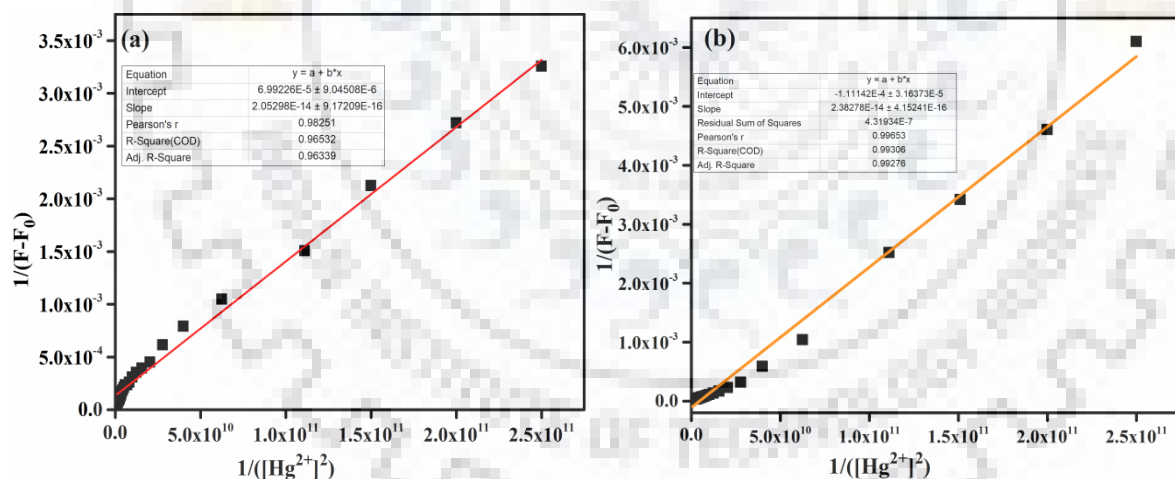


Figure 4.12 Benesi-Hildebrand Plot for K_a determination of (a) **L4**, (b) **L5** towards Hg^{2+} .

4.3.7 Selectivity Studies

The specificity of the chemosensors towards Hg^{2+} was further attested by monitoring their preference in the presence of other possible interfering metal ions (Na^+ , K^+ , Ba^{2+} , Ca^{2+} , Mg^{2+} , Cr^{3+} , Mn^{2+} , Co^{2+} , Ni^{2+} , Cu^{2+} , Zn^{2+} , Pb^{2+} , Ag^+ , Fe^{2+} , Fe^{3+} , Al^{3+} , and Cd^{2+}) (Figure 4.13). The chemosensors **L4** and **L5** were treated with 10 equivalents of different metal ions in the presence of 1 equivalent Hg^{2+} ion. The mixing of other cations into mixture of chemosensors and Hg^{2+} did not impose any change to fluorescence intensity enhancement inflicted by Hg^{2+}

ion, which showed outstanding selectivity. The excellent selectivity of the chemosensors in the presence of potential interfering metal ions was essentially due to stronger affinity of thio groups of the amino acids to Hg^{2+} .

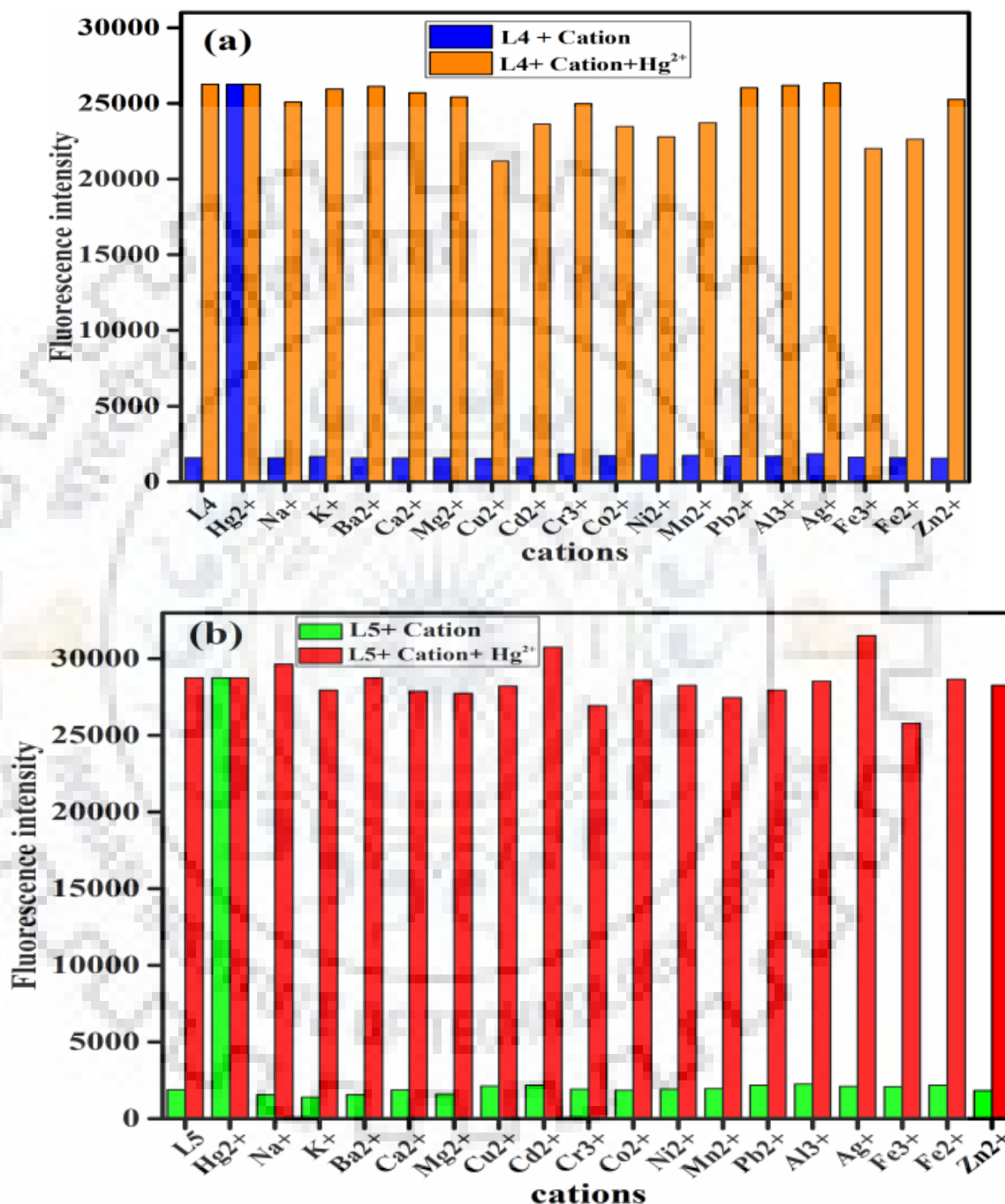


Figure 4.13 Interference effect of various cations, with (a) **L4** emission spectra at 395 nm (Blue bars represent the fluorescence intensity of **L4**+cations and orange bars show the fluorescence intensity of **L4**+ Hg^{2+} +other cations, and (b) **L5** emission spectra at 386 nm (green bars represent the fluorescence intensity of **L5**+cations and red bars show the fluorescence intensity of **L5**+ Hg^{2+} +other cations).

4.3.8 Binding Mode of L4 and L5 with Hg²⁺

The binding mode of **L4** and **L5** with Hg²⁺ were established by recording IR, ¹H NMR and HRMS spectra of **L4** and **L5** in the absence and presence of Hg²⁺ ion.

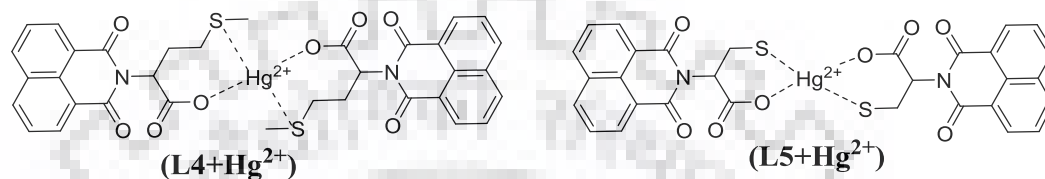
L4 shows a characteristic vibration bands at 3258 (acid –OH), 1759 (acid –C=O), 1695, 1656 (amide –C=O) and 722, 667 (C–S–C) among the major ones. Upon addition of Hg²⁺, the peaks corresponding to (C–S–C) and the acid group were diminished in intensity with slight shift (Figure 4.26) reveals the coupling of Hg²⁺ with the thio ether and acidic group of the amino acid. The characteristic bands of amide group of naphthalimide ring shows no significant change confirms that naphthalimide moiety is not involved in the coordination.

The binding mode was further investigated by ¹H NMR spectroscopy (Figure 4.27). The addition of Hg²⁺ to **L4** in DMSO-d₆ leads to deprotonation of –COOH and a slight change of chemical shifts in other protons. The –CH proton nearby carboxylic group shows up-field shift from 5.71 ppm to 5.69 ppm, while the –CH₃ shifted downfield from 2.00 ppm to 2.10 ppm and the four protons of the two CH₂ groups at 2.55 ppm (s, 4H) of amino acid chain were resolved into 2 different peaks at 2.63 ppm (s, 2H) and 2.55 ppm (s, 2H) indicating Hg²⁺ is binding with carboxylic and thiol ether group.

L5 exhibited a distinctive stretching vibration bands at 3476 cm⁻¹ and 2927 cm⁻¹ (acid –OH), 2604 cm⁻¹ (–SH), 1771 cm⁻¹ and 1743 (acid –C=O), 1701 and 1650 (amide –C=O) and 655 cm⁻¹ (C–SH) among the major ones. Upon addition of Hg²⁺, the peaks corresponding to (–SH) at 2604 cm⁻¹ and the acid group at 1771 cm⁻¹ were disappeared, while the –C–S band at 655 cm⁻¹ was shifted to 648 cm⁻¹ and the peak at 1743 (acid –C=O) was decreased in intensity (Figure 4.28), reveals the coupling of Hg²⁺ with –SH and acidic group of the amino acid and the insignificant shift in the amide (N–C=O) of the naphthalimide ring shows naphthalimide moiety is not involved in the coordination. The binding mode was further investigated by ¹H NMR spectroscopy as shown in Figure 4.28 the treatment of **L5** with Hg²⁺ ion leads to deprotonation of –SH and –COOH groups and a noticeable change of chemical shifts in other protons. The CH proton nearby carboxylic group shows up-field shift from 5.81 ppm to 5.72 ppm and the protons of the CH₂ group of amino acid chain were shifted towards downfield by 0.2 ppm (from 3.57 to 3.77) while the naphthalimide ring protons show little up-

field shift. The IR and ^1H NMR analysis suggested that Hg^{2+} ion is coordinated with carboxylic and thiol groups by $\text{Hg}-\text{O}$ and $\text{Hg}-\text{S}$ bond.

As per the spectroscopic data from IR, NMR and HRMS and the stoichiometric calculation, **L4** and **L5** coordinate with Hg^{2+} through acidic oxygen and sulphur of thio groups in 2:1 binding. Based on those observations, the probable binding mechanism of chemosensors with Hg^{2+} is presented in scheme 2



Scheme 2. Proposed sensing mechanism of chemosensors with Hg^{2+}

4.3.9 pH Selection

The choice of a suitable pH value has enormous significance for the detection procedure, because the spectroscopic properties of the carboxylic acid derivatives strongly depend on pH. The pKa for 4-methylthiobutyric acid (in **L4**) is 4.80 and pKa for 3-mercaptopropionic acid (in **L5**) is 4.34 [58]. At lower pH the carboxylic acids functionality will be in protonated form, while they will be deprotonated at higher pH.

The investigation of suitable pH value for sensing application was studied at pH range of (3-10) with and without Hg^{2+} ion. It was observed that high fluorescence emission of free chemosensors and low fluorescence intensity of complex was shown at low pH and the decreasing in the intensity at higher pH ranges was observed for both free chemosensors and complexes which might be due to deprotonation of chemosensors and mercury hydroxide formation. The overall pH effect for the fluorescence intensity for both chemosensors (**L4** and **L5**) and complexes (**L4+Hg²⁺** and **L5+Hg²⁺**) were constant in the pH range of 6-9 (Figure 4.14). This wide range pH stability is an important for its practical applications in both environmental and biological analysis. On this bases, we have selected the neutral pH ($\text{CH}_3\text{OH}:\text{H}_2\text{O}$ 1:99 v/v, HEPES buffer, pH 7.0) as optimized experimental condition for our study.

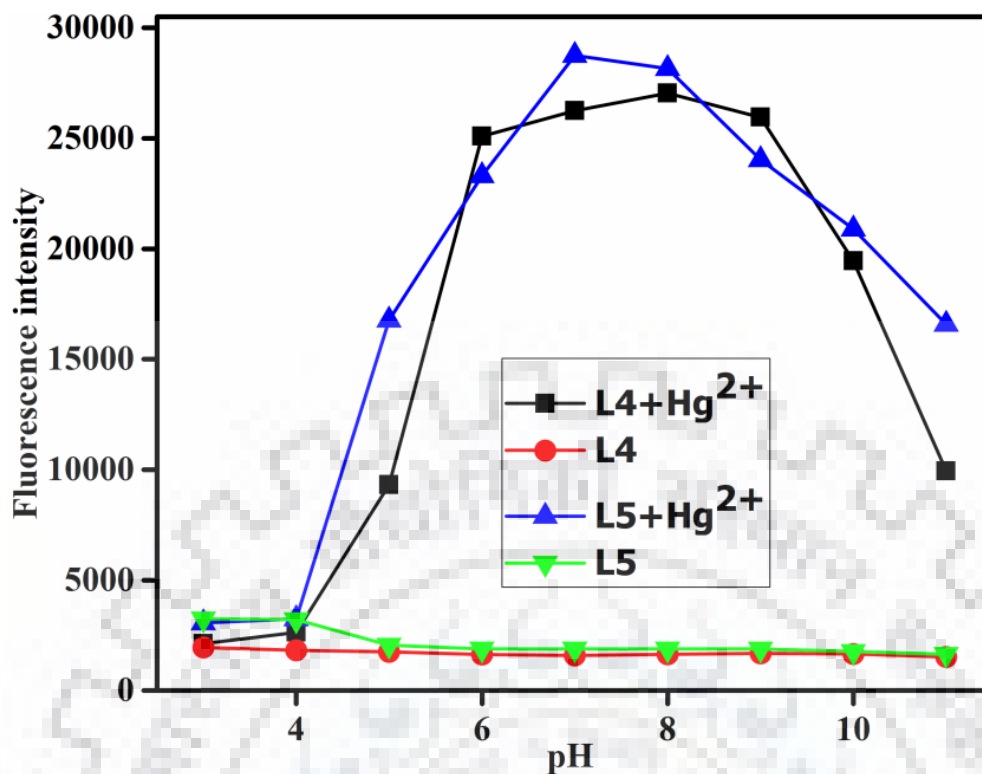


Figure 4.14 Fluorescence intensity of chemosensors (L4 and L5) and complexes (L4 + Hg²⁺ and L5 + Hg²⁺) at different pH values.

4.3.10 Reversibility Studies

It is very useful if a sensor is reversible and can be reused. The reusability of chemosensors (L4 and L5) for Hg²⁺ sensing was studied *via* addition of KI to the complex of chemosensor (L4 or L5) and Hg²⁺ in MeOH/H₂O (1:99, v/v, HEPES buffer, pH 7.0) solution. Importantly, chemosensors (L4 or L5) exhibits high reversibility (Figure 4.15), upon addition of 10 equiv. of KI, the fluorescence intensity returned almost to the free chemosensors which can be further reused. This is by the virtue of the high affinity of I⁻ to Hg²⁺ ion, it is possible to form stable mercury iodide complex [59–63].

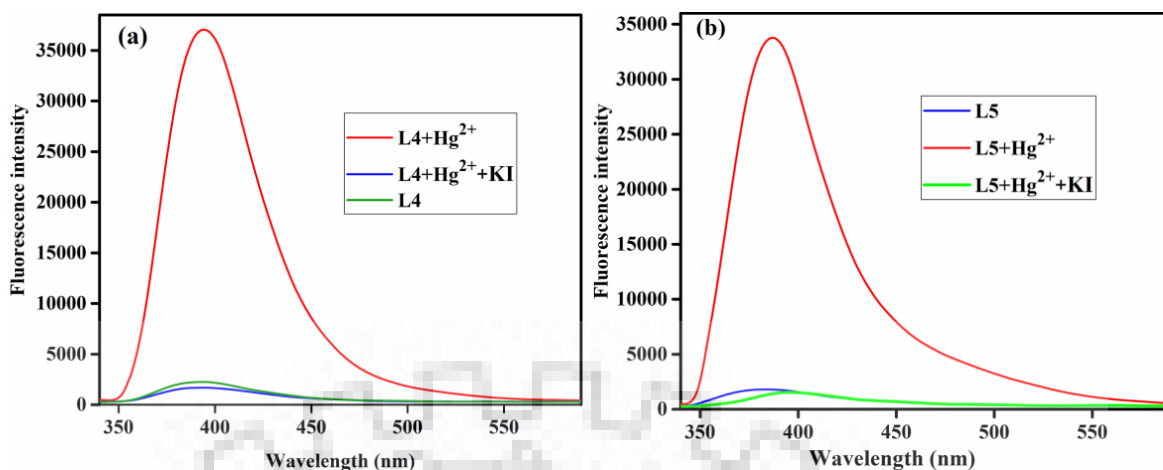


Figure 4.15 Fluorometric reversibility (a) L4, (b) L5 upon sequential addition of Hg²⁺ and KI.

4.4 Conclusion

Our new method presented several important features such as rapid detection, high sensitivity and selectivity towards Hg²⁺ versus other interfering tested metal ions. The uniqueness of the present work over the previous ones is possessing Hg²⁺ selectivity *via* chelation-mediated aggregation-induced emission enhancement (AIEE) in (In MeOH/H₂O (1:99, v/v) solution. The substrates employed in this work, the amino acids and 1,8-naphthalamide are biologically compatible and they can be further used for biological study. The ability of L4 and L5 to form chelated coordination complexes with Hg²⁺ ions is an important aspect in governing the fluorescence response; therefore, it could have great potential as a simple, cost effective selective and sensitive chemosensor for Hg²⁺ ion detection in aqueous solution.

Spectral Characterization of L4, L5, L4+Hg²⁺ and L5+Hg²⁺ by IR, NMR and HRMS

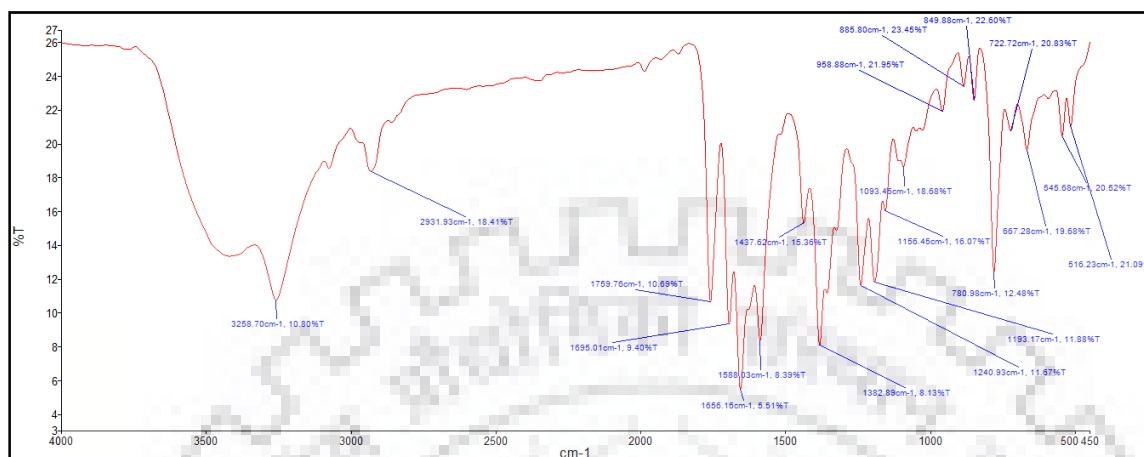


Figure 4.16 IR spectrum of receptor L4 recorded in KBr pellet.

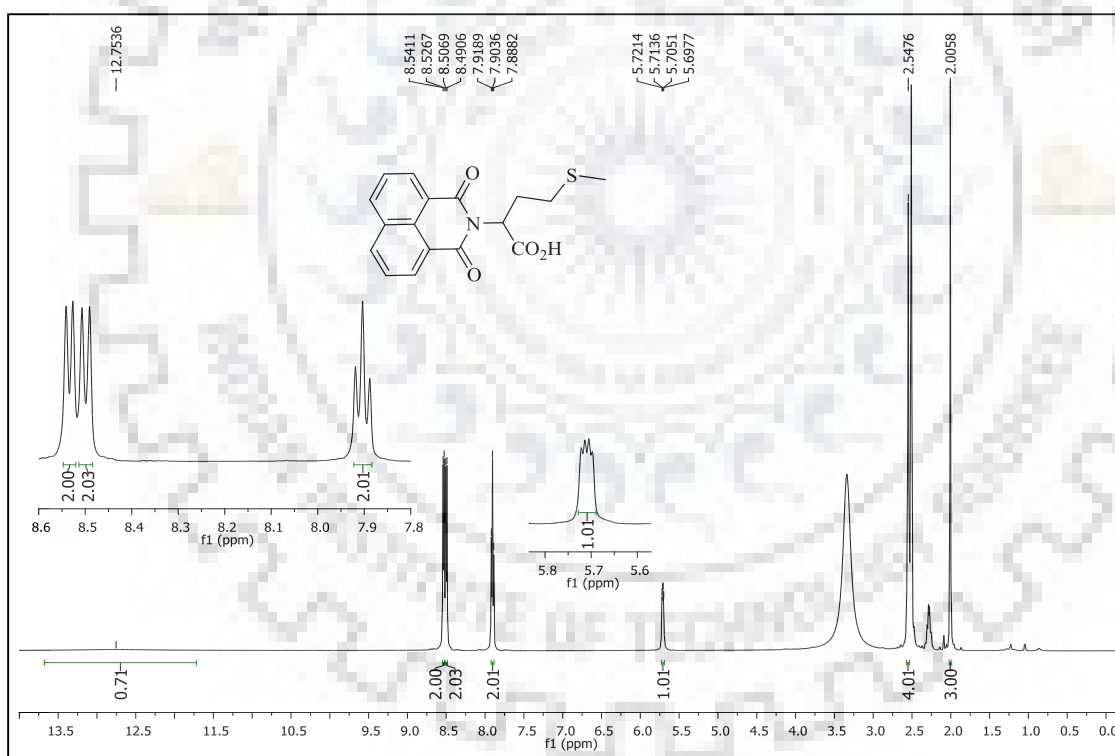


Figure 4.17 ¹H-NMR spectrum of receptor L4 recorded in DMSO-*d*₆.

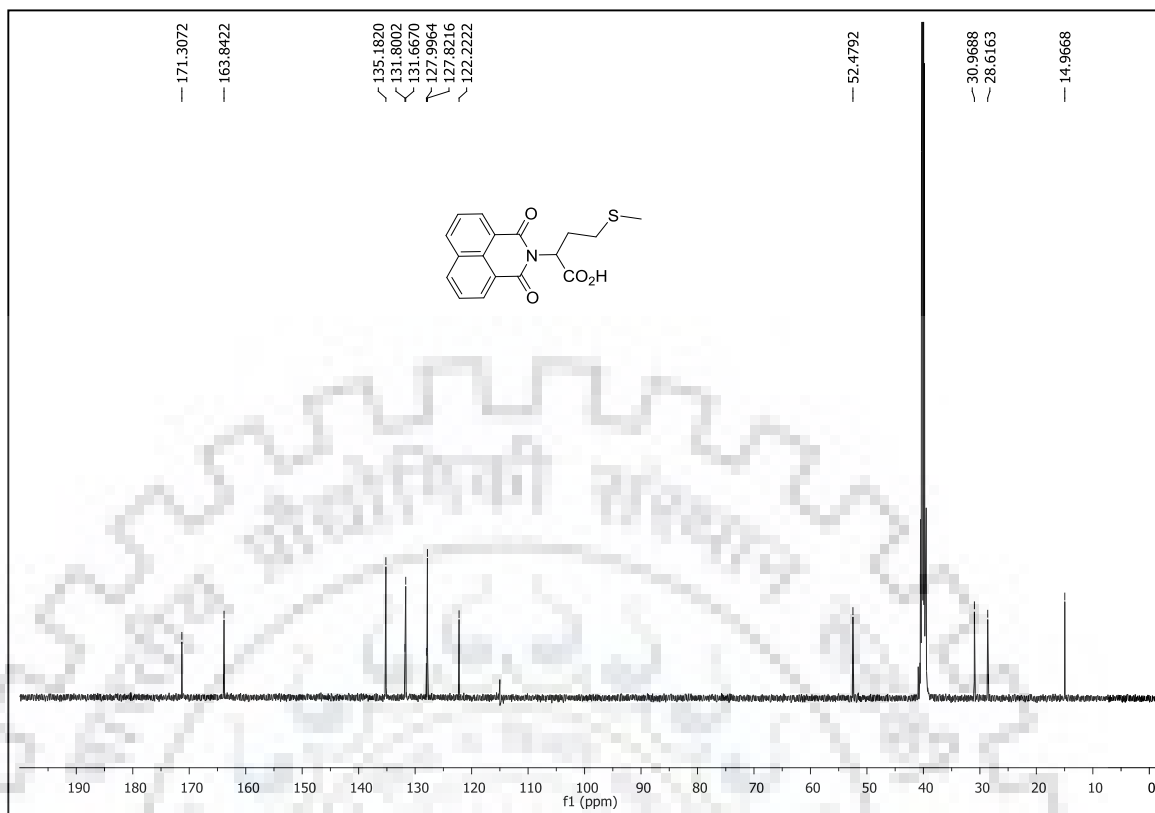


Figure 4.18 ^{13}C -NMR spectrum of receptor L4 recorded in $\text{DMSO-}d_6$.

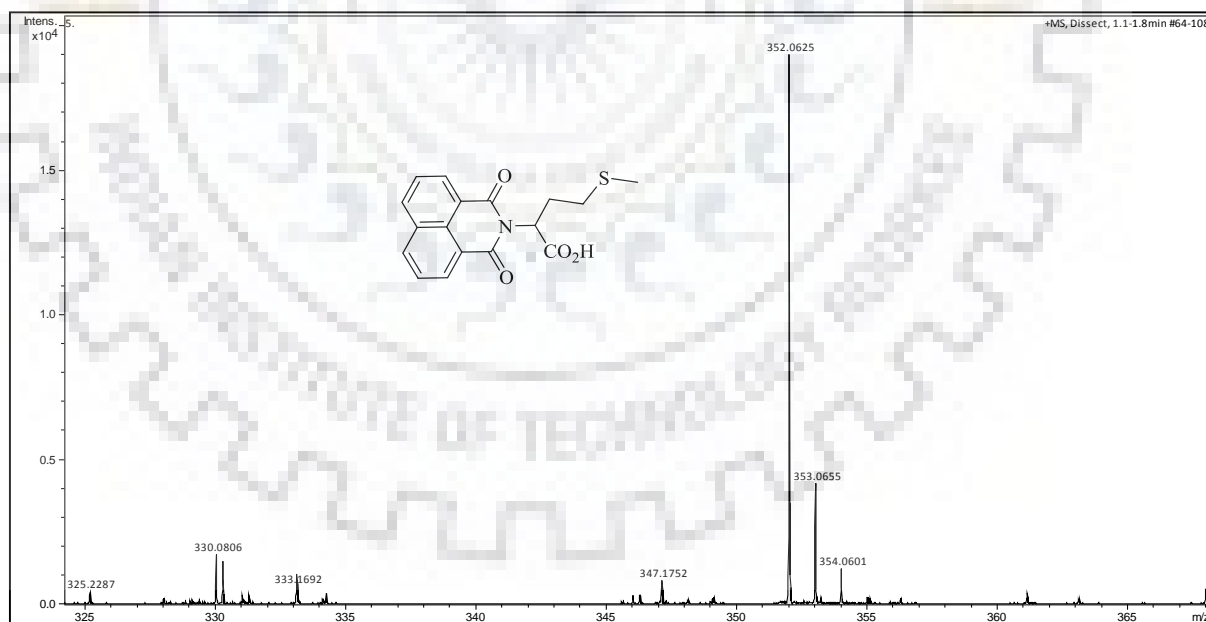


Figure 4.19 HRMS of receptor L4 recorded in CH_3CN .

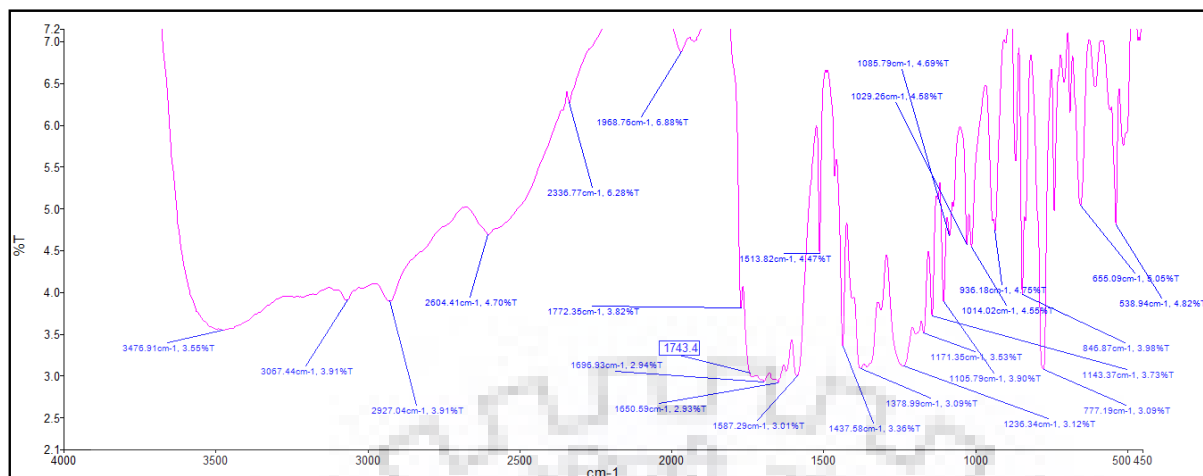


Figure 4.20 IR spectrum of receptor L5 recorded in KBr pellet.

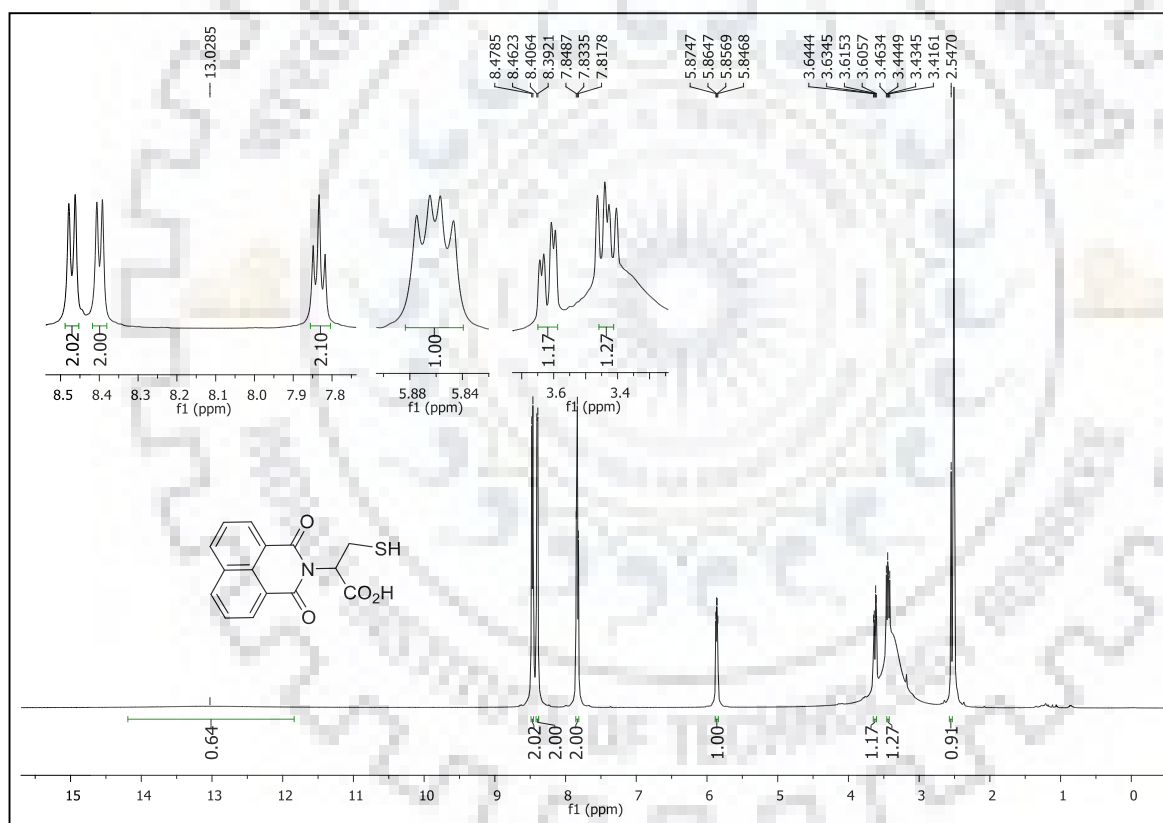


Figure 4.21 ¹H-NMR spectrum of receptor L5 recorded in DMSO-d₆.

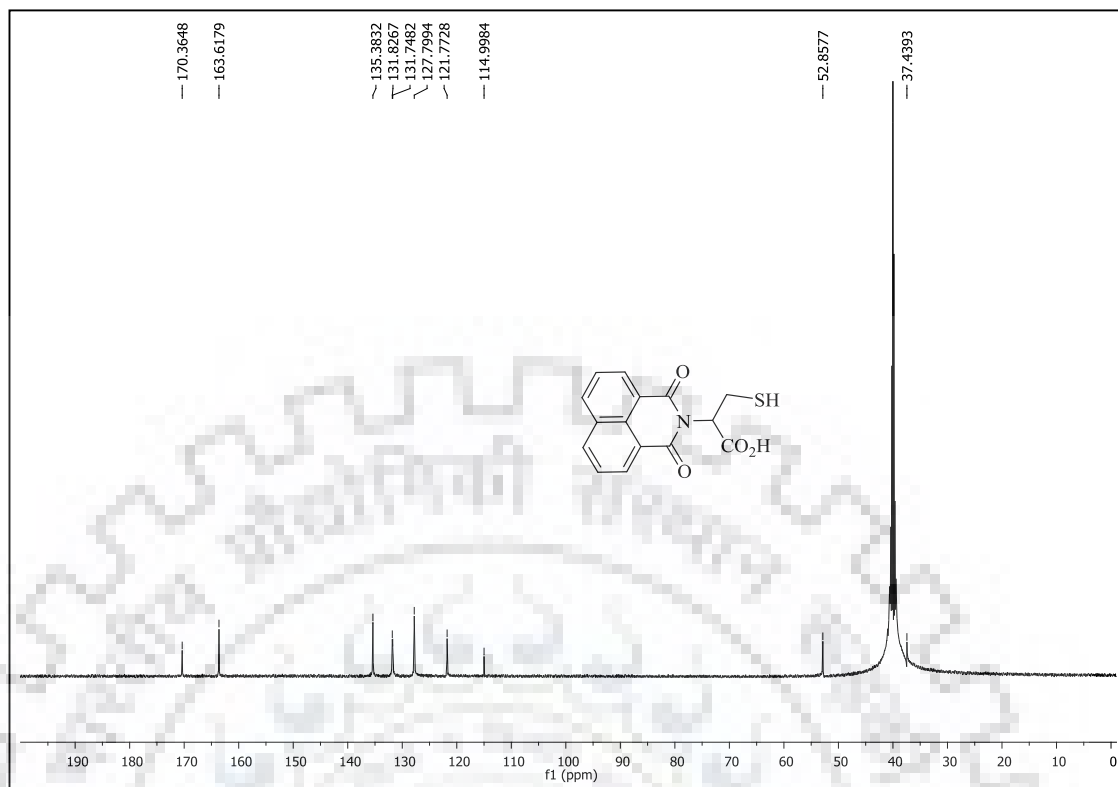


Figure 4.22 ^{13}C -NMR spectrum of receptor L5 recorded in DMSO-d_6 .

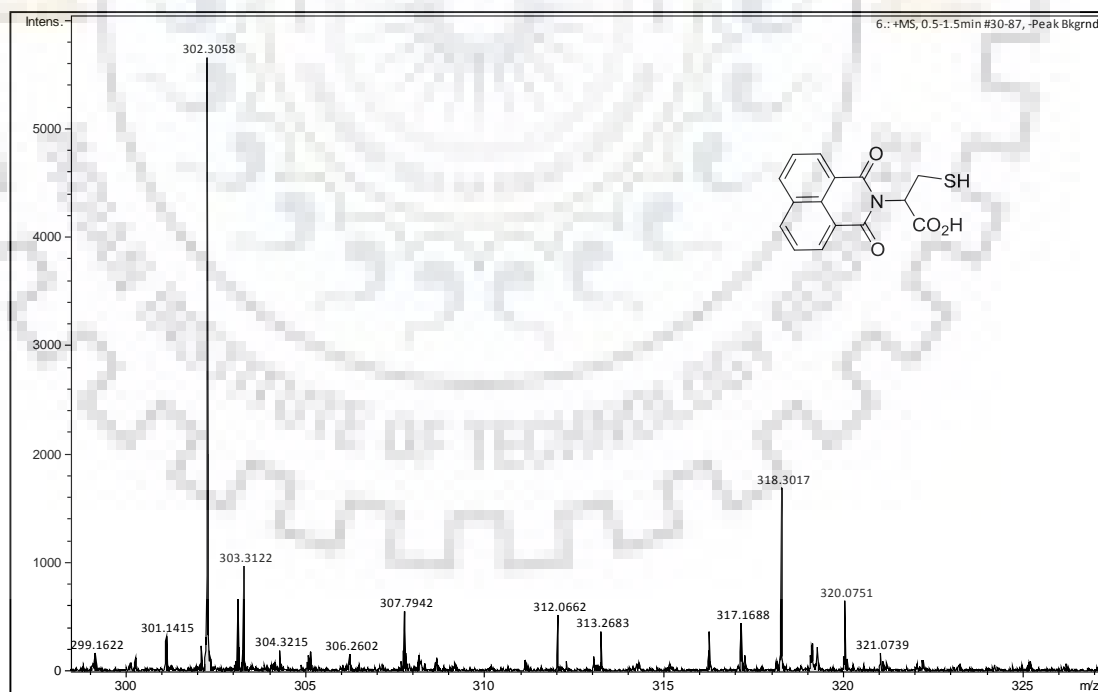


Figure 4.23 HRMS of receptor L5 recorded in CH_3CN .

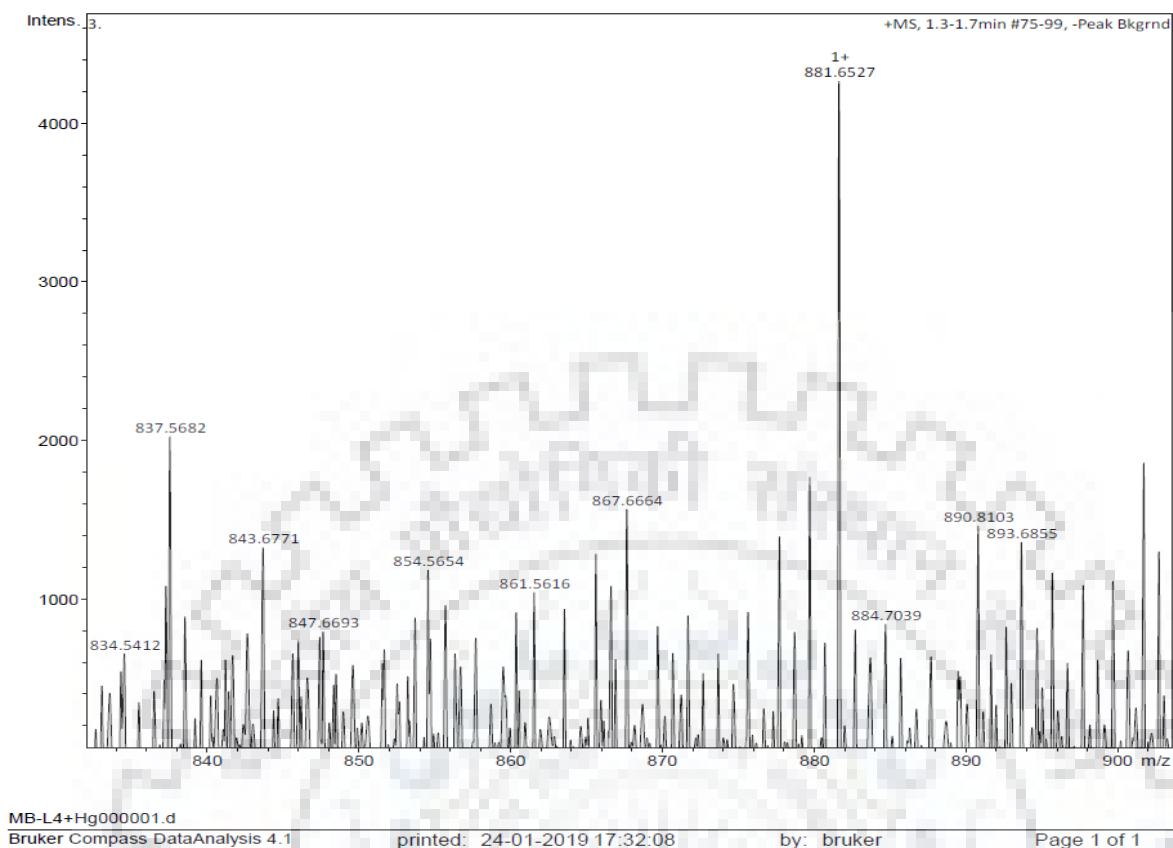


Figure 4.24 HRMS of receptor **L4+Hg²⁺** recorded in CH₃CN.

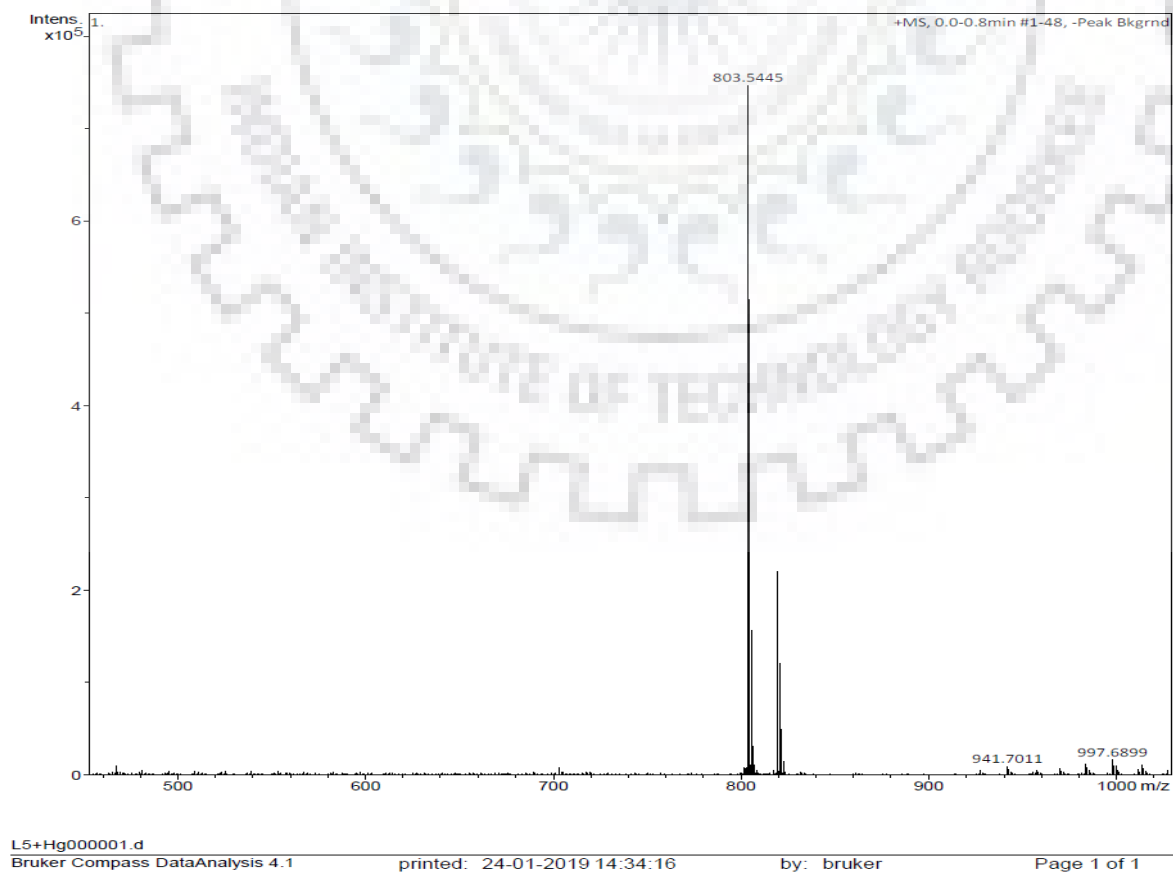


Figure 4.25 HRMS of receptor **L5+Hg²⁺** recorded in CH₃CN.

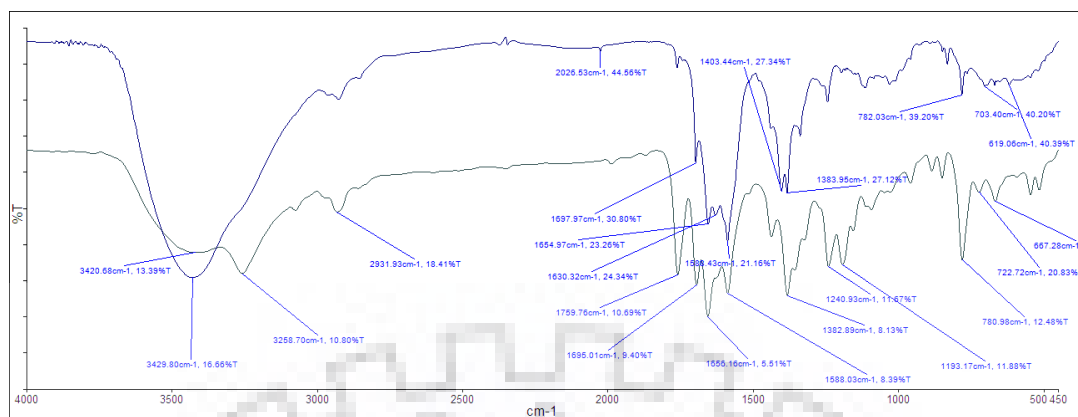


Figure 4.26 IR spectrum of receptor L4+Hg²⁺ recorded in KBr pellet

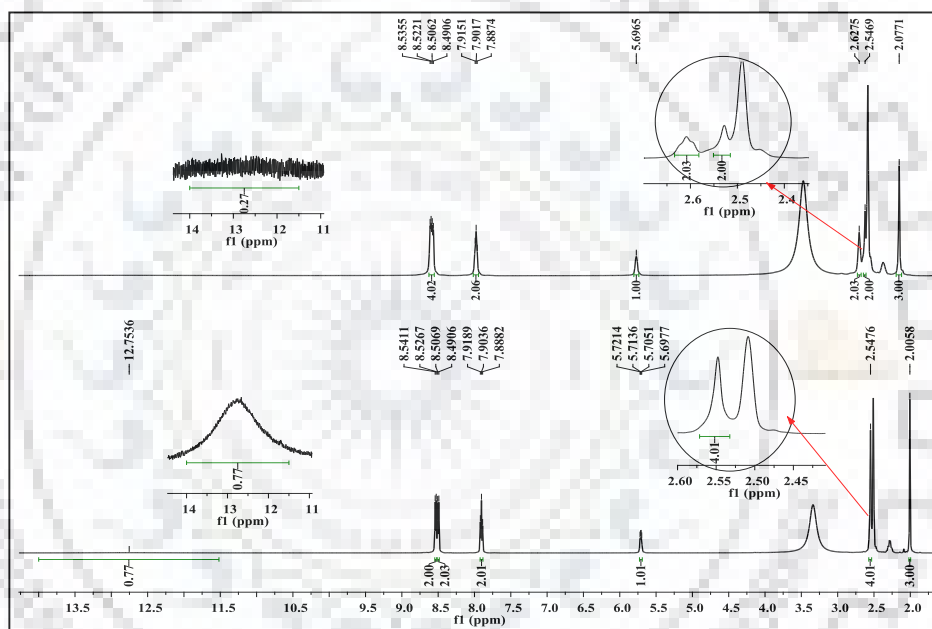


Figure 4.27 ¹H-NMR spectra of L4 with Hg²⁺ as HgCl₂ in DMSO-*d*₆.

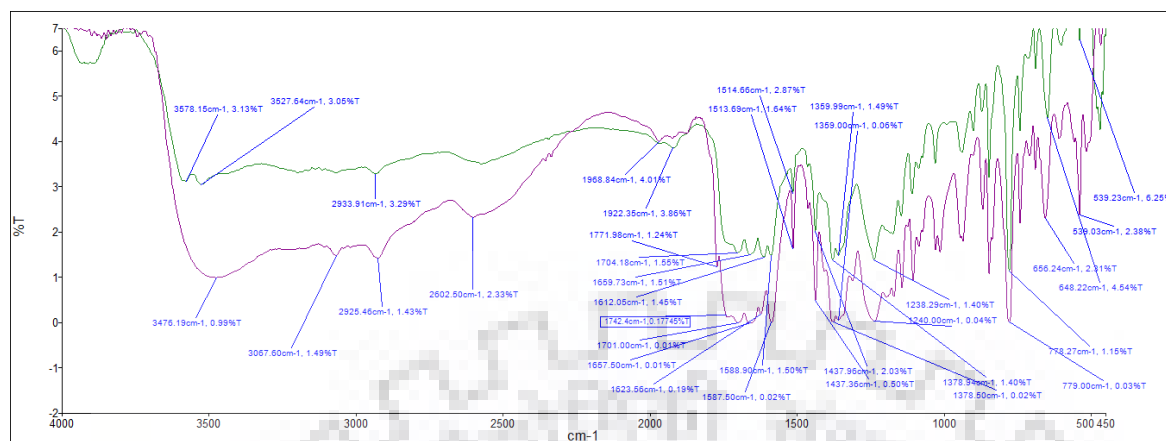


Figure 4.28 IR spectrum of receptor L5+Hg²⁺ recorded in KBr pellet

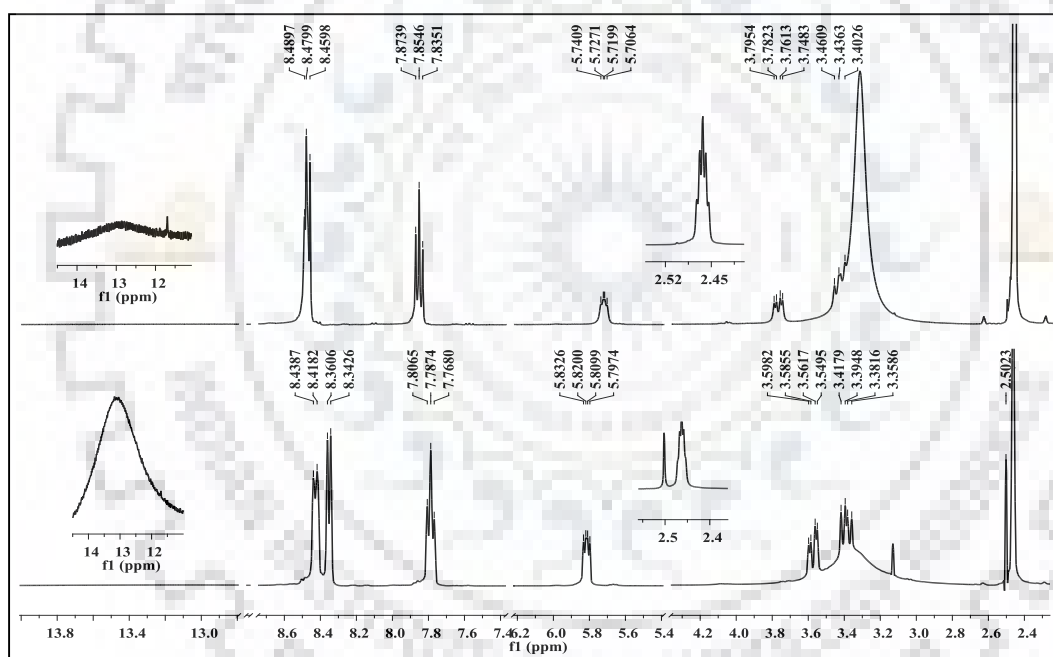


Figure 4.29 ¹H-NMR spectra of L5 with Hg²⁺ as HgCl₂ in DMSO-*d*₆.

4.5 References

- [1] A.T. Jan, M. Azam, K. Siddiqui, A. Ali, I. Choi, Q.M.R. Haq, Heavy metals and human health: Mechanistic insight into toxicity and counter defense system of antioxidants, *Int. J. Mol. Sci.* 16 (2015) 29592–29630. doi:10.3390/ijms161226183.
- [2] M. Jaishankar, T. Tseten, N. Anbalagan, B.B. Mathew, K.N. Beeregowda, Toxicity, mechanism and health effects of some heavy metals, *Interdiscip. Toxicol.* 7 (2014) 60–72. doi:10.2478/intox-2014-0009.
- [3] S. Jadoon, A. Malik, DNA Damage by Heavy Metals in Animals and Human Beings: An Overview, *Biochem. Pharmacol.* 6 (2017). doi:10.4172/2167-0501.1000235.
- [4] V. Poornimaa, V. Alexandarb, S. Iswariyaa, P.T. Perumalc, T.S. Uma, Gold nanoparticle based nano systems for the colorimetric detection of Hg²⁺ ion contamination in the environment, *RSC Adv.* 3 (2016) 1–13. doi:10.1039/x0xx00000x.
- [5] L.B. Poole, The basics of thiols and cysteines in redox biology and chemistry, *Free Radic. Biol. Med.* 80 (2015) 148–157. doi:10.1016/j.freeradbiomed.2014.11.013.
- [6] Z. Yan, M. Yuen, L. Hu, P. Sun, C. Lee, Advances for the colorimetric detection of Hg²⁺ in aqueous solution, *RSC Adv.* 4 (2014) 48373–48388. doi:10.1039/c4ra07930b.
- [7] G. Chen, Z. Guo, L. Tang, Fluorescent and colorimetric sensors for environmental mercury detection, *Analyst.* 140 (2015) 5400–5443. doi:10.1039/c5an00389j.
- [8] X. Wen, Q. Wang, Z. Fan, Highly selective Turn-On fluorogenic chemosensor for Zn(II) detection based on aggregation-induced emission, *J. Lumin.* 194 (2018) 366–373. doi:10.1016/j.jlumin.2017.10.064.
- [9] Y. Hong, W.Y. Lam, B. Zhong, Aggregation-induced emission, *Chem. Soc. Rev.* 40 (2011) 5361–5388. doi:10.1039/c1cs15113d.
- [10] M. Yang, P. Thirupathi, K. Lee, Selective and Sensitive Ratiometric Detection of Hg(II) Ions Using a Simple Amino Acid Based Sensor, *Org. Lett.* 13 (2011) 5028–5031. doi:10.1021/ol201683t.
- [11] S. Hutschenreiter, L. Neumann, U. Radler, L. Schmitt, R. Tampe, Metal-chelating amino acids as building blocks for synthetic receptors sensing metal ions and histidine-tagged proteins, *ChemBioChem.* 4 (2003) 1340–1344. doi:10.1002/cbic.200200455.
- [12] R.C.M. Ferreira, M.M.M. Raposo, S.P.G. Costa, Heterocyclic amino acids as fluorescent reporters for transition metals: Synthesis and evaluation of novel furyl-benzoxazol-5-yl-l-alanines, *New J. Chem.* 42 (2018) 3483–3492. doi:10.1039/c7nj04459c.

- [13] C. Klomsiri, P.A. Karplus, L.B. Poole, Cysteine-Based Redox Switches in Enzymes, *Antioxid Redox Signal.* 14 (2011) 1065–1077. doi:10.1089/ars.2010.3376.
- [14] B.R. White, M. Liljestrang, J.A. Holcombe, A ‘Turn-On’ FRET peptide sensor based on the mercury binding protein MerP, *RCS Anal.* 133 (2008) 65–70. doi:10.1039/b711777a.
- [15] L. Ma, Y. Liu, Y. Wu, A tryptophan-containing fluoroionophore sensor with high sensitivity to and selectivity for lead ion in water, *Chem. Commun.* 2 (2006) 2702–2704. doi:10.1039/b604623a.
- [16] L. Subha, C. Balakrishnan, S. Natarajan, M. Theetharappan, Water soluble and efficient amino acid Schiff base receptor for reversible fluorescence Turn-On detection of Zn^{2+} : Quantum chemical calculations and detection of bacteria, *Spectrochim. Acta Part A Mol. Biomol. Spectro.* 153 (2016) 249–256. doi:10.1016/j.saa.2015.08.033.
- [17] L.N. Neupane, J. Park, J.H. Park, K. Lee, Turn-On Fluorescent Chemosensor Based on an Amino Acid for Pb(II) and Hg(II) ions in Aqueous Solutions and Role of Tryptophan for Sensing, *Org. Lett.* 15 (2013) 254–257. doi:10.1021/ol3029516.
- [18] H. Li, Y. Li, Y. Dang, Y. Wu, G. Hou, L. Wu, An easily prepared hypersensitive water-soluble fluorescent probe for Mercury (II) ions, *Chem. Commun.* (2009) 4453–4455. doi:10.1039/b907386h.
- [19] B.P. Joshi, J. Park, W.I. Lee, K.-H. Lee, Ratiometric and Turn-On monitoring for heavy and transition metal ions in aqueous solution with a fluorescent peptide sensor, *Talanta.* 78 (2009) 903–909. doi:10.1016/j.talanta.2008.12.062.
- [20] H. Xu, S. Gao, Q. Liu, D. Pan, L. Wang, S. Ren, M. Ding, J. Chen, G. Liu, A highly sensitive and selective competition assay for the detection of cysteine using mercury-specific DNA, Hg^{2+} and Sybr green I, *Sensors.* 11 (2011) 10187–10196. doi:10.3390/s111110187.
- [21] M.B. Colovic, V.M. Vasic, D.M. Djuric, D.Z. Krstic, Sulphur-containing amino acids: protective role against free radicals and heavy metals., *Curr. Med. Chem.* 25 (2018) 1–12. doi:10.1109/HPCC.2012.229.
- [22] H. Xu, M. Hepel, “Molecular Beacon” based fluorescent assay for selective detection of glutathione and cysteine, *Anal. Chem.* 83 (2011) 813–819. doi:10.1021/ac102850y.
- [23] H. Wang, Y. Chen, Y. Li, H. Zhang, J. Cao, A rapid, sensitive and label-free sensor for Hg(II) ion detection based on blocking of cysteine-quenching of fluorescent poly(thymine)-templated copper nanoparticles, *RSC Adv.* 5 (2015) 94099–94104. doi:10.1039/c5ra18906c.

- [24] A. Banerjee, D. Karak, A. Sahana, S. Guha, S. Lohar, D. Das, Methionine–pyrene hybrid based fluorescent probe for trace level detection and estimation of Hg (II) in aqueous environmental samples: Experimental and computational studies, *J. Hazard. Mater.* 186 (2011) 738–744. doi:10.1016/j.jhazmat.2010.11.060.
- [25] A. Aliberti, P. Vaiano, A. Caporale, M. Consales, M. Ruvo, A. Cusano, Fluorescent chemosensors for Hg²⁺ detection in aqueous environment, *Sensors Actuators B. Chem.* 247 (2017) 727–735. doi:10.1016/j.snb.2017.03.026.
- [26] H. Dai, H. Xu, A water-soluble 1,8-naphthalimide-based ‘Turn On’ fluorescent chemosensor for selective and sensitive recognition of mercury ion in water, *Bioorg. Med. Chem. Lett.* 21 (2011) 5141–5144. doi:10.1016/j.bmcl.2011.07.085.
- [27] Y. Li, L. Li, J. Sun, C. Tian, Y. Wu, A protein-supported fluorescent reagent for the highly-sensitive and selective detection of mercury ions in aqueous solution and live cells, *Chem. Commun.* (2008) 6345–6347. doi:10.1039/b815281k.
- [28] M.H. Yang, C.R. Lohani, H. Cho, K.H. Lee, A methionine-based Turn-On chemical sensor for selectively monitoring Hg²⁺ ions in 100% aqueous solution, *Org. Biomol. Chem.* 9 (2011) 2350–2356. doi:10.1039/c0ob00780c.
- [29] Z. Zhang, Y. Chen, D. Xu, L. Yang, A. Liu, A new 1,8-naphthalimide-based colorimetric and "Turn-On" fluorescent Hg²⁺ sensor, *Spectrochim. ACTA PART A Mol. Biomol. Spectrosc.* 105 (2013) 8–13. doi:10.1016/j.saa.2012.11.113.
- [30] K.N. Hearn, T.D. Nalder, R.P. Cox, H.D. Maynard, T.D.M. Bell, F.M. Pfeffer, T.D. Ashton, Modular synthesis of 4-aminocarbonyl substituted 1,8-naphthalimides and application in single molecule fluorescence detection, *Chem. Commun.* 53 (2017) 12298–12301. doi:10.1039/c7cc07922b.
- [31] H. Ulla, B. Garudachari, M.N. Satyanarayan, G. Umesh, A.M. Isloor, Blue organic light emitting materials: Synthesis and characterization of novel 1,8-naphthalimide derivatives, *Opt. Mater.(Amst).* 36 (2014) 704–711. doi:10.1016/j.optmat.2013.11.017.
- [32] N. V Marinova, N.I. Georgiev, V.B. Bojinov, Synthesis and photophysical properties of novel 1,8-naphthalimide light- harvesting antennae based on benzyl aryl ether architecture, *J. Lumin.* 204 (2018) 253–260. doi:10.1016/j.jlumin.2018.08.011.
- [33] Z. Zhang, S. Lu, C. Sha, D. Xu, A single thiourea-appended 1,8-naphthalimide chemosensor for three heavy metal ions: Fe²⁺, Pb²⁺, and Hg²⁺, *Sensors Actuators, B Chem.* 208 (2015) 258–266. doi:10.1016/j.snb.2014.10.136.
- [34] Y.M. Zhang, K.P. Zhong, J.X. Su, X.P. Chen, H. Yao, T.B. Wei, Q. Lin, A novel histidine-functionalized 1,8-naphthalimide-based fluorescent chemosensor for the

- selective and sensitive detection of Hg^{2+} in water, *New J. Chem.* 41 (2017) 3303–3307. doi:10.1039/c6nj03930h.
- [35] J.S. Chen, R.Z. Liu, Y. Yang, T.S. Chu, Intramolecular charge transfer and sensing mechanism for a colorimetric fluoride sensor based on 1,8-naphthalimide derivatives, *Theor Chem Acc.* 133 (2014) 1411. doi:10.1007/s00214-013-1411-3.
- [36] M. Bahta, N. Ahmed, Design and synthesis of 1, 4-benzothiazine hydrazide as selective and sensitive colorimetric and Turn-On fluorometric sensor for Hg^{2+} detection in aqueous medium, *J. Photochem. Photobiol. A Chem.* 357 (2018) 41–48. doi:10.1016/j.jphotochem.2018.02.022.
- [37] M. Bahta, N. Ahmed, A novel 1,8-naphthalimide as highly selective naked-eye and ratiometric fluorescent sensor for detection of Hg^{2+} ions, *J. Photochem. Photobiol. A Chem.* 373 (2019) 157–161. doi:10.1016/j.jphotochem.2019.01.009.
- [38] K.A. Macgregor, M.J. Robertson, K.A. Young, L. Von Kleist, W. Stahlschmidt, A. Whiting, N. Chau, P.J. Robinson, V. Haucke, A. Mccluskey, Development of 1,8-Naphthalimides as Clathrin Inhibitors, *J. Med. Chem.* 57 (2014) 131–143. doi:10.1021/jm4015263.
- [39] R. Araya, V. Andino-pavlovsky, R. Yuste, R. Etchenique, Two-Photon Optical Interrogation of Individual Dendritic Spines with Caged Dopamine, *ACS Chem. Neurosci.* 4 (2013) 1163–1167. doi:10.1021/cn4000692.
- [40] X. Zhang, X. Gan, S. Yao, W. Zhu, J. Yu, Z. Wu, H. Zhou, Y. Tian, J. Wu, Branched triphenylamine-core compounds: aggregation induced two-photon absorption, *RSC Adv.* 6 (2016) 60022–60028. doi:10.1039/c6ra09701d.
- [41] A. Emission, K. Santhiya, S.K. Sen, R. Natarajan, R. Shankar, D–A–D Structured Bisacylhydrazone Exhibiting Aggregation-Induced Emission, Mechanochromic Luminescence, and Al(III) Detection, *J. Org. Chem.* 83 (2018) 10770–10775. doi:10.1021/acs.joc.8b01377.
- [42] Q. Zhao, J. Liu, H. Wang, M. Li, K. Zhou, H. Yangab, Y. Han, Balancing the H- and J-aggregation in DTS(PTTh2)2/PC70BM to yield a high photovoltaic efficiency, *J. Mater. Chem. C.* 3 (2015) 8183–8192. doi:10.1039/c5tc01205h.
- [43] X. He, H. Tian, Lightning Up Membrane Receptors with Fluorescent Molecular Probes and Supramolecular Materials, *Chem.* 4 (2017) 1–23. doi:10.1016/j.chempr.2017.11.006.
- [44] M. Gao, C.K. Sim, C. Wai, T. Leung, Q. Hu, G. Feng, F. Xu, B.Z. Tang, B. Liu, A fluorescent light-up probe with AIE characteristics for specific mitochondrial imaging

- to identify differentiating brown adipose cells, *Chem. Commun.* 50 (2014) 8312–8315. doi:10.1039/c4cc00452c.
- [45] Y. Hong, W.Y.J. Lam, B.Z. Tang, Aggregation-induced emission: phenomenon, mechanism and applications, *Chem. Commun.* (2009) 4332–4353. doi:10.1039/b904665h.
- [46] M.T. Gabr, F.C. Pigge, A selective fluorescent sensor for Zn^{2+} based on aggregation-induced emission (AIE) activity and metal chelating ability of bis(2-pyridyl)-diphenylethylene, *Dalton Trans.* 45 (2016) 14039–14043. doi:10.1039/c6dt02657e.
- [47] E. Ravindran, N. Somanathan, Efficient white-light emission from a single polymer system with “spring-like” self-assemblies induced emission enhancement and intramolecular charge transfer characteristics, *J. Mater. Chem. C.* (2017). doi:10.1039/C7TC01036B.
- [48] S. Mukherjee, P. Thilagar, Molecular flexibility tuned emission in “v” shaped naphthalimides: Hg(II) detection and aggregation-induced emission enhancement (AIEE), *Chem. Commun.* 49 (2013) 7292–7294. doi:10.1039/c3cc43351j.
- [49] A. Dvivedi, S. Kumar, M. Ravikanth, Nucleophilic addition of CN^- ion to $-C=N$ bond of aza-BODIPY leading to Turn-On fluorescence sensor, *Sensors Actuators B Chem.* 224 (2016) 364–371. doi:org/10.1016/j.snb.2015.10.045.
- [50] Y. Ren, J.W.Y. Lam, Y. Dong, B.Z. Tang, K.S. Wong, Enhanced Emission Efficiency and Excited State Lifetime Due to Restricted Intramolecular Motion in Silole Aggregates, *J. Phys. Chem. B.* 109 (2005) 1135–1140. doi:10.1021/jp046659z.
- [51] D.P. Bhopate, G.B. Kolekar, K.M. Garadkar, S.R. Patil, Cetyltrimethylammonium bromide stabilized perylene nanoparticles for fluorimetric estimation of bicarbonate (HCO_3^-) anion: spectroscopic approach, *Anal. Methods.* 5 (2013) 5324–5330. doi:10.1039/c3ay41049h.
- [52] P.G. Mahajan, D.P. Bhopate, G.B. Kolekar, S.R. Patil, N-methyl isatin nanoparticles as a novel probe for selective detection of Cd^{2+} ion in aqueous medium based on chelation enhanced fluorescence and application to environmental sample, *Sensors Actuators B Chem.* 220 (2015) 864–872. doi:10.1016/j.snb.2015.05.119.
- [53] D.P. Bhopate, P.G. Mahajan, K.M. Garadkar, G.B. Kolekar, S.R. Patil, Pyrene nanoparticles as a novel FRET probe for detection of rhodamine 6G : spectroscopic ruler for textile effluent Characterization of PyNPs, *RSC Adv.* 5 (2014) 63866–63874. doi:10.1039/c4ra13555e.
- [54] M. Kumar, L.K. Kumawat, V.K. Gupta, A. Sharma, Rational design of the first

- furoquinolinol based molecular systems for easy detection of Cu^{2+} with potential applications in the area of membrane sensing, *RSC Adv.* 5 (2015) 106030–106037. doi:10.1039/c5ra21862d.
- [55] M. Li, W. Feng, H. Zhang, G. Feng, An aza-coumarin-hemicyanine based near-infrared fluorescent probe for rapid, colorimetric and ratiometric detection of bisulfite in food and living cells, *Sensors Actuators, B Chem.* 243 (2017) 51–58. doi:10.1016/j.snb.2016.11.132.
- [56] E. Desimoni, B. Brunetti, About Estimating the Limit of Detection by the Signal to Noise Approach, *Pharm. Anal. Acta.* 6 (2015). doi:10.4172/2153-2435.1000355.
- [57] N. Maurya, S. Bhardwaj, A.K. Singh, Selective colorimetric and fluorescence ‘Turn-On’ sensor for Ag^+ and in-situ sensing of CN^- (off–on–off) via displacement approach, *Mater. Sci. Eng. C.* 74 (2017) 55–61. doi:10.1016/j.msec.2016.12.131.
- [58] M. Catellani, E. Kozma, G. Grisci, K. Pagano, F. Galeotti, A. Eckstein-andicsov, Water-soluble aminoacid functionalized perylene diimides: The effect of aggregation on the optical properties in organic and aqueous media, *Dye. Pigment.* 125 (2016) 201–209. doi:10.1016/j.dyepig.2015.10.019.
- [59] C. Song, X. Zhang, C. Jia, P. Zhou, X. Quan, C. Duan, Highly sensitive and selective fluorescence sensor based on functional SBA-15 for detection of Hg^{2+} in Aqueous Media, *Talanta.* 81 (2010) 643–649. doi:10.1016/j.talanta.2009.12.047.
- [60] G. Gangatharan, V. Kumar, M. Palsamy, A. Tamilselvi, A reversible fluorescent for the rapid detection of Hg^{2+} in an aqueous solution: Its logic gates behavior, *Sensors Actuators B. Chem.* 273 (2018) 305–315. doi:10.1016/j.snb.2018.06.067.
- [61] Z. Wang, J. Yang, Y. Li, Q. Zhuang, J. Gu, Zr-Based MOFs integrated with a chromophoric ruthenium complex for specific and reversible Hg^{2+} sensing, *Dalton Trans.* 47 (2018) 5570–5574. doi:10.1039/c8dt00569a.
- [62] R.X. Zhang, P.F. Li, W.J. Zhang, N. Li, N. Zhao, A highly sensitive fluorescent sensor with aggregation-induced emission characteristics for the detection of iodide and mercury ions in aqueous solution, *J. Mater. Chem. C.* 4 (2016) 10479–10485. doi:10.1039/c6tc03696a.
- [63] E. Coronado, R. Gala, C. Martí, E. Palomares, J.R. Durrant, M. Gratzel, Reversible Colorimetric Probes for Mercury Sensing, *J. Am. Chem. Soc.* 127 (2005) 12351–12356. doi:10.1021/ja0517724.

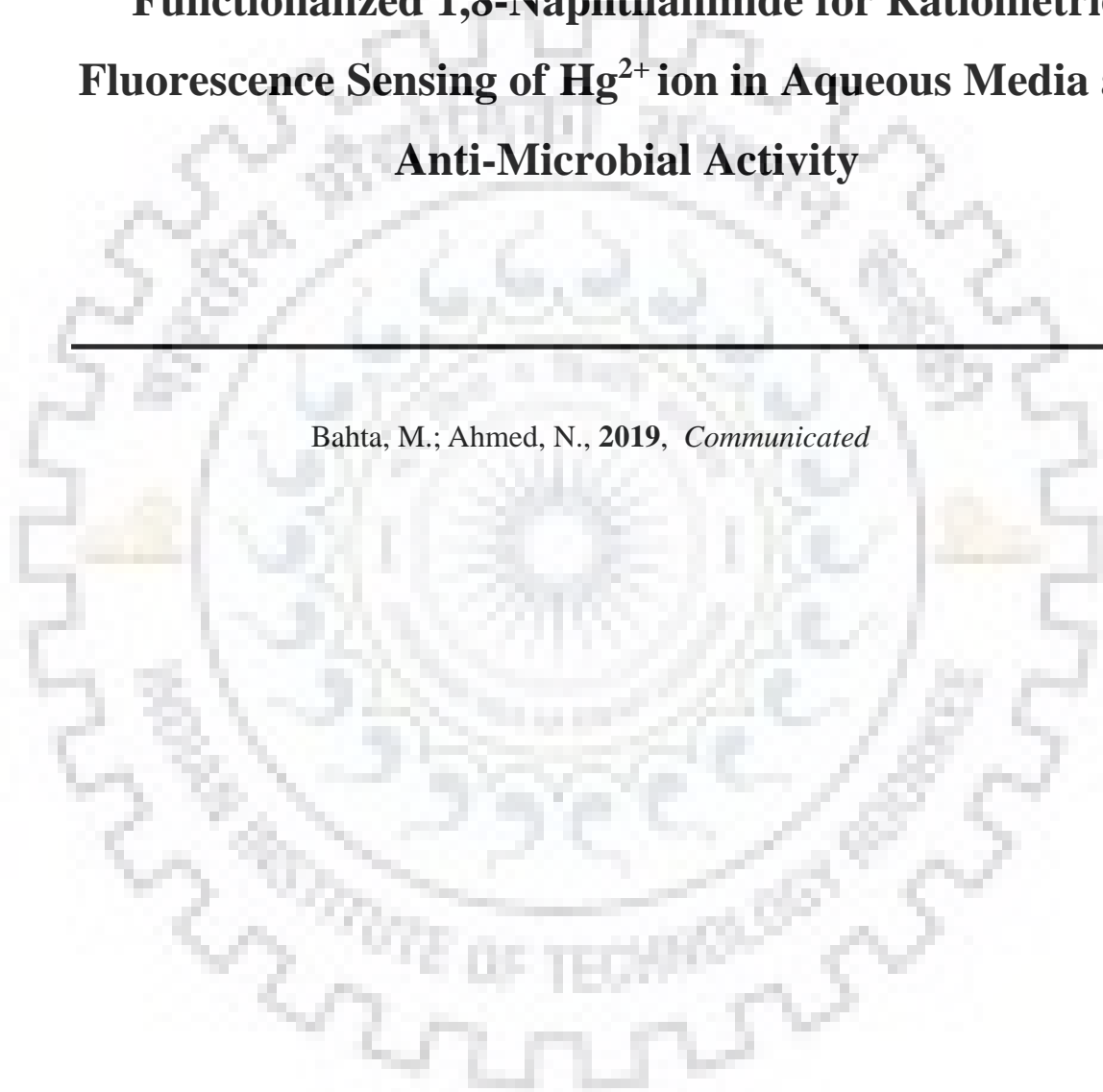




Chapter 5

Synthesis and Evaluation of AIEE Active Sulfamethizole Functionalized 1,8-Naphthalimide for Ratiometric Fluorescence Sensing of Hg²⁺ ion in Aqueous Media and Anti-Microbial Activity

Bahta, M.; Ahmed, N., 2019, *Communicated*





5.1 Introduction

The development of organic sensors with high selectivity and sensitivity for the toxic heavy metal ions has rigorous impact on both human health and the environment [1,2]. Mercury (Hg^{2+}) ion has been getting more attention for its pain-staking threats as highly toxic heavy metals, and its prolonged effects to environment and biological system [3–5]. It could build up in our body from the food chain through the utilization of contaminated sea-food and agro-products [6]. Hg^{2+} ion exposure is particularly serious due to the strong affinity to sulphur-functionalities of proteins and enzymes [7], can lead dysfunction of proteins and enzymes, which causes wide variety of diseases related to neurotoxicity, and hepatotoxicity [8–11]. Therefore, over the past years, lots of efforts have been made to develop a specific and selective detection of Hg^{2+} ion [12].

Fluorescence chemosensors are more attractive and implemented in broad research areas due to operational simplicity, excellent specificity and sensitivity, fast response, real-time application, small sample size applicability and non-destructive sample handling [13]. Nevertheless, mostly organic fluorophores possess strong fluorescence emission with only in diluted solutions, while increasing their concentration largely weakened or quench their fluorescence intensity due to aggregation [14]. The aggregation caused quenching (ACQ) phenomenon might be resulted due to strong π - π stacking and non radiative decay [15,16], especially the detection of analyte in aqueous medium, in which the hydrophobic organic fluorophores tend to aggregate and experience ACQ which limits the sensitivity [17]. To overcome this limitation, researchers have been putting big effort to develop fluorophores with new fluorescence features over the past few decades. Tang *et al.* in 2001 [19] revealed a new class of fluorogenic molecules which are strong fluorescent in an aggregated state, but weak or non-fluorescent when get diluted [20]. This unique photophysical property which is happened as a result of the restriction of intermolecular motion (RIM) closes the non-radiative the non-radiative relaxation pathway and opens radiative relaxation is known as aggregation induced emission (AIE) [21,22]. Subsequently, owing to their Turn-On character, AIE based fluorescent probes for detection of various ions has been developed rapidly and attracted tremendous research interest.

The ratiometric fluorescence sensors with well resolved dual emission have many excellent advantages over the single emission band intensity based fluorescence Turn-On or turn-off counter parts [23]. The analyte induced two emission intensities change at separate wave

lengths in ratiometric fluorescent sensors overcomes some disadvantages of the intensity based sensors by minimizing the dependence in sensor concentration and increasing signal to noise ratio [24–26]. Therefore, designing of non-cytotoxic, AIE active and ratiometric sensor for Hg^{2+} in aqueous medium would be highly demanding.

Naphthalimide scaffolds are explored extensively in various applications [27] and considered as one of the most excellent fluorophore due to their high stability, high quantum yield and N-imides site which can be modified easily by introducing different functionalities under cost-effective synthetic routes [28], and they are well known to form aggregation in aqueous solution [29–31]. Another important feature of the naphthalimide derivatives is their significant potential in medicinal chemistry [32] owing to their capabilities to impart biological activities such as anti-cancer [33], and anti-microbial [34].

Other important group of compounds is sulfonamides (sulfa-drugs) are an important kind of widely used antibiotic drugs and were the first effective chemotherapeutic agents employed systematically for the prevention and treatment of bacterial infection in humans [35–37]. And N-Substituted sulfonamides are well-known anti-bacterial drugs [38], the modification of substituent on a ligand might improve the efficacy of the antimicrobial by supporting in drug transport across the cell membrane, rising the viable does or enabling targeting to the active agent of drug [39]. Furthermore, it has been well accepted that hybrid molecules *via* the combination of different scaffolds into a single molecule may lead to the improved cytotoxic effectiveness of compounds with synergistic effect [40,41]. In this regard, recently researchers are trying to modify the sulfonamide group and prepare novel compound with better anti-microbial activity by conjugating sulfonamide with various scaffolds [42]. Accordingly, incorporating photophysical and anti-microbial nature of naphthalimide derivatives with the biological active sulfonamide might give very active pharmaceutical and photo-physical quality.

Considering the binding affinity of naphthalimide scaffolds for Hg^{2+} [43,44] and Ag^+ [45] ions of reported chemosensors, biological and environmental compatibility of sulfonamide group, and fluorogenic property, herein, we report synthesis, characterization and fluorescence sensing and biological activity of novel fluorescent sulfamethizole functionalized 1,8 naphthalimide based AIE active ratiometric chemosensor Hg^{2+} ion detection and Ag^+ complex of the chemosensor for biological application. The chemosensor is designed by introducing a sulfamethizole into recognition unit and naphthalimide as a fluorogenic moiety. A novel hybrid chemosensor was synthesized by combining the structural features of naphthalimide

and sulfamethizole compound using straight forward and convenient method. Naphthalimide moieties monomer emits at around 380 nm are known to form excimers emission at visible wavelength range higher than 450 nm [46,47]. Hg^{2+} ion binding with the sulfamethizole moieties could bring the naphthalimide moieties monomer molecules close to engage in intramolecular excimers formation *via* metal ion-induced assembly that Turn On the fluorescence intensity of the excimer and off the monomer emission. In the absence of Hg^{2+} ion, **L6** exhibits monomeric emission at 390 nm, addition of Hg^{2+} ion inflicts gradual monomer emission quenching and excimer emission enhancement, this monomer-excimer conversion induced fluorescence intensity variation at 390 nm and 483 nm which gives a ratiometric result. Furthermore, the chemosensor and its silver complex exhibited excellent biological activity. The chemosensor have three basic advantages (i) the ligand exhibit AIE activity, (ii) ratiometric character, with splendid selectivity and low detection limit and (iii) outstanding biological activity.

5.2 Experimental Section

5.2.1 Reagents and Instrumentation

Sulfamethizole and 1,8-naphthalimide were purchased from Sigma-Aldrich (India) and all cations solutions were prepared using their salts of perchlorate and solvents of AR grade were obtained from different commercial suppliers and were used without further purification. The reactions were monitored by thin layer chromatography (TLC) on 0.25 mm silica gel plates using UV light for visualization. The IR spectra were recorded in the range 4000-400 cm^{-1} by Alpha-FTIR spectrometer BRUKER using KBr pellet. All ^1H -NMR and ^{13}C -NMR spectra were recorded on JEOL 400 MHz spectrophotometer in $\text{DMSO}-d_6$ solvent and TMS internal standard were used, and the chemical shift were reported as parts per million (ppm) scales downfield from TMS. The multiplicities were reported as abbreviations *viz* s = singlet, d = doublet, t = triplet and m = multiplet. Absorption was recorded via Specord S600 PC double beam spectrophotometer, while SHIMADZU RF-5301PC spectro fluorophotometry was used for emission study with 1cm standard quartz cell. DMSO and deionized water was used for absorption and emission studies as per requirements. HORIBA Jobin Yvon, fluorocube fluorescence Lifetime system was used for fluorescence lifetime.

5.2.2 General Procedure

The stock solution of compound **L6** (1 mM) was prepared in DMSO and further diluted to 10 μM in DMSO/water (1:99 v/v, HEPES buffer pH 7.2). Metal ion solutions were prepared in

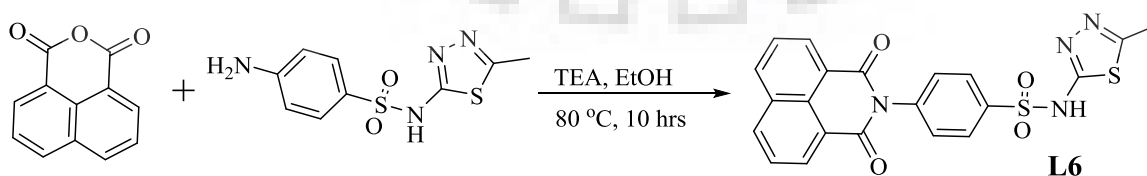
deionized water using their respective perchlorate salts. 340 nm was used as excitation wavelength and the fluorescence emission was recorded in the range of 350-600 nm. And the experiments were carried out at room temperature. The excitation wavelength was 340 nm, and the emission was measured from 350 to 600 nm. All the experiments were performed at room temperature.

5.2.3 Synthesis and Characterization of Chemosensor

Synthesis of 4-(1,3-dioxo-1H-benzo[de]isoquinolin-2(3H)-yl)-N-(5-methyl-1,3,4-thiadiazol-2-yl)benzenesulfonamide was prepared from sulfamethizole and 1,8-naphthalic anhydride by amidation reaction following the reported procedure [48]. To a suspension of 1.2 mmol of sulfamethizole and 1.0 mmol 1,8-naphthalic anhydride in 5 ml of ethanol in round-bottom flask 10 drops of triethylamine was added and the reaction mixture was refluxed at 80 °C for 10 hrs (Scheme 5.1). After stirring for 10hrs the reaction mixture was slowly cooled down to room temperature and diluted with dil. HCl solution was added slowly to the reaction mixture, and it was stirred to get white solid, yield of 85% was obtained after washing with water and air dried. Then, the product was characterized by IR, ¹H-NMR, ¹³C-NMR, and HRMS spectroscopy (Figure 5.10-5.13).

4-(1,3-dioxo-1H-benzo[de]isoquinolin-2(3H)-yl)-N-(5-methyl-1,3,4-thiadiazol-2-yl)benzene sulfonamide (L6):

white solid, 85% yield; MP: 169.6 °C; IR (KBr, $\bar{\nu}/\text{cm}^{-1}$): 3445 (-NH), 1775-1649 (N-C=O), 1548 (C=C aromatic), 1438 (thiadiazole ring), 1235, 1187 (SO₂), and 923 (N-S of SO₂), 697 (C-S-C); ¹H NMR (400 MHz, DMSO-*d*₆, δ/ppm): 14.09 (s, 1H), 8.47 (m, 4H), 7.91 (d, *J* = 8.5 Hz, 2H), 7.87 (t, *J* = 7.6 Hz, 2H), 7.58 (d, *J* = 8.5 Hz, 2H), 2.46 (s, 3H). ¹³C NMR (100 MHz, DMSO-*d*₆, δ/ppm): 168.8, 164.1, 155.4, 142.32, 140.2, 135.2, 131.94, 131.4, 130.7, 128.4, 127.8, 127.0, 123.0, 16.6. HRMS (ESI+) *m/z* calcd. C₂₁H₁₄N₄O₄S₂ [M+H]⁺: 451.0535 found 451.0512.



Scheme 5.1. Synthesis of chemosensor L6.

5.2.4 Synthesis and Characterization of Silver Complex

To a suspension of 1.0 mmol of 4-(1,3-dioxo-1H-benzo[de]isoquinolin-2(3H)-yl)-N-(5-methyl-1,3,4-thiadiazol-2-yl)benzenesulfonamide and 1.0 mmol of silver nitrate (AgNO_3) in 5 ml water in round bottom flask, 2.0 mmol of KOH in 2 ml of water were added and the mixture was stirred at room temperature for 3 hrs [49,50]. Diluted with more water and filtered to get black solid, it washed with water and air dried, obtained 93% yield, and characterized by IR, $^1\text{H-NMR}$ and $^{13}\text{C-NMR}$ (Figure 5.14-5.16).

L6+Ag⁺ complex: black, MP: 314.5 °C; IR (KBr, $\bar{\nu}/\text{cm}^{-1}$): 3445, 1700, 1650, 1561, 1440, 1376, 1355, 1271, 1235, 1186, 1080, 1028, 985, 775, and 685; $^1\text{H NMR}$ (400 MHz, DMSO-*d*₆, δ/ppm): 8.38 (d, $J = 8.3$ Hz, 2H), 8.33 (d, $J = 7.2$ Hz, 2H), 7.99 (d, $J = 8.3$ Hz, 2H), 7.74 (t, $J = 7.7$ Hz, 2H), 7.47 (d, $J = 8.3$ Hz, 2H), 1.78 (s, 3H). $^{13}\text{C NMR}$ (125 MHz, DMSO-*d*₆, δ/ppm): 165.9, 164.0, 141.51, 140.4, 135.2, 131.9, 131.4, 130.7, 128.2, 127.7, 127.1, 122.7, 16.7.

5.3 Results and Discussion

5.3.1 Aggregation Induced Emission (AIE) Character of L6

Initially absorption spectrum of the chemosensor **L6** was studied in DMSO and DMSO/water mixtures. The Absorption maximum of **L6** at 281 nm was blue shifted by 14 nm to 264 nm and the π - π absorption band was red shifted by 10 nm from 333 nm to 343 nm in DMSO and DMSO/water (1:99 v/v) respectively (Figure 5.1a). In general, the absorption spectra tailing and red-shift implies the formation of nano-aggregates [51,52], possibly due to J-aggregates [53]. The red shift accompanied by tailing in DMSO/water (1:99 v/v) of **L6** might be due to light-scattering effects, which indicates the formation of aggregates in aqueous.

For further exploration of the AIE properties of **L6**, the fluorescence intensity of **L6** was scanned in various fractions of DMSO/water mixtures. The AIE profile of **L6** showed that the emission intensity of **L6** at 390 nm increased along with increasing water fraction in the DMSO/water mixtures. The fluorescence intensity of the ligand enhances rapidly with increasing water fraction is 90% (Figure 5.1b). However, **L6** showed no fluorescence enhancement until the fraction of water reaches 30%. This result clearly indicates that the chemosensor underwent aggregation. Naphthalimide moieties have large π -conjugation which increases the hydrophobicity which helps it to exhibit π - π stacking in an aqueous medium which subsequently results in AIE nature.

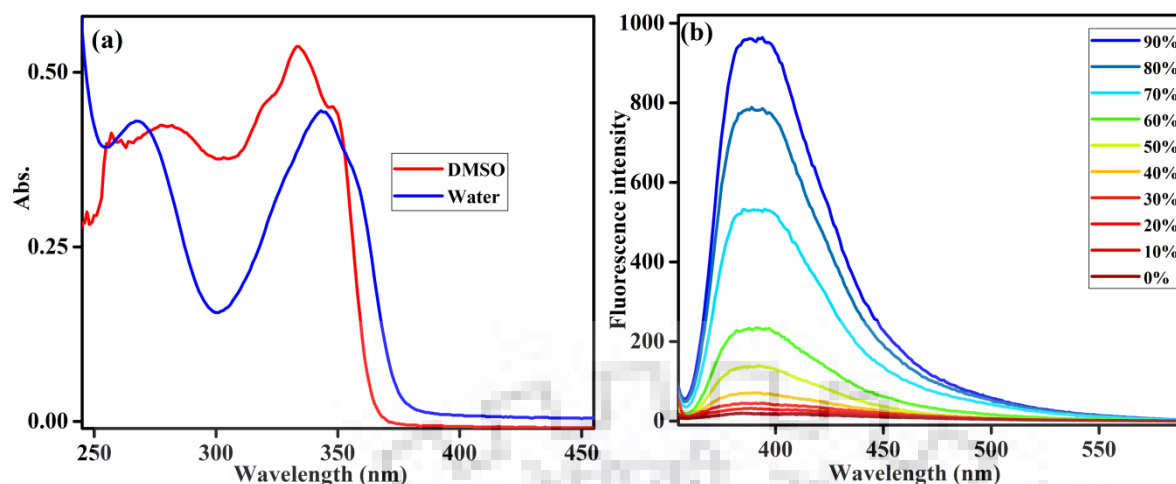


Figure 5.1 (a) The absorption spectrum of **L6** in DMSO and DMSO/water (1:99 v/v), (b) Fluorescence intensity of **L6** (10 μM) solution in DMSO with various water fraction (0, 10, 20, 40, 60, 80, 90%).

5.3.2 Absorption Behaviour towards Various Cations

The UV-visible absorption spectra of **L6** in the presence of various biological and environmental important metal ions (Na^+ , K^+ , Mg^{2+} , Ba^{2+} , Mn^{2+} , Zn^{2+} , Cu^{2+} , Co^{2+} , Ni^{2+} , Ag^+ , Al^{3+} , Fe^{2+} , Fe^{3+} , Pb^{2+} , Cd^{2+} , Cr^{3+} , and Hg^{2+}) have been done in DMSO/water(1:99, v/v, HEPES buffer, pH 7.2) solution as revealed in Figure 5.2a, **L6** exhibits absorption centered at 267 nm and 343 nm, Hg^{2+} ion addition undergoes increases in absorbance at 267 nm with slight red shift with hypochromic effect at 343 nm. The UV titration disclose in Figure 5.3a, gradual addition of Hg^{2+} employs distinct increase in absorption intensity at 267 nm and decreasing in absorption intensity at 343 nm along with two isosbestic points at 320 nm and 362 nm, this indicates the complex formation of **L6** with Hg^{2+} ion. And gradually addition of Ag^+ ion undertake increases in absorbance at 267 nm and decreases in absorbance at 343 nm with slight blue shift to 339 nm (Figure 5.3b) with two isosbestic points at 327 nm and 365 nm. Hence, there was no significant effect induced by other tested metal ions.

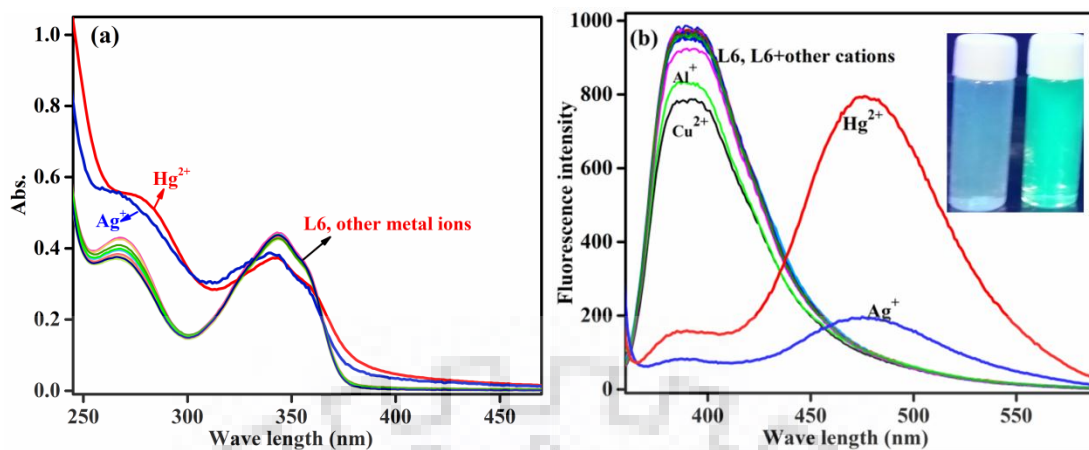


Figure 5.2(a). Absorption spectra (b). Fluorescence spectra **L6** (10 μM) in the presence of various metal ions (10 equiv.)

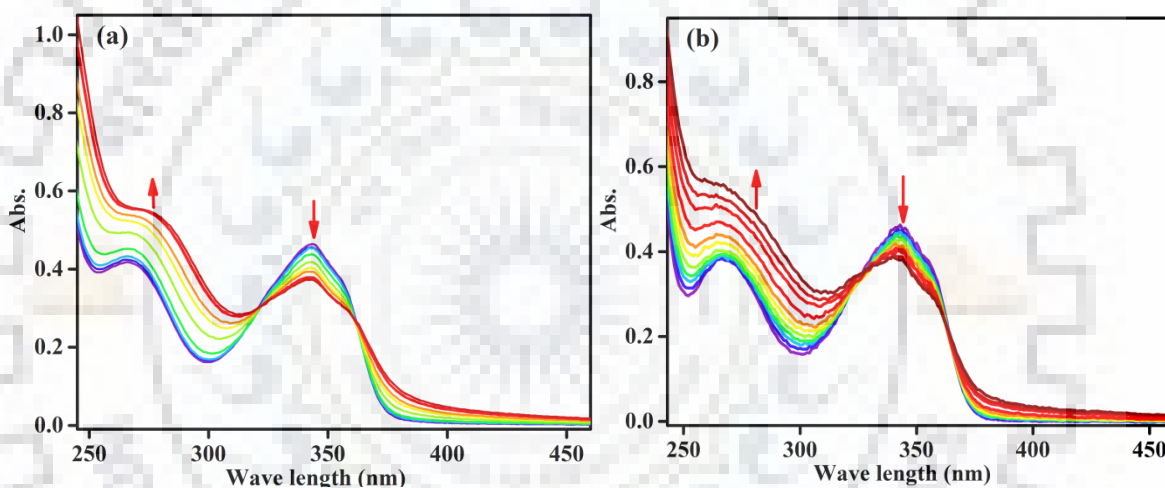


Figure 5.3 UV-visible absorption titration spectra of **L6** (10 μM) towards varying concentrations (0-5 equiv.) (a) Hg^{2+} ion, (b) Ag^{+} ion (in DMSO/water (1:99, v/v, HEPES buffer, pH 7.2)).

5.3.3 Fluorescence Emission Change towards Various Metal ions

Selectivity is a significant parameter for evaluating performance of fluorescence sensing. To assess the binding competence of the chemosensors to be used for metal ion-sensing, the fluorescence emission spectra of chemosensors were recorded in the presence of 10 equivalent of variety of metal ions (Na^{+} , K^{+} , Mg^{2+} , Ba^{2+} , Mn^{2+} , Zn^{2+} , Cu^{2+} , Co^{2+} , Ni^{2+} , Ag^{+} , Al^{3+} , Fe^{2+} , Fe^{3+} , Pb^{2+} , Cd^{2+} , Cr^{3+} , and Hg^{2+}) using 340 nm as excitation wave length in DMSO-water (1:99 v/v, HEPES buffer pH 7.2). **L6** exhibited characteristic monomeric emission at 390 nm. The monomeric emission spectra of **L6** were quenched and a new band centered at 483 nm and 478 nm was appeared in the presence of Hg^{2+} and Ag^{+} ions respectively, whereas no significant response was shown by other metal ions (Figure 5.2b).

The fluorescence spectra were monitored with consecutive addition of Hg^{2+} and Ag^+ ions concentrations under optimized condition. As shown in Figure 5.4a upon increasing in Hg^{2+} ion concentration the emission intensity centered at 390 nm was quenching gradually while the excimeric emission at 483 nm was enhanced significantly with iso-emissive point at 445 nm with remarkable fluorescence color change from blue to green which can detect by naked eye under a UV lamp (Inset Figure 5.2b). As per Ag^+ ion, when the concentration increases, the emission band centered at 478 nm start to emerge with progressive quenching at 390 nm gives iso-emissive point at 455 nm (figure 5.4b). The red shifted emission centered at 483 nm can be due to an excimeric species obtained from the intramolecular interaction between the naphthalimide moieties in the completion of **L6** with Hg^{2+} ion. Addition of Hg^{2+} alight a ratiometric response with considerable increase in intensity ratio (I_{483}/I_{390}) from 0.19 to 6.63 in pure **L6** and in addition of 5 equivalent of Hg^{2+} ion respectively. Hg^{2+} ion at 5 equivalents was enough to saturate the fluorescence intensity. Considering the change in the emission intensity of **L6** in the absence and presence of Hg^{2+} ion at 390 nm, and 483 nm showed “OFF–ON” switch to Hg^{2+} ion (in DMSO/water (1:99, v/v, HEPES buffer, pH 7.2).

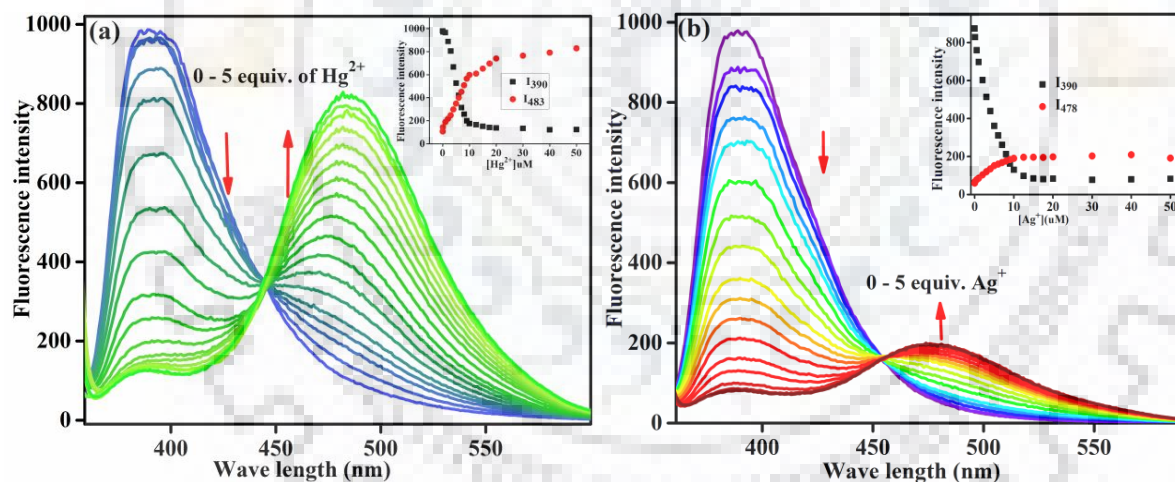


Figure 5.4 Fluorescence emission titration responses of **L6** (10 μM) towards varying (a) Hg^{2+} ion concentrations, (b) Ag^+ ion concentrations (0 -5 equiv.) ion (in DMSO/water (1:99, v/v, HEPES buffer, pH 7.2).

5.3.4 Competitive Experiment

To evaluate the selective ratiometric detection of the sensor for Hg^{2+} ion, the selectivity of the sensor was tested by competitive experiment to determine the possible interferences by other cations. The fluorescence changes of 10 μM **L6** in DMSO/water (1:99, v/v, HEPES buffer, pH 7.2) were carried out in the presence of 1 equivalent Hg^{2+} blend with 5 equivalents of various metal ions (Figure 5.5). The ratiometric response (I_{483}/I_{390}) of **L6** and **L6**- Hg^{2+} system

remained the same with or without the other metal ions (Figure 5). Hg^{2+} and Ag^+ ions induced a selective ratiometric response, and the competitive experiment between Hg^{2+} and Ag^+ was done by addition of Hg^{2+} to a mixed solution of **L6** and Ag^+ the chemosensor was selective to Hg^{2+} ion over Ag^+ ion with insignificant effect in the fluorescence ratio. All the results confirmed the selectivity and sensitivity of **L6** towards Hg^{2+} ion.

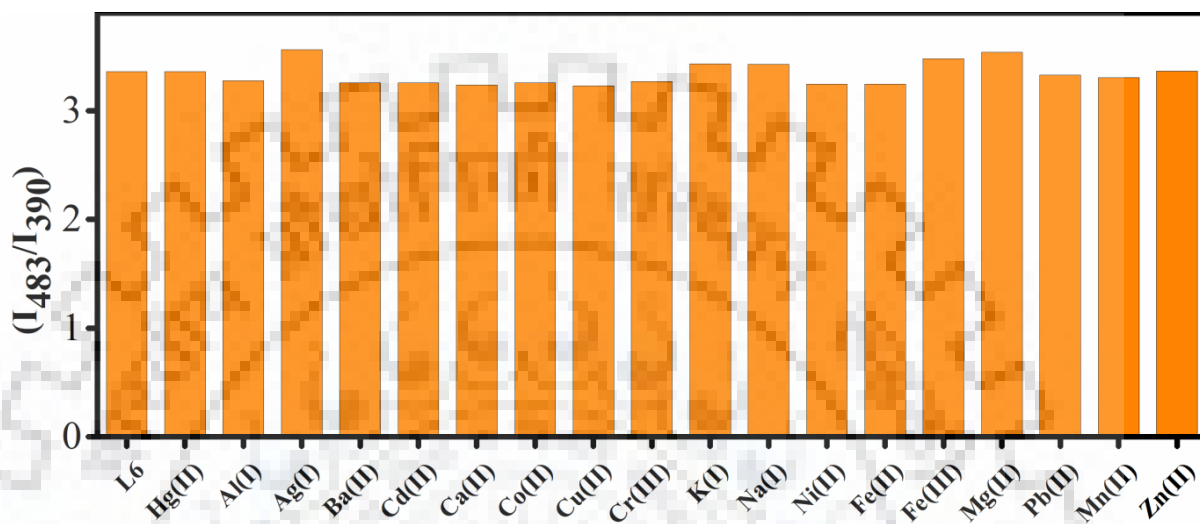


Figure 5.5 Interference effect of various cations with **L6**- Hg^{2+} (fluorescence intensity ratio (I_{483}/I_{390}) of **L6** + Hg^{2+} + other cations (1:1:10 equiv.)

5.3.5 Stoichiometry and Limit of Detection (LOD)

The Job's plot of fluorescence intensity ratio (I_{483}/I_{390}) (Figure 5.6a) that is dependent on the complex formation was plotted as a function of mole fraction of Hg^{2+} to determine the stoichiometry between **L6** and Hg^{2+} and the maximum of the plot was obtained at 0.34 mole fraction, exemplify 2:1 stoichiometry between **L6** and Hg^{2+} ion [54]. The detection limit of **L6** for Hg^{2+} ion detection was calculated from the fluorescence titration data. The emission intensity ratio (I_{483}/I_{390}) of **L6** was measured 7 times for calculation of the standard deviation of the blank receptor and the obtained standard deviation was used for determination of limit of detection. The slope of linear fit graph of fluorescence intensity ratio response (I_{483}/I_{390}) of fluorescence titration measurements was plotted against the concentration of Hg^{2+} ion to determine the slope (Figure 5.6b). Calculated from the slope and standard deviation as Limit of detection = 3 s/m [55,56] and found to be 14.7 nM.

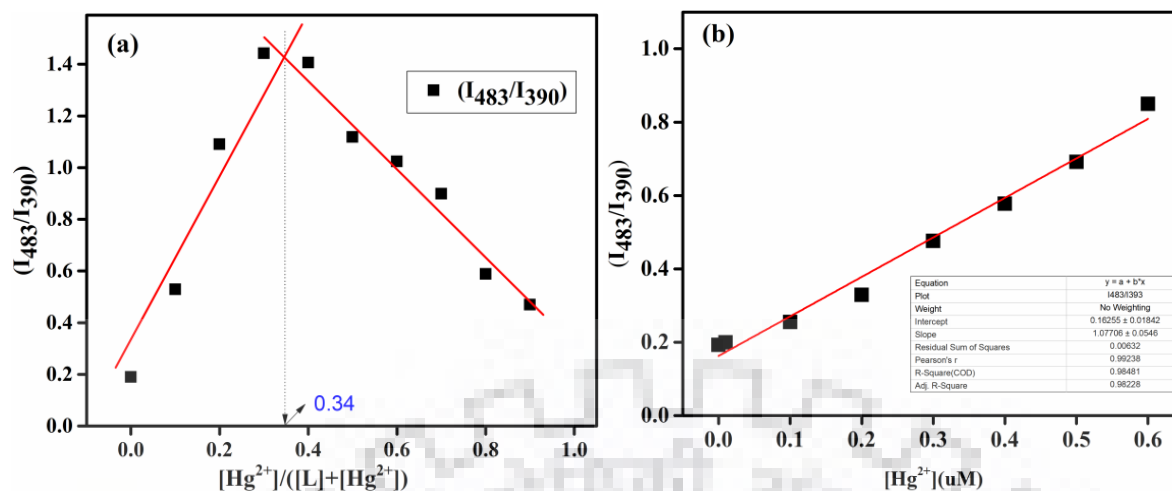


Figure 5.6 (a) Job's plot (the total concentration were 10 μM), (b) The linear fit graph of intensity ratio (I_{483}/I_{390}) as a function of Hg^{2+} ion concentration. (in DMSO-water (1:99 v/v, HEPES buffer pH 7.2))

5.3.6 Fluorescence Lifetime

As shown in Figure 5.7, the fluorescence lifetime of **L6** at 390 nm was 2.64 ns and after the addition of Hg^{2+} it decreased to 1.43 ns, and the fluorescence lifetime of **L6+Hg²⁺** at 483 nm was 14.8 ns. These results validate fluorescence quenching at 390 nm is due to conversion of the monomers to the excimer that results a red shift in fluorescence to 483 nm. The long emission lifetime at 483 nm confirms the excimeric nature of the emitting species, as it is known excimers have significantly longer life time than monomer aggregates this is due to the excimer formation time associated with migration of the free excited molecules to the excimer-formation sites [57].

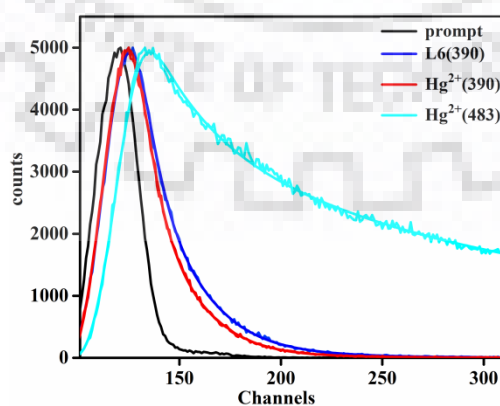
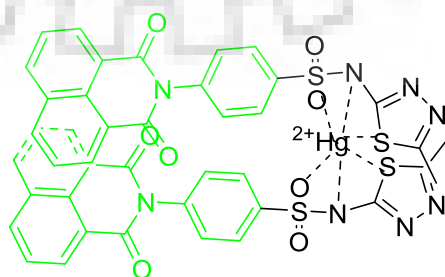


Figure 5.7 Fluorescence lifetime decay profile of **L6** in the absence and presence of Hg^{2+} ion (in DMSO/water (1:99 v/v, HEPES buffer pH 7.2), $\lambda_{ex} = 340$ nm)

5.3.7 Binding Mode of L6 with Hg²⁺ ion

The complex formation was established by IR, and ¹H-NMR to understand the binding mode of **L6** with Hg²⁺. The FT-IR spectrum experiment was carried out in the absence and presence of Hg²⁺. **L6** exhibited a characteristic series of stretching vibrations among which are 3445 (-NH), 1775-1649 (N-C=O), 1548 (C=C aromatic), 1438 (thiadiazole ring), 1235, 1187 (SO₂), and 923 (N-S of SO₂), and 697(C-S-C) bands and respectively. Upon addition of Hg²⁺, the three strong bands corresponding to SO₂ group showed significant changes of 1235 to 1239 cm⁻¹ and 1187 and 923 cm⁻¹ get disappeared respectively, which could be ascribed to binding of Hg²⁺ to SO₂ functional group. While, thiadiazole ring vibration band is shifted to 1412 cm⁻¹ and 697 cm⁻¹ of C-S-C stretching in thiadiazole ring diminished in the complex (Figure 5.17). Which implies the coupling of Hg²⁺ with (-SO₂) and thiadiazole ring of sulfamethizole moiety. Moreover, the binding mode was investigated by ¹H NMR (Figure 5.18), the ¹H NMR titration shows that the -NH proton peak appeared as a singlet at 14.09 ppm is vanished upon addition of Hg²⁺, this reveals that the deprotonation of -NH proton by Hg²⁺ and noticeable change of chemical shifts in other protons. The four proton of naphthalimide ring (H-3, 5) that appeared as multiplet at 8.47 ppm divided into two resolved doublets and up field to 8.44 ppm (H-3) and 8.40 ppm (H-5) at the same time the doublet (H-2) at 7.91 ppm is down field shift to 7.92 ppm while triplet (H-4) at 7.87 ppm and doublet (H-1) at 7.58 ppm also shifted to 7.81 and 7.54 ppm. The shift in the naphthalimide ring shows that the heavy metal effect in binding of Hg²⁺ ion and the downfield of (H-2) in the Meta and up-field shift of (H-1) in the ortho position to sulfamethizole moiety illustrates the interactions of Hg²⁺ with the sulfonamide. Accordingly, the spectroscopic data from IR, NMR and the Stoichiometric calculation **L6** coordinate with Hg²⁺ through (-NH), (-SO₂) and thiadiazole ring of sulfamethizole moiety in 2:1 stoichiometry. Based on those observations, the possible binding interaction of **L6** with Hg²⁺ ion is demonstrated in scheme 5.2.



Scheme 5.2: proposed mode of binding of **L6** with Hg²⁺

5.3.8 pH Selection

The pH effect in the photophysical properties of **L6** were examined in the absence and presence of 5 equivalent of Hg^{2+} in the pH range of 3 to 12 in DMSO:H₂O (1:99, v/v). The fluorescence intensity of **L6** was not changed significantly in pH range of 3-8, the fluorescence intensity was remarkably high in acidic media while quenched in basic media, this might be due to the solubility difference of **L6**; at low pH the chemosensor become less soluble and it can encapsulate into nano-aggregate which enhance the fluorescence intensity and in the basic pH range above 8 the chemosensor solubility increases which weaken the fluorescence intensity (Figure 5.19a). While, upon addition of Hg^{2+} , at pH 3 there were no obvious change in fluorescence intensity, this indicates there were no binding of Hg^{2+} , and at pH 4 fluorescence intensity of at 390 nm start to decreases and the new peak centered at 483 nm shows up. The less significant change in acidic media might be due to formation of stable nano aggregates or protonation of imide and $-\text{NH}$ group of **L6**. In pH range of 5-10, **L6** shows good ratiometric response to Hg^{2+} , however, a decrease in the fluorescence intensity at 390 nm and total quenching at 483 nm was observed in **L6**- Hg^{2+} at higher pH range (Figure 5.19b). The overall pH effect for the fluorescence intensity ratio (I_{483}/I_{390}) for the **L6** and **L6**- Hg^{2+} was substantial stable in 5-10 pH range (Figure 5.8). This wide range pH stability is an imperative for application of Hg^{2+} ion detection in biological and environmental samples. Hence all experiments were carried out in physiological pH ((in DMSO/water (1:99, v/v, HEPES buffer, pH 7.2).as optimized experimental condition.

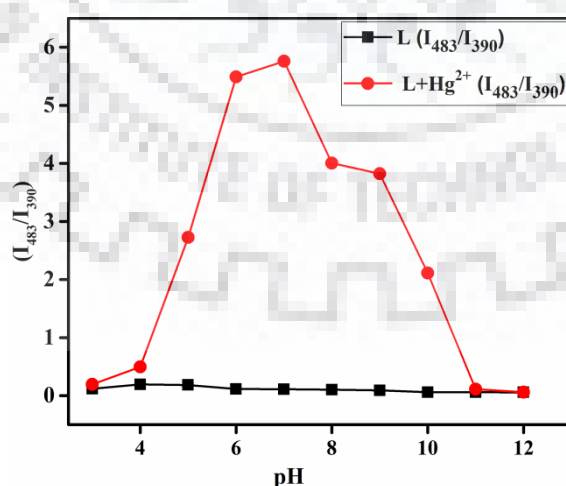


Figure 5.8 Fluorescence intensity ratio (I_{483}/I_{390}) for **L6** and **L6**- Hg^{2+} at different pH values.

5.3.9 Reversibility Studies Applied as Logic Circuit Devices

It is very practical if a sensor can be reversed and reused. The strong binding affinity of Hg^{2+} ion to iodide ion is well-known [58–61]. Therefore, we use KI for competitive binding of Hg^{2+} by I⁻ from the **L6**– Hg^{2+} complex. To identify the reusability of **L6** for Hg^{2+} sensing, the reversibility of **L6** toward Hg^{2+} ion was examined by addition of KI to **L6**– Hg^{2+} solution in DMSO/water (1:99, v/v, HEPES buffer, pH 7.2). As expected, splendid reversibility was acquired, indicating that **L6** can be reused reputedly for detection of Hg^{2+} ion, confirming the high KI affinity towards Hg^{2+} ion while there was KI alone induces no change in the fluorescence intensity of **L6** (Figure 5.9a). Hg^{2+} ion imposes remarkably increasing fluorescence intensity ratio (I_{483}/I_{390}) of **L6** due to the excimer formation up on coordination of **L6** with Hg^{2+} ion, thus acting as an ON switch. Treatment of **L6**– Hg^{2+} complex with KI induces the excimer to return to monomer **L6**, which is accompanied by the noticeably decreases in emission intensity at 483 nm whereas the intensity of emission at 390 nm increased, this slims down the intensity ratio (I_{483}/I_{390}) thus assigned as an OFF switch. The repeated the **ON/OFF** behaviour of fluorescence intensity ratio (I_{483}/I_{390}) and fluorescence color changes under Uv-light from blue to green and then back to blue (Inset Figure 5.9a) reveals the applicability of **L6** as naked eye and ratiometric **ON/OFF/ON** reversible and reusable Hg^{2+} ion sensor.

Furthermore, the **ON/OFF/ON** cycle could be repeated numerous times with negligible reduction in emission ratio (I_{483}/I_{390}) by alternating the addition of Hg^{2+} and KI. Subsequently, two input and two output INHIBIT logic gate has been constructed on the basis of the repeated On-Off behaviour of **L6** by Hg^{2+} and KI as two input signals, in inputs system the presence and absence of Hg^{2+} and KI are defined as 1 and 0 respectively [62] and in output the quenching and enhancement of fluorescence intensity at 390 and 483 nm is represented as 0 and 1 respectively as shown in the truth table (Figure 5.9b). This can be symbolized as a combination of IMPLICATION and INHIBIT gates for outputs at 390 and 483 nm respectively [63–65]. The combined effect in the ratiometric (I_{483}/I_{390}) output gives INHIBIT logic gate (Figure 5.9c). The combination of these intrinsic properties with diverse chemical inputs permits the implementation in designing molecular logic gate Circuit devices [66].

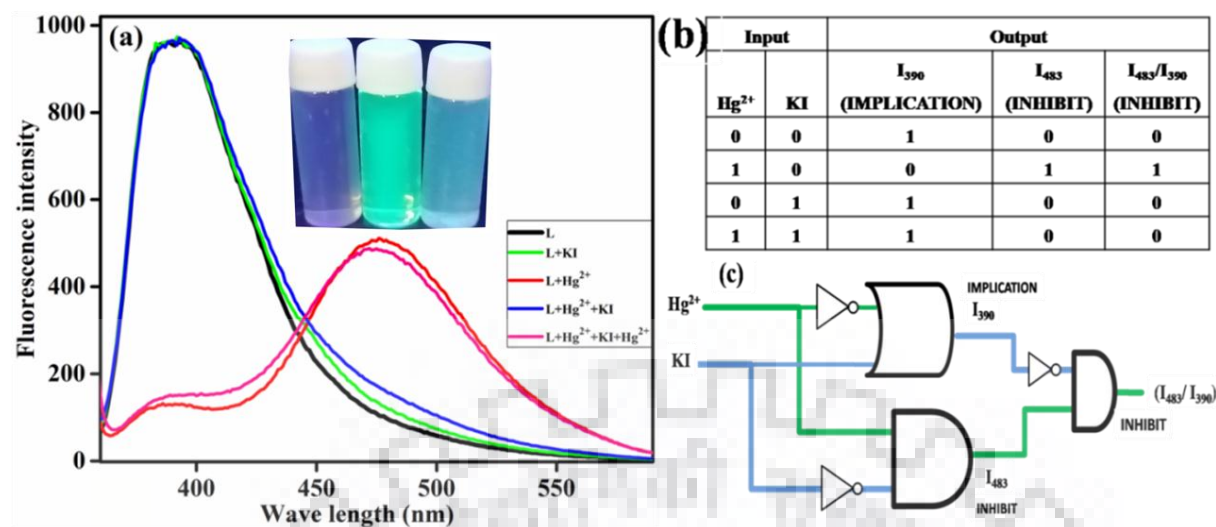


Figure 5.9 (a) Fluorometric reversibility. (Inset: visual fluorometric reversibility) (b) Truth table corresponding to a logic gate based on Hg²⁺ and KI. (c) Switch circuit diagram.

5.4 Biological Application of Ligand-Silver Complex

Silver complexes have been widely used for disinfection and silver sulfonamides complexes are known for their biological activity [36,49,67]. Therefore, we also screened the **L6** and **L6-Ag** complex as antimicrobial agents and reported in Table 5.1. The anti-microbial activities were tested against Gram negative strain due to more pathogenic in nature. Under similar concentrations, these compounds have shown better anti-microbial activities than the most of the antibiotics available in the market (Table 5.1).

Table 5.1 Anti-microbial activities of **L6** and **L6-Ag⁺** compounds

Strain	L6	L6+Ag ⁺	Amikacin	Cefotaxime	Cefazidime	Imipenem	Meropenem
AK-83	256	16	2	512	1024	512	512
AK-44	512	32	4096	512	1024	512	256
AK-68	512	4	1024	1024	1024	1024	1024
AK-67	512	4	1024	1024	1024	1024	1024
AK-92	1024	64	1024	1024	1024	1024	1024

(Bacterial strain AK-83, AK-44, AK-68, AK-67, AK-92 are Gram negative).

5.5 Conclusion

An effective ratiometric Hg^{2+} ion chemosensor was established. The Hg^{2+} -prompted monomer-excimer conversion induced fluorescence intensity variation of monomer emission quenching and excimer emission enhancement based on chelation enhanced fluorescence emission, with larger bathochromic shift from 390 nm to 483 nm which gave a ratiometric result. The proposed sensor display high selectivity and splendid sensitive to Hg^{2+} ion over a variety of tested metal ions in the physiological pH range in aqueous solution, and with detection limit as low as 14.7 nM. In addition, the better anti-microbial activities of **L6** and **L6-Ag⁺** complex have been investigated and compared with antibiotics available in the market.



Spectral Characterization of L6, L6+Ag⁺ and L6+Hg²⁺ by IR, NMR and HRMS

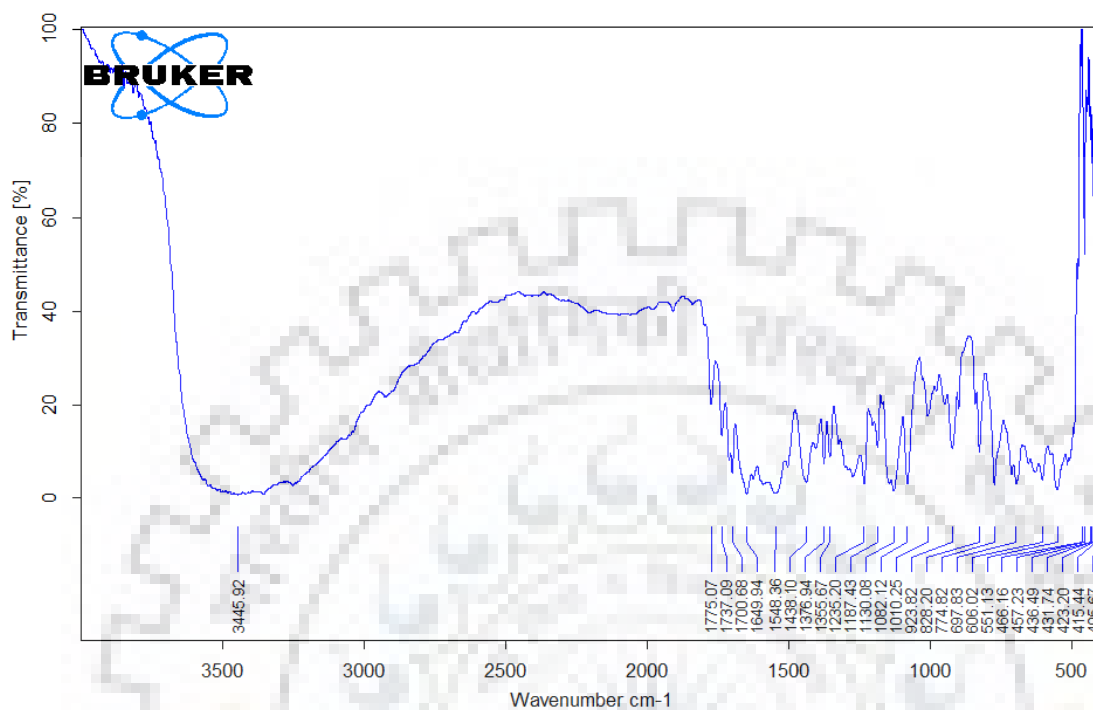


Figure 5.10 IR spectrum of receptor L6 recorded in KBr pellet.

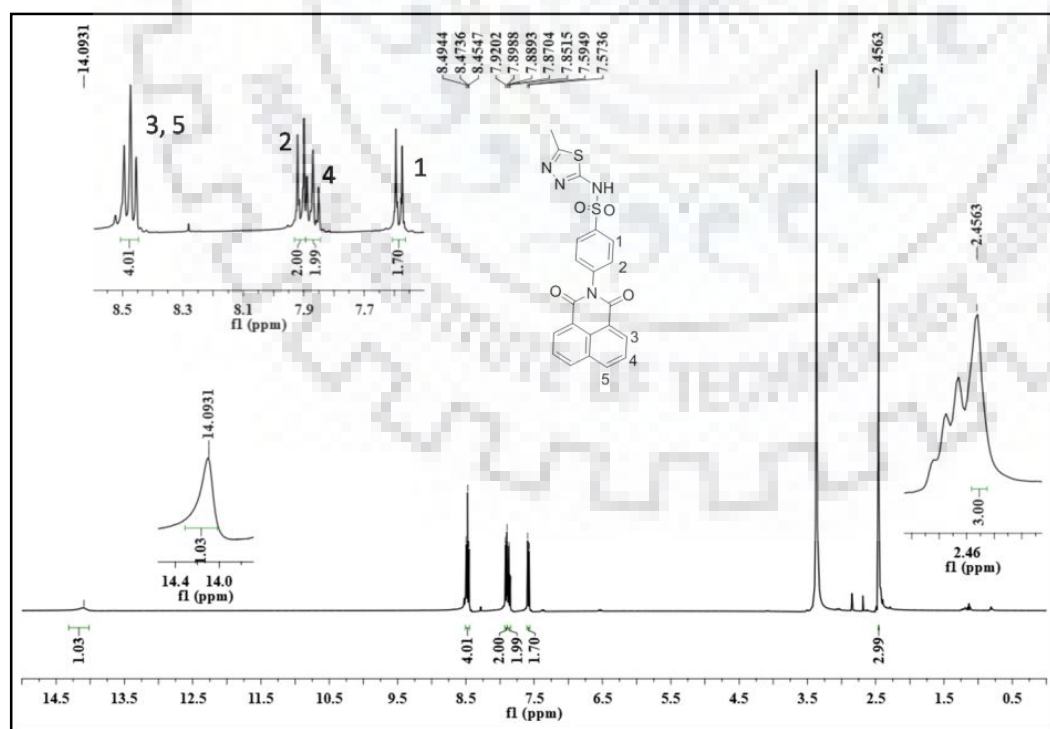


Figure 5.11 ¹H-NMR spectrum of receptor L6 recorded in DMSO-*d*₆.

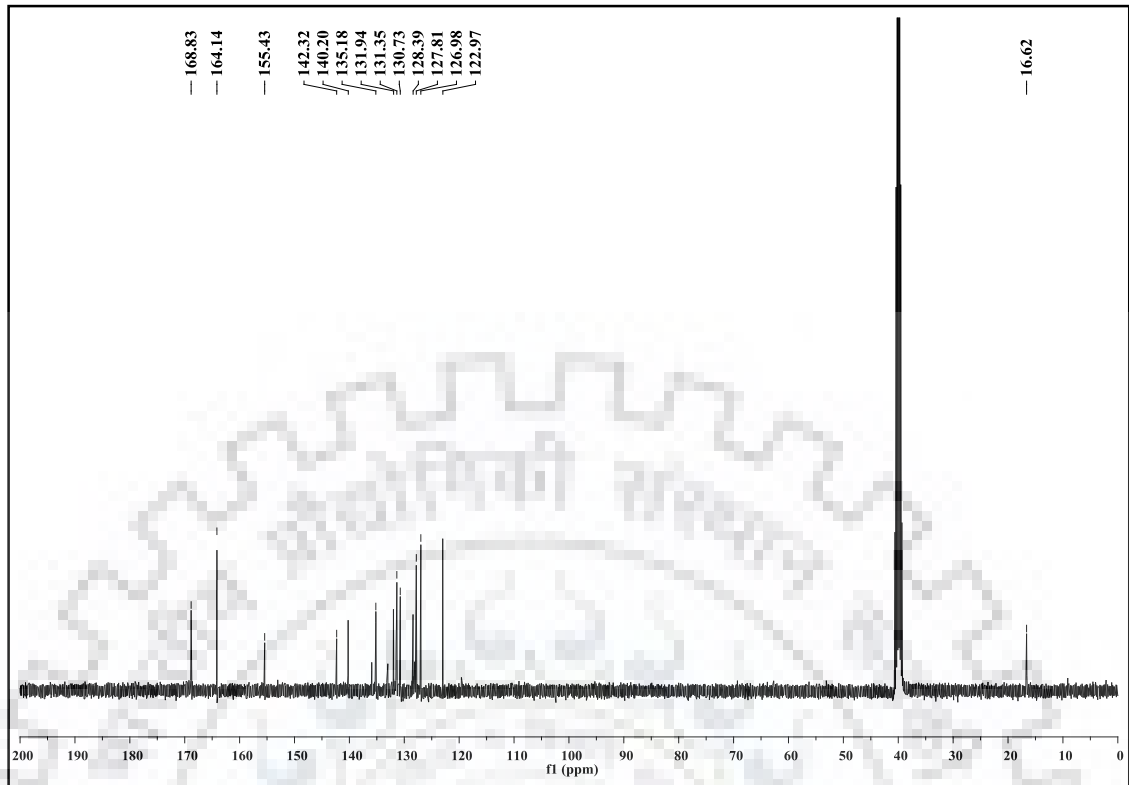


Figure 5.12 ^{13}C -NMR spectrum of receptor L6 recorded in $\text{DMSO}-d_6$.

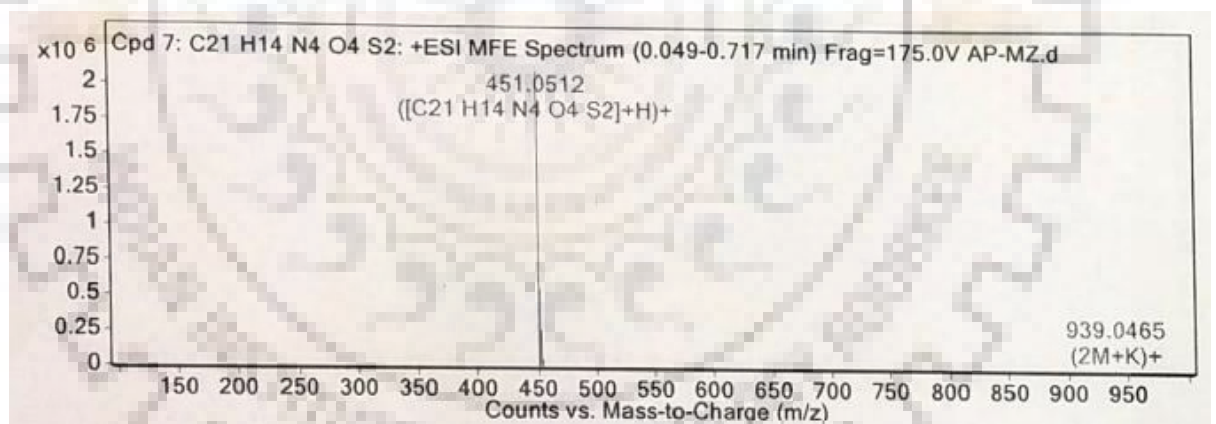


Figure 5.13 HRMS of L6

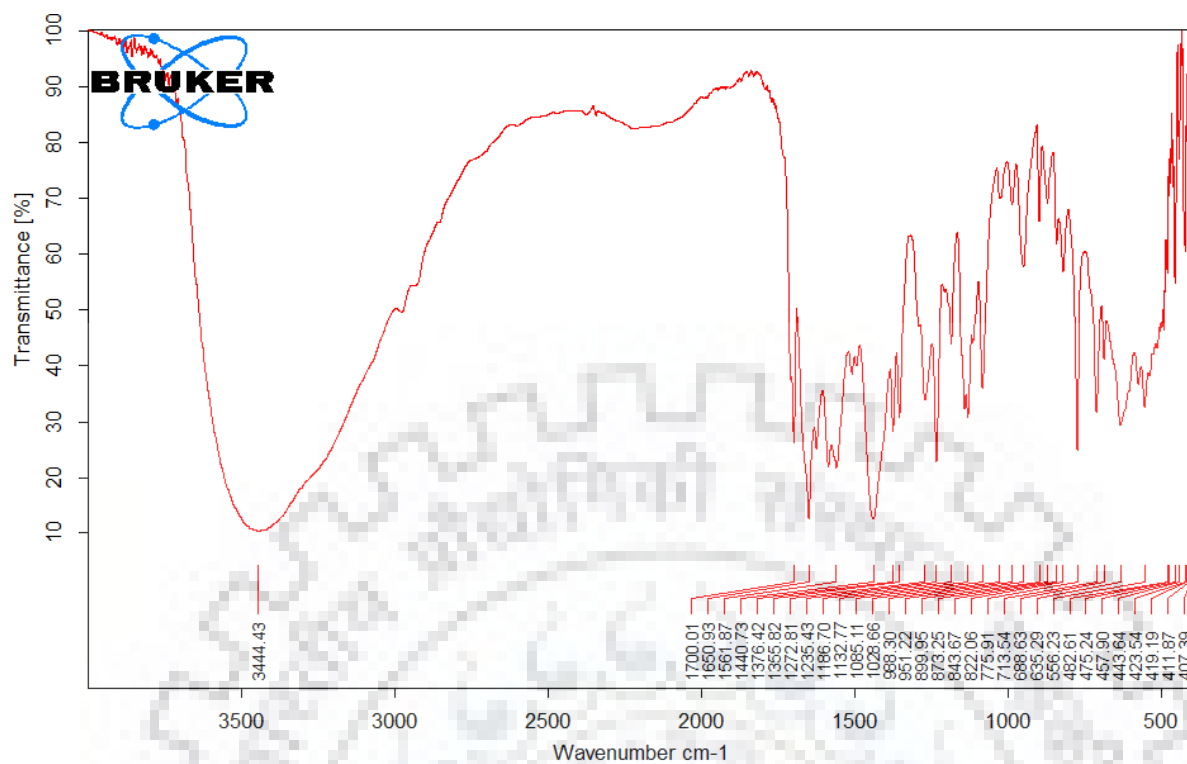


Figure 5.14 IR spectrum of receptor **L6+Ag⁺** recorded in KBr pellet.

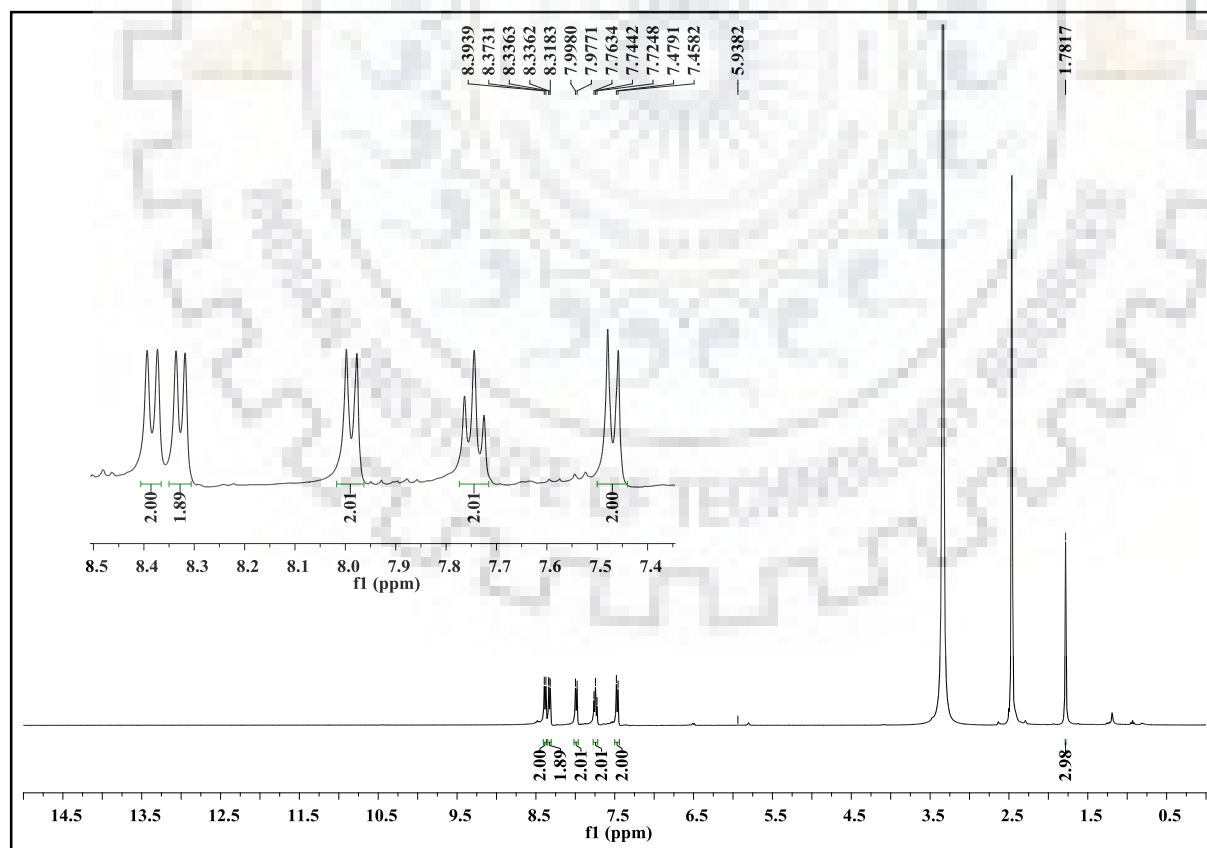


Figure 5.15 ¹H-NMR spectrum of receptor **L6+Ag⁺** complex recorded in DMSO-d₆.

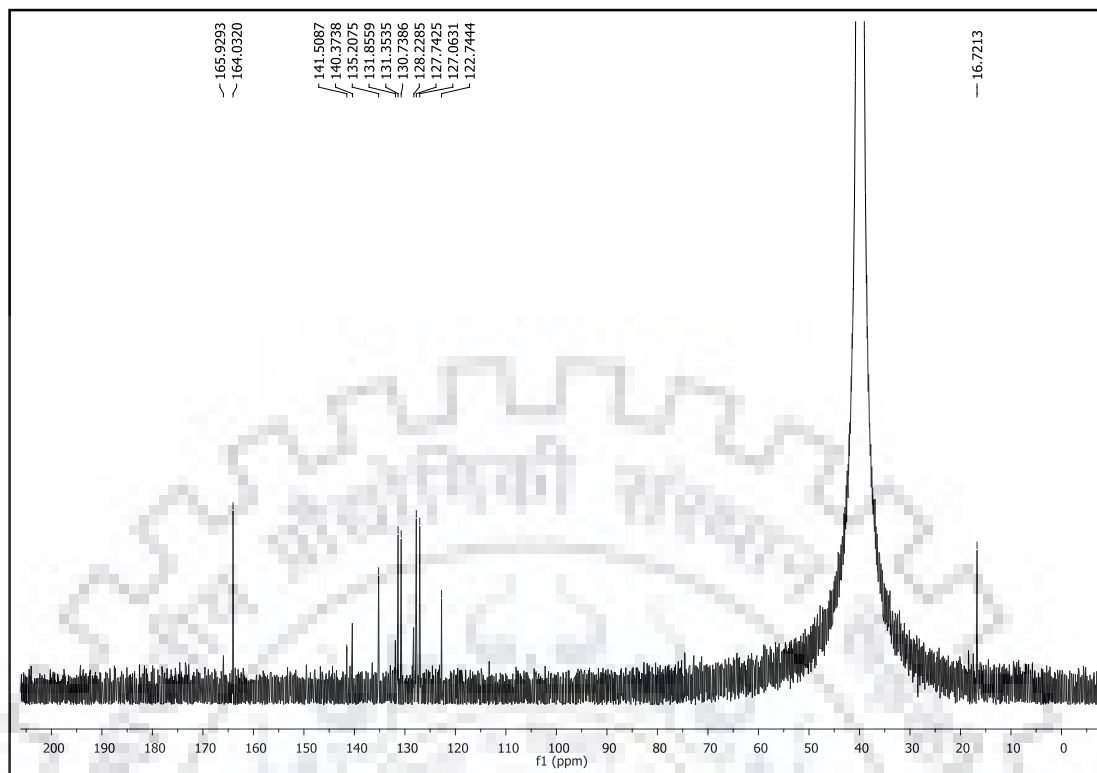


Figure 5.16 ^{13}C -NMR spectrum of receptor **L6**+ Ag^+ recorded in DMSO-d_6 .

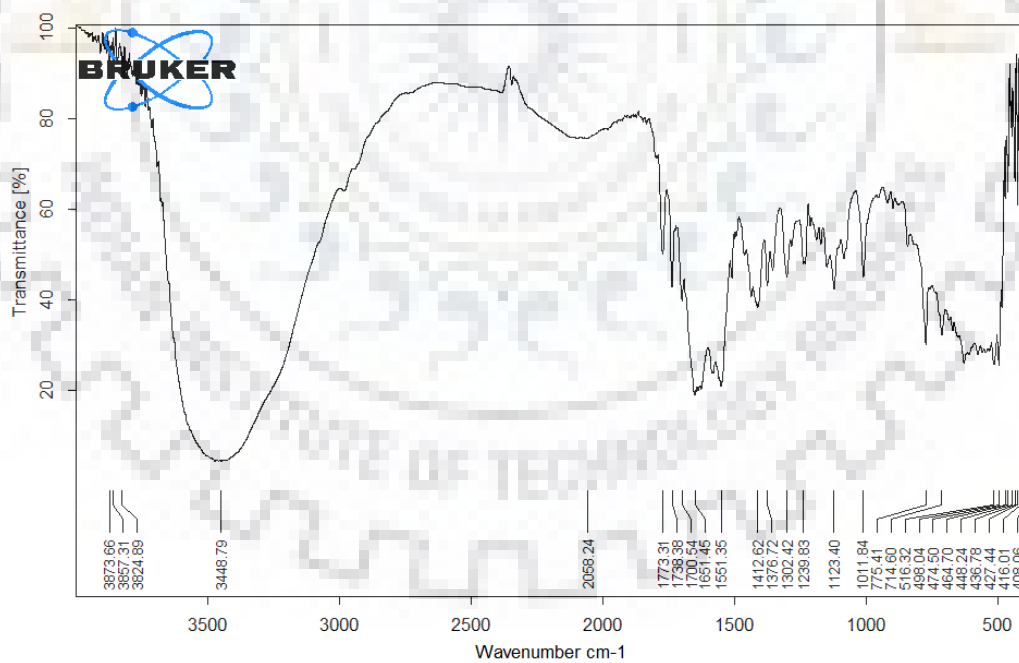


Figure 5.17 IR spectrum of **L6**+ HgCl_2 recorded in KBr pellet.

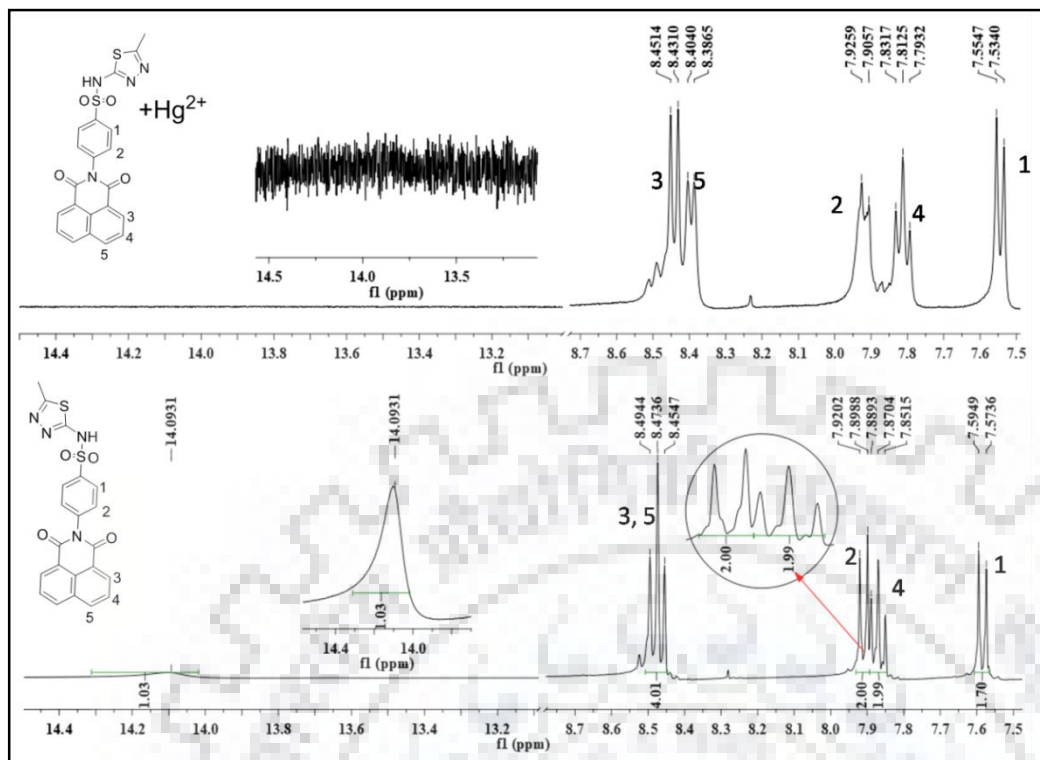


Figure 5.18 $^1\text{H-NMR}$ spectra of **L6** with Hg^{2+} (as HgCl_2) in $\text{DMSO-}d_6$.

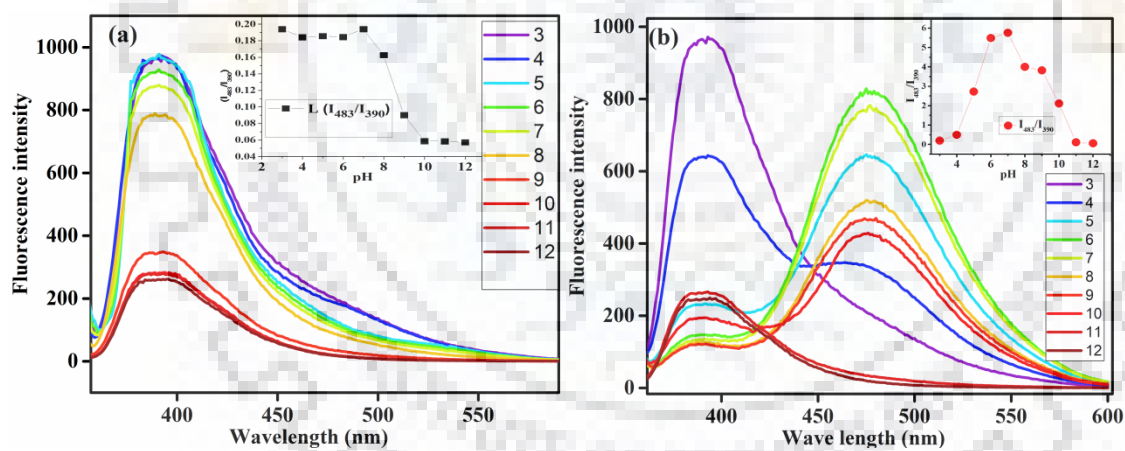


Figure 5.19 Fluorescence intensity of (a). **L6**, (b). **L6-Hg $^{2+}$** at different pH value.

5.6 Reference

- [1] Y. Ding, Y. Tang, W. Zhu, Y. Xie, Fluorescent and colorimetric ion probes based on conjugated oligopyrroles, *Chem. Soc. Rev.* 44 (2015) 1101–1112. doi:10.1039/c4cs00436a.
- [2] N. Ullah, M. Mansha, I. Khan, A. Qurashi, Nanomaterial-based optical chemical sensors for the detection of heavy metals in water: Recent advances and challenges, *Trends Anal. Chem.* 100 (2018) 155–166. doi:10.1016/j.trac.2018.01.002.
- [3] Y. Ding, S. Wang, J. Li, L. Chen, Nanomaterial-based optical sensors for mercury ions, *Trends Anal. Chem.* 82 (2016) 175–190. doi:10.1016/j.trac.2016.05.015.
- [4] S.A. El-Safty, M.A. Shenashen, S.A. El-Safty, Mercury-ion optical sensors, *Trends Anal. Chem.* 38 (2012) 98–115. doi:10.1016/j.trac.2012.05.002.
- [5] G. Chen, Z. Guo, L. Tang, Fluorescent and colorimetric sensors for environmental mercury detection, *Analyst.* 140 (2015) 5400–5443. doi:10.1039/c5an00389j.
- [6] Y. Jiang, Q. Duan, G. Zheng, L. Yang, J. Zhang, Y. Wang, H. Zhang, J. He, H. Sun, D. Ho, An ultra-sensitive and ratiometric fluorescent probe based on the DTBET process for Hg²⁺ detection and imaging applications, *Analyst.* 144 (2019) 1353–1360. doi:10.1039/c8an02126k.
- [7] B.D. de Greñu, J. García-Calvo, J. Cuevas, G. García-Herbosa, B. García, N. Busto, S. Ibeas, T. Torroba, B. Torroba, A. Herreras, S. Pons, Chemical Science solution and HEK cells nuclei by means of DNA interacting fluorogenic probes, *Chem. Sci.* 6 (2015) 3757–3764. doi:10.1039/c5sc00718f.
- [8] M. Goudarzi, M. Kalantar, H. Kalantar, The Hepatoprotective Effect of Gallic Acid on Mercuric Chloride-Induced Liver Damage in Rats, *Jundishapur J Nat Pharm Prod.* 12 (2017). doi:10.5812/jjnpp.12345.Research.
- [9] M.H. Hazelhoff, M.S. Trebucovich, T.R. Stoyanoff, A.A. Chevalier, A.M. Torres, Amelioration of mercury nephrotoxicity after pharmacological manipulation of organic anion transporter 1 (Oat1) and multidrug resistance- associated protein 2 (Mrp2) with furosemide, *Toxicol. Res.* 2 (2015) 1324–1332. doi:10.1039/c5tx00100e.
- [10] M.T. Boroushaki, H. Mollazadeh, A. Rajabian, K. Dolati, A. Hoseini, M. Paseban, M. Farzadnia, Protective effect of pomegranate seed oil against mercuric chloride-induced nephrotoxicity in rat Protective effect of pomegranate seed oil against mercuric chloride-induced nephrotoxicity in rat, *Ren Fail.* 6049 (2014) 1581–1586. doi:10.3109/0886022X.2014.949770.

- [11] B. Du, P. Li, X. Feng, G. Qiu, J. Zhou, L. Maurice, Mercury Exposure in Children of the Wanshan Mercury Mining Area, Guizhou, China, *Int. J. Res. Public Heal.* 13 (2016) 1107. doi:10.3390/ijerph13111107.
- [12] P.D. Selid, H. Xu, E.M. Collins, M.S. Face-collins, J.X. Zhao, Sensing Mercury for Biomedical and Environmental Monitoring, *Sensors.* 9 (2009) 5446–5459. doi:10.3390/s90705446.
- [13] T. Puangsamlee, Y. Tachapermpon, P. Kammalun, K. Sukrat, C. Wainiphithapong, J. Sirirak, N. Wanichacheva, Solvent control bifunctional fluorescence probe for selective detection of Cu^{2+} and Hg^{2+} via the excimer of pyrenylacetamide subunits, *J. Lumin.* 196 (2018) 227–235. doi:10.1016/j.jlumin.2017.11.048.
- [14] F. Wu, G. Xu, X. Zeng, L. Mu, C. Redshaw, G. Wei, Characterization of the Aggregation-Induced Enhanced Emission of N,N'-bis (4 -methoxysalicylide) benzene-1,4-diamine, *J Fluoresc.* 25 (2015) 1183–1189. doi:10.1007/s10895-015-1605-2.
- [15] L. Le Bras, K. Chaitou, S. Aloïse, C. Adamoac, A. Perrier, Aggregation-caused quenching versus crystallization induced emission in thiazolo[5,4-b]thieno[3,2-e]-pyridine (TTP) derivatives: theoretical insights, *Phys.Chem.Chem.Phys.* (2019) 46–56. doi:10.1039/C8CP04730H.
- [16] Y. Bao, De Keersmaecker, Herlinde, S. Corneillie, F. Yu, H. Mizuno, G. Zhang, J. Hofkens, B. Mendrek, A. Kowalczyk, M. Smet, Tunable Ratiometric Fluorescence Sensing of Intracellular pH by Aggregation-Induced Emission-Active Hyperbranched Polymer Nanoparticles, *Chem. Mater.* 27 (2015) 3450–3455. doi:10.1021/acs.chemmater.5b00858.
- [17] M. Yeh, C. Huang, T. Lai, F. Chen, N. Chu, D.T. Tseng, S. Hung, H. Lin, Effect of Peptide Sequences on Supramolecular Interactions of Naphthaleneimide/Tripeptide Conjugates, *Langmuir.* 32 (2016) 7630–7638. doi:10.1021/acs.langmuir.6b01809.
- [18] Y. Sun, X. Liang, S. Wei, J. Fan, X. Yang, Fluorescent Turn-On detection and assay of water based with aggregation-induced emission enhancement, *Spectrochim. Acta Part A Mol. Biomol. Spectrosc.* 97 (2012) 352–358. doi:10.1016/j.saa.2012.06.017.
- [19] J. Luo, Z. Xie, J.W.Y. Lam, L. Cheng, H. Chen, C. Qiu, H.S. Kwok, X. Zhan, Y. Liu, D. Zhu, B.Z. Tang, Aggregation-induced emission of 1-methyl-1,2,3,4,5-pentaphenylsilole, *Chem. Commun.* (2001) 1740–1741. doi:10.1039/b105159h.
- [20] X. Wen, Q. Wang, Z. Fan, Highly selective Turn-On fluorogenic chemosensor for Zn(II) detection based on aggregation-induced emission, *J. Lumin.* 194 (2018) 366–373. doi:10.1016/j.jlumin.2017.10.064.

- [21] Y. Chen, X. Min, X. Zhang, F. Zhang, S. Lu, L. Xu, X. Lou, F. Xia, X. Zhang, S. Wang, AIE-based superwetable microchips for evaporation and aggregation induced fluorescence enhancement biosensing, *Biosens. Bioelectron.* 111 (2018) 124–130. doi:10.1016/j.bios.2018.04.011.
- [22] X. Wen, Q. Wang, Z. Fan, An active fluorescent probe based on aggregation-induced emission for intracellular bioimaging of Zn^{2+} and tracking of interactions with, *Anal. Chim. Acta.* 1013 (2018) 79–86. doi:10.1016/j.aca.2018.01.056.
- [23] Y. Wang, H. Wu, W. Wu, Y. Yu, X. Zhao, Z. Xu, Z. Xu, Y. Fan, Aggregation-induced ratiometric emission active monocarbazone: Ratiometric fluorescent probe for Cu^{2+} in either solution or aggregation states, *J. Lumin.* 204 (2018) 289–295. doi:10.1016/j.jlumin.2018.08.042.
- [24] Y. Zhou, X. He, H. Chen, Y. Wang, S. Xiao, N. Zhang, D. Li, K. Zheng, An ESIPT/ICT modulation based ratiometric fluorescent probe for sensitive and selective sensing Hg^{2+} , *Sensors Actuators B. Chem.* 247 (2017) 626–631. doi:10.1016/j.snb.2017.03.085.
- [25] L. Long, L. Zhou, L. Wang, S. Meng, A. Gong, C. Zhang, ratiometric fluorescent probe for iron (III) and its application for detection of iron (III) in human blood serum, *Anal. Chim. Acta.* 812 (2014) 145–151. doi:10.1016/j.aca.2013.12.024.
- [26] L. Wu, Y. Wang, T.D. James, A hemicyanine based ratiometric fluorescence probe for mapping lysosomal pH during heat stroke in living cells, *Chem. Commun.* 54 (2018) 5518–5521. doi:10.1039/c8cc02330a.
- [27] Y. Sun, X. Liang, J. Fan, Q. Han, Studies on the photophysical properties of 1,8-naphthalimide derivative and aggregation induced emission recognition for casein, *J. Lumin.* 141 (2013) 93–98. doi:10.1016/j.jlumin.2013.02.053.
- [28] P. Gopikrishna, N. Meher, P.K. Iyer, Functional 1,8-Naphthalimide AIE/AIEEgens: Recent Advances and Prospects, *ACS Appl. Mater. Interfaces.* 10 (2018) 12081–12111. doi:10.1021/acsami.7b14473.
- [29] C. Liu, Y. Hang, T. Jiang, J. Yang, X. Zhang, J. Hua, A light-up fluorescent probe for citrate detection based on bispyridinium amides with aggregation-induced emission feature, *Talanta.* 178 (2018) 847–853. doi:10.1016/j.talanta.2017.10.026.
- [30] S. Ge, B. Li, X. Meng, H. Yan, M. Yang, B. Dong, Y. Lu, Aggregation-induced emission, multiple chromisms and self-organization of N-substituted-1,8-naphthalimides, *Dye. Pigment.* 148 (2018) 147–153. doi:10.1016/j.dyepig.2017.08.013.
- [31] A. Kumar, P.S. Chae, New 1,8-naphthalimide-conjugated sulfonamide probes for TNP sensing in water, *Sensors Actuators B. Chem.* 240 (2017) 1–9.

doi:10.1016/j.snb.2016.08.149.

- [32] S. Banerjee, E.B. Veale, C.M. Phelan, S.A. Murphy, G.M. Tocci, L.J. Gillespie, D.O. Frimannsson, J.M. Kelly, T. Gunnlaugsson, Recent advances in the development of 1,8-naphthalimide based DNA targeting binders, anticancer and fluorescent cellular imaging agents, *Chem. Soc. Rev.* 42 (2013) 1601–1618. doi:10.1039/c2cs35467e.
- [33] A. Wu, P. Mei, Y. Xu, X. Qian, Novel Naphthalimide–Benzoic Acid Conjugates as Potential Apoptosis-Inducing Agents: Design, Synthesis, and Biological Activity, *Chem Biol Drug Des.* 78 (2011) 941–947. doi:10.1111/j.1747-0285.2011.01232.x.
- [34] S. Radha, K.K. Mothilal, A. Thamarachelvan, Elangovana, Synthesis, characterization and biological studies of sulfadiazine drug based transition metal complexes, *J. Chem. Pharm. Res.* 8 (2016) 202–211.
- [35] M. Meshki, M. Behpour, S. Masoum, Application of Fe doped ZnO nanorods-based modified sensor for determination of sulfamethoxazole and sulfamethizole using chemometric methods in voltammetric studies, *J. Electroanal. Chem.* 740 (2015) 1–7. doi:10.1016/j.jelechem.2014.12.008.
- [36] S. Alyar, S. Cihan, H. Alyar, S. Adem, A. Kalkanci, U.O. Ozdemir, Synthesis, characterization, antimicrobial activity, carbonic anhydrase enzyme inhibitor effects, and computational studies on new Schiff bases of Sulfa drugs and their Pd(II), Cu(II) complexes, *J. Mol. Struct.* 1171 (2018) 214–222. doi:10.1016/j.molstruc.2018.06.004.
- [37] M. Mondelli, F. Pavan, P.C. De Souza, C.Q. Leite, J. Ellena, O.R. Nascimento, G. Facchin, M.H. Torre, Study of a series of cobalt(II) sulfonamide complexes: Synthesis, spectroscopic characterization, and microbiological evaluation against *M.tuberculosis* Crystal structure of $[\text{Co}(\text{sulfamethoxazole})_2(\text{H}_2\text{O})_2]\text{H}_2\text{O}$, *J. Mol. Struct.* 1036 (2013) 180–187. doi:10.1016/j.molstruc.2012.09.064.
- [38] G. Alzuet, J. Borra´s, F. Estevan, M. Liu-González, F. Sanz-Ruiz, Zinc complexation to N-substituted sulfonamide ligands Preparation, properties and crystal structure of copper (II) doped $\{[\text{Zn}(\text{sulfamethizolate})_2(\text{py})]\times\text{H}_2\text{O}\}$, *Inorganica Chim. Acta.* 343 (2003) 56–60.
- [39] B.D. Wright, P.N. Shah, L.J. McDonald, M.L. Shaeffer, P.O. Wagers, M.J. Panzner, J. Smolen, J. Tagaev, C.A. Tessier, C.L. Cannon, W.J. Youngs, Synthesis, characterization, and antimicrobial activity of silver carbene complexes derived from 4,5,6,7-tetrachlorobenzimidazole against antibiotic resistant bacteria, *Dalton Trans.* 41 (2012) 6500–6506. doi: 10.1039/C2DT00055E.
- [40] C. Dilek, K. Ismail, L. Nabih, D. Mustafa, A. Suleyman, S.C. T, Synthesis and

- cytotoxic activities of novel copper and silver complexes of 1,3-diaryltriazene-substituted sulfonamides, *J. Enzyme Inhib. Med. Chem.* 34 (2018) 116–122. doi:10.1080/14756366.2018.1530994.
- [41] G. Borthagaray, M. Mondelli, M.H. Torre, Essential Transition Metal Ion Complexation as a Strategy to Improve the Antimicrobial Activity of Organic Drugs, *J. Infect. Dis. Epidemiol.* 2 (2016) 1–8. doi:10.23937/2474-3658/1510014.
- [42] H. Shaki, A. Khosravi, K. Gharanjig, A. Mahboubi, photophysical and biological properties of derivatives Investigation of synthesis, characterization, photophysical and biological properties of novel antimicrobial fluorescent naphthalimide derivatives, *Mater. Technol.* 31 (2016) 322–331. doi:10.1179/1753555715Y.0000000058.
- [43] A. Kumar, H. Kim, N-(3-Imidazolyl) propyl dansylamide as a selective Hg^{2+} sensor in aqueous media through electron transfer, *Spectrochim. Acta Part A.* 148 (2015) 250–254. doi:10.1016/j.saa.2015.03.091.
- [44] P. Thirupathi, P. Saritha, K. Lee, Ratiometric fluorescence chemosensor based on tyrosine derivatives for monitoring mercury ions in aqueous solutions, *Org. Biomol. Chem.* 12 (2014) 7100–7109. doi:10.1039/c4ob01044b.
- [45] H. Goh, T.N. Kyu, A. Singh, N. Singh, D.O. Jang, Dipodal colorimetric sensor for Ag^+ and its resultant complex for iodide sensing using a cation displacement approach in water, *Tetrahedron Lett.* 58 (2017) 1040–1045. doi:10.1016/j.tetlet.2017.01.098.
- [46] M. Licchelli, O. Biroli, A. Poggi, D. Sacchi, C. Sangermani, M. Zema, Excimer emission induced by metal ion coordination in 1,8-naphthalimide-tethered iminopyridine ligands, *Dalton Trans.* (2003) 4537–4545. doi:10.1039/B308439F.
- [47] D.W. Cho, M. Fujitsuka, K.H. Choi, M.J. Park, U.C. Yoon, T. Majima, Intramolecular Exciplex and Intermolecular Excimer Formation of 1,8-naphthalimide Linker Phenothiazine Dyads, *J. Phys. Chem. B.* 110 (2006) 4576–4582. doi:10.1021/jp056078p.
- [48] K.A. Macgregor, M.J. Robertson, K.A. Young, L. Von Kleist, W. Stahlschmidt, A. Whiting, N. Chau, P.J. Robinson, V. Haucke, A. McCluskey, Development of 1,8-Naphthalimides as Clathrin Inhibitors, *J. Med. Chem.* 57 (2014) 131–143. doi:10.1021/jm4015263.
- [49] L. Megumi, J. Helena, B. Nunes, M. Antônio, A. Maria, W. Rogério, P. Paulo, Copper(II) and silver(I) complexes with sulfamethizole: synthesis, spectroscopic characterization, ESI-QTOF mass spectrometric analysis, crystal structure and antibacterial activities, *Polyhedron.* 138 (2017) 168–176.

doi:10.1016/j.poly.2017.09.034.

- [50] J. Helena, B. Nunes, R. Enoque, F. De Paiva, A. Cuin, W. Rogério, P. Paulo, Silver complexes with sulfathiazole and sulfamethoxazole: Synthesis, spectroscopic characterization, crystal structure and antibacterial assays, *Polyhedron*. 85 (2015) 437–444. doi:10.1016/j.poly.2014.09.010.
- [51] X. Zhang, X. Gan, S. Yao, W. Zhu, J. Yu, Z. Wu, H. Zhou, Y. Tian, J. Wu, Branched triphenylamine-core compounds: aggregation induced two-photon absorption, *RSC Adv.* 6 (2016) 60022–60028. doi:10.1039/c6ra09701d.
- [52] A. Emission, K. Santhiya, S.K. Sen, R. Natarajan, R. Shankar, D–A–D Structured Bis-acylhydrazone Exhibiting Aggregation-Induced Emission, Mechanochromic Luminescence, and Al(III) Detection, *J. Org. Chem.* 83 (2018) 10770–10775. doi:10.1021/acs.joc.8b01377.
- [53] Q. Zhao, J. Liu, H. Wang, M. Li, K. Zhou, H. Yangab, Y. Han, Balancing the H- and J-aggregation in DTS(PTTh₂)₂/PC70BM to yield a high photovoltaic efficiency, *J. Mater. Chem. C*. 3 (2015) 8183–8192. doi:10.1039/c5tc01205h.
- [54] S. Qu, C. Zheng, G. Liao, C. Fan, G. Liu, S. Pu, A fluorescent chemosensor for Sn²⁺ and Cu²⁺ based on a carbazole-containing diarylethene, *RSC Adv.* 7 (2017) 9833–9839. doi:10.1039/C6RA27339D.
- [55] K.H. Jung, S. Oh, J. Park, Y.J. Park, S. Park, K. Lee, A novel fluorescent peptidyl probe for highly sensitive and selective ratiometric detection of Cd(II) in aqueous and bio-samples *via* metal ion-mediated self-assembly, *New J. Chem.* 42 (2018) 18143–18151. doi:10.1039/c8nj02298d.
- [56] H. Tang, Y. Gao, B. Li, C. Li, Y. Guo, Reaction-based colorimetric and ratiometric fluorescent probe for highly selective detection of silver ions, *Sensors Actuators B. Chem.* 270 (2018) 562–569. doi:10.1016/j.snb.2018.05.064.
- [57] O.P. Dimitriev, Y.P. Piryatinski, Y.L. Slominskii, Excimer Emission in J-Aggregates, *J. Phys. Chem. Lett.* 9 (2018) 2138–2143. doi:10.1021/acs.jpcelett.8b00481.
- [58] E.M. Nolan, M.E. Racine, S.J. Lippard, Selective Hg(II) Detection in Aqueous Solution with Thiol Derivatized Fluoresceins, *Inorg. Chem.* 45 (2008) 2742–2749. doi:10.1021/ic052083w.
- [59] E. Coronado, R. Gala, C. Marti, E. Palomares, J.R. Durrant, M. Gratzel, Reversible Colorimetric Probes for Mercury Sensing, *J. Am. Chem. Soc.* 127 (2005) 12351–12356. doi:10.1021/ja0517724.
- [60] Z. Wang, J. Yang, Y. Li, Q. Zhuang, J. Gu, Zr-Based MOFs integrated with a

- chromophoric ruthenium complex for specific and reversible Hg^{2+} sensing, *Dalton Trans.* 47 (2018) 5570–5574. doi:10.1039/c8dt00569a.
- [61] G. Gangatharan, V. Kumar, M. Palsamy, A. Tamilselvi, A reversible fluorescent chemosensor for the rapid detection of Hg^{2+} in an aqueous solution: Its logic gates behavior, *Sensors Actuators B. Chem.* 273 (2018) 305–315. doi:10.1016/j.snb.2018.06.067.
- [62] S. Madhu, R. Kalaiyarasi, S.K. Basu, S. Jadhavb, M. Ravikanth, A boron-dipyrrin-Hg(II) complex as a fluorescence Turn-On sensor for chloride and applications towards logic gates, *J. Mater. Chem. C* 2 (2014) 2534–2544. doi:10.1039/c3tc32188f.
- [63] Y. Wu, J. You, K. Jiang, J. Xie, S. Li, D. Cao, Z. Wang, Colorimetric and ratiometric fluorescent sensor for F^- based on benzimidazole-naphthalene conjugate: Reversible and reusable study & design of logic gate function, *Dye. Pigment.* 140 (2017) 47–55. doi:10.1016/j.dyepig.2017.01.025.
- [64] S. Erbas-Cakmak, S. Kolemen, A.C. Sedgwick, T. Gunnlaugsson, T.D. James, J. Yoon, E.U. Akkaya, Molecular logic gates: the past, present and future, *Chem. Soc. Rev.* 47 (2018) 2228–2248. doi:10.1039/c7cs00491e.
- [65] W. Li, G. Wu, W. Qu, Q. Li, J. Lou, Q. Lin, H. Yao, Y. Zhang, T. Wei, A colorimetric and reversible fluorescent chemosensor for Ag^+ in aqueous solution and its application in IMPLICATION logic gate, *Sensors Actuators B. Chem.* 239 (2017) 671–678. doi:10.1016/j.snb.2016.08.016.
- [66] R. Gao, S. Shi, Y. Zhu, H. Huang, T. Yao, A RET-supported logic gate combinatorial library to enable modeling and implementation of intelligent logic functions, *Chem. Sci.* 7 (2016) 1853–1861. doi:10.1039/C5SC03570H.
- [67] J. Nunes, R.E.F. De Paiva, A. Cuin, W.R. Lustri, P.P. Corbi, Silver complexes with sulfathiazole and sulfamethoxazole: Synthesis, spectroscopic characterization, crystal structure and antibacterial assays, *Polyhedron.* 85 (2015) 437–444. doi:10.1016/j.poly.2014.09.010.